2003

平成15年度

金沢医科大学
奨励研究成果報告書

平成17年12月

金沢医科大学

はじめに

平成15年度金沢医科大学奨励研究成果報告書を発刊しましたのでお手元にお届けいたします。本学の研究助成は、学術研究を活性化させる目的で学内公募のもと継続されていますが、平成15年度から装いを新たにして始まりました。本学は、平成15年度から大学院が改組され、医学部と総合医学研究所を含む全学的な教育・研究体制が構築されました。その大学院改組の年である平成15年から新しい形で共同研究が始まりましたが、同時に研究基盤を充実させるため、将来を嘱望され、特徴ある独創的な企画の研究に対して助成することとしました。平成15年度は、学内公募で申請があった39件のうち12件が採択されました。この奨励研究が共同研究と併せて本学の学術研究をさらに推進することを期待します。

最後に、本報告書の取りまとめの労をとられた研究推進評価特別委員会、研究助成センター事務課並びに関係各位に感謝します。

平成17年12月

金沢医科大学
学長　山本　達

目　　次

1．研究課題名：　各種脂肪酸・抗酸化ビタミン摂取量、血清高感度 CRP と血圧との関連に関する大規模疫学研究（研究番号 S2003-1）

2．キーワード：1）脂肪酸（fatty acids）
2）抗酸化ビタミン（antioxidant vitamins）
3）高感度 CRP（C-reactive protein）
4）血圧（blood pressure）
5）疫学（epidemiology）

3．研究者氏名：　三浦克之・医学部・助教授・健康増進予防医学(公衆衛生学)

4．研究目的

高血圧は動脈硬化性循環器疾患の最大の危険因子の一つであり、その予防はわが国の国民的課題となっている。高血圧は、食塩、飲酒などの生活習慣が大きな原因とされてきたが、近年新たに様々な栄養素と血圧との関連が示唆されてきている。特に注目されるのは米国 DASH 研究が豊富な野菜・果物・魚摂取・低脂肪乳製品という食事パターン（DASH 食）による効果的な血圧低下を証明したことであり、そのメカニズムとして、少ない飽和脂肪酸、多い植物性（多価不飽和）脂肪酸、魚に多い n-3 系脂肪酸、抗酸化ビタミンなどが推察されているがいまだ明らかになっておらず、国際的に大きな課題となっている。一方、新たな動脈硬化危険因子として炎症反応指標である血清高感度 CRP が注目されているが、脂質・ビタミン類など酸化ストレス関連要因との関連や、血圧との関連については明らかになっていない。

本研究では大規模な成人集団において各種脂肪酸(飽和脂肪酸、一価不飽和脂肪酸、多価不飽和脂肪酸、n-3 系脂肪酸、n-6 系脂肪酸）および各種抗酸化ビタミン（ビタミン A, C, E, B 群）の摂取量を厳密に評価し、血清高感度 CRP および血圧値との関連を検討することを目的とする。

5．研究計画

北陸地方の製造業事業所従業員の 20-60 歳の成人男女約 7000 人を対象として、食物摂取状況調査および血清高感度 CRP 測定、厳密に標準化された２回の血圧測定を行った。

食物摂取状況調査は 15 ページにわたる自記式調査であり、量頻度法を主にするものである。国立健康・栄養研究所佐々木敏氏の開発によるもので、佐々木氏との共同研究にて実施した。本調査法の妥当性・信頼性は、３日間食事記録法、24 時間蓄尿、血中指標等を用いて確認がされており、各種脂肪酸摂取量および各種抗酸化ビタミン摂取量についても精度の高い結果が得られる。調査票は 6527 人から回収され回収率は 89.3%であった。

血清高感度CRPは35-60歳の従業員男女3621人においてラテックスネフェロメトリー法にて測定された（Behring Nephelometer Analyzer II, Behring)。血圧測定は標準化された自動血圧計を用い、7306人の対象者において5分間の座位安静後2回厳密に測定された。

解析においては、各種脂肪酸・抗酸化ビタミンを始めとした各種摂取素摂取量と高感度 CRP、血圧との関連を、多変量解析を用いて年齢・肥満度・飲酒・喫煙等の交絡要因の影響を調整して明らかにした。血清高感度 CRP については 10mg/L 以上の人は除外し、対数変換値を用いて解析した。

6．研究成果

まず、性・年齢階級別の各種栄養素・食品群摂取量を比較した。総脂肪摂取量は若年層ほど多く、20歳代男 59g、女 52g に対し 50歳代男 43g、女 45g と大きな差を示した。20歳代女の脂肪エネルギー比は 28%であった。飽和脂肪酸エネルギー比も 20歳代が最も高かった。n-6/n-3 脂肪酸比は年齢が高いほど低くなった。葉酸、ビタミン B6、ビタミン B12 摂取量は男女とも年齢が高いほど多い傾向があった。ビタミン A、ビタミン C 摂取量は 50 歳代女性が最も高かった。一方、食品群で見ると、魚介類の摂取量、野菜・果物の摂取量は 50 歳代が最も多く、50 歳代女の野菜・果物平均摂取量は 300g を越えていた。50 歳代の魚摂取量は男女とも 79g であった。大豆蛋白、葉酸、食物繊維、マグネシウム摂取量も 50 歳代が最も高かった。

血清高感度 CRP は女性より男性で統計学的に有意に高く($p<0.001$)、男性では年齢により有意差は認められないが、女性は年齢が高くなるにつれ統計学的に有意に高くなった($p<0.001$)。また BMI が大きくなるにつれ男女とも血清高感度 CRP は統計学的に有意に高くなった($p<0.001$)。

血清高感度 CRP と各種栄養素摂取量（エネルギー調整値）との関連を、重回帰分析を用いて年齢、肥満度、飲酒、喫煙を調整し、男女別に検討した。男性においては、総脂肪摂取、飽和脂肪摂取、一価不飽和脂肪摂取、多価不飽和脂肪摂取、n-3 系脂肪酸摂取、n-6 系脂肪酸摂取のいずれとも血清高感度 CRP との関連は認めなかった。各種脂肪酸それぞれとの関連も有意なものは認めなかった。一方、ビタミン類については、総カロテン摂取($p<0.05$)、βカロテン摂取($p<0.05$)、αカロテン摂取($p<0.01$) との有意な正の関連を示した。その他のビタミン類との有意な関連は示さなかった。

女性においては、血清高感度 CRP は総脂肪摂取量と負の関連($p<0.01$)、総炭水化物摂取量と正の関連($p<0.001$)を示した。また、飽和脂肪摂取、一価不飽和脂肪摂取、多価不飽和脂肪摂取、n-3 系脂肪酸摂取、n-6 系脂肪酸摂取のいずれとも有意な負の関連を示した。脂肪酸別に見るとオレイン酸およびリノール酸と最も強い負の関連を示した($p<0.01$)。ビタミン類については、ビタミン B6 摂取と有意な負の関連を示したが($p<0.05$)、そのほかのビタミン類との関連は認めなかった。

次に、収縮期血圧と各種栄養素摂取量（エネルギー調整値）との関連を、重回帰分析を用いて年齢、肥満度、飲酒、喫煙を調整し、男女別に検討した。男性においては総炭水化物摂取量と負の有意な関連を示した($p<0.01$)。しかし、各種の脂肪摂取量の指標及びビタミン類摂取量との関連は示さなかった。女性においては、総脂肪摂取、飽和脂肪摂取、一価不飽和脂肪摂取、多価不飽和脂肪摂取、および n-6 系脂肪酸摂取と有意な負の関連を示したが、n-3 系脂肪酸摂取との関連は示さなかった。各種脂肪酸の中では、オレイン酸摂取との負の関連が最も強かった($p<0.01$)。ビタミン類では、レチノール及びビタミン A との有意な負の関連を示した($p<0.001$)。

7．研究の考察・反省

血清高感度 CRP は近年新たな循環器疾患リスクファクターとして注目され、その科学的根拠が確立してきた。全身の動脈硬化の進行自体が低レベルの炎症を引き起こし、高感度 CRP 値は動脈硬化の進行度のマーカーであるとする考えもあるが、一方で、酸化ストレスや代謝症候群が炎症を促進し動脈硬化の原因になるとする説もある。高感度 CRP は一般に加齢とともに上昇し、また肥満による上昇も多くの疫学研究で確認されており、今回の我々の検討においても同様の知見が得られた。しかし食事要因が血清高感度 CRP にどのように影響するかは未だ明らかになっていない。今回我々は大規模な日本人の集団における詳細な栄養調査から栄養摂取と高感度 CRP との関連を検討し、女性において一価不飽和脂肪酸であるオレイン酸摂取および多価不飽和脂肪酸であるリノール酸摂取との強い負の関連が明らかになった。最近の研究ではオレイン酸の豊富な地中海式食事による高感度 CRP の低下も報告されており、これに一致するものである。しかし抗酸化ビタミン類との関連は明らかでなく、男性ではカロテン類との正の関連が見られた。近年βカロテン補充による循環器疾患予防効果には否定的な報告が多く、これに関連する可能性がある。一方、血圧と各種脂肪摂取との関連については現在様々な議論があるが、本研究において女性の血圧とオレイン酸摂取との負の関連が認められたことは注目される。また女性の血圧とビタミン A 摂取との負の関連も興味深い。今後他の栄養素の影響を考慮した多変量解析にてさらに詳細に検討する必要がある。また近年、各種の食品群摂取と高感度 CRP または血圧との関連についても重要な研究課題となっており、本データベースを用いてさらに研究を進めたい。

1．研究課題名：ウイルス感染症を伴う肥満者におけるアディポサイトカインの診断及び治療への応用
(研究番号 S2003-2)

2．キーワード：1）肥満（obesity）
2）ウイルス感染症（viral infection）
3）アディポサイトカイン（adipocytokine）

3．研究者氏名：高橋　孝・医学部・講師・総合内科学(総合診療科)

4．研究目的

現代病と言われている肥満は、糖代謝異常や内分泌異常を惹起し、易感染性や感染症の重篤化を招く場合が多いと言われている。これまでは、感染症との関わりを糖代謝及び内分泌の病的な状況という視点から説明されてきた。

しかし、脂肪組織が生体最大の内分泌臓器であるという概念から、肥満と感染症との直接的な関わりを検証する重要性があり、この点が本研究の意義である。これまでに、敗血症におけるレプチンの生体防御を示唆する報告はあるが、ウイルス感染症に対するレプチンの役割は検証されていない。SARS ウイルスを含む新興感染症が人類の生命を脅かす社会情勢においては、本研究が解明したい感染症に対する脂肪組織特異的な内分泌蛋白質の解析が急務であると考える。

そこで、本研究は、サイトカインの感染性疾患への関わりを脂肪組織特異的な生理活性物質(アディポサイトカイン)の視点から解析することによって、ウイルス感染症を伴う肥満者に対するアディポサイトカインの臨床診断(特に、予後予測因子の同定)、そして治療への応用を展開したい。そして、感染症を伴う肥満者に対するサイトカイン補充療法という治療方法の開発が期待できる。

5．研究計画

レプチン欠損肥満マウス(*ob* マウス)を用いて、encephalomyocarditis (EMC) ウイルスを接種させることによってウイルス性心筋炎という疾患モデルを作製する。

① 致死的なウイルス感染症（ウイルス性心筋炎）の発症下において、疾患マウスの生存率を評価する共に、アディポサイトカインの血中レベルの経時的変動を検討する。その結果から、本病態の予後を推測するマーカーを同定する。

② 感染症病巣（心臓局所）におけるアディポサイトカイン及びその mRNA の発現量と EMC ウイルスの力価定量との関連性を解析する。その結果に基づいて、局所でのウイルス力価と関連するアディポサイトカインを推定する。

③ 上記の病態における予後改善に関与するアディポサイトカインを判定するために、外因性の同サイトカイン投与による生存観察や心筋障害を評価する。その結果から、予後の観点から見たアディポサイトカイン治療を想定する。

6．研究成果

① *ob* マウスにおいて発症したウイルス性心筋炎において、野生型マウスでのウイルス性心筋炎と比較して、重篤な心筋壊死と共に、ウイルス接種後 10 日間という短期間において有意に低い生存率が観察された。*ob* マウスへのウイルス接種と共に、組換えマウスレプチン(300 μg/day 腹腔

内投与)を補充した場合、生存率の改善が認められた。しかし、ウイルス感染後4日目と8日目に各群において測定した血中アディポネクチン値に有意な差は見られず、長寿因子である同サイトカインが肥満におけるウイルス感染症の予後マーカーであるというエビデンスは今回得られなかった。

② ウイルス接種後8日目に*ob*マウスより得られた心臓におけるアディポネクチンmRNA発現レベル(Real-time RT-PCR)及び蛋白質発現レベル(ELISA)は、野生型マウスと比較して、局所でのEMCウイルス高力価と共に有意な低値を示した。一方、同時期の*ob*マウスにおける心臓内TNF-α mRNA及び蛋白質発現レベルは、野生型と比べて、有意に増加した。免疫組織化学を用いたアディポネクチン及びTNF-αの心筋細胞における発現に関しても、同様な結果が認められた。

③ ①に提示したように、*ob*マウスにおけるウイルス性心筋炎は、重篤な心筋障害と低い生存率を示したが、組換えマウス全長アディポネクチン(30 μg/g/day 皮下投与)をウイルス接種と同時に連日補充することによって、心筋細胞におけるアディポネクチン受容体の発現増強と共に有意な心筋障害の抑制作用が認められた。そして、生存率の上昇という短期的な予後改善効果が確認された。

<アディポネクチン補充療法と心筋障害抑制>

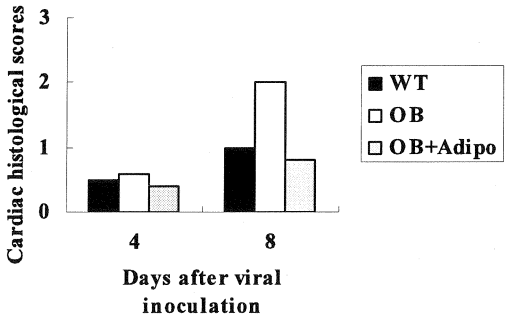

WT:野生型マウス、OB:*ob*マウス、OB+Adipo:*ob*マウスにアディポネクチン補充

7．研究の考察・反省

① 肥満マウスにおける致死的なウイルス感染症のモデルは確立され、野生型マウスと比較して重篤な心筋障害と有意な生存率の減少が確認された。しかし、血中レベルでのアディポネクチンが予後因子となり得るという所見は認められず、今後、本病態の予後改善を推測する他の血中バイオマーカーを同定する必要がある。

② ウイルス力価と関連する局所発現のサイトカインとしてアディポネクチンやTNF-αが推定され、心筋細胞のアディポネクチン発現による自己防御機構の可能性が示唆された。今後は、心筋細胞あるいは脾臓細胞の培養系を確立して、アディポネクチンとウイルス複製抑制との直接的な関連性を確認したい。

③ ウイルス性心筋炎を伴う肥満マウスへのアディポネクチン補充療法による予後の改善が確認された。しかし、アディポネクチンの至適な投与量の設定には至っておらず、今後、同サイトカイン投与量の調整を検討したい。長期的な予後改善効果の確認も今後の課題である。

8．研究発表

Takahashi T, Zhu S, Sumino H, Saegusa S, Nakahashi T, Iwai K, Morimoto S, Kanda T. Inhibition of cyclooxygenase-2 enhances myocardial damage in a mouse model of viral myocarditis. Life Sci 2005; 78: 195-204. (in press) (MLDB)

Takahashi T, Saegusa S, Sumino H, Nakahashi T, Iwai K, Morimoto S, Kanda T. Adiponectin replacement therapy attenuates myocardial damage in leptin-deficient mice with viral myocarditis. J Int Med Res 2005; 33: 207-214. (MLDB)

Takahashi T, Saegusa S, Sumino H, Nakahashi T, Iwai K, Morimoto S, Nojima T, Kanda T. Adiponectin, T-cadherin and tumor necrosis factor-a in damaged cardiomyocytes from autopsied specimens. J Int Med Res 2005; 33: 236-244. (MLDB)

Kotajima N, Takahashi T, Ito H, Sumino H, Fukumura Y, Kurabayashi M, Murakami M, Kanda T. Clinical features associated with circulating concentration of soluble leptin receptor in patients with diabetes. J Int Med Res 2005; 33: 61-67. (MLDB)

Goto M, Takahashi T, Kanda T, Iwamoto A. Detection of *Toxoplasma gondii* by polymerase chain reaction in cerebrospinal fluid from human immunodeficiency virus-1-infected Japanese patients with focal neurological signs. J Int Med Res 2004; 32: 665-670. (MLDB)

The Journal of International Medical Research
2005; 33: 207 – 214

Adiponectin Replacement Therapy Attenuates Myocardial Damage in Leptin-deficient Mice with Viral Myocarditis

T TAKAHASHI[1], S SAEGUSA[1], H SUMINO[3], T NAKAHASHI[2], K IWAI[2], S MORIMOTO[2] AND T KANDA[1]

[1]Department of General Medicine and [2]Department of Geriatric Medicine, Kanazawa Medical University, Ishikawa, Japan; [3]Second Department of Internal Medicine, Gunma University School of Medicine, Gunma, Japan

The effects of adiponectin replacement therapy on myocardial damage were studied in leptin-deficient (OB) mice with acute viral myocarditis. Encephalomyocarditis virus was injected intraperitoneally into OB and wild-type (WT) mice. One subgroup of OB mice received no intervention and another subgroup received daily adiponectin replacement, simultaneously with viral inoculation. Differences in heart weight, cardiac histological score, numbers of infiltrating or apoptotic cells in the myocardium and the immunoreactivity of adiponectin receptors in myocytes were determined. The reactivity of adiponectin receptor 1 in myocytes from OB mice on day 4 and day 8 after viral inoculation was significantly decreased compared with that in myocytes from WT mice; the OB mice also had elevated cardiac weights and severe inflammatory myocardial damage. Adiponectin replacement in OB mice inhibited the development of severe myocarditis by augmenting myocyte adiponectin receptor 1 reactivity. Exogenously administered adiponectin may inhibit the progression of viral myocarditis through binding to the adiponectin receptor 1 in leptin-deficient conditions.

KEY WORDS: ADIPONECTIN; VIRAL MYOCARDITIS; LEPTIN DEFICIENCY; MYOCARDIAL DAMAGE

Introduction

Several studies have reported an association between leptin and cardiovascular conditions such as hypertension and chronic heart failure with cachexia. Reduced leptin concentrations may diminish the degree of cardiac adaptation in heart failure,[1] and plasma leptin levels were inappropriately low in patients with cachectic chronic heart failure.[2] We have recently found that leptin deficiency enhanced myocardial necrosis and lethality in a mouse model of viral myocarditis. However, leptin replacement inhibited the development of severe myocarditis, suggesting a protective role for leptin against myocyte damage,[3] although the mechanisms involved are unclear.

Adiponectin, also known as adipocyte complement-related protein of 30 kDa,[4] is a cytokine secreted by adipocytes that has anti-diabetic and anti-atherogenic effects.[5] Concentrations of adiponectin in blood are diminished in obesity, insulin resistance and type 2 diabetes.[4] The adiponectin gene and the obese gene, which encodes leptin, show several striking similarities in humans.[6] Both genes are composed of three exons and have a long first intron, and are expressed specifically in adipose tissues.[6] Adiponectin and leptin control fuel homeostasis, body weight and insulin sensitivity. Amelioration of insulin resistance, pancreatic β-cell degranulation and diabetes after crossing leptin-deficient mice with globular domain adiponectin transgenic mice has been described, indicating that globular adiponectin and leptin may have overlapping functions.[5] Thus, adiponectin may also possess functions similar to those of leptin in the development of heart failure.

In this study, we hypothesized that adiponectin could play a protective role against the progression of severe viral myocarditis in leptin deficiency. We examined the effects of adiponectin replacement therapy on myocardial damage in leptin-deficient mice with acute viral myocarditis.

Materials and methods

INFECTION PROTOCOL

Six-week-old female leptin-deficient *ob/ob* mice and C57BL wild-type mice were obtained from the Jackson Laboratory (Bar Harbor, ME, USA). A myocarditic variant of the encephalomyocarditis (EMC) virus was obtained from Dr Y Seto (Keio University, Tokyo, Japan). The viral preparations were stored at –80 °C in Eagle's minimum essential medium supplemented with 0.1% fetal bovine serum. Ethical approval for this study was obtained from the animal experimental committee in Kanazawa Medical University. All animals were treated in accordance with the Kanazawa Medical University guidelines for the care and use of laboratory animals. All animals were inoculated intraperitoneally with 500 plaque-forming units of EMC virus suspended in 0.1 ml of saline.

TREATMENT PROTOCOL

The leptin-deficient mice were randomly assigned to one of two groups. The first group did not receive interventional therapy (OB group). The second group received daily subcutaneous injections of recombinant mouse full-length adiponectin (30 μg/g per day, starting simultaneously with the EMC virus injection) (OB + Adipo group).[7]

HISTOLOGICAL EXAMINATION OF THE HEART

The mice were weighed and then killed by cervical dislocation on either day 4 or day 8 after viral inoculation. Cardiac tissues were immediately extracted, weighed, fixed in 10% buffered formalin and stained with haematoxylin and eosin (H&E). Two transverse sections of the ventricular myocardium were assessed for the severity of necrosis and mononuclear cell infiltration by an experienced pathologist who had no knowledge of the study design. Sections were scored according to the following scale: 1, lesions involving < 25% of the ventricular myocardium; 2, lesions involving 25 – 50% of the myocardium; 3, lesions involving 50 – 75% of the myocardium; and 4, lesions involving > 75% of the myocardium. The sections were also stained for myosin in order to confirm the presence of myocyte necrosis.

Five high-power fields (HPFs) (magnification × 400) were randomly selected from each transverse section of the myocardium, and the number of infiltrating cells counted. The number of apoptotic cells per section in these HPFs was also determined using *in situ*

terminal deoxynucleotidyl transferase-mediated deoxyuridine triphosphate nick-end labelling, as described previously.[8]

IMMUNOREACTIVITY OF ADIPONECTIN RECEPTORS IN MYOCYTES

To examine the immunoreactivity of adiponectin receptors 1 and 2 (AdipoR1 and AdipoR2), immunohistochemical staining using a streptavidin biotin complex method (K0675 and E0353, DAKO Cytomation Co. Ltd, Kyoto, Japan) was performed on serial sections of transverse ventricular myocardium from different mice on day 4 or day 8 after viral inoculation. The immunoreactivity of AdipoR1 and AdipoR2 in vessels and macrophages from a normal wild-type mouse that had not received viral inoculation or adiponectin administration was used as a positive control.

Rabbit polyclonal anti-mouse AdipoR1 and AdipoR2 antibodies (ADIPOR11-A and ADIPOR21-A, Alpha Diagnostic International Inc., San Antonio, TX, USA) were applied at a dilution of 1:50. Control slides were treated with normal diluted rabbit serum.

The slides were blindly reviewed by the same pathologist. The degree of adiponectin receptor reactivity was assessed in 30 randomly selected myocytes corresponding to surviving cells found on the respective H&E and myosin-stained slides, and was semi-quantitatively graded according to the degree of immunoreactivity: 0, absence of staining; 1+, weak staining; 2+, moderate staining; and 3+, strong staining.[9] The slides were also compared with the respective control slides to exclude non-specific staining.

STATISTICAL ANALYSIS

Data were expressed as the mean ± SD. Analysis of variance was used to evaluate differences in body and cardiac weights, cardiac histological scores, numbers of infiltrating or apoptotic cells in the myocardium and immunoreactivity of adiponectin receptors in myocytes between the groups. A P-value < 0.05 was considered to be statistically significant.

Results

Eight wild-type and 28 leptin-deficient mice were inoculated with EMC virus. Eighteen of the leptin-deficient mice did not receive interventional therapy (OB group); the remaining 10 leptin-deficient mice received daily injections of adiponectin (OB + Adipo group).

Eight of the mice in the OB group died from viral myocarditis during the study protocol; there were no deaths in the wild-type (WT) or OB + Adipo groups over the same period. The numbers of mice killed on day 4 and day 8 after viral inoculation were four and four, respectively, in the WT group, six and four, respectively, in the OB group, and five and five, respectively, in the OB + Adipo group.

BODY AND CARDIAC WEIGHTS

Body weights on days 0, 4 and 8 after viral inoculation were significantly higher ($P < 0.05$) in the OB and OB + Adipo groups than in the WT group (Table 1). Cardiac weights in the OB mice on day 8 after viral inoculation were significantly increased ($P < 0.05$) compared with those in the WT mice (Table 1). There was no significant difference in cardiac weight between the OB + Adipo group and the WT group.

HISTOLOGICAL FINDINGS

The histological scores of myocardial necrosis, and the numbers of infiltrating and apoptotic cells per HPF, in hearts from the different types of mice on day 4 and day 8 after viral inoculation are shown in Fig. 1. Hearts from the OB group showed severe myocardial necrosis and mononuclear cell

TABLE 1:
Body weight and cardiac weight after viral inoculation in various types of mice

	Body weight (g)			Cardiac weight (mg)	
Type	Day 0	Day 4	Day 8	Day 4	Day 8
WT	18.3 ± 1.5	18.7 ± 1.8	19.1 ± 1.5	96 ± 8	102 ± 10
OB	37.5 ± 2.4*	37.8 ± 2.9*	38.4 ± 3.1*	103 ± 7	121 ± 9*
OB + Adipo	37.8 ± 2.2*	37.3 ± 2.8*	35.6 ± 3.9*	94 ± 6	98 ± 12

WT, wild-type mice; OB, leptin-deficient ob/ob mice; OB + Adipo, OB mice receiving adiponectin.
Data are the mean ± SD.
*$P < 0.05$ compared with WT mice.

infiltration. The histological scores, numbers of infiltrating cells and numbers of apoptotic cells were significantly higher ($P < 0.05$ for all) in the OB group than in the WT group on day 8 (Fig. 1). There were no significant differences in the histological scores or the number of infiltrating or apoptotic cells between the OB + Adipo group and the WT group.

IMMUNOREACTIVITY OF ADIPONECTIN RECEPTORS

In the normal WT group, immunoreactivity for AdipoR1 was found in the arterial walls and immunoreactivity for AdipoR2 was found in macrophages. The degrees of immunoreactivity for AdipoR1 and AdipoR2 in myocytes from different mice on day 4 and day 8 are shown in Fig. 2. In the OB group, the AdipoR1 reactivity in myocytes was significantly reduced ($P < 0.05$) compared with reactivity observed in the WT group on day 4 and day 8 (Fig. 2A), but the AdipoR1 reactivity was similar in the OB + Adipo group and the WT group. There were no significant differences in the immunoreactivity for AdipoR2 among the groups (Fig. 2B).

Discussion

Circulating levels of leptin and adiponectin are either undetectable or decreased in OB mice.[10] The protective role of adiponectin against fatty liver diseases has recently been demonstrated in non-alcoholic OB mice with insulin resistance and dyslipidaemia.[11] Replacement therapy with adiponectin could in part compensate for the absence of leptin in terms of ameliorating hepatomegaly and steatosis and decreasing serum alanine aminotransferase levels,[11] although such therapy would not alter the primary aetiology. Injection of adiponectin has also been reported to elevate insulin sensitivity and alleviate hyperlipidaemia.[11] Consistent with these findings, adiponectin administration to OB mice receiving EMC viral inoculation in the present study was found to protect the OB mice from inflammatory myocardial damage.

Complementary DNA encoding the two adiponectin receptors AdipoR1 and AdipoR2, which are distantly related to the family of seven-transmembrane spanning G protein-coupled receptors, has been cloned.[12] AdipoR1 and AdipoR2 are expressed ubiquitously in most organs, with AdipoR1 being especially expressed in skeletal muscle and AdipoR2 in liver.[12] Pancreatic β-cells have also been shown to express adiponectin receptors in a cell culture system.[13] These receptors have seven transmembrane domains and activate signalling molecules

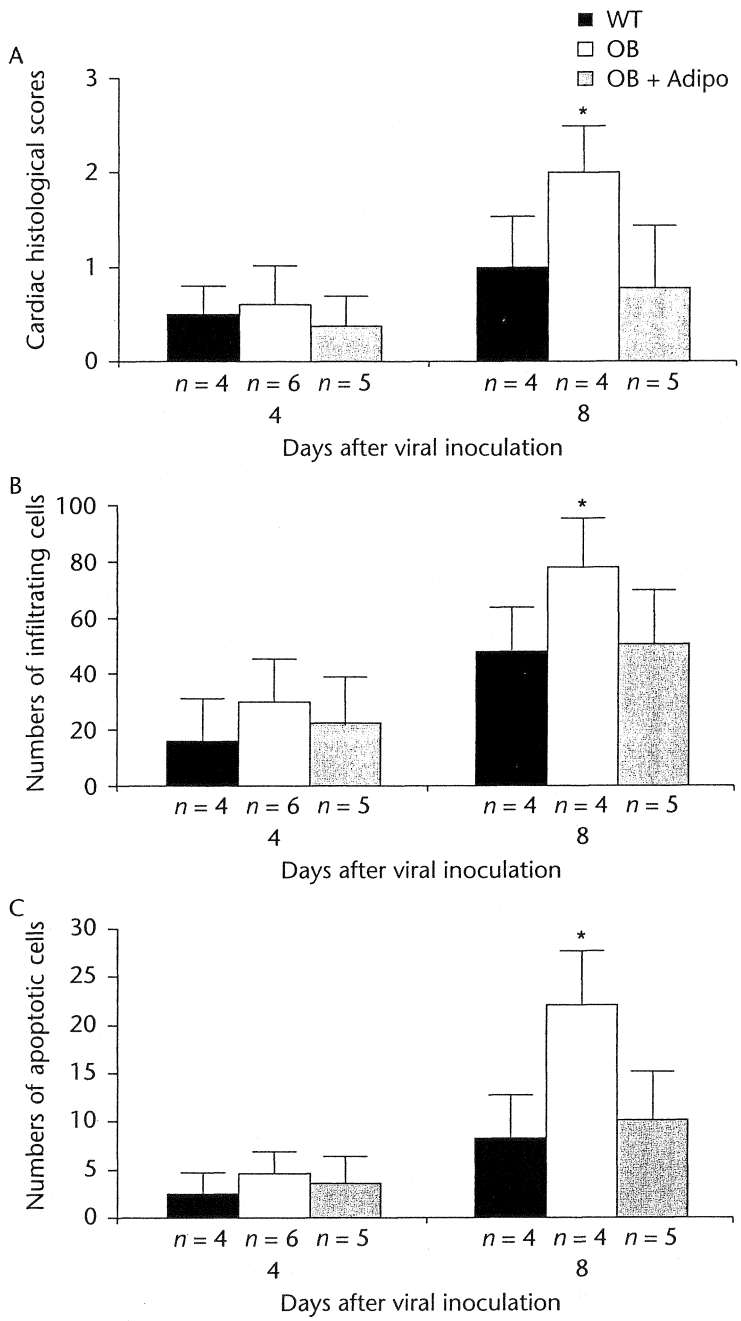

FIGURE 1: Results of histological examination of myocardial sections. (A) Histological scores, (B) numbers of infiltrating cells and (C) numbers of apoptotic cells in different types of mice on day 4 and day 8 after viral inoculation. Data are expressed as the mean ± SD. WT, wild-type mice; OB, leptin-deficient ob/ob mice; OB + Adipo, OB mice receiving subcutaneous administration of mouse adiponectin (30 μg/g daily, starting simultaneously with viral inoculation). $^*P < 0.05$ compared with WT group

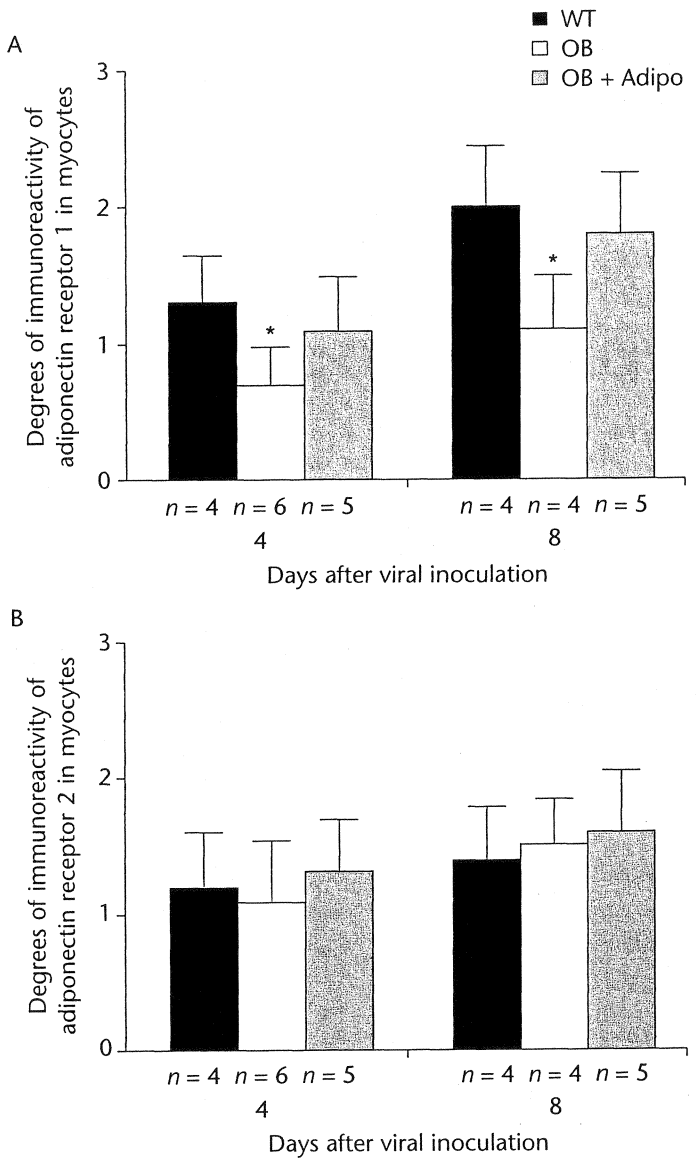

FIGURE 2: Degrees of immunoreactivity of adiponectin receptor 1 (A) or adiponectin receptor 2 (B) in myocytes from different types of mice on day 4 and day 8 after viral inoculation. Data are expressed as the mean ± SD. WT, wild-type mice; OB, leptin-deficient *ob/ob* mice; OB + Adipo, OB mice receiving subcutaneous administration of mouse adiponectin (30 μg/g daily, starting simultaneously with viral inoculation). $^*P < 0.05$ compared with WT group

such as peroxisome proliferator-activated receptor-α, adenosine monophosphate-activated protein kinase, and mitogen-activated protein kinase.[12] Possible alterations to adiponectin utilization in the coronary artery and/or heart have been described in type 2 diabetic patients compared with non-diabetic patients based on the transcardiac gradient of adiponectin levels from aortic root to coronary sinus.[14]

One mechanism of impaired transcardiac utilization of adiponectin in subjects with diabetes seems to be a decreased receptor-binding ability of adiponectin in the cardiac myocytes.[14] Interestingly, in the present study we found decreased AdipoR1 immunoreactivity in damaged myocytes from OB mice with viral myocarditis, and adiponectin replacement therapy in OB mice led to recovery of the suppressed AdipoR1 reactivity. These results indicate that adiponectin may act through binding to the AdipoR1, leading to protection against the progression of myocardial inflammation.

In summary, we determined the effects of adiponectin replacement therapy on myocardial damage in OB mice with viral myocarditis. There was significantly decreased reactivity of AdipoR1 in damaged myocytes from OB mice on day 4 and day 8 after viral inoculation compared with that in myocytes from WT mice, together with elevated cardiac weights and severe inflammatory myocardial damage. Replacement of adiponectin in the OB mice inhibited the development of severe myocarditis through augmentation of the AdipoR1 reactivity in the injured myocytes. Our data suggest that exogenously administered adiponectin may inhibit the progression of viral myocarditis through binding to the AdipoR1 in leptin-deficient conditions.

Acknowledgements

This study was supported in part by Grant for Promoted Research from Kanazawa Medical University (S2003-2 and S2004-2), Grant for Project Research from the High Technology Centre of Kanazawa Medical University (H2004-7) and the Science Research Promotion Fund of the Promotion and Mutual Aid Corporation for Private Schools of Japan.

Conflicts of interest

No conflicts of interest were declared in relation to this article.

• Received for publication 24 October 2004 • Accepted subject to revision 2 November 2004
• Revised accepted 4 December 2004

References

1 Makris TK, Stavroulakis GA, Krespi PG, Hatzizacharias AN, Kyriaki DK, Chronakis EV, *et al*: Elevated plasma immunoreactive leptin levels preexist in healthy offspring of patients with essential hypertension. *Am Heart J* 1999; **138:** 922 – 925.
2 Murdoch DR, Rooney E, Dargie HJ, Shapiro D, Morton JJ, McMurray JJ: Inappropriately low plasma leptin concentration in the cachexia associated with chronic heart failure. *Heart* 1999; **82:** 352 – 356.
3 Kanda T, Takahashi T, Kudo S, Takeda T, Tsugawa H, Takekoshi N: Leptin deficiency enhances myocardial necrosis and lethality in a murine model of viral myocarditis. *Life Sci* 2004; **75:** 1435 – 1447.
4 Hu E, Liang P, Spiegelman BM: *AdipoQ* is a novel adipose-specific gene dysregulated in obesity. *J Biol Chem* 1996; **271:** 10697 – 10703.
5 Yamauchi T, Kamon J, Waki H, Imai Y, Shimozawa N, Hioki K, *et al*: Globular adiponectin protected *ob/ob* mice from diabetes and ApoE-deficient mice from atherosclerosis. *J Biol Chem* 2003; **278:** 2461 – 2468.
6 Saito K, Tobe T, Minoshima S, Asakawa S, Sumiya J, Yoda M, *et al*: Organization of the gene for gelatin-binding protein (GBP28). *Gene* 1999; **229:** 67 – 73.
7 Berg AH, Combs TP, Du X, Brownlee M, Scherer PE: The adipocyte-secreted protein Acrp30 enhances hepatic insulin action. *Nat Med* 2001; **7:** 947 – 953.
8 Kanda T, Koike H, Arai M, Wilson JE, Carthy CM, Yang D, *et al*: Increased severity of viral myocarditis in mice lacking lymphocyte maturation. *Int J Cardiol* 1999; **68:** 13 – 22.
9 Kanazawa K, Kawashima S, Mikami S, Miwa Y, Hirata K, Suematsu M, *et al*: Endothelial constitutive nitric oxide synthase protein and mRNA increased in rabbit atherosclerotic aorta despite impaired endothelium-dependent

vascular relaxation. *Am J Pathol* 1996; **148**: 1949 – 1956.
10 Yamauchi T, Kamon J, Waki H, Terauchi Y, Kubota N, Hara K, *et al*: The fat-derived hormone adiponectin reverses insulin resistance associated with both lipoatrophy and obesity. *Nat Med* 2001; **7**: 941 – 946.
11 Xu A, Wang Y, Keshaw H, Xu LY, Lam KS, Cooper GJ: The fat-derived hormone adiponectin alleviates alcoholic and nonalcoholic fatty liver diseases in mice. *J Clin Invest* 2003; **112**: 91 – 100.
12 Yamauchi T, Kamon J, Ito Y, Tsuchida A, Yokomizo T, Kita S, *et al*: Cloning of adiponectin receptors that mediate antidiabetic metabolic effects. *Nature* 2003; **423**: 762 – 769.
13 Kharroubi I, Rasschaert J, Eizirik DL, Cnop M: Expression of adiponectin receptors in pancreatic beta cells. *Biochem Biophys Res Commun* 2003; **312**: 1118 – 1122.
14 Furuhashi M, Ura N, Moniwa N, Shinshi Y, Kouzu H, Nishihara M, *et al*: Possible impairment of transcardiac utilization of adiponectin in patients with type 2 diabetes. *Diabetes Care* 2004; **27**: 2217 – 2221.

Address for correspondence
Dr T Kanda
Department of General Medicine, Kanazawa Medical University, 1-1 Daigaku, Uchinada-machi, Kahoku-gun, Ishikawa, 920-0293, Japan.
E-mail: kandat@kanazawa-med.ac.jp

The Journal of International Medical Research
2005; 33: 236 – 244

Adiponectin, T-cadherin and Tumour Necrosis Factor-α in Damaged Cardiomyocytes from Autopsy Specimens

T TAKAHASHI[1], S SAEGUSA[1], H SUMINO[4], T NAKAHASHI[2], K IWAI[2], S MORIMOTO[2], T NOJIMA[3] AND T KANDA[1]

[1]Department of General Medicine, [2]Department of Geriatric Medicine and [3]Department of Clinical Pathology, Kanazawa Medical University, Ishikawa, Japan; [4]Second Department of Internal Medicine, Gunma University School of Medicine, Gunma, Japan

This study determined the presence of adiponectin, T-cadherin (an adiponectin receptor) and tumour necrosis factor-α (TNF-α) in damaged myocytes from autopsied patients with acute or old myocardial infarction (MI) or dilated cardiomyopathy (DCM), using immunohistochemical staining. The enrolled patients included eight with acute MI, six with old MI and seven with DCM. Four autopsied individuals with no cardiac lesions were also enrolled as controls. Adiponectin and TNF-α were not observed in normal myocytes from control subjects, but T-cadherin was weakly detected. Immunoreactivity for adiponectin and T-cadherin was observed at the periphery of damaged myocytes from MI and DCM patients; intracellular reactivity for TNF-α was also seen. There were no statistically significant differences in the degree of reactivity for each molecule in the myocytes between the MI and DCM patients. These results suggest that the presence of adiponectin and TNF-α in damaged myocytes may contribute to the processes of myocardial injury occurring in MI and DCM.

KEY WORDS: MYOCARDIAL INFARCTION; DILATED CARDIOMYOPATHY; ADIPONECTIN; T-CADHERIN; TUMOUR NECROSIS FACTOR-α

Introduction

Adiponectin, which is also known as adipocyte complement-related protein of 30 kDa,[1] is a hormone secreted by adipocytes that acts as an anti-diabetic and anti-atherogenic cytokine.[2] It has structural homology to the protein C1q, and is found in the serum as three distinct oligomers: a trimer, a hexamer and a high molecular weight (HMW) species.[3] Concentrations of adiponectin in blood are decreased in obesity, insulin resistance and type II diabetes.[1] Adiponectin administration has been reported to lower glucose and improve insulin resistance in mice,[4] whereas adiponectin-deficient mice develop insulin resistance and diabetes.[5] This effect of adiponectin appears to be mediated by an elevation in fatty acid oxidation through activation of adenosine monophosphate-activated protein kinase[6] and peroxisome proliferator-activated receptor-α.[2]

Cadherins comprise a large family of cell-surface proteins involved in calcium-mediated cell–cell interactions and signalling. T-cadherin was initially described in the central nervous system, but its tissue distribution is more widespread; the highest expression is found in the cardiovascular system, with low levels in muscle. In the vasculature, T-cadherin is localized to the intima and media and is expressed on endothelial and smooth muscle cells. Expression was shown to be upregulated in the neointima of mouse carotid artery after injury caused by a balloon catheter.[7] Interestingly, T-cadherin has recently been reported to be a receptor for the hexameric and HMW forms of adiponectin; this was demonstrated using a series of expression-cloning studies with panned infected cells on recombinant adiponectin linked to magnetic beads.[8]

Heart failure is generally considered to begin with myocyte damage caused by a variety of pathological conditions, including ischaemia, toxins and myocardial infection. The heart compensates by dilatation and cellular hypertrophy, and eventually decompensates, leading to heart failure. The pro-inflammatory cytokine tumour necrosis factor-α (TNF-α) has been postulated to be one of the pathogenetic factors responsible for the progression from compensated to decompensated heart failure.[9] Yokoyama and colleagues[10] demonstrated that the non-failing human heart does not express TNF-α, whereas the failing human heart expresses significant amounts of this cytokine. Moreover, TNF-α immediately inhibits contractility of isolated cardiac myocytes in a dose-dependent manner; this negative inotropic action is completely reversible upon removal of TNF-α.[10]

In the light of these different findings, we hypothesized that adiponectin, its receptor T-cadherin and TNF-α may contribute to the processes of myocardial injury. In this study, the presence or absence of adiponectin, T-cadherin and TNF-α in damaged myocytes obtained from autopsied patients with acute or old myocardial infarction (MI) or dilated cardiomyopathy (DCM) was determined using immunohistochemical staining. In addition, we analysed differences in the degree of reactivity for each molecule in the myocardium between the two groups.

Patients and methods

PATIENTS

Patients with a confirmed histopathological diagnosis of acute or old MI or a diagnosis of DCM, in whom autopsy examinations were performed in the Department of Clinical Pathology, Kanazawa Medical University Hospital, Ishikawa, Japan, between 1984 and 2004, were randomly selected for inclusion in the study. Autopsied cases from the same period with no cardiac lesions of any kind were also enrolled as normal controls. All individuals were autopsied within 6 h of death. Ethical approval from our institution was not needed, since written consent for each autopsy examination was obtained from each patient's family members.

PREPARATION OF SPECIMENS

In the controls, normal myocardial tissue and surrounding pericardial tissue were dissected from the left ventricle and ventricular septum. In individuals with MI or DCM, the myocardial lesion and surrounding pericardium were dissected in the same manner. Specimens were fixed with 10% neutral buffered formaldehyde and embedded in paraffin, and thin sections were treated with haematoxylin and eosin and Azan–Mallory staining. Based on the histopathological findings, each MI lesion was staged as follows: stage I, early MI; stage II, established myocardial necrosis; stage III, macrophage infiltration; stage IV, granulation formation; stage V, scar formation.[11]

IMMUNOHISTOCHEMICAL STAINING

Immunohistochemical staining was performed on subserial transverse ventricular myocardium and pericardium paraffin sections, using a streptavidin biotin complex method (K0675 or E0466, Dako Cytomation Co. Ltd, Kyoto, Japan). The following primary antibodies were used: rabbit polyclonal anti-human adiponectin antibody at a dilution of 1:500 (AB3784P, Chemicon International Inc., Temecula, CA, USA); rabbit polyclonal anti-human T-cadherin antibody at a dilution of 1:200 (sc-7940, Santa Cruz Biotechnology Inc., Santa Cruz, CA, USA); and goat polyclonal anti-human TNF-α antibody at a dilution of 1:500 (RC210, Dako Cytomation). The immunostaining was visualized by treating the slides with 3,3'-diaminobezidine tetrahydrochloride and counterstaining with haematoxylin. Negative control slides were treated with normal diluted rabbit or goat serum. For each slide, an area containing approximately 50 myocytes corresponding to the damaged areas found on haematoxylin and eosin and Azan–Mallory staining was blindly reviewed by a pathologist and semiquantitatively graded according to the degree of immunoreactivity for adiponectin, T-cadherin and TNF-α: 0, no staining; 1+, focal staining; 2+, diffuse weak staining; 3+, diffuse moderate staining; 4+, diffuse strong staining.[12] The slides were also compared with the respective negative control slides to exclude non-specific staining.

STATISTICAL ANALYSIS

Differences in the degree of immunoreactivity for each molecule in the damaged myocytes between the MI and the DCM group were analysed using the Mann–Whitney *U*-test. A *P*-value of < 0.05 was considered to be statistically significant.

Results

PATIENT CHARACTERISTICS

Fourteen patients with a confirmed histopathological diagnosis of acute ($n = 8$) or old ($n = 6$) MI, seven patients with DCM and four controls were included in the study. Of the 14 patients with MI, nine were male and five were female. On histopathological examination, two were stage I, three were stage II, three were stage III, four were stage IV and two were stage V. The mean age of the MI patients was 74.9 ± 14.1 years (range 36 – 88 years). Of the seven patients with DCM, five were male and two were female, and the mean age was 51.4 ± 24.5 years (range 17 – 76 years). Of the four control patients without cardiac lesions, three were male and one was female, and the mean age was 55.0 ± 21.0 years (range 33 – 78 years). The main histopathological diagnoses at autopsy for the control subjects were subarachnoid haemorrhage, acute leukaemia, liver cirrhosis and pancreatic cancer, respectively.

IMMUNOREACTIVITY IN NORMAL CARDIOMYOCYTES

Adiponectin and TNF-α were not seen in non-damaged myocytes obtained from the four control subjects, but positive reactivity for adiponectin was observed in pericardial adipocytes. T-cadherin was weakly detected in normal myocytes and the surrounding vessel walls.

IMMUNOREACTIVITY IN DAMAGED CARDIOMYOCYTES

Moderate to strong immunoreactivity for adiponectin was seen at the periphery of injured myocytes from MI and DCM patients (Fig. 1). There was also weak to moderate reactivity for T-cadherin at the periphery of damaged myocytes (Fig. 2). In addition, moderate to strong intracellular reactivity for TNF-α was seen in the myocytes (Fig. 3).

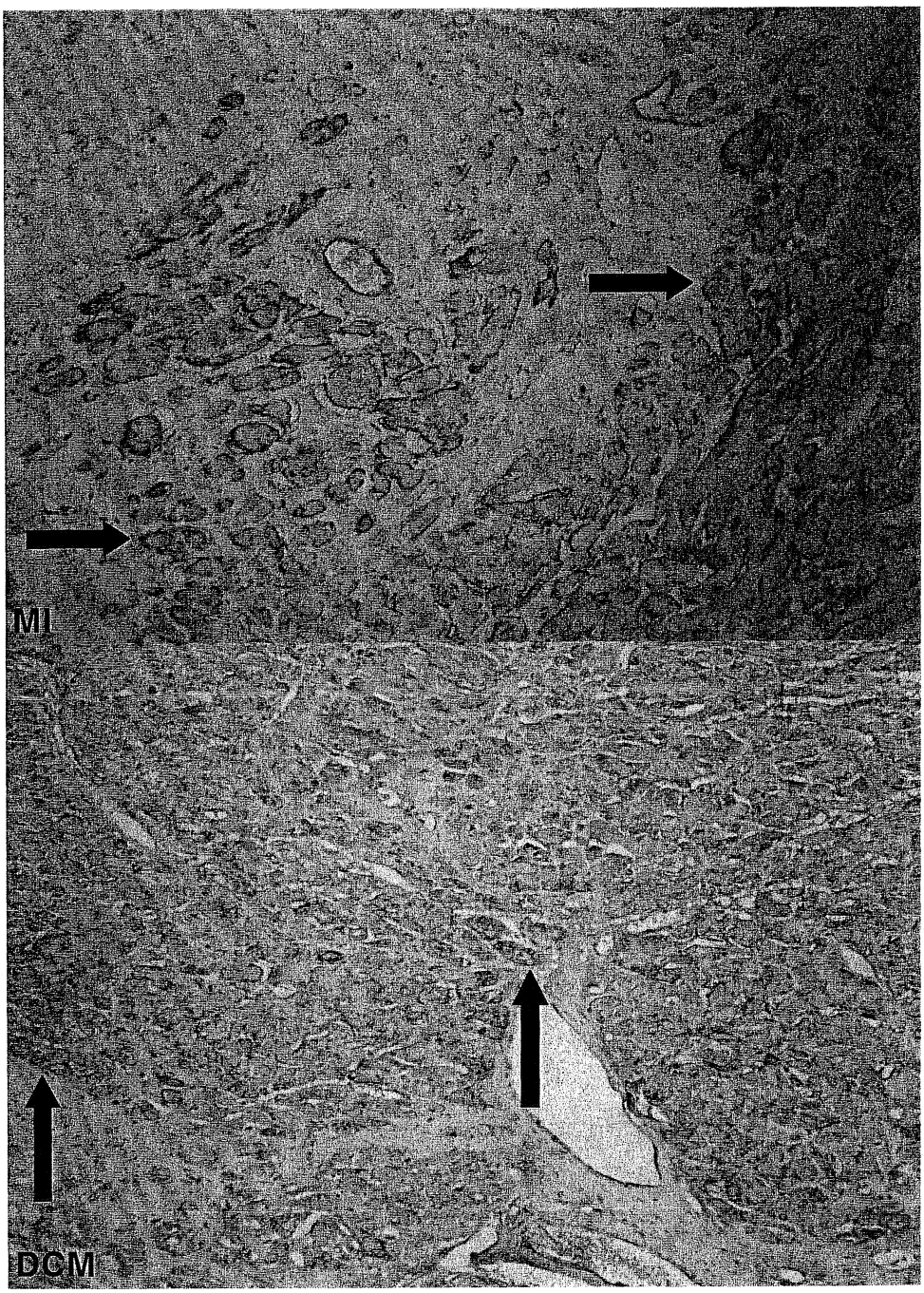

FIGURE 1: Photomicrograph showing moderate to strong adiponectin reactivity (arrows) in autopsy myocardial specimens from patients with myocardial infarction (MI) or dilated cardiomyopathy (DCM). × 75

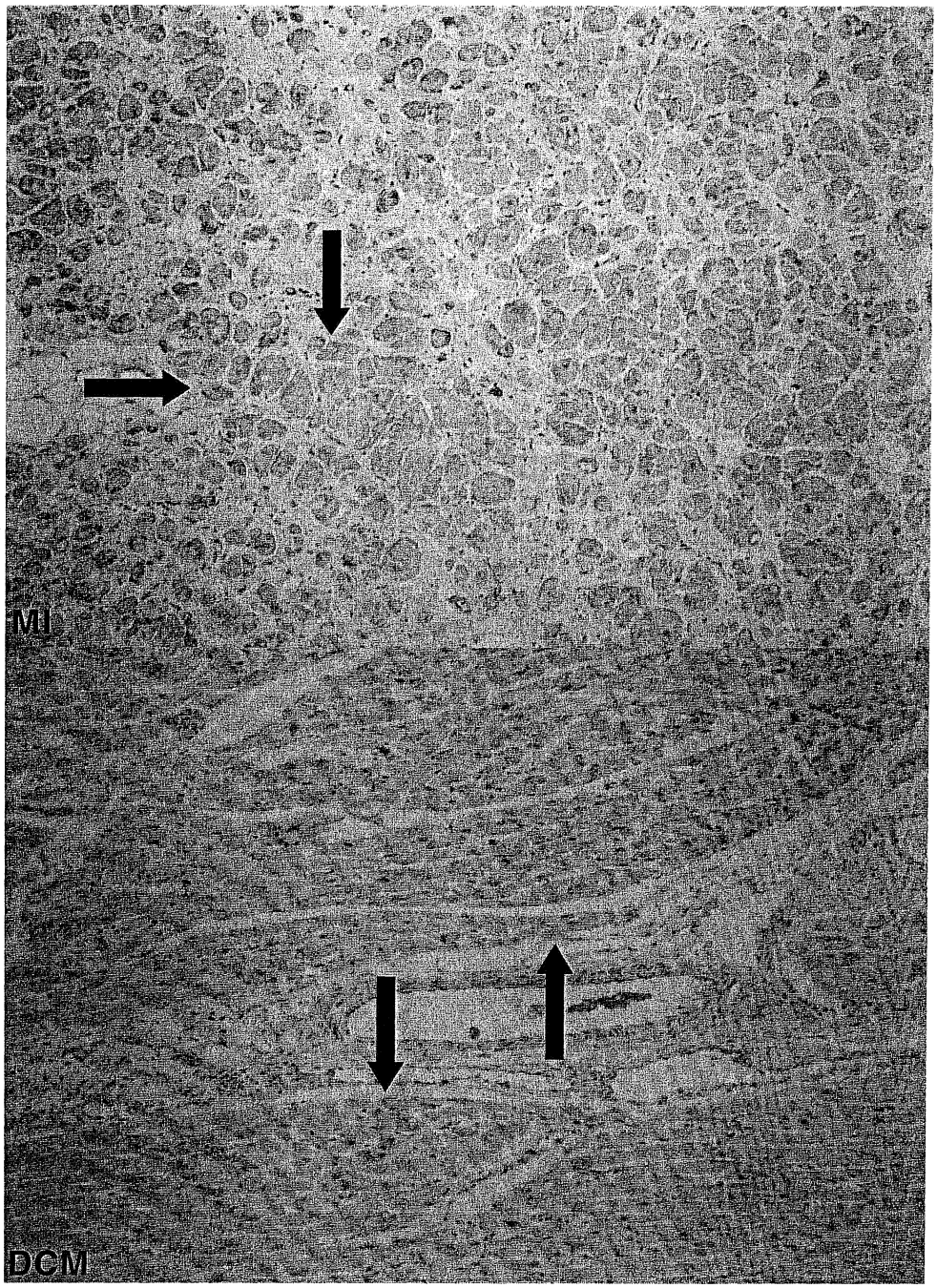

FIGURE 2: Photomicrograph showing weak to moderate T-cadherin reactivity (arrows) in autopsy myocardial specimens from patients with myocardial infarction (MI) or dilated cardiomyopathy (DCM). × 75

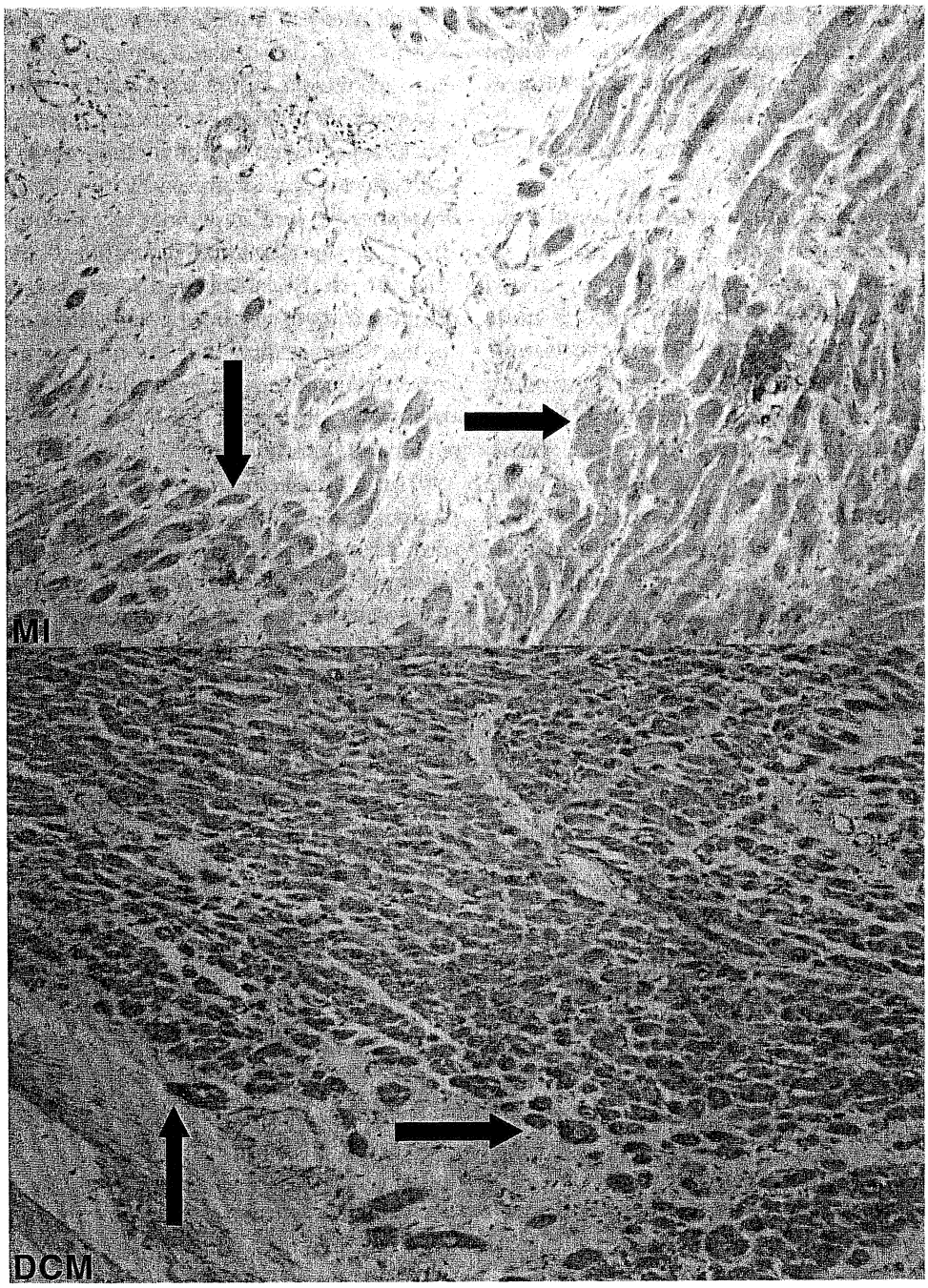

FIGURE 3: Photomicrograph showing moderate to strong intracellular tumour necrosis factor-α reactivity (arrows) in autopsy myocardial specimens from patients with myocardial infarction (MI) or dilated cardiomyopathy (DCM). × 75

The degrees of reactivity for each molecule in the damaged myocytes from individuals with MI or DCM are shown in Fig. 4. There were no statistically significant differences between the two patient groups.

Discussion

High plasma adiponectin concentrations were associated with a lower risk of MI during 6 years of follow-up in a nested case–control study among 18 225 male participants aged 40 – 75 years.[13] Possible utilization of adiponectin in the coronary artery and/or heart has been described for non-diabetic patients based on a trans-cardiac gradient of adiponectin levels from aortic root to coronary sinus.[14] It is interesting that immunostaining for adiponectin was observed at the periphery of damaged cardiomyocytes in lesions at the granulative stage obtained from autopsied hearts with infarction.[15] In another immunohistochemical analysis, the boundaries of mouse hepatocytes were positive for adiponectin after 3 – 6 h of carbon tetrachloride treatment, and the cytoplasm was intensely stained after 18 h of treatment.[16] The authors suggested that adiponectin was produced by the damaged hepatocytes, and undergoes tissue damage-induced transcriptional regulation.[16] In the present study, adiponectin was seen in damaged myocytes from both DCM and MI patients, suggesting that the adipose tissue-specific cytokine adiponectin may have important implications for the processes of myocardial damage.

The adiponectin receptors AdipoR1 and AdipoR2 are expressed ubiquitously in most organs, but in particular AdipoR1 is found in skeletal muscle and AdipoR2 in liver.[17] Complementary DNA for these receptors has been cloned, and they have been shown to be distantly related to the family of seven-

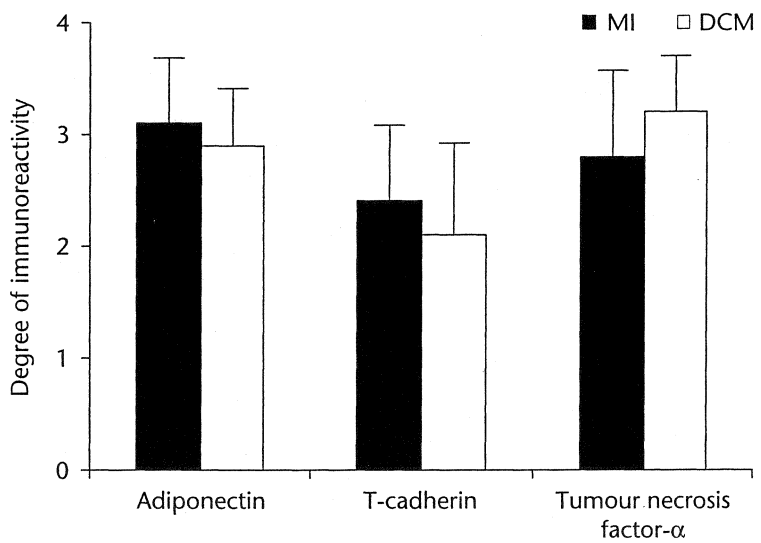

FIGURE 4: Degrees of immunoreactivity for adiponectin, T-cadherin and tumour necrosis factor-α in damaged myocytes obtained from 14 autopsied patients with myocardial infarction (MI) or dilated cardiomyopathy (DCM)

transmembrane-spanning G protein-coupled receptors.[17] However, these receptors have an inverted topology with an intracellular N terminus, unlike other seven-transmembrane spanning receptors.[8] In addition, the extracellular portion of these molecules is small, which is distinct from the members of this class of receptors that bind peptide hormone.[8] T-cadherin, a glycosylphosphatidylinositol-anchored extracellular protein, has been shown to be a novel receptor for the hexameric and HMW forms of adiponectin.[8] In the present study, both T-cadherin and adiponectin were seen in damaged myocardial cells from autopsied MI or DCM patients. This indicates that damaged cardiac cells may possess an adiponectin autocrine system, which leads to protection against the progression of myocardial injury. TNF-α expression was also observed in the damaged myocytes from subjects with DCM and MI using immunohistochemical staining as previously demonstrated.[9] We found cytoplasmic or perinuclear distribution of TNF-α expression in the damaged myocytes, and peripheral distribution of adiponectin expression in the injured cells.

In conclusion, the results of the present study suggest that the presence of adiponectin and TNF-α in damaged myocytes may contribute to the processes of myocardial injury occurring in MI and DCM.

Acknowledgements

This study was supported in part by a Grant for Promoted Research from Kanazawa Medical University (S2003-2 and S2004-2), a Grant for Project Research from the High-Technology Centre of Kanazawa Medical University (H2004-7) and the Science Research Promotion Fund of the Promotion and Mutual Aid Corporation for Private Schools of Japan.

Conflicts of interest

No conflicts of interest were declared in relation to this article.

• Received for publication 30 September 2004 • Accepted subject to revision 7 October 2004
• Revised accepted 19 November 2004

References

1 Hu E, Liang P, Spiegelman BM: AdipoQ is a novel adipose-specific gene dysregulated in obesity. *J Biol Chem* 1996; **271**: 10697 – 10703.
2 Yamauchi T, Kamon J, Waki H, Imai Y, Shimozawa N, Hioki K, *et al*: Globular adiponectin protected ob/ob mice from diabetes and ApoE-deficient mice from atherosclerosis. *J Biol Chem* 2003; **278**: 2461 – 2468.
3 Tsao TS, Tomas E, Murrey HE, Hug C, Lee DH, Ruderman NB, *et al*: Role of disulfide bonds in Acrp30/adiponectin structure and signaling specificity. Different oligomers activate different signal transduction pathways. *J Biol Chem* 2003; **278**: 50810 – 50817.
4 Berg AH, Combs TP, Du X, Brownlee M, Scherer PE: The adipocyte-secreted protein Acrp30 enhances hepatic insulin action. *Nat Med* 2001; **7**: 947 – 953.
5 Maeda N, Shimomura I, Kishida K, Nishizawa H, Matsuda M, Nagaretani H, *et al*: Diet-induced insulin resistance in mice lacking adiponectin/ACRP30. *Nat Med* 2002; **8**: 731 – 737.
6 Yamauchi T, Kamon J, Minokoshi Y, Ito Y, Waki H, Uchida S, *et al*: Adiponectin stimulates glucose utilization and fatty-acid oxidation by activating AMP-activated protein kinase. *Nat Med* 2002; **8**: 1288 – 1295.
7 Ivanov D, Philippova M, Antropova J, Gubaeva F, Iljinskaya O, Tararak E, *et al*: Expression of cell adhesion molecule T-cadherin in the human vasculature. *Histochem Cell Biol* 2001; **115**: 231 – 242.
8 Hug C, Wang J, Ahmad NS, Bogan JS, Tsao TS, Lodish HF: T-cadherin is a receptor for hexameric and high-molecular-weight forms of Acrp30/adiponectin. *Proc Natl Acad Sci USA* 2004; **101**: 10308 – 10313.
9 Torre-Amione G, Kapadia S, Lee J, Durand JB, Bies RD, Young JB, *et al*: Tumor necrosis factor-alpha and tumor necrosis factor receptors in the failing human heart. *Circulation* 1996; **93**: 704 – 711.

10 Yokoyama T, Vaca L, Rossen RD, Durante W, Hazarika P, Mann DL: Cellular basis for the negative inotropic effects of tumor necrosis factor-alpha in the adult mammalian heart. *J Clin Invest* 1993; **92:** 2303 – 2312.
11 Lodge-Patch I: The aging of cardiac infarcts, and its influence on cardiac rupture. *Br Heart J* 1951; **13:** 37 – 42.
12 Wong SC, Fukuchi M, Melnyk P, Rodger I, Giaid A: Induction of cyclooxygenase-2 and activation of nuclear factor-κB in myocardium of patients with congestive heart failure. *Circulation* 1998; **98:** 100 – 103.
13 Pischon T, Girman CJ, Hotamisligil GS, Rifai N, Hu FB, Rimm EB: Plasma adiponectin levels and risk of myocardial infarction in men. *JAMA* 2004; **291:** 1730 – 1737.
14 Furuhashi M, Ura N, Moniwa N, Shinshi Y, Kouzu H, Nishihara M, *et al*: Possible impairment of transcardiac utilization of adiponectin in patients with type 2 diabetes. *Diabetes Care* 2004; **27:** 2217 – 2221.
15 Ishikawa Y, Akasaka Y, Ishii T, Yoda-Murakami M, Choi-Miura NH, Tomita M, *et al*: Changes in the distribution pattern of gelatin-binding protein of 28 kDa (adiponectin) in myocardial remodelling after ischaemic injury. *Histopathology* 2003; **42:** 43 – 52.
16 Yoda-Murakami M, Taniguchi M, Takahashi K, Kawamata S, Saito K, Choi-Miura NH, *et al:* Changes in expression of GBP28/adiponectin in carbon tetrachloride-administrated mouse liver. *Biochem Biophys Res Commun* 2001; **285:** 372 – 377.
17 Yamauchi T, Kamon J, Ito Y, Tsuchida A, Yokomizo T, Kita S, *et al*: Cloning of adiponectin receptors that mediate antidiabetic metabolic effects. *Nature* 2003; **423:** 762 – 769.

Address for correspondence
Dr T Kanda
Department of General Medicine, Kanazawa Medical University, 1-1 Daigaku,
Uchinada-machi, Kahoku-gun, Ishikawa, 920-0293, Japan.
E-mail: kandat@kanazawa-med.ac.jp

The Journal of International Medical Research
2005; 33: 61 – 67

Clinical Features Associated with Circulating Concentration of Soluble Leptin Receptor in Patients with Diabetes

N KOTAJIMA[1], T TAKAHASHI[3], H ITO[2], H SUMINO[2], Y FUKUMURA[1], M KURABAYASHI[2], M MURAKAMI[1], AND T KANDA[3]

[1]Department of Laboratory Medicine and Medical Laboratory Centre, and [2]Second Department of Internal Medicine, Gunma University School of Medicine, Gunma, Japan; [3]Department of General Medicine, Kanazawa Medical University, Ishikawa, Japan

We aimed to determine if there were any clinical features that were significantly associated with the circulating concentration of soluble leptin receptor (OB-Re) in 67 Japanese subjects with diabetes mellitus. The characteristics evaluated included age, height, body weight, body mass index (BMI), systolic and diastolic blood pressure, duration of diabetes, haemoglobin A_{1C} and blood lipid concentrations, urinary albumin excretion rate, circulating concentrations of leptin, tumour necrosis factor-α (TNF-α), TNF-α receptor 1 and genotypes of the angiotensin-converting enzyme (ACE) gene. We found statistically significant negative correlations between circulating OB-Re concentration and body weight, BMI, diastolic blood pressure, concentrations of leptin and TNF-α receptor 1. Serum OB-Re concentration was not associated with any of the other clinical characteristics that were measured, or with the different ACE genotypes. Our results suggest that OB-Re might have an important influence on the biological activity of leptin in diabetic subjects.

KEY WORDS: SOLUBLE LEPTIN RECEPTOR; LEPTIN; BODY MASS INDEX; DIASTOLIC BLOOD PRESSURE; SOLUBLE TUMOUR NECROSIS FACTOR-α RECEPTOR 1

Introduction

Leptin is an adipocyte-specific hormone of 167 amino acids that derives its name from the Greek 'leptos', meaning 'thinness'.[1] In *ob/ob* mice, the gene encoding leptin is mutated, resulting in morbid obesity and related conditions, including hyperphagia, hypothermia, diabetes and infertility. Leptin is produced and secreted in response to eating, and acts on the central nervous system to inhibit feeding in animals. This adipocytokine has been shown to play a role in regulating body fat, energy expenditure and metabolism of glucose and lipids.[2] Circulating leptin concentrations correlate well with body weight, body mass index (BMI) and body adiposity,[3] especially in obese individuals and in women.[4]

The leptin receptor (OB-R) is a member of the cytokine receptor family.[5] OB-R is encoded by the diabetes (*db*) gene, mutation of which also results in morbid obesity and other abnormalities similar to those observed in *ob/ob* mice. This receptor is alternatively spliced into at least five

transcripts from a single gene. These transcripts encode proteins that have been designated the long (OB-Rb), short (OB-Ra, c and d), and soluble (OB-Re) forms of the leptin receptor. OB-Rb plays an essential role in mediating leptin's weight-reducing and other biological effects.[6] OB-Re is capable of binding leptin at a ratio of 1:1,[7] and it has been postulated that OB-Re forms approximately 10% of the leptin-binding proteins found in human serum samples.[8] Observational and interventional studies in humans have recently shown that circulating OB-Re concentration is regulated by gender, adiposity, sex steroids and leptin,[9] but clinical reports regarding OB-Re in patients with diabetes are rare.

We aimed to determine if there was any significant association between the concentration of OB-Re and age, height, body weight, BMI, systolic and diastolic blood pressure, duration of disorder, haemoglobin A_{1C} and blood lipid concentrations, urinary albumin excretion rate, and circulating concentrations of leptin, tumour necrosis factor-α (TNF-α), and TNF-α receptor 1 in Japanese subjects with diabetes mellitus. We also aimed to determine if there was any correlation between OB-Re concentration and an insertion/deletion (I/D) polymorphism in intron 16 of the angiotensin-converting enzyme (ACE) gene (17q23).

Patients and methods

PATIENTS

Subjects with diabetes mellitus who visited Gunma University Hospital and received conventional treatment in 2000 were voluntarily enrolled into this study. The treatment that they received aimed to maintain haemoglobin A_{1C} levels < 7.0% and blood pressure < 140/90 mmHg. Subjects were requested to maintain appropriate levels of exercise and to adhere to the recommended diet. They were instructed not to take any over-the-counter medications during the study.

The study protocol was approved by the Institutional Committee of Gunma University Hospital, and informed written consent was obtained from all subjects.

CLINICAL AND LABORATORY ASSESSMENTS

Age, height, body weight, BMI, duration of diabetes, and systolic and diastolic blood pressure were recorded for each subject.

Blood samples were taken from each person's right cubital vein when they attended the clinic for their other assessments (detailed above). Serum was separated by centrifugation and stored at –80 °C until analysed.

Haemoglobin A_{1C} concentration and urine concentration of albumin were measured using high-performance liquid chromatography and radioimmunoassay, respectively, as routine analyses in the clinical biochemistry department of the University Hospital. The urinary albumin excretion rate was calculated using timed overnight urine samples. Serum concentrations of triglyceride (TG), total cholesterol, high-density lipoprotein (HDL) cholesterol, and remnant-like lipoprotein (RLP) cholesterol were measured using standard laboratory methods.

Serum concentrations of leptin (ng/ml) were measured by a radioimmunoenzymatic assay using a commercially available kit (LINCO Research, St Louis, MO, USA). The intra- and inter-assay variations were 4.98% and 4.5%, respectively, and the limit of sensitivity was 0.5 ng/ml. Serum OB-Re concentration (U/ml) was measured using a commercially available enzyme-linked immunosorbent assay (ELISA; BioVendor

Laboratory Medicine, Brno, Czech Republic), with a sensitivity of 0.4 μl (or 0.8 ng/ml) and an intra-assay coefficient of variation (CV) of 3.9 – 5.6% for 16.9 – 69.5 U/ml. The measurement of TNF-α concentration (pg/ml) was performed with an ELISA (Pharmingen, San Diego, CA, USA). The intra- and inter-assay CVs were < 5.8% and < 13.8%, respectively, and the limit of sensitivity was 4 pg/ml. An immunoenzymometric assay was used to determine the concentration of soluble TNF-α receptor 1 (pg/ml) in sera (BioSource, Fleunes, Belgium). The minimum detectable concentration was estimated to be 50 pg/ml, and the intra- and inter-assay CVs were < 6.5% and < 8.9%, respectively.

GENE ANALYSIS

Genomic DNA was extracted by standard phenol-chloroform methods from peripheral blood collected on ethylene-diamine-tetra-acetic acid. Polymerase chain reaction (PCR) was performed to detect the two ACE I/D alleles. The polymorphic region in intron 16 of the ACE gene was amplified using primers, and PCR-cycling conditions were as described previously.[10] Two PCR products, a 190 bp fragment (D allele) and a 490 bp fragment (I allele), were separated by agarose gel electrophoresis. Each sample that was found to have the DD genotype was subjected to a second PCR amplification with an insertion-specific primer.

STATISTICAL ANALYSES

Correlation coefficients between serum OB-Re concentration and the clinical characteristics of age, height, body weight, BMI, systolic and diastolic blood pressure, duration of diabetes, haemoglobin A_{1C} and blood lipid concentrations, urinary albumin excretion rate, and circulating concentrations of leptin, TNF-α, and soluble TNF-α receptor 1 were analysed by linear regression analysis. The differences in the mean OB-Re concentration among patients with various ACE genotypes were determined using one-way analysis of variance.

A *P*-value of < 0.05 was considered to be statistically significant.

Results

Sixty-seven subjects enrolled in this study; two subjects with type 1 diabetes mellitus and 65 subjects with type 2 diabetes mellitus. The study participants had a mean age (± SD) of 59 ± 19 years (range: 29 – 82 years), and the male to female ratio was 0.86:1. Around half of the diabetic subjects (33; 49.3%) had the II genotype of the ACE gene compared with 11 subjects (16.4%) with the DD genotype and 23 subjects (34.3%) with the ID genotype.

Table 1 shows the results of the coefficient of correlation analyses that were carried out between serum OB-Re concentration and the clinical characteristics of age, height, body weight, BMI, systolic and diastolic blood pressure, duration of diabetes, haemoglobin A_{1C} and blood lipid concentrations, urinary albumin excretion rate, and circulating concentrations of leptin, TNF-α and soluble TNF-α receptor 1. We observed statistically significant negative correlations between circulating OB-Re concentration and body weight, BMI, diastolic blood pressure, concentration of leptin, and soluble TNF-α receptor 1 concentration. There was no association between OB-Re concentration and any of the other characteristics evaluated in this study.

No significant difference was observed in mean OB-Re concentration among the groups of subjects with different ACE genotypes (Fig. 1).

Discussion

Several studies have recently described the relationship between OB-Re and body weight. Weight loss has been shown to

TABLE 1:
Results of the coefficient of correlation analyses performed between serum soluble leptin receptor (OB-Re) concentration and the clinical characteristics of the study participants (n = 67)

Clinical characteristics	Coefficient value	*P*-value
Age (y)	–0.133	NS
Height (cm)	–0.110	NS
Body weight (kg)	–0.256	0.036
Body mass index (kg/m^2)	–0.285	0.019
Duration of diabetes (y)	0.006	NS
Systolic blood pressure (mmHg)	–0.239	NS
Diastolic blood pressure (mmHg)	–0.272	0.026
Haemoglobin A_{1C} (%)	0.076	NS
Urinary albumin excretion rate (μg/min)	0.002	NS
Triglyceride (mg/dl)	–0.211	NS
Total cholesterol (mg/dl)	–0.147	NS
HDL cholesterol (mg/dl)	0.033	NS
RLP cholesterol (mg/dl)	–0.161	NS
Leptin (ng/ml)	–0.263	0.018
Tumour necrosis factor-α (pg/ml)	0.039	NS
Soluble tumour necrosis factor-α receptor 1 (pg/ml)	–0.241	0.048

HDL, high density lipoprotein; RLP, remnant-like lipoprotein.

increase OB-Re concentration,[11] and obesity was reported to be associated with decreasing concentration of circulating OB-Re in humans.[12] Consistent with these findings, we found a significant negative correlation between serum OB-Re concentrations and body weight and BMI in subjects with diabetes.

Leptin concentration is associated with several indicators of the metabolic syndrome, such as plasma triglyceride and apolipoprotein B concentrations, and with systolic blood pressure, independent of BMI and glucose disposal rate.[13] Plasma leptin concentration was also demonstrated to be a novel, independent risk factor for cardiovascular disease in a large prospective study.[14] There was no correlation between circulating OB-Re concentration and blood lipids (TG, total cholesterol, HDL cholesterol, RLP cholesterol) in our study, but OB-Re concentration was found to be negatively associated with diastolic blood pressure. Further study is needed to evaluate whether OB-Re concentrations correlate with a risk of cardiovascular disease in a large number of individuals with diabetes.

Monteleone *et al.*[15] reported that significant inverse correlations were demonstrated between plasma concentrations of leptin and

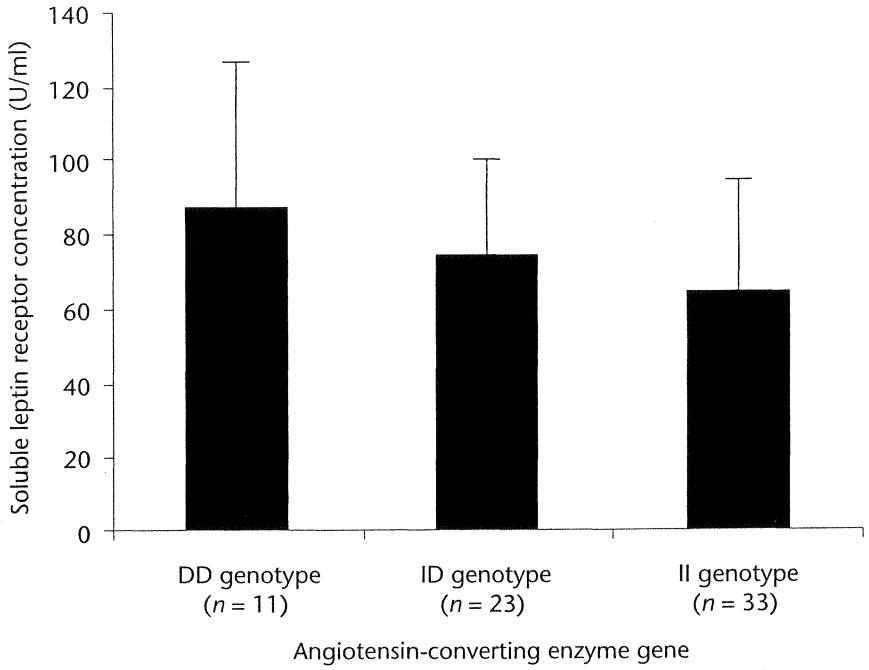

FIGURE 1: Mean soluble leptin receptor concentration and angiotensin-converting enzyme genotype found in the 67 subjects with diabetes mellitus who enrolled in this study

those of OB-Re in patients with conditions within the eating disorder spectrum (anorexia nervosa, bulimia nervosa and binge-eating disorder). In our study, OB-Re concentration was also negatively correlated with leptin concentration in subjects with diabetes. Plasma soluble TNF-α receptor 1 concentration was shown to be correlated with leptin concentration and BMI in normal weight and overweight individuals.[16,17] Interestingly, for the first time, we demonstrated that an inverse correlation exists between the circulating concentration of soluble TNF-α receptor 1 and OB-Re in subjects with diabetes.

In summary, we aimed to determine if any clinical characteristics were associated with serum OB-Re concentration in 67 Japanese subjects with diabetes. We observed significant inverse correlations between circulating OB-Re concentration and body weight, BMI, diastolic blood pressure, concentrations of leptin and TNF-α receptor 1. There was no association between OB-Re concentration and any of the other characteristics measured: age, height, systolic blood pressure, duration of disease, haemoglobin A_{1C} and blood lipid concentrations, urinary albumin excretion rate and the circulating concentration of TNF-α. No association was found with the ACE genotypes either, despite a report that the D allele polymorphism is a potent risk factor for developing microalbuminuria in patients with type 2 diabetes.[18] Our results suggest that OB-Re might have an influence on the biological activity of leptin in subjects with diabetes.

Acknowledgements

This study was supported in part by a Grant for Promoted Research from Kanazawa Medical University (S2003-2 and S2004-2), a Grant for Project Research from the High-Technology Center of Kanazawa Medical University (H2004-7), and by funding from the Science Research Promotion Fund of the Promotion and Mutual Aid Corporation for Private Schools of Japan.

Conflicts of interest

No conflicts of interest were disclosed in relation to this article.

• Received for publication 6 June 2004 • Accepted subject to revision 19 June 2004
• Revised accepted 8 September 2004

References

1 Zhang Y, Proenca R, Maffei M, Barone M, Leopold L, Friedman JM: Positional cloning of the mouse obese gene and its human homologue. *Nature* 1994; **372:** 425 – 432.
2 Maffei M, Halaas J, Ravussin E, Pratley RE, Lee GH, Zhang Y, *et al*: Leptin levels in human and rodent: measurement of plasma leptin and *ob* RNA in obese and weight-reduced subjects. *Nat Med* 1995; **1:** 1155 – 1161.
3 Dua A, Hennes MI, Hoffmann RG, Maas DL, Krakower GR, Sonnenberg GE, *et al*: Leptin: a significant indicator of total body fat but not of visceral fat and insulin insensitivity in African-American women. *Diabetes* 1996; **45:** 1635 – 1637.
4 Christensen JQ, Svendsen OL, Hassager C, Christiansen C: Leptin in overweight post-menopausal women: no relationship with metabolic syndrome X or effect of exercise in addition to diet. *Int J Obes Relat Metab Disord* 1998; **22:** 195 – 199.
5 Tartaglia LA, Dembski M, Weng X, Deng N, Culpepper J, Devos R, *et al*: Identification and expression cloning of a leptin receptor, OB-R. *Cell* 1995; **83:** 1263 – 1271.
6 Lee GH, Proenca R, Montez, JM, Carroll KM, Darvishzadeh JG, Lee JI, *et al*: Abnormal splicing of the leptin receptor in diabetic mice. *Nature* 1996; **379:** 632 – 635.
7 Devos R, Guisez Y, Van der Heyden J, White DW, Kalai M, Fountoulakis M, *et al*: Ligand-independent dimerization of the extracellular domain of the leptin receptor, and determination of the stoichiometry of leptin binding. *J Biol Chem* 1997; **272:** 18304 – 18310.
8 Sinha MK, Opentanova I, Ohannesian JP, Kolaczynski JW, Heiman ML, Hale J, *et al*: Evidence of free and bound leptin in human circulation. Studies in lean and obese subjects and during short-term fasting. *J Clin Invest* 1996; **98:** 1277 – 1282.
9 Chan JL, Bluher S, Yiannakouris N, Suchard MA, Kratzsch J, Mantzoros CS: Regulation of circulating soluble leptin receptor levels by gender, adiposity, sex steroids, and leptin: observational and interventional studies in humans. *Diabetes* 2002; **51:** 2105 – 2112.
10 Cambien F, Poirier O, Lecerf L, Evans A, Cambou JP, Arveilier D, *et al*: Deletion polymorphism in the gene for angiotensin-converting enzyme is a potent risk factor for myocardial infarction. *Nature* 1992; **359:** 641 – 644.
11 Laimer M, Ebenbichler CF, Kaser S, Sandhofer A, Weiss H, Nehoda H, *et al*: Weight loss increases soluble leptin receptor levels and the soluble receptor bound fraction of leptin. *Obes Res* 2002; **10:** 597 – 601.
12 Ogier V, Ziegler O, Mejean L, Nicolas JP, Stricker-Krongrad A: Obesity is associated with decreasing levels of the circulating soluble leptin receptor in humans. *Int J Obes Relat Metab Disord* 2002; **26:** 496 – 503.
13 Haffner SM, Mykkanen L, Rainwater DL, Karhapaa P, Laakso M: Is leptin concentration associated with the insulin resistance syndrome in nondiabetic men? *Obes Res* 1999; **7:** 164 – 169.
14 Wallace AM, McMahon AD, Packard CJ, Kelly A, Shepherd J, Gaw A, *et al*: Plasma leptin and the risk of cardiovascular disease in the west of Scotland coronary prevention study (WOSCOPS). *Circulation* 2001; **104:** 3052 – 3056.
15 Monteleone P, Fabrazzo M, Tortorella A, Fuschino A, Maj M: Opposite modifications in circulating leptin and soluble leptin receptor across the eating disorder spectrum. *Mol Psychiatry* 2002; **7:** 641 – 646.
16 Chu NF, Spiegelman D, Rifai N, Hotamisligil GS, Rimm EB: Glycemic status and soluble tumor necrosis factor receptor levels in relation to plasma leptin concentrations among normal weight and overweight US men. *Int J Obes Relat Metab Disord* 2000; **24:** 1085 – 1092.
17 Bullo M, Garcia-Lorda P, Salas-Salvado J: Plasma soluble tumor necrosis factor alpha receptors and leptin levels in normal-weight and obese women: effect of adiposity and diabetes. *Eur J Endocrinol* 2002; **146:** 325 – 331.

18 Okuno S, Utsugi T, Ohno T, Ohyama Y, Uchiyama T, Tomono S, *et al*: Angiotensin-converting enzyme gene polymorphism as a potent risk factor for developing microalbuminuria in Japanese patients with type 2 diabetes mellitus: a 9-year follow-up study. *J Int Med Res* 2003; **31**: 290 – 298.

Address for correspondence
Dr T Takahashi
Department of General Medicine, Kanazawa Medical University,
1-1 Daigaku, Uchinada-machi, Kahoku-gun, Ishikawa, 920-0293, Japan.
E-mail: taka2si@kanazawa-med.ac.jp

The Journal of International Medical Research
2004; 32: 665 – 670

Detection of *Toxoplasma gondii* by Polymerase Chain Reaction in Cerebrospinal Fluid from Human Immunodeficiency Virus-1-infected Japanese Patients with Focal Neurological Signs

M GOTO[1], T TAKAHASHI[2], T KANDA[2] AND A IWAMOTO[1]

[1]Division of Infectious Diseases, Advanced Clinical Research Centre, Institute of Medical Science, University of Tokyo, Tokyo; [2]Department of General Medicine, Kanazawa Medical University, Ishikawa, Japan

We aimed to determine the effectiveness of using the polymerase chain reaction (PCR) to detect *Toxoplasma gondii* in cerebrospinal fluid (CSF) specimens from Japanese patients infected with human immunodeficiency virus (HIV)-1. Twenty-six HIV-positive individuals presenting with focal neurological signs and a possible diagnosis of *T. gondii* encephalitis (TE) were enrolled in the study between April 1997 and March 2003. Eight patients were diagnosed as having TE using the accepted diagnostic criteria; PCR amplified the *T. gondii B1* gene in CSF samples from five of these eight patients. CSF samples from the 18 patients without TE were negative for *T. gondii* DNA. The sensitivity, specificity and positive and negative predictive values for detecting *T. gondii* in CSF using PCR were 62.5%, 100%, 100% and 85.7%, respectively. These results suggest that PCR might be a clinically useful technique for detecting *T. gondii* DNA in patients infected with HIV showing focal neurological signs. Improvements in sensitivity are needed, however.

KEY WORDS: *TOXOPLASMA GONDII*; *B1* GENE; POLYMERASE CHAIN REACTION; CEREBROSPINAL FLUID; HUMAN IMMUNODEFICIENCY VIRUS; JAPANESE

Introduction

Toxoplasma gondii encephalitis (TE) has been reported in 3 – 50% of patients with acquired immunodeficiency syndrome (AIDS); it is the most common central nervous system complication of AIDS in Europe.[1] Histopathologically, brain abscesses characterize TE and the neurological features are associated with the location and extent of the brain lesions and perilesional oedema.

Classical techniques for diagnosing TE include demonstrating the presence of *T. gondii*-specific antibody and isolating *T. gondii* by tissue culture or mouse inoculation. These methods are inadequate when applied to patients with AIDS and suspected TE, however. When used to assess patients with AIDS the test for demonstrating the presence of *T. gondii*-specific intrathecal

antibody has a sensitivity and specificity of 63% and 68%, respectively;[2] *T. gondii* could be isolated from cerebrospinal fluid (CSF) or blood in fewer than 40% of cases.[3]

Clinical diagnosis of TE is based on the results of a computed tomography (CT) scan or magnetic resonance imaging (MRI), clinical signs, seropositivity for *T. gondii* and response to anti-toxoplasma therapy with pyrimethamine and sulphadiazine or pyrimethamine and clindamycin.[4] Patients who fail to respond to treatment are candidates for a brain biopsy as TE can be diagnosed by examining haematoxylin and eosin and Wright–Giemsa-stained tissue. Sensitivity may be enhanced by immunocytochemistry but, in a number of cases, even histopathological examination fails to detect evidence of *T. gondii* infection.[1] Brain biopsy is an invasive process and in patients with AIDS it may be associated with a risk of developing further complications.[5]

We aimed to determine the effectiveness of using the polymerase chain reaction (PCR) to detect *T. gondii* in Japanese patients infected with human immunodeficiency virus (HIV)-1 and presenting with focal neurological signs. We used CSF samples and aimed to detect the presence of the *T. gondii B1* gene, a 35-fold-repetitive gene.[6]

Patients and methods

PATIENTS

Japanese patients infected with HIV, presenting with focal neurological signs and requiring confirmation or elimination of TE were enrolled in the study. All patients presented to the hospital associated with the Institute of Medical Science, University of Tokyo between April 1997 and March 2003. Patients were excluded from the study if they had received treatment, other than with anti-toxoplasma agents, for the neurological deficits (e.g. radiotherapy) before the CSF samples were obtained.

Informed consent was obtained from each individual. Ethical approval was not sought as an ethics committee had not been established when the study started.

DIAGNOSIS AND SAMPLE COLLECTION

Patients were examined and routine tests to aid diagnosis performed. The diagnosis of TE was based on the results of a CT scan or MRI, clinical signs, seropositivity for *T. gondii* and response to anti-toxoplasma therapy with pyrimethamine and sulphadiazine or pyrimethamine and clindamycin for 2 weeks.[4]

Seropositivity was determined using an enzyme-linked immunosorbent assay (ELISA; Platelia II Toxo IgG test, Sanofi Diagnostics Pasteur, Marne La Cornette, France). Peripheral blood was collected on the first visit to the hospital and the serum samples immediately stored at –80 °C until use. A $CD4^+$ T lymphocyte count was also undertaken using these blood samples (taken before the start of anti-toxoplasma therapy) and standard procedures.[7]

Cerebrospinal fluid specimens were collected before the start of anti-toxoplasma treatment with pyrimethamine and sulphadiazine, or pyrimethamine and clindamycin. A lumbar puncture was performed and 5 ml of CSF collected in a sterilized tube as previously described.[3] All samples were immediately stored at 4 °C for rapid processing.

DNA EXTRACTION FROM CEREBROSPINAL FLUID

Cerebrospinal fluid samples were frozen and thawed three times before DNA extraction to disrupt the rigid cell walls of the protozoan. DNA was extracted from 100 µl of CSF using a commercially available extraction kit (SMI test EX-R&D [Sumitomo Metal Industries Ltd, Tokyo, Japan] or QIAamp DNA Mini Kit [Qiagen Inc., Valencia, CA, USA]) according

to the manufacturer's instructions. The DNA was re-suspended in 10 µl of distilled water.

POLYMERASE CHAIN REACTION

We used two pairs of oligonucleotide primers specific for the *T. gondii B1* gene and nested PCR to generate a 194 base pair PCR product as previously described:[8]

- Single PCR: forward, 5'-CATTTTCGCAG TACACCAGG-3'; reverse, 5'-GGAGTGAA GTCATCCGCAGT-3'
- Nested PCR: forward, 5'-GGAACTGCAT CCGTTCATGAG-3'; reverse, 5'-TCTTTAA AGCGTTCGTGGTC-3'.

The first round PCR mixture contained 20 µl template DNA, 5 µl PCR buffer (2 mM $MgCl_2$), 1 µM each PCR primer, 0.25 mM of each deoxynucleoside triphosphate, and 20 IU/ml of *Ex-Taq* DNA polymerase (Takara Shuzo Co., Shiga, Japan) in a total volume of 50 µl. After an initial denaturation step (94 °C for 1 min), the samples were amplified by repeating the following cycle 40 times: denaturation at 94 °C for 30 s, annealing at 42 °C for 30 s, and extension at 72 °C for 1 min. The reaction mixture was incubated at 72 °C for 2 min for the final extension.

Nested PCR was performed on 2 µl of first round product using the same reagent concentrations and PCR parameters.

To avoid contaminating the PCR mixtures, mixture preparation and template DNA addition were carried out in separate rooms. Tachyzoites of the *T. gondii* RH-strain (donated by Professor S Kojima, Department of Parasitology, Institute of Medical Science, University of Tokyo) were used as a positive control. DNA was extracted from 4×10^6 tachyzoites, which were propagated in the peritoneum of a ddY mouse. The DNA was suspended in 100 µl of distilled water, and 10-fold dilutions of the positive control were used. To avoid false-positive results, all procedures were carried out carefully and a DNA-free negative control consisting of distilled water was tested simultaneously. Each specimen was examined in duplicate.

ELECTROPHORESIS

One tenth of the nested PCR product was loaded onto a 1.5% agarose gel containing ethidium bromide (0.5 µg/ml) for electrophoresis, and the gel visualized under ultraviolet illumination.

DATA ANALYSIS

The sensitivity and specificity of the technique were evaluated using binomial distribution confidence intervals. The predictive values of a positive and negative PCR test were assessed using *a priori* prevalence levels for the patients.

Results

DIAGNOSIS

Of the 26 patients enrolled in the study, eight were diagnosed as having TE based on the accepted criteria.[4] All patients with TE were male and seropositive for *T. gondii* (result of ≥ 5 IU/ml using the ELISA test). The mean count of $CD4^+$ T lymphocytes was 36.3/mm^3 (range, 2 – 133/mm^3). The remaining 18 patients were diagnosed with primary central nervous system lymphoma, progressive multifocal leucoencephalopathy, cytomegalovirus encephalitis or AIDS dementia.

PCR ANALYSIS

The *T. gondii B1* gene was amplified by PCR from the CSF of five out of the eight patients diagnosed with TE (Table 1; Fig. 1). CSF specimens from the 18 patients without TE were negative for *T. gondii* DNA (Table 1).

We observed that the sensitivity, specificity and positive and negative predictive values for detecting *T. gondii* DNA in CSF using PCR were 62.5%, 100%, 100% and 85.7%, respectively.

TABLE 1:
Detection of the *Toxoplasma gondii B1* gene by polymerase chain reaction (PCR) in cerebrospinal fluid samples from HIV-positive Japanese patients with or without a diagnosis of *T. gondii* encephalitis (TE)

PCR result	Number of patients with TE	Number of patients without TE
Positive	5	0
Negative	3	18

Discussion

The PCR method can detect pathogen DNA when approximately five to 10 parasites are present in the CSF or blood sample.[3] The high biological sensitivity is possible when primers flanking repetitive genes of *T. gondii*, i.e. the *B1* gene[6] or ribosomal DNA repetitive sequences are used.[3] Dupon *et al.*[3] reported a positive PCR result for CSF and/or blood samples in 10 out of 25 HIV-infected subjects with TE, while for one patient the presence of *T. gondii* was shown by culture of the CSF sample. Unlike tissue culture, PCR techniques are able to demonstrate TE in HIV-positive individuals.

Several studies have reported the potential of PCR on CSF for detecting the *T. gondii B1* gene in AIDS-associated TE patients (Table 2).[4,8 - 12] The sensitivity of detecting *T. gondii* DNA by this method varies between 44% and 100%, but was reported to be between 50% and 70% in studies where more than 20 subjects were enrolled (Table 2). The specificity was always high, at between 94% and 100% (Table 2). In a previous study the positive and negative predictive values of the PCR technique were estimated to be 100% and 87%,[8] which were similar to our results (100% and 85.7%, respectively).

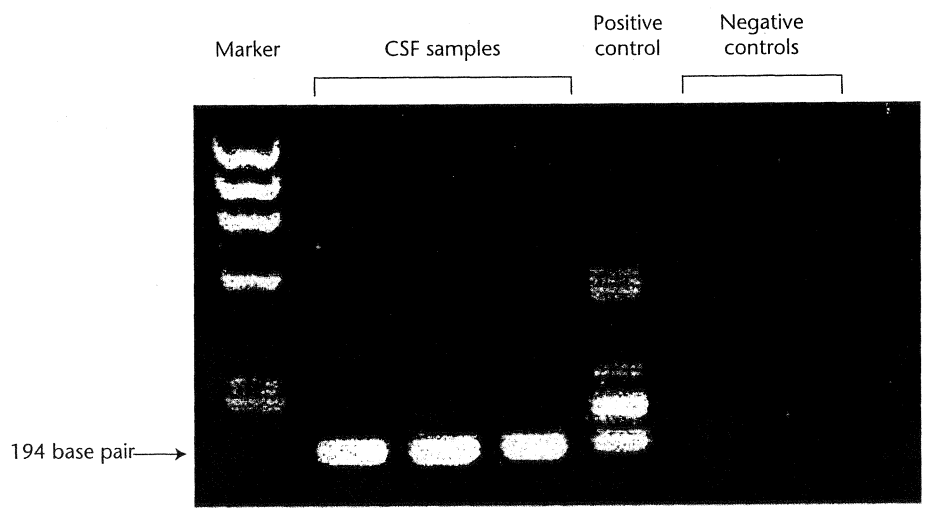

FIGURE 1: Products from the nested polymerase chain reaction (PCR) of cerebrospinal fluid samples from Japanese patients who were HIV-positive and had *Toxoplasma gondii* encephalitis. The PCR reaction used primers specific for the *T. gondii B1* gene and amplification products were electrophoresed through a 1.5% agarose gel containing ethidium bromide (0.5 µg/ml)

TABLE 2:
Results of published studies using the polymerase chain reaction (PCR) to detect *Toxoplasma gondii B1* gene DNA in cerebrospinal fluid samples from HIV-positive subjects

Publication year and reference number	Population	Number of patients enrolled	Diagnostic standard	PCR method	PCR sensitivity (%)	PCR specificity (%)
1992[9]	Danish	13	Clinical Dx	Nested	100	100
1992[4]	American	14	Clinical Dx	Single	44.4	100
1993[8]	Dutch	33	Clinical Dx	Single	65	100
1993[10]	Belgian	33	Clinical Dx	Nested	67	96
1994[11]	Italian	82	Histology or clinical Dx	Nested	51	100
2002[12]	Italian	46	Clinical Dx	Nested	59.3	94.7
This study	Japanese	26	Clinical Dx	Nested	62.5	100

Dx, diagnosis.

To improve the sensitivity of PCR methods the techniques used during sample preparation and nucleic acid extraction are important. In previous studies extraction of DNA from the encapsulated yeast *Cryptococcus neoformans* was achieved using three cycles of freezing in liquid nitrogen and boiling to disrupt the rigid cell walls of the fungus.[13,14] We used a similar procedure to extract sufficient DNA from the CSF samples.

We conclude that PCR using specific primers can detect *T. gondii B1* gene DNA in CSF specimens from HIV-infected Japanese patients with TE and represents a different way of diagnosing TE in these patients. The test is very specific and has a high positive predictive value (both 100%). Diagnostic sensitivity needs to be improved and a simple DNA extraction procedure adopted before this test could be used routinely in clinical practice, however.

Acknowledgements

This study was supported in part by grants for Promoted Research from Kanazawa Medical University (S2003-2 and S2004-2), for Project Research from the High-Technology Center of Kanazawa Medical University (H2004-7), and from the Science Research Promotion Fund of the Promotion and Mutual Aid Corporation for Private Schools of Japan.

• Received for publication 14 June 2004 • Accepted subject to revision 19 June 2004
• Revised accepted 19 August 2004

References

1 Cinque P, Scarpellini P, Vago L, Linde A, Lazzarin A: Diagnosis of central nervous system complications in HIV-infected patients: cerebrospinal fluid analysis by the polymerase chain reaction. *AIDS* 1997; **11**: 1 – 17.
2 Potasman I, Resnick L, Luft BJ, Remington JS: Intrathecal production of antibodies against

Toxoplasma gondii in patients with toxoplasmic encephalitis and the acquired immunodeficiency syndrome (AIDS). *Ann Intern Med* 1988; **108**: 49 – 51.
3 Dupon M, Cazenave J, Pellegrin JL, Ragnaud JM, Cheyrou A, Fischer I, *et al*: Detection of *Toxoplasma gondii* by PCR and tissue culture in cerebrospinal fluid and blood of human immunodeficiency virus-seropositive patients. *J Clin Microbiol* 1995; **33**: 2421 – 2426.
4 Parmley SF, Goebel FD, Remington JS: Detection of *Toxoplasma gondii* in cerebrospinal fluid from AIDS patients by polymerase chain reaction. *J Clin Microbiol* 1992; **30**: 3000 – 3002.
5 Cohn JA, McMeeking A, Cohen W, Jacobs J, Holzman RS: Evaluation of the policy of empiric treatment of suspected Toxoplasma encephalitis in patients with the acquired immunodeficiency syndrome. *Am J Med* 1989; **86**: 521 – 527.
6 Burg JL, Grover CM, Pouletty P, Boothroyd JC: Direct and sensitive detection of a pathogenic protozoan, *Toxoplasma gondii*, by polymerase chain reaction. *J Clin Microbiol* 1989; **27**: 1787 – 1792.
7 Yerly S, Kaiser L, Race E, Bru JP, Clavel F, Perrin L: Transmission of antiretroviral-drug-resistant HIV-1 variants. *Lancet* 1999; **354**: 729 – 733.
8 Schoondermark-van de Ven E, Galama J, Kraaijeveld C, van Druten J, Meuwissen J, Melchers W: Value of the polymerase chain reaction for the detection of *Toxoplasma gondii* in cerebrospinal fluid from patients with AIDS. *Clin Infect Dis* 1993; **16**: 661 – 666.
9 Lebech M, Lebech A-M, Nelsing S, Vuust J, Mathiesen L, Petersen E: Detection of *Toxoplasma gondii* DNA by polymerase chain reaction in cerebrospinal fluid from AIDS patients with cerebral toxoplasmosis. *J Infect Dis* 1992; **165**: 982 – 983.
10 Verhofstede C, Reniers S, Colebunders R, van Wanzeele F, Plum J: Polymerase chain reaction in the diagnosis of Toxoplasma encephalitis. *AIDS* 1993; **7**: 1539 – 1541.
11 Novati R, Castagna A, Morsica G, Vago L, Tambussi G, Ghezzi S, *et al*: Polymerase chain reaction for *Toxoplasma gondii* DNA in the cerebrospinal fluid of AIDS patients with focal brain lesions. *AIDS* 1994; **8**: 1691 – 1694.
12 Contini C, Cultrera R, Seraceni S, Segala D, Romani R, Fainardi E, *et al*: The role of stage-specific oligonucleotide primers in providing effective laboratory support for the molecular diagnosis of reactivated *Toxoplasma gondii* encephalitis in patients with AIDS. *J Med Microbiol* 2002; **51**: 879 – 890.
13 Bialek R, Weiss M, Bekure-Nemariam K, Najvar LK, Alberdi MB, Graybill JR, *et al*: Detection of *Cryptococcus neoformans* DNA in tissue samples by nested and real-time PCR assays. *Clin Diagn Lab Immunol* 2002; **9**: 461 – 469.
14 Takahashi T, Goto M, Kanda T, Iwamoto A: Utility of testing bronchoalveolar lavage fluid for cryptococcal ribosomal DNA. *J Int Med Res* 2003; **31**: 324 – 329.

Address for correspondence
T Takahashi
Department of General Medicine, Kanazawa Medical University,
1-1 Daigaku, Uchinada-machi, Kahoku-gun, Ishikawa 920-0293, Japan.
E-mail: taka2si@kanazawa-med.ac.jp

1．研究課題名：RNA interference における二本鎖 RNA 依存性プロテインキナーゼ PKR の関与（研究番号 S2003-3）

2．キーワード：1）RNA 干渉（RNA interference, RNAi）
2）二本鎖 RNA（double-stranded RNA, dsRNA）
3）二本鎖 RNA 依存性プロテインキナーゼ（dsRNA-activated protein kinase, PKR）

3．研究者氏名：松井　理・医学部・助手・ゲノム医科学（生化学Ⅰ）

4．研究目的

RNA interference（RNAi）は、short interfering RNA（siRNA）と呼ばれる 21～23 塩基対（base pair, bp）の短い二本鎖 RNA（dsRNA）がそれと同じ配列を持つ mRNA に作用しその分解を誘導するという原理に基づく遺伝子発現抑制機構である。RNAi は比較的簡単な操作で特定遺伝子の発現を抑制できるため癌の遺伝子治療など臨床への応用が期待されているが、その作用機構には未だ不明な点も多く安全性が疑問視されている。特に、細胞内には dsRNA の関与する重要な系が他にもいくつか知られており、これらへの影響が懸念されている。そこで本研究では、このような dsRNA 分子を活性化因子とする二本鎖 RNA 依存性プロテインキナーゼ（PKR）の機能に対して、siRNA のような短い dsRNA がどのような影響を及ぼすかを明らかにすることを目的に研究を行う。PKR はウイルス感染などの細胞ストレス下でのサイトカイン産生やアポトーシス誘導など重要な生理現象において中心的な役割を担っており、PKR と RNAi との関連を明らかにすることは生物学的・医学的に大いに意義があると思われる。

5．研究計画

(1) PKR 組換え蛋白質と様々な鎖長の dsRNA を作製し、それらを用いて、dsRNA の PKR 活性化に及ぼす効果を in vitro の実験によって調べることにより、siRNA が PKR 活性化能を有するかを明らかにする。

(2) 培養細胞へ様々な鎖長の dsRNA を導入し、これらの細胞内 PKR 活性に与える影響を調べることにより、RNAi 経路の PKR 経路への影響を明らかにする。

6．研究成果

(1) PKR 組換え蛋白質（PKR-His）の作製

PKR の dsRNA 結合ドメインは N 末端近くに存在する。このため、dsRNA による PKR の活性化を解析するために、C 末端に精製用タグとして Gly-$(His)_6$のわずか 7 アミノ酸残基を付加した新規の PKR 組換え蛋白質（PKR-His）を作製した。T7 発現系を

用いて大腸菌内でPKR-Hisの発現を行いNi-NTAアガロースビーズを用いてHisタグ蛋白質を精製したところ、目的のサイズ（～68kDa）の蛋白質の他にそれよりもやや小さな～60kDaの蛋白質がほぼ同量得られた。この小さなサイズの蛋白質のN末端アミノ酸配列を調べたところ、PKRのN末端側98残基が欠けたものであることが判明した。そこで、60kDa蛋白質のN末端付近のDNA配列を調べたところ、98番目のアミノ酸残基がMetでありさらにそのすぐ上流にA、Gに富む大腸菌の翻訳開始シグナル（SD配列）様の配列が存在することからMet98コドンが擬似的な開始コドンとして機能していることが予想された。そこで、Met98をAlaに置換したところ、予想通り60kDa蛋白質の発現は完全に抑制された。さらに、アミノ酸置換を伴わないで60kDa蛋白質の発現のみを抑制するために、Met98の上流のSD様配列内の数ヌクレオチド残基を置換した変異体（internal SD-like sequence mutant、iSDm）を作製したところ、60kDa蛋白質の発現のみを抑制することに成功した。iSDmの発現系より生産されたPKR-His は野生型と同じアミノ酸配列であり、これをNi-NTAアガロースビーズ、phosphocellulose カラムクロマトグラフィーによって精製し、精製PKR-His標品を得た。

(2) 様々な長さの合成dsRNAの作製

様々な長さのdsRNAの作製は以下の手順にて行った。まずpGEM-3Zf(+)（Promega）のSP6プロモーターの下流に二本鎖合成DNAをクローニングし、11～61 bpのdsRNA領域を持つhairpin RNA合成プラスミドを構築した。次にこれらのプラスミドを鋳型として用い、SP6 RNA polymeraseによってin vitroでhairpin RNAを合成した。このhairpin RNAの一本鎖領域をMung Bean nucleaseで消化し、ポリアクリルアミドゲル電気泳動によって分離した後、ゲル片からdsRNAを抽出・回収し、精製dsRNA標品を得た。

(3) PKRの活性化におけるdsRNAの鎖長の依存性

様々な鎖長のdsRNAについて、PKR-Hisの自己リン酸化活性に対するdsRNAの依存性を調べた。その結果、siRNAのサイズ（21～23 bp）付近を境に、それよりも大きなdsRNA（26～61 bp）では明らかなPKR-Hisの自己リン酸化の促進が観察されたのに対し、それよりも小さなdsRNA（11, 16 bp）ではPKR-Hisの自己リン酸化は全く促進されなかった。また、上記のPKRの自己リン酸化を促進するdsRNAの場合でも、コントロールとして用いた長鎖（数百～数千bp）の合成二本鎖RNA、Poly(I)・Poly(C)の場合と比較すると、活性化の効果は非常にわずかであった。この結果から、二本鎖RNAによるPKRの活性化は二本鎖RNAの鎖長に依存しており、21～23 bp程度の鎖長であるsiRNAはPKRの活性化因子として機能しないことが予想された。

(4) dsRNAとPKRとの相互作用およびdsRNAによるPKRの構造変化

(3) で明らかになったdsRNAの鎖長の違いによるPKR活性化能の違いが、dsRNAとPKRとの相互作用の違いに基づくものなのかどうかを明らかにするためゲルシフ

トアッセイを行った。その結果、PKR 活性化能を持つ 26 bp 以上の dsRNA だけでなく PKR 活性化能を持たない 11～21 bp の dsRNA についても dsRNA と PKR との間の相互作用が検出された。さらにゲルシフトアッセイの結果を詳しく調べると、プローブ dsRNA 量が一定の場合、21 bp 以上の dsRNA では PKR の量を増加させると移動速度の遅いシフトバンドが新たに観察された。このことは、PKR が多量体化していることを示している。この結果から、PKR の活性化に対する二本鎖 RNA の鎖長依存性は、PKR への結合能の違いによるものではなく、おそらく活性化中間体である PKR 多量体形成能の違いによるものと推察された。

(5) Dicer による hairpin RNA の分解における dsRNA 部分の長さの影響

動物細胞の RNAi の場合、siRNA はまず hairpin RNA 前駆体としてとして転写された後、drosha や dicer などのヌクレアーゼでプロセッシングされることにより、最終的に成熟 siRNA となる。そこで、動物細胞において様々な長さの dsRNA の影響を調べる前に、本研究で用いる前駆体 hairpin RNA の dicer による分解を in vitro で調べた。その結果、21 bp のステムを持つ hairpin RNA (HR21) は dicer で速やかにプロセッシングされ 21～23 bp の dsRNA となるのに対し、51 bp のステムを持つ haripin RNA (HR51) は dicer によって分解されにくいことが明らかになった。また、in vitro の実験により HR21 の dicer 分解物は PKR 活性化能が極めて低く、HR51 は高い PKR 活性化能を持つことから、HR21 および HR51 を動物細胞で発現させた場合、前者は PKR 活性を抑制し後者は PKR 活性を促進することが予想された。

(6) 細胞内で発現させた hairpin RNA の細胞内 PKR 活性への影響

Hairpin RNA を動物細胞で発現させるために、pSilencer1.0-U6 (Ambion) の U6 プロモーターの下流に合成 DNA をつなげ、hairpin RNA 発現プラスミドを作製した。これをヒト培養細胞に導入した後、細胞内 PKR 活性をルシフェラーゼレポーター遺伝子の発現でモニターした。その結果、HR21 だけでなく HR51 を導入した場合も PKR 活性が著しく阻害された。これはおそらく in vitro 実験の場合と異なり細胞内で合成された HR51 が dicer あるいは drosha などのヌクレアーゼによってプロセッシングされ短い dsRNA になったためであると推察された。

7．研究の考察・反省

本研究の結果から、細胞内で合成させた siRNA は PKR を活性化しないだけでなく、PKR 活性を著しく阻害することが明らかになった。この作用機構としてはおそらく、siRNA が PKR 活性化能を持つ dsRNA と PKR との結合を競合的に阻害するからだと考えられる。PKR は前述のように抗ウイルス作用に関わる蛋白質である。したがって、RNAi を臨床に応用する場合、本研究の結果によると、siRNA によって引き起こされる PKR 機能の低下により人体がウイルスの感染に対して無防備になることが懸念される。今後は、さらに詳細な解析を継続しつつ、論文として公表することを目指す。

1. 研究課題名：心筋梗塞の新しい治療法の開発－体性幹細胞を用いた再生治療
（研究番号 S2003-4）

2. キーワード：1）心筋梗塞、心不全（myocardial infarction,heart failure）
2）再生（regenaration）
3）体性幹細胞、骨髄間葉系細胞細胞（stem cell,mesenchymal stem cell）
4）SP細胞（side population cell）
5）心筋細胞（cardiac myocyte）

3. 研究者氏名：赤澤純代（久藤）・医学部・助手・循環制御学（循環器内科学）
（現 生活習慣病センター）

4. 研究目的

高齢化、食生活の欧米化によりわが国において種々の動脈硬化性疾患が増加している。その代表が心筋梗塞でその終末像は心不全である。心筋梗塞は30～40％が発症時に死亡、10％が病院内で死亡する。また、死を逃れた半数も心不全や不整脈により QOL が低下するため、早急に克服すべき極めて重要な疾患である。

心筋梗塞には高血圧、高脂血症、喫煙といった、発症を促進する危険因子があり、食事療法や薬物療法等により危険因子を予防することで、心筋梗塞の発症をある程度減少させることができるが限界がある。心筋梗塞は心臓を養っている冠動脈が閉塞し心筋細胞が、虚血となる結果、細胞がネクローシスやアポトーシスにより死ぬ病態で、その結果、筋肉としてのポンプ機能が喪失し心不全を呈する。これまで心筋梗塞の治療法としては、閉塞した部位を一刻も早く再開通させるといった血栓溶解療法や血管形成術しかなく、それによっても虚血に弱い心筋を救うことは困難であった。発症後6時間以上たった場合には治療のすべはなく、それ以上梗塞範囲が広がらないように心臓の負荷をとるような姑息的な手段しかなかった。つまり心筋細胞にはほとんど再生能がないことより、一担死んでしまった心筋の機能を回復させることは不可能であった。そこで本研究においては今までと全く異なる新しい治療法として、心筋の再生療法の可能性について検討する。

5. 研究計画

1）骨髄間葉系細胞の心筋細胞への分化の機序について
2）筋芽細胞等組織幹細胞の心筋細胞への分化の有無の2つについて検討する。

1）骨髄間葉系細胞の心筋細胞への分化

骨髄間葉系細胞は脂肪、骨、軟骨、骨格筋など種々の細胞に分化することが知られており、マウスではin vitroおよびin vivo において心筋細胞に分化することも示されている。心筋梗塞時にG-CSFとSCFを投与することにより、おそらく骨髄より幹細胞が末梢に動員される結果、梗

塞部に心筋細胞が再生し、梗塞巣が縮小して心機能が改善すると報告された。本研究においては、骨髄間葉系細胞中のどの分画が心筋細胞に分化するのか、また心筋の幹細胞とも呼べるそのような細胞にはどのような特徴があるのかについて解析する。具体的には抗体を用いない新しい幹細胞純化方法SP(side population)細胞を用いて行う。これは、幹細胞が膜透過性が高く生細胞の状態でDNAのAT塩基配列にとりこまれる色素Hoechst33342を排出する性質がありこの特徴を用い、その分画side populationをFACSにて選別し、心臓へ注入したり、心筋細胞と共培養することによって心筋細胞への分化を検討する。SP細胞が心筋細胞との共培養により心筋細胞に分化した場合、その機序について液性因子や接着因子の役割を中心に解析する。

2)組織幹細胞の心筋細胞への分化

骨格筋芽細胞は一種の組織幹細胞(体性幹細胞)として、骨格筋ばかりでなく血液細胞、脂肪細胞等他の細胞にも分化する。そこで骨格筋芽細胞が心筋細胞に分化するか否かを検討する。GFP をマーカーとして利用するために GFP トランスジェニックマウスの骨格筋より骨格筋芽細胞を培養し、一部を心筋細胞と共培養し、心筋細胞に分化するか否かを自律拍動および心筋特異的分子に対する抗体で検討する。また、報告された骨格筋 SP 細胞には中胚葉性幹細胞との類似点が多いことより、骨格筋細胞の中から SP 細胞をとり、心臓に注入ないし心筋細胞との共培養により心筋細胞に分化するか否かを同様に検討する。

6. 研究成果

1)骨髄間葉系細胞の心筋細胞への分化

心筋細胞分化誘導の in vitro での機構を検討するために、研究協力者とともに GFP transgenic mouse より単離した骨格筋細胞を新生仔ラット心筋細胞と共培養し、骨格筋細胞に心筋蛋白が発現するかについて免疫細胞染色法により検討した。その結果、GFP 陽性骨格筋由来細胞の一部は cTnT、ANP、GATA4、CSX/Nkx2.5 を発現し、また、周囲の心筋細胞との細胞間接着部位に cadherin と connexin43 を発現して電気的機械的接着部位を形成することが明らかになった。また、骨格筋の幹細胞が多く含まれる分画として、FACS により得られた SP(side population)分画とを骨格筋初代培養上清中の遅延接着細胞群を、それぞれ心筋細胞と共培養した。

骨髄間葉系細胞を心筋細胞と共培養することにより、骨髄間葉系細胞は心筋細胞特異的な遺伝子および蛋白を発現した。異なる色素にて予めラベルしておくことにより、骨髄間葉系細胞の心筋細胞化は2種類の細胞の融合によることがわかった。興味深いことに、融合した細胞は心筋細胞の形質をもち、しかも分裂能を獲得した。骨髄間葉系細胞以外にも骨格筋由来の細胞、内皮細胞、内皮前駆細胞、心臓線維芽細胞が心筋細胞との共培養にて融合し、いずれも心筋細胞の形質を示した。骨格筋由来の細胞、内皮細胞をマウスの心臓に注入したところ、in vivo においても、心筋細胞と融合し、心筋細胞特異的蛋白を発現した。また心臓に凍結傷害をくわえたところ、心筋細胞は周囲の内皮細胞と融合した。

2) 組織幹細胞の心筋細胞への分化

心臓より幹細胞を単離する目的で、FACS により SP(side population)分画を採取に成功した。SP 分画細胞はヘキスト dye を排出する分子である bcrp を発現していた。SP 細胞はオキシトシンの処理により、急速に分裂増殖し、3－4週後には自律拍動する心筋細胞に分化した。また培養条件をかえることにより、心臓由来 SP 細胞は脂肪細胞や骨細胞に分化した。

7. 研究の考察・反省

世界レベルの展開で見ると、これまでは骨髄由来の造血や間葉系幹細胞を主体に心筋細胞への分化や移植実験が進められてきた。造血幹細胞によるものは最近の報告によって否定的な意見も出ている。骨髄間葉系幹細胞は様々な検討により、心筋細胞への分化度は極めて低く、骨や脂肪組織への分化が主たるものと考えられている。幹細胞を心筋細胞に高率に分化させるためには、分化の 詳細な分子機序と分化を促進する因子を解明する必要があると考えられる。

組織幹細胞の存在がわかり、今後、さらに誘導、大量培養、シート作成などが可能となると思われる。心筋細胞の本質的な再生はとにかく複雑で難しい。再生医療の実現に対する周りの期待の大きさとは反対に学問的には深いものと思われる。

また、今後は心筋細胞の分化・再生のメカニズムを解明し再生医療の実現へと発展することを強く願う。末期重症心不全の治療には移植以外には再生療法などしかなく、究極的治療の開発には心筋細胞および血管再生という二面の相補的なサポートおよび工学的な手法の組み合わせによる治療が期待されると思われる。この分野の研究は大変な時間と研究費がかかるために継続してゆくことは困難と思われた。

1. 研究課題名：レトロウイルス発現系を用いたタイラーウイルス増殖メカニズムにおけるL*蛋白の役割の解明（研究番号 S2003-5）

2. キーワード：1）タイラーウイルス（Theiler's murine encephalomyelitis virus）
2）L*蛋白（L* protein）
3）マクロファージ（macrophage）
4）ウイルス増殖（virus propagation）
5）レトロウイルス発現系（retrovairal expression system）

3. 研究者氏名： 姫田敏樹・医学部・助手・生体感染防御学 (微生物学)
（現 徳島大学）

4. 研究目的

タイラーウイルスは、ピコルナウイルス科に属し、マウスに急性致死性の灰白脳脊髄炎を引き起こす急性亜群（GDVII 株）と、脊髄に持続感染して脱髄を引き起こす慢性亜群（DA 株）に分類され、その脱髄は多発性硬化症の動物モデルとして注目されている。DA 亜群では、ポリ蛋白の開始コドンの 13 塩基下流にある別の読み枠の開始コドンから約 18kDa の L*と呼ばれる蛋白が合成される。一方、GDVII 亜群では、この AUG が ACG となっており、L*蛋白は合成されない。このように L*蛋白は DA 亜群でのみ合成されることから、持続感染・脱髄を規定している重要な因子の一つであると考えられている。これまで、L*蛋白の機能解析は DA 株の L*蛋白の開始コドン AUG を ACG に点変異させた DAL*-1 ウイルスを用いた"loss-of-function"の系で行われており、L*蛋白を合成する DA 株ではマクロファージで増殖するものの、L*蛋白非産生 DAL*-1 ウイルスはマクロファージで増殖しないことが明らかとなった。すなわち、L*蛋白はマクロファージにおけるウイルス増殖（ウイルスゲノムの維持）に寄与し、持続感染に重要な役割を果たしていると考えられる。本研究の目的は、L*蛋白発現マクロファージを作製し"gain-of-function"の系で上記の現象の裏づけをとることである。

5. 研究計画

1）目的蛋白の恒常的な発現を可能にするレトロウイルス発現系を用いて、L*蛋白とその N 末端側に 3xFLAG を融合させた 3xFLAGL*融合蛋白をそれぞれ発現するマクロファージ細胞株 J774 を樹立する。

2）抗 L*ポリクローナル抗体および抗 FLAG モノクローナル抗体を用いた Western blotting にて、単離した各細胞における L*蛋白の発現を確認する。

3）マクロファージ内でのウイルス増殖に対する L*蛋白の役割を明らかにするために、L*蛋白非産生ウイルス DAL*-1 を L*蛋白発現細胞に感染させ、その増殖をプラークア

ッセイにより検討する。

4) L*蛋白がウイルス増殖過程のどの段階で影響を及ぼしているのかを知るために、ウイルス RNA 複製および蛋白合成について、それぞれ RNase protection assay および Western blotting により検討する。

6. 研究成果

1) 形質導入したマクロファージ細胞株 J774 を限界希釈し、L*蛋白発現細胞 L*/J774 および 3xFLAGL*融合蛋白発現細胞 3xFLAGL*/J774 を樹立した。

2) 抗 L*ポリクローナル抗体および抗 FLAG モノクローナル抗体を用いた Western blotting により、単離した各細胞における L*蛋白の発現が確認された。

3) L*/J774 細胞を用いた DAL*-1 ウイルスの増殖検討から、DAL*-1 は感染後 12 時間（3-6x10^5 pfu/ml）にピークを示す増殖が認められた。一方、3xFLAGL*/J774 および L*蛋白を発現しないコントロール細胞（control/J774）では DAL*-1 の増殖は認められなかった。

4) RNase protection assay によるウイルス RNA の複製および抗 VP-1 モノクローナル抗体を用いた Western blotting によるウイルスカプシド蛋白合成の解析では、いずれの細胞においても差は認められなかった。

7. 研究の考察・反省

本研究において樹立した L*蛋白発現細胞 L*/J774 を用いた DAL*-1 ウイルスの増殖を検討したところ、L*蛋白非産生ウイルス DAL*-1 は L*蛋白の発現により増殖能を回復した。しかしコントロール細胞では DAL*-1 ウイルスはまったく増殖しなかった。すなわち、マクロファージにおけるタイラーウイルス DA 株の増殖には L*蛋白が不可欠であることが"gain-of-function"の系からも証明された。また、3xFLAGL*/J774 を用いた増殖検討でも DAL*-1 ウイルスは増殖せず、L*蛋白の機能発現にはその N 末端領域の構造が重要であることが示唆された。しかしながら、L*蛋白はウイルスゲノムの複製およびカプシド蛋白合成に影響を与えないことが示され、このことから L*蛋白はウイルス粒子の assembly に影響を及ぼしていると考えられた。

以上の結果から、L*蛋白の存在によって、DAL*-1 がマクロファージで増殖可能ということは、持続感染に必須なウイルスゲノムの維持に L*蛋白が重要な役割を担っていると考えられる。

今回作製した L*蛋白発現マクロファージ細胞株は、ウイルス本体を変化させることなく L*蛋白の機能を解析できることから、持続感染に重要とされる L*蛋白の更なる機能解明において有用な材料となることが期待される。今後、宿主細胞側に及ぼす L*蛋白の影響を調べるために、アポトーシスへの関与の可能性が報告されているマクロファージ細胞株 P388D1 の L*蛋白発現細胞株を樹立し、L*蛋白とアポトーシスの関係

について調べていく必要がある。

8. 研究発表

Toshiki Himeda, Yoshiro Ohara, Kunihiko Asakura, Yasuhide Kontani, Manabu Murakami, Hiromi Suzuki, Makoto Sawada. A lentiviral expression system demonstrates that L^* protein of Theiler's murine encephalomyelitis virus (TMEV) is essential for virus growth in a murine macrophage-like cell line. Virus Research 2005; 108: 23-28. (MLDB)

Available online at www.sciencedirect.com
SCIENCE DIRECT®
ELSEVIER
Virus Research 108 (2005) 23–28
Virus Research
www.elsevier.com/locate/virusres

A lentiviral expression system demonstrates that L* protein of Theiler's murine encephalomyelitis virus (TMEV) is essential for virus growth in a murine macrophage-like cell line

Toshiki Himeda[a], Yoshiro Ohara[a,*], Kunihiko Asakura[a], Yasuhide Kontani[a], Manabu Murakami[b], Hiromi Suzuki[c], Makoto Sawada[c]

[a] *Department of Microbiology, Kanazawa Medical University, 1-1 Uchinada, Ishikawa 920 0293, Japan*
[b] *Division of Basic Science, Medical Research Institute, Kanazawa Medical University, 1-1 Uchinada, Ishikawa 920 0293, Japan*
[c] *Institute for Comprehensive Medical Science, Fujita Health University, Aichi 470 1192, Japan*

Received 14 April 2004; received in revised form 14 July 2004; accepted 19 July 2004
Available online 17 September 2004

Abstract

The DA subgroup strains of Theiler's murine encephalomyelitis virus (TMEV) synthesize L* protein, which is translated out of frame with the polyprotein from an alternative AUG, 13 nucleotides downstream from the authentic polyprotein AUG. By a 'loss of function' experiment using a mutant virus, DAL*-1, in which the L* AUG is mutated to an ACG, L* protein is shown to play an important role in virus persistence, TMEV-induced demyelination, and virus growth in macrophages. In the present study, we established an L* protein-expressed macrophage-like cell line and confirmed the importance of L* protein in virus growth in this cell line.

Keywords: Theiler's murine encephalomyelitis virus; L* protein; Lentiviral vector; Virus growth; Macrophages

Theiler's murine encephalomyelitis virus (TMEV) belongs to the genus *Cardiovirus* of the family *Picornaviridae* and is divided into two subgroups (Ohara and Roos, 1987; Lipton and Jelachich, 1997; Obuchi and Ohara, 1998; Roos, 2002). DA (or TO) subgroup strains induce a non-fatal polioencephalomyelitis in weanling mice followed by virus persistence and chronic demyelination in the spinal cords. This late demyelinating disease serves as an experimental model of the human demyelinating disease, multiple sclerosis. In contrast, GDVII subgroup strains cause acute fatal polioencephalomyelitis without demyelination. The precise mechanisms of virus persistence and demyelination caused by DA subgroup strains are still unknown. A 17 kDa protein, called L*, is translated out of frame with the polyprotein from an alternative AUG, 13 nucleotides downstream from the authentic polyprotein AUG (Kong and Roos, 1991; Obuchi and Ohara, 1998; Roos, 2002). L* protein is only synthesized in the DA subgroup strains since the L* AUG is present in DA subgroup strains, but not in GDVII subgroup strains (Michiels et al., 1995; Obuchi and Ohara, 1998; Roos, 2002). Therefore, L* protein is thought to be a key protein regulating DA biological activities. A 'loss-of-function' experiment using a mutant virus, DAL*-1, in which the L* AUG initiation codon is mutated to an ACG, demonstrated that L* protein plays an important role in DA persistence and demyelination (Chen et al., 1995; Ghadge et al., 1998). However, that finding is still controversial since the absence of the L* AUG initiation codon in a different DA infectious clone had only a weak influence on the persistence of DA strain (van Eyll and Michiels, 2000, 2002).

We previously reported that DA strain grows in J774-1 cells, an $H\text{-}2^d$ macrophage-like cell line derived from a tumor of a BALB/c mouse (Ralph et al., 1975), while the GDVII

* Corresponding author. Tel.: +81 76 218 8096; fax: +81 76 286 3961.
E-mail address: ohara@kanazawa-med.ac.jp (Y. Ohara).

0168-1702/$ – see front matter © 2004 Elsevier B.V. All rights reserved.
doi:10.1016/j.virusres.2004.07.009

strain does not (Obuchi et al., 1997). This phenomenon is of great interest since a major site for TMEV persistence is thought to be macrophages (Lipton and Jelachich, 1997; Obuchi and Ohara, 1998; Roos, 2002). The important role of L* protein in this in vitro phenomenon can be demonstrated by using DAL*-1 virus. DAL*-1 virus does not grow in murine monocyte/macrophage lineage cell lines, but it does grow in other cell lines, including neural cells (Obuchi et al., 1999). A recombinant virus, DANCL*/GD, which has the DA 5′ noncoding and L* protein coding regions replacing the corresponding regions of GDVII and therefore synthesizes L* protein, had a rescue of growth activity in J774-1 cells, suggesting that L* protein plays an important role in virus growth in macrophages (Obuchi et al., 2000).

A challenge in research related to L* protein is that its sequence overlaps with that of the polyprotein, making it impossible to introduce the DA L* coding sequence into the parental GDVII strain without changing the polyprotein sequence. The generation of macrophage cells that constitutively express L* protein would allow a confirmation of the role of this protein in virus growth with a 'gain of function' experiment. This system would also allow the synthesis of L* protein in the cytoplasm, as has been described (Obuchi et al., 2001), without being incorporated into virions. Therefore, the goal of the present study was to establish a macrophage cell line that constitutively expresses L* protein.

We used a lentiviral expression system in order to achieve a stable and efficient gene transfer of L* protein. The vector was constructed by using the transfer vector plasmid pCSII-EF-MCS-IRES-hrGFP, constructed by Dr. Hiroyuki Miyoshi and Dr. Tomoyuki Yamaguchi, Laboratory of Genetics, The Salk Institute for Biological Studies. The plasmid has sequences of a human elongation factor (EF) 1 α subunit gene promoter, a multiple cloning site (MCS), an internal ribosome entry site (IRES), and the coding region of a 'humanized, red-shifted' green fluorescent protein (hrGFP) in tandem. L* coding sequence was inserted into MCS, resulting in the production of L* protein independently from hrGFP and not as a fusion protein. The expression of both proteins is regulated by one promoter. Another construct, in which the 3xFLAG epitope sequence is tagged to the N-terminus of L* protein, was generated as an additional control since the 5′ one third of the L* protein coding region is important for its function (Obuchi et al., 2001). In order to generate vesicular stomatitis virus (VSV) G protein-pseudotyped lentiviral vector particles, the transfer vector plasmid pCSII-EF-(cDNA of L* or 3xFLAGL* protein)-IRES-hrGFP with the packaging plasmid pMDLg/pRRE, pRSV-Rev, and the VSV-G protein envelope plasmid pMD.G (Naldini et al., 1996) were tansfected into subconfluent 293T cells, a human embryonic kidney epithelial cell line expressing the simian virus 40 large T antigen, using a high-efficiency calcium-phosphate-mediated transfection method (Miyoshi et al., 1997; Miyoshi et al., 1998; Sambrook and Russell, 2001). High-titer virus stocks were prepared by centrifugation (43,600 × *g*, 3 h, 21 °C). The infectious titers were determined by counting the number of GFP-positive cells by fluorescence-activated cell sorting (FACS) analysis (FACSCalibur: BD Biosciences, San Jose, CA). J774-1 cells (2×10^5) were infected and transduced at a multiplicity of infection (M.O.I.) of 5. After the infection, the third subculture of L*-transduced and 3xFLAGL*-transduced J774-1 cells were seeded at a density of 0.5 cells per well onto 360 wells and 1200 wells of HLA plates (Greiner bio-one, Tokyo, Japan), respectively.

Cell propagation was observed in 27 wells of L*-transduced cells and 105 wells of 3xFLAGL*-transduced cells. During the first several passages, the cells in approximately 50% of wells were GFP-positive and propagated more slowly than the original J774-1 cells. Some showed a different morphology, such as enlargement (20–30 μm, about 1.5-fold larger in diameter) and an amoebic shape. We selected four L*-expressed (L*/J774) and eight 3xFLAGL*-expressed (3xFLAGL*/J774) clones by FACS analysis using expression of GFP. The cells formed clusters easily when replated in new culture dishes. These properties reverted to those of the original J774-1 cells after seven passages. When both cells were seeded in a 35 mm plastic culture dish at the density of 1×10^5 cells/ml, the cultures reached to the density of 1×10^6 cells/ml within about four days, with a doubling time of 24–30 h. Seven empty vector-transduced clones (control/J774) were also obtained from the empty vector-transduced J774-1 cells and served as a control. The properties of these cells were not different from those of the original J774-1 cells. Fig. 1 shows the histograms of L*/J774/6, 3xFLAGL*/J774/33 and control/J774/6 clones, which gave the highest GFP expression.

The expression of L* and 3xFLAGL* proteins was further confirmed by Western blotting using polyclonal rabbit anti-L* antibody (Ab) (Obuchi et al., 2000, 2001) or monoclonal mouse anti-FLAG M2 Ab (Sigma, St. Louis, MO). Enhanced chemiluminescence reagents, ECL plus (Amersham Biosciences, Buckinghamshire, UK), detected biotinylated secondary Ab and horseradish peroxidase-conjugated streptavidin (Fig. 2). The expression of L* or 3xFLAGL* protein was stable after forty passages of culture.

We examined and compared the growth kinetics of DAL*-1 virus in those cells. The culture supernatants and cell lysates of 1.5×10^6 cells infected with DAL*-1 virus at an M.O.I. of 10 PFU per cell were harvested at 0, 3, 6, 12, 24, and 48 h post-infection (p.i.), and the infectivity was assayed by a standard plaque assay on BHK-21 cells. In L*/J774/6 cells, the titers of cell-free and cell-associated DAL*-1 virus reached a peak at 12 h p.i. (6.3×10^5 and 3.8×10^5 PFU/ml, respectively) and then gradually decreased (Fig. 3B). On the other hand, the titers gradually decreased in control/J774/6 cells (Fig. 3A). The data indicated that L* protein is essential for DA growth in J774-1 cells. The titers of DAL*-1 virus also gradually decreased in 3xFLAGL*/J774/33 cells (Fig. 3C), suggesting that the N-terminus is important for the function of L* protein, as previously reported (Obuchi et al., 2001). In addition, even though the 3xFLAG epitope is a small peptide (2.7 kDa), it may have changed the higher-order structure of

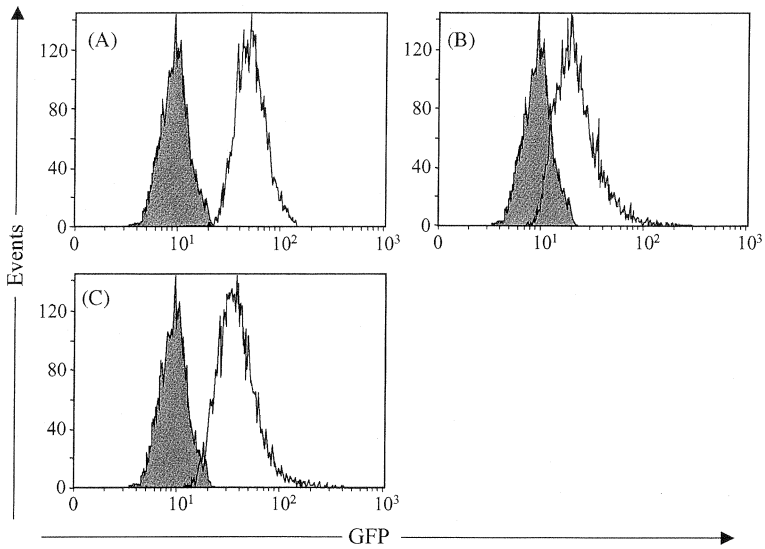

Fig. 1. Flow cytometric analysis of green fluorescent protein (GFP) fluorescence. J774-1 cells were infected and transduced with lentiviral vector containing the L* or 3xFLAGL* protein sequence. The transduced cells were cloned by a limiting dilution. Figure shows the histograms of GFP fluorescence in the representative clone of the vector-transduced J774-1 cells (open area). The original J774-1 cells served as a control (closed area). (A) Control/J774/6, which was transduced by an empty vector as described in the text; (B) L*/J774/6, which was transduced by the vector containing the L* sequence; (C) 3xFLAGL*/J774/33, which was transduced by the vector containing the 3xFLAGL* sequence.

L* protein since L* protein is relatively small (17 kDa). Also, the predicted hydrophilicity of 3xFLAG epitope may have interfered with the strong hydrophobicity of L* protein (Ohara et al., 1988; Obuchi et al., 2001), and thereby disturbed the function of L* protein.

To further investigate which step of virion formation is affected by L* protein, viral RNA synthesis of DAL*-1 virus following the infection of those cells was analyzed by RNase protection assay (RPA) (Fig. 4A). RPA was performed with the BD RiboQuant™ Non-Radioactive RPA system (BD Biosciences, San Jose, CA), according to the manufacturer's instructions. Briefly, pDAFL3, a full-length infectious DA cDNA clone (Roos et al., 1989), was cleaved at the *Hinc*II site (nt 7783) in the viral genome in order to prepare an antisense probe. The linearized plasmid was transcribed by an in vitro transcription system with T3 RNA polymerase in the presence of biotin-16-UTP (Roche Diagnostics GmbH, Mannheim, Germany). The biotin-labeled RNA probe con-

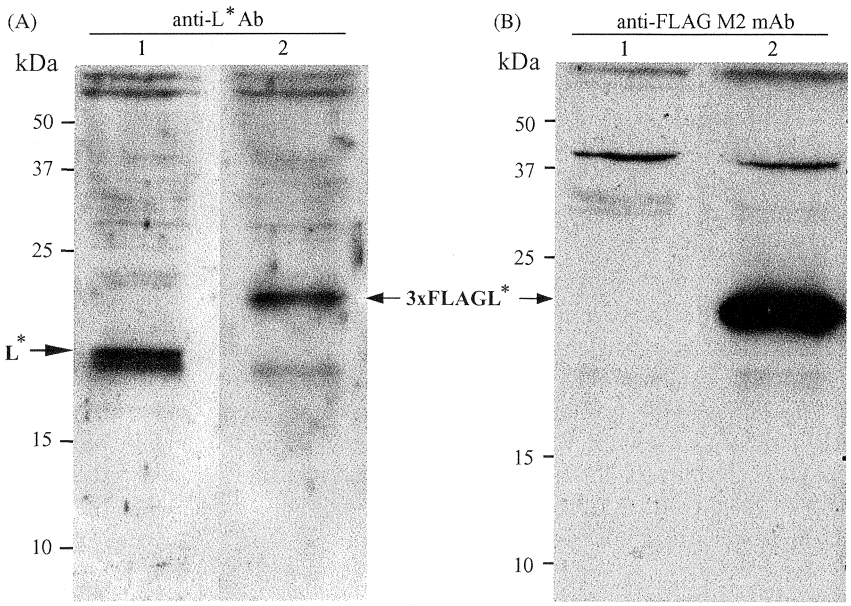

Fig. 2. Protein expression of the transgenes (L* and 3xFLAGL* sequences) in L*/J774/6 and 3xFLAGL*/J774/33 cells. The expression of L* gene in L*/J774/6 cells or 3xFLAGL* gene in 3xFLAGL*/J774/33 cells was analyzed by Western blotting as described in the text. L* (lane 1) and 3xFLAGL* (lane 2) proteins were detected with anti-L* antibody (A) and anti-FLAG M2 monoclonal antibody (B), respectively.

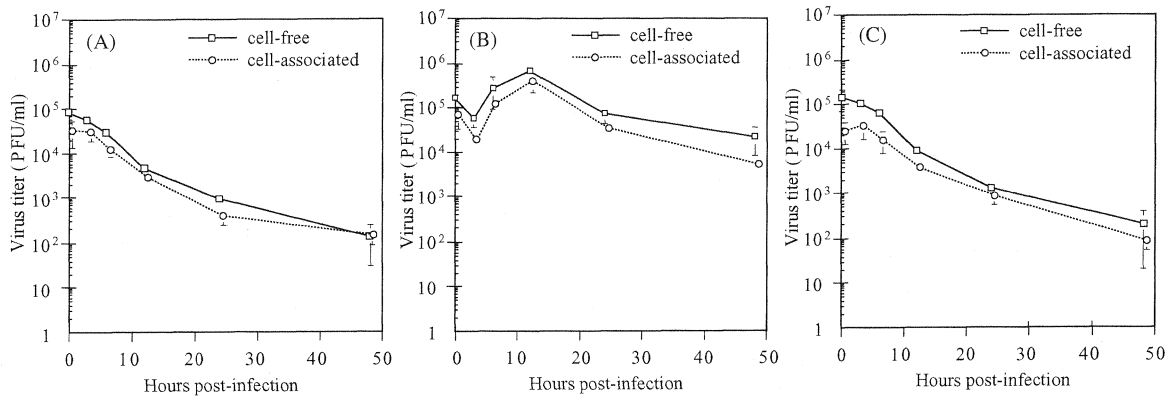

Fig. 3. Growth kinetics of DAL*-1 virus in control/J774/6 (A), L*/J774/6 (B), and 3xFLAGL*/J774/33 (C) cells. The culture supernatants (solid lines, open squares) and cell lysates (broken lines, open circles) of cells infected at a multiplicity of infection (M.O.I.) of 10 were harvested at indicated time points and subjected to titer determination by a standard plaque assay on BHK-21 cells. Data are expressed as the mean ± standard deviation (S.D.) in three independent experiments.

tained 310 nt of sequence complementary to the 3' region of the viral genome and 52 nt of vector sequence (Ohara et al., 1988; Roos et al., 1989). At 0, 3, 6, and 9 h p.i., total RNA was extracted and purified from 9.3 × 10^4 virus-infected cells by using RNeasy Mini Kit (QIAGEN, Tokyo, Japan). The RNA and 10 ng of biotin-labeled RNA probe were hybridized, and then treated with RNase A and RNase T1. The protected RNA probes were separated by electrophoresis on 5% polyacrylamide gels containing 8 M urea, and transferred to positively-charged nylon membranes by electroblotting. The signals were detected by chemiluminescent detection system. As shown in Fig. 4A, the amount of viral RNA of DAL*-1 virus clearly increased and reached a peak 6 h p.i. in all the cells examined.

Viral protein synthesis was also examined in those cells. At 3, 6, and 9 h p.i., 1 × 10^6 cells infected with DAL*-1 virus were scraped and dissolved in sample buffer (0.01 M Tris-Cl [pH 6.8], 1 mM EDTA, 2.5% SDS, 5% 2-mercaptoethanol, 10% glycerol, 0.005% bromophenol blue). The cell lysates were analyzed by Western blotting with DA-neutralizing monoclonal antibody, DA mAb 2, which reacts to VP1 capsid protein of DA strain (kindly provided from Dr. Raymond P. Roos, University of Chicago, IL) (Fig. 4B). The amount of VP1 capsid protein of DAL*-1 virus increased rapidly from

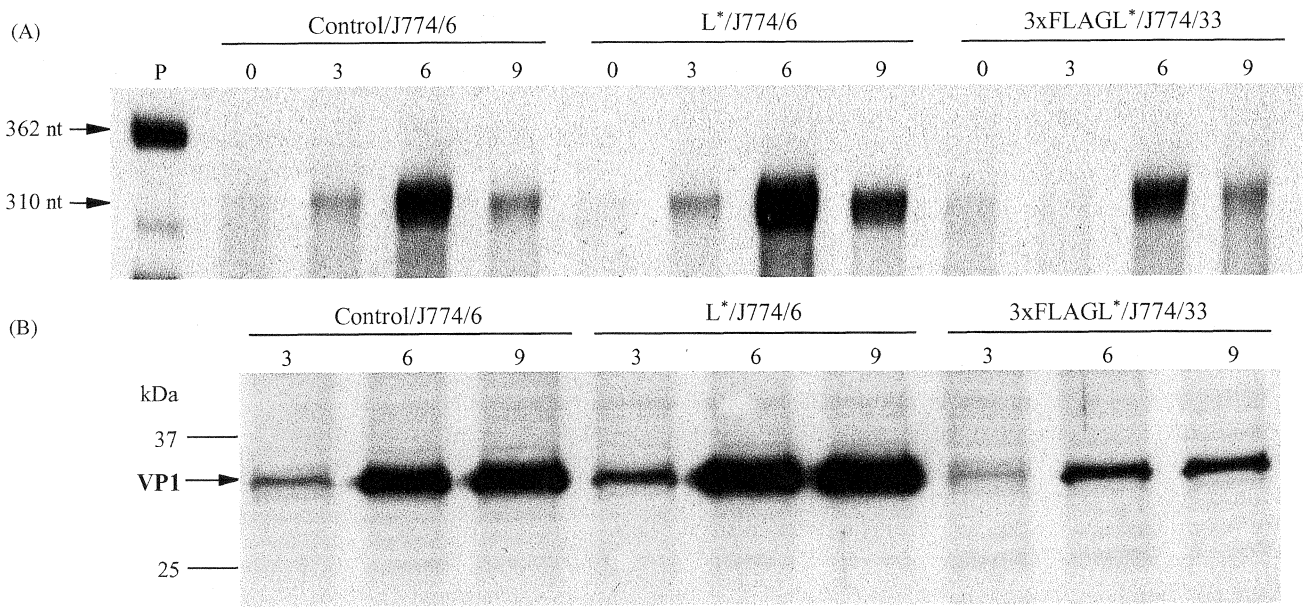

Fig. 4. (A) Viral RNA synthesis of DAL*-1 virus in control/J774/6, L*/J774/6, and 3xFLAGL*/J774/33 cells. Total RNA extracted from the virus infected-cells (9.3 × 10^4 cells) was subjected to RNase protection assay as described in the text. The numbers at the top of panel indicate hours post-infection (p.i.). Lane P is the starting probe. (B) Synthesis of viral protein in control/J774/6, L*/J774/6, and 3xFLAGL*/J774/33 cells. The cells were infected with DAL*-1 virus at an M.O.I. of 10. After the infection, the cell lysates were analyzed by Western blotting with DA mAb 2 as described in the text. The numbers at the top of panel indicate hours p.i.

3 h p.i., reaching a plateau at 6 to 9 h p.i. in L*/J774/6 cells. The same tendency was observed in both control/J774/6 and 3xFLAGL*/J774/33 cells.

The data obtained in the L*-expressed system have confirmed that L* protein is essential for virus growth in J774-1 cells. In fact, GDVII strain, which does not grow in J774-1 cells (Obuchi et al., 1997), also had a rescue of the growth activity in L*/J774/6 cells (data not shown). As described elsewhere (Obuchi et al., 1997), DA strain infects and actively replicates in J774-1 cells, with only a minimal damage on these cells. This property is clearly important to set the stage for a persistent infection of DA strain in macrophages in vivo. Therefore, DA strain may be able to maintain its genome in macrophages in the presence of L* protein, leading to virus persistence and consequently to demyelination.

As shown in Fig. 4A and B, L* protein had no effects on viral RNA replication and viral protein translation. These results differ from our previous reports (Takata et al., 1998; Obuchi et al., 1999, 2000) that suggested that L* protein probably interferes with viral RNA replication, however, only two time-points (3 and 9 h p.i.) were examined in these previous studies. No effects of L* protein on virus attachment were found in a previous report (Obuchi et al., 1999). As shown in Fig. 3, the titers of cell-associated virus almost paralleled those of cell-free virus in all cells, strongly suggesting that the release of virions are not influenced by the presence or the absence of L* protein. Therefore, L* protein may have some effect(s) on the step of virion assembly. The effect of L* protein is presumably in *trans*.

The formation of viral particles of picornaviruses is reported to be coupled to RNA replication, both events occurring on the surface of virus-induced membranous vesicles found in the cytoplasm of infected cells (Blondel et al., 1998). The poliovirus-induced vesicles are formed closely related on the surface of intracellular membranes, such as the endoplasmic reticulum (ER) (Suhy et al., 2000). Proteins of the poliovirus replication complex, especially 2BC and 3A, accumulate in patches on the ER. Double membrane vesicles derive from the ER (Suhy et al., 2000). Microtubules are known to be closely associated with the ER (Lodish et al., 1995). It may be that the association of L* protein with microtubules is important in TMEV assembly in J774-1 cells or other macrophage cell lines. Of interest, the importance of L* protein to DA growth is not observed in other types of cells (Obuchi et al., 1999). Some unknown host cell factor(s) may have a key interaction with L* protein that is important for virus growth. This may foster DA persistence in a cell key to carrying out DA-induced demyelination. Two-hybrid system may identify this factor(s), and the study is under progress. The restricted growth and persistence of TMEV in macrophages may be critical to the white matter disease. Therefore, the identification of this factor(s) interacting with L* protein may clarify the mechanism(s) of TMEV-induced demyelinating disease.

Acknowledgements

This work was supported by a Grant-in-Aid for Scientific Research from the Ministry of Education, Science, Sports and Culture; and a Grant for Project Research from High-Technology Center of Kanazawa Medical University (H2002-7) and a Grant for Promoted Research from Kanazawa Medical University (S2003-5).

References

Blondel, B., Duncan, G., Couderc, T., Delpeyroux, F., Pavio, N., Colbere-Garapin, F., 1998. Molecular aspects of poliovirus biology with a special focus on the interactions with nerve cells. J. NeuroVirol. 4, 1–26.

Chen, H.-H., Kong, W.-P., Zhang, L., Ward, P.L., Roos, R.P., 1995. A picornaviral protein synthesized out of frame with the polyprotein plays a key role in a virus-induced immune-mediated demyelinating disease. Nat. Med. 1, 927–931.

Ghadge, G.D., Ma, L., Sato, S., Kim, J., Roos, R.P., 1998. A protein critical for a Theiler's virus-induced immune system-mediated demyelinating disease has a cell type-specific antiapoptotic effect and a key role in virus persistence. J. Virol. 72, 8605–8612.

Kong, W.-P., Roos, R.P., 1991. Alternative translation initiation site in the DA strain of Theiler's murine encephalomyelitis virus. J. Virol. 65, 3395–3399.

Lipton, H.L., Jelachich, M.L., 1997. Molecular pathogenesis of Theiler's murine encephalomyelitis virus-induced demyelinating disease in mice. Intervirology 40, 143–152.

Lodish, H., Baltimore, D., Berk, A., Zipursky, S.L., Matsudaira, P., Darnell, J., 1995. Microtubules and intermediate filaments. In: Lodish, H., Baltimore, D., Berk, A., Zipursky, S.L., Matsudaira, P., Darnell, J. (Eds.), Molocular cell biology, third ed. Scientific American books, New York, pp. 1072–1075.

Michiels, T., Jarousse, N., Brahic, M., 1995. Analysis of the leader and capsid coding regions of persistent and neurovirulent strains of Theiler's virus. Virology 214, 550–558.

Miyoshi, H., Takahashi, M., Gage, F.H., Verma, I.M., 1997. Stable and efficient gene transfer into the retina using an HIV-based lentiviral vector. Proc. Natl. Acad. Sci. U.S.A. 94, 10319–10323.

Miyoshi, H., Blömer, U., Takahashi, M., Gage, F.H., Verma, I.M., 1998. Development of a self-inactivating lentivirus vector. J. Virol. 72, 8150–8157.

Naldini, L., Blömer, U., Gallay, P., Ory, D., Mulligan, R., Gage, F.H., Verma, I.M., Trono, D., 1996. In vivo gene delivery and stable transduction of nondividing cells by a lentiviral vector. Science 272, 263–267.

Obuchi, M., Ohara, Y., Takegami, T., Murayama, T., Takada, H., Iizuka, H., 1997. Theiler's murine encephalomyelitis virus subgroup strain-specific infection in a murine macrophage-like cell line. J. Virol. 71, 729–733.

Obuchi, M., Ohara, Y., 1998. Theiler's murine encephalomyelitis virus and mechanisms of its persistence. Neuropathology 18, 13–18.

Obuchi, M., Yamamoto, J., Uddin, M.N., Odagiri, T., Iizuka, H., Ohara, Y., 1999. Theiler's murine encephalomyelitis virus (TMEV) subgroup strain-specific infection in neural and non-neural cell lines. Microbiol. Immunol. 43, 885–892.

Obuchi, M., Yamamoto, J., Odagiri, T., Uddin, M.N., Iizuka, H., Ohara, Y., 2000. L* protein of Theiler's murine encephalomyelitis virus is required for virus growth in a murine macrophage-like cell line. J. Virol. 74, 4898–4901.

Obuchi, M., Odagiri, T., Asakura, K., Ohara, Y., 2001. Association of L* protein of Theiler's murine encephalomyelitis virus with microtubules in infected cells. Virology 289, 95–102.

Ohara, Y., Roos, R.P., 1987. The antibody response in Theiler's virus infection: new perspectives on multiple sclerosis. Prog. Med. Virol. 34, 156–179.

Ohara, Y., Stein, S., Fu, J., Stillman, L., Klaman, L., Roos, R.P., 1988. Molecular cloning and sequence determination of DA strain of Theiler's murine encephalomyelitis viruses. Virology 164, 245–255.

Ralph, P., Prichard, J., Cohn, M., 1975. Reticulum cell sarcoma: An effector cell in antibody-dependent cell-mediated immunity. J. Immunol. 114, 898–905.

Roos, R.P., Stein, S., Ohara, Y., Fu, J., Semler, B.L., 1989. Infectious cDNA clones of the DA strain of Theiler's murine encephalomyelitis virus. J. Virol. 63, 5492–5496.

Roos, R.P., 2002. Pathogenesis of Theiler's murine encephalomyelitis virus-induced disease. In: Semler, B.L., Wimmer, E. (Eds.), Molecular Biology of Picornaviruses. ASM Press, Washington, DC, pp. 427–435.

Sambrook, J., Russell, D.W., 2001. Alternative protocol: high-efficiency calcium-phosphate-mediated transfection of eukaryotic cells with plasmid DNAs, third ed. In: Sambrook, J., Russell, D.W. (Eds.), Molecular Cloning: A Laboratory Manual, vol. 3. Cold Spring Harbor Laboratory Press, Cold Spring Harbor, New York, pp. 16.19–16.20.

Suhy, D.A., Giddings Jr., T.H., Kirkegaard, K., 2000. Remodeling the endoplasmic reticulum by poliovirus infection and by individual viral proteins: an autophagy-like origin for virus-induced vesicles. J. Virol. 74, 8953–8965.

Takata, H., Obuchi, M., Yamamoto, J., Odagiri, T., Roos, R.P., Iizuka, H., Ohara, Y., 1998. L* protein of DA strain of Theiler's murine encephalomyelitis virus is important for virus growth in a murine macrophage-like cell line. J. Virol. 72, 4950–4955.

van Eyll, O., Michiels, T., 2000. Influence of the Theiler's virus L* protein on macrophage infection, viral persistence, and neurovirulence. J. Virol. 74, 9071–9077.

van Eyll, O., Michiels, T., 2002. Non-AUG-initiated internal translation of the L* protein of Theiler's virus and importance of this protein for viral persistence. J. Virol. 76, 10665–10673.

1．研究課題名：日本人の白内障病型別有所見率・発症率と発症・進行予測および危険因子探索
(研究番号　S2003-6)

2．キーワード：1）白内障（Cataract）
2）水晶体（Crystalline lens）
3）疫学（Epidemiology）
4）有所見率（Prevalence）
5）WHO 白内障分類（WHO cataract grading system）

3．研究者氏名：佐々木　洋・医学部・教授・感覚機能病態学（眼科学）

4．研究目的

加齢白内障は現在の高齢化社会を象徴する代表的な眼疾患であり、わが国でものその患者数が着実に増加していることは厚生省労働省による患者調査でも明らかである。また治療としての白内障手術件数も年々増加の一途を辿り逼迫する医療経済の中で問題になっていることもよく知られている。先進国全般にかかわる現象であり、世界的にもこれへの対応を模索しているところであるが、国レベルでその検討が行われている地域は米国、オーストラリア、フランスなどまだ限られている。わが国でもこの立場からの白内障疫学研究が行われているが、申請者らの研究グループのみの研究にとどまっており、国際的な検討の場でも申請者らのこれまでの検討結果が議論のベースとなっている。本研究では本邦では初めてとなる無作為対象での日本人水晶体病型別の有所見率、手術施行例の頻度、5 年での発症率、進行率、壮年代初期を境に明らかに進行する水晶体透明度の低下に眼部紫外線被曝推定蓄積総量をはじめとする種々の危険因子がどの程度関与するのか等に視点を置いて検討することにある。既に申請者らはアイスランドで行った Reykjavik Eye Study で 5 年経過の 1,000 余名の無作為対象群から、今回意図した病型別発症率、進行率が明らかにすることができた。本研究の結果は世界最長寿国である日本での白内障の実態を明らかにし、欧米先進諸国での検討結果との差異を明確にし、同じ目的をもつ先進諸国の研究グループへも大きく貢献するはずである。

申請者らのグループはこれまで、能登地区、鹿児島県奄美地区、シンガポール、アイスランドで眼疫学調査を行ってきた。これらの調査では全て本研究代表者が細隙灯顕微鏡検査および白内障画像診断を行っており、全ての調査対象間での比較が可能である。本研究の特色は①、日本人にみられる白内障病型別の有所見率、進行率、発症率、手術受領率および白内障病型と視機能（視力、今トラス感度）の関係を明らかにすることであり、得られた結果は今後の日本での眼科医療保険制度を再検討する際の基礎的データとなり得るはずである。②また、生活様式と白内障発症の関連については問診結果から検討するが、これと白内障発症前水晶体の散乱光強度を新たな指標として検討をする予定である。申請者らは散乱光強度と層間厚から水晶体の加齢変化の指標となり得る Lens Transparent Property（LTP）の有用性を報告している。これまでに散乱光強度を指標とした危険因子探索の検討はなく、この点も本研究の特色の 1 つである。③危険因子の中でも太陽紫外線被曝との関連についてはこれまでの調査でも検討を行ってきたが、マネキンモデルを用いた実験から申請者らが提唱する“推定眼部紫外線被曝蓄積量”と水晶体混濁との関連・これに対する防御指針を本研究ではより具体的に提唱したい。国内はもとより海外でも眼部紫外線

被曝量と白内障との関連についての研究は緒についたばかりであり、申請者らはこの領域では他の研究グループより一歩先んじた研究の蓄積があることより、本研究から白内障発症に至る眼部紫外線総被曝量の閾値が提唱できればと考えている。

5．研究計画

申請者らのグループが1998年から能登地域で行っている眼疫学調査Monzen Eye Study の対象（無作為対象群；50歳以上の2,000名）について、すでに終了している1次調査の画像解析と5年目の縦断的調査を行う。1次調査では対象の60%以上について問診および水晶体撮影を含む眼科的検査を行った。本研究期間中に1次調査で収集したデータの解析と1次調査から5年を経過した症例を対象に2次調査を行う。2次調査では原則として1次調査で施行した全ての眼科的検査を行う。水晶体の解析は他のフィールド調査でも使用している前眼部解析装置での撮影画像を用いて行う。水晶体画像解析は1）水晶体散乱光強度、2）水晶体形状、3）3主病型（皮質、核、後嚢下混濁）の混濁程度の評価について行う予定である。生活視力の指標であるコントラスト感度と白内障病型の関連についての検討も行う。また、問診の結果について、全身疾患、眼疾患、内服薬、食生活、推定紫外線被爆量と水晶体混濁との関連を検討し、白内障発症および進行の予測、危険因子探索を行う。申請者らが提唱する“推定眼部紫外線被曝蓄積量”については、マネキンモデルでの実験から我々のグループが提唱した予測式を用い被爆量算出する。

6．研究成果

これまで石川県門前町の50歳以上の一般住民（無作為抽出）を対象に行った第1回の眼疫学調査の対象者1105名中、本年度終了時点で約400名について5年目の2次検診が終了した。1次調査の結果からグレード1以上の皮質、核、後嚢下混濁の有病率は、それぞれ36.6%、8.5%、3.0%であった。いずれの病型も有病率は、加齢にともない有意に増加した。グレード1以上の皮質混濁の頻度は、女性（40.0%）が男性（32.8%）に比べ有意に高値であった。核、後嚢下では男女間に有意差はなかった。 CEN の有所見率は、50、60、70、80歳代でそれぞれ4.2、19.9、39.8、50%であった。白内障の手術をすでに受けていた者は全対象例の3.4%で年代別では50、60、70、80歳代でそれぞれ0.5、1.7、6.1、15.2%であり、女性(4.1%)が男性(2.4%)に比して有意に高率であった。

最終的な白内障の発症率、進行率、手術受療率、5年間での白内障有所見率や手術症例数の変化などは来年度の検診が終了した時点で算出する予定であるが、これまでの結果では3主病型(皮質、核、後嚢下白内障）の発症は加齢に伴い増加する傾向がみられている。白内障の進行については、年齢との明らかな相関は見られていない。研究者らがアイスランド一般住民を対象に行ったReykjavik Eye Study でも同様の傾向が見られおり興味深い結果と考える。2次検診では白内障3主病型（皮質、核、後嚢下）以外の混濁病型についても検討を行っている。2次検診でこれまで行ってきた途中経過でのデータでは3主病型以外の混濁病型、i)Fiber folds、ii)Water clefts、iii)Vacuoles、iv)Focal dots、v)Retrodots、vi)Coronary cataract のそれぞれの有所見率は29.1%、41.4%、21.1%、28.6%、22.5%、11.5%であった。i)、ii)、v)、は加齢に伴い増加していた。i)がみられた症例の91%は皮質混濁に伴うものであった（投稿中)。6病変中には視機能障害につながるものがあり、日本人での有所見率を明らかにすることは重要で、2次検診終了時点で最終的な年齢別、性別の有所見率を算出する予定である。

３主病型とRetrodots混濁のコントラスト感度への影響を検討した。皮質白内障はCENがない場合はコントラストへの影響は少ないが、WHO分類の程度２以上でCENを合併するとコントラストの有意な低下をきたす。核白内障は程度１ではコントラストに影響はなく、２以上で低下が見られる。後嚢下白内障は程度１でも有意なコントラストの低下を生じる。混合型混濁のコントラスト感度は各単独混濁による低下量の（log(MAR)）の増加量）の加算値にほぼ相当した。この結果はWHO白内障分類から白内障の手術適応を判定する際、有用な基準となる可能性がある。Retrodots混濁では程度２以上で有意なコントラスト感度の低下をきたした。今後は他の白内障副病型と３主病型の合併例での視機能についても検討し、日本人での白内障手術の適応基準を提唱したいと考えている。

問診とマネキンモデルでの予測式から求めた紫外線総被曝量（CUV: Cumulative UV exposure）眼部紫外線総被曝量（COUV: Cumulative ocular UV exposure）と皮質の関連について検討した。門前町での疫学調査に加え、これまで行ってきたアイスランド、シンガポールでの調査の結果についても検討した。CUVはシンガポール>門前>アイスランドであったが、COUVはシンガポール＝門前>アイスランドであった。皮質白内障とCUV、COUVに関して門前、アイスランドでは有意な相関はみられなかった。一方、シンガポールの女性ではCUVの下位25%に対する上位25%の皮質白内障のオッズ比は2.84(1.14-6.94, $p<0.01$)であった。COUVも上位25%で高い傾向があったが有意ではなかった。門前でも同様の傾向が見られたが有意ではなかった。

７．研究の考察・反省

北陸地域の農村部、石川県門前町一般住民におけるWHO分類での白内障有病率および白内障手術受療頻度が明らかになった。WHO分類を用いた評価では、皮質白内障が主病型であり、特に皮質単独混濁が多いことが特徴と考えられた。白内障手術受療頻度は、女性が男性の1.7倍であり、女性は手術に至る可能性が男性より高い可能性が示唆された。

３主病型以外の副病型の有所見率に関しての予備的なデータを出すことができた。副病型については眼科医でも正確に診断できるものは少なく、その認知度は低い。しかし、副病型の中には単独でも高度の視機能障害を生じるものがあり、本邦での有所見率および視機能との関連を明らかにする意義は大きい。平成18年度中に終了する２次検診の結果からこれらの副病型の詳細を明らかにしていく予定である。

LTPと白内障発症の関連については本研究では行うことができなかった。５年観察終了症例が蓄積した後に、初回検診時のLTPと各種白内障の関連について検討したい。

眼部紫外線総被曝量と皮質白内障の関連については予想していた有意な関連はみられなかった。紫外線と皮質白内障の関係は現在まで多くの疫学調査で証明されているが、本研究レベルでの個人の眼部紫外線被曝との関連について検討したものはない。今後はさらに眼部紫外線被曝に関する予測式の精度に関する検討が必要であるとともに、紫外線被曝と白内障の関連について、その寄与危険度を再検討する必要があると考えられた。

８．研究発表

Sasaki K, Sasaki H, Jonasson F, Kojima M, Cheng HM. Racial Differences of Lens Transparency Property with Aging and Prevalence of Age Related Cataract Applying a WHO Classification System.. Ophthalmic Res 2004; 36 : 332-340. (MLDB)

Original Paper

Ophthalmic Research

Ophthalmic Res 2004;36:332–340
DOI: 10.1159/000081636

Racial Differences of Lens Transparency Properties with Aging and Prevalence of Age-Related Cataract Applying a WHO Classification System

Kazuyuki Sasaki[a] Hiroshi Sasaki[a] Fridbert Jonasson[b] Masami Kojima[a] Hong Ming Cheng[c]

[a]Department of Ophthalmology, Kanazawa Medical University, Uchinada, Japan; [b]Department of Ophthalmology, Iceland University, Reykjavik, Iceland; [c]Schepens Retina Association Foundation, Boston, Mass., USA

Key Words

Lens transparency property · Age-related cataract · WHO cataract classification system · Nuclear cataract · Reykjavik Eye Study · Japan-Singapore Cooperative Cataract Study · Monzen Eye Study

Abstract

Purpose: To investigate racial differences of lens transparency properties and the prevalence of lens opacification by age. ***Methods:*** Lenses of randomly selected Asian (1,038 Japanese and 517 Singaporeans) and Caucasian (1,045 Icelanders) subjects were evaluated for their lens transparency property (LTP). The prevalence of lens opacification was determined with a newly proposed WHO cataract classification system. ***Results:*** LTP increased with aging for all nationalities. Light scattering intensity was significantly higher in the Singaporeans followed by the Icelandic subjects. The prevalence of cortical opacification in Singaporeans was significantly higher than those of the other nationalities up to the age of 60, and the prevalence in Asians was significantly higher than that in Caucasians aged 60–69. Cortical opacification was more prevalent than the other types for both Japanese and Icelanders in their 50s, 60s and 70s. Regarding the central optical zone, the prevalence in the Singaporeans was significantly higher than in the other two groups in their 50s and 60s. The prevalence of nuclear opacification in Singaporeans was markedly higher than those of the two other groups for all ages. Subcapsular cataract was the least prevalent type for all age groups and nationalities; however, the highest prevalence was observed in Singaporeans. ***Conclusions:*** Lens transparency decreased with age in the Singaporeans more markedly than in the other two groups. The high prevalence of nuclear opacification in Singaporeans is considered to be due to environmental rather than race-specific factors.

This work was presented as an Ophthalmic Research Lecture during the EVER 2003 meeting.

Introduction

Since the late 1990s, cataract epidemiologic studies undertaken in industrialized countries have employed several systems for recording opacified lens morphology and used them as diagnostic tools. Although further methodologic improvements may yet be made, it is fair to say that the quality of investigations has improved compared with those performed before the late 1990s.

KARGER

Fax +41 61 306 12 34
E-Mail karger@karger.ch
www.karger.com

0030–3747/04/0366–0332$21.00/0

Accessible online at:
www.karger.com/ore

Kazuyuki Sasaki, MD, PhD
Department of Ophthalmology, Kanazawa Medical University
Daigaku-machi 1-1, Uchinada, Ishikawa 920-0293 (Japan)
Tel. +81 76 286 2211, ext. 3956, Fax +81 76 286 9020
E-Mail sasaki-k@kanazawa-med.ac.jp

Table 1. Persons examined

Age, years	Reykjavik			Singapore			Monzen		
	males	females	total	males	females	total	males	females	total
50–59	166	194	360	84	127	211	77	126	203
60–69	145	210	355	107	116	223	167	251	418
70–79	118	136	254	42	31	73	163	212	375
≥80	033	43	76	5	5	10	19	23	42
Total	462	583	1,045	238	279	517	426	612	1,038

To date, such epidemiologic studies have yielded a lot of important information including prevalence, incidence, type, severity of opacity and risk factors. As far as we know, there have been very few studies comparing age-related changes of lens transparency in different races. We have proposed lens transparency property (LTP), calculated from lens layer thickness and light scattering intensity measured by Scheimpflug slit images, as an index of age-related changes in lens transparency. This index is higher in diabetic subjects, in whom prevalence and rates of surgical intervention are higher than in nondiabetic populations, compared with nondiabetic volunteers [1]. Based on experience, we believe that LTP may be a useful tool for predicting lens opacification. Since it is unclear whether light scattering intensities and thickness of lens layers differ between races, measuring LTP in different races could offer a new aspect for investigating variation of age-related lens transparency in the normal population. A comparison of LTP measures of three climatically and racially different subject groups is presented in this article. In addition, comparison of cataract prevalence in the same subject groups was performed applying a newly proposed cataract classification system by the WHO [2].

Cataract researchers interested in the incidence or prevalence of cataract by type, age, gender, race or other variables may find themselves thwarted when reviewing the literature, because comparison of findings is difficult due to the lack of a universal or 'gold standard' cataract classification system. To overcome this situation, the WHO study group proposed the newly established cataract classification system [2]. For purposes of this study, and to assist other researchers to make such comparisons, from our own Japanese Cooperative Cataract Epidemiology Study Group system (JCCESG system) [3], data of the same subjects from previous surveys [4–6] have been converted in accordance with the new WHO classification system.

Methods

Residents of Monzen, Japan, Singapore and Reykjavik, Iceland, aged 50 years and older were surveyed. The local government of Monzen randomly contacted 2,000 citizens aged from 50 to 80 years. Of those, 214 had deceased or were unable to be contacted, leaving 1,786 from whom 1,105 (61.7% of the eligible) responded and were subsequently examined. For reporting prevalence, a further 67 cases were excluded due to lack of useful images; thus, 1,038 cases were re-evaluated (table 1).

Details of the other studies have been described elsewhere [4–6]. There were 1,045 participants in Iceland and 517 in Singapore. All subjects gave informed consent, and all procedures adhered to the provisions of the Helsinki declaration. From the above populations, cases aged from 50 to 69 years with grade 0 for cortical, nuclear and posterior subcapsular cataracts, according to the JCCESG system, were selected as subjects for LTP analysis. Since the WHO grade 0 for cortical and posterior subcapsular cataract includes the early stage of that type of opacity, we used the JCCESG system to investigate the characteristic change in transparent lenses. Cases with diabetes mellitus were excluded from the LTP study. The number of subjects for LTP analysis in Monzen, Singapore and Iceland was 147, 153 and 386, respectively (table 2).

All of the subjects in Monzen were Japanese, those in Iceland were Caucasian and 98% of those in Singapore were Chinese Singaporeans. The climatic environments of the survey locations are shown in table 3.

The same methodology was used for all the surveys. With a maximally dilated pupil, participants were examined by slitlamp microscopy, and Scheimpflug slit images of lenses were documented by the anterior eye segment analysis system [7] (EAS 1000, Nidek).

Methodology for the LTP Study

In order to calculate LTP, measurement of the lens thickness and densitometry for detecting the light scattering intensities were performed along the theoretical optical axis of the eye. As, in several eyes, pupil dilatation was not optimal and the whole lens thickness had increased with aging, it was impossible to detect the posterior capsule in some lenses. Since the authors have previously reported that there is a very high correlation ($r = 0.91$) between the anterior half of the lens and the full lens thickness [7], the distance from the anterior capsule to the central clear zone was used to indicate lens thickness. The intensity of light scattering was evaluated in 256 gray steps digital values for the three representative

Table 2. Number of cases with transparent lenses

	50s	60s	Total	Mean age ± SD years
Reykjavik				
Males	99 (170)	68 (108)	167 (278)	57.7 ± 6.0
Females	130 (223)	89 (143)	219 (366)	57.7 ± 5.6
All	229 (393)	157 (251)	386 (644)	57.7 ± 5.8
Singapore				
Males	45 (82)	15 (25)	60 (107)	56.5 ± 4.6
Females	68 (123)	25 (37)	93 (160)	55.8 ± 4.7
All	113 (205)	40 (62)	153 (267)	56.1 ± 4.7
Monzen				
Males	29 (52)	41 (70)	70 (122)	59.7 ± 4.8
Females	43 (81)	34 (62)	77 (143)	58.5 ± 5.4
All	72 (133)	75 (132)	147 (265)	59.1 ± 5.1

LTP analysis was performed for the cases with bilateral transparent lenses. Figures in parentheses indicate number of eyes.

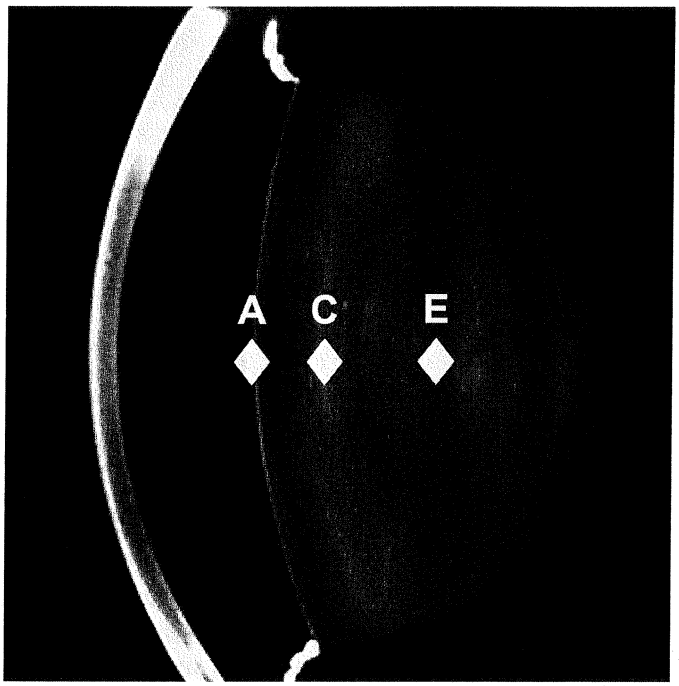

Fig. 1. The points of lens layers (A, C, E) where light scattering was measured: A = light scattering intensity of the anterior capsule; B = light scattering intensity of the anterior adult nucleus; C = light scattering intensity of the central clear zone.

Table 3. Location and climatic conditions of the three survey places

	Location	Altitude m	Annual average temperature °C	Relative humidity %	Rainfall mm/year	UVB kJ/m^2
Reykjavik	64°08' N 21°58' W	18.0	4.4	82	798	5.5
Singapore	0°17' N 103°51' E	32.0	26.7	84	2,172	29.2
Monzen	36°11' N 135°23' E	5.6	15.1	71	2,881	17.6

layers: A = the anterior capsular area including a part of the anterior clear zone of disjunction; C = the anterior adult nuclear area including a part of the deep cortical layer; E = the central clear zone (fig. 1). LTP was calculated from the light scattering intensities of the three lens layers and the distance of the layers according to the previous report [1]:

$$LTP = A + C \cdot AC + E \cdot AE,$$

where A, C and E refer to the light scattering intensities and AC and AE are the thicknesses of the lens layers.

Methodology for the Prevalence Study

Grading Definition of Lens Opacification. Photographed images from the Reykjavik Eye Study [4] and the Singapore-Japan Cooperative Cataract Study [5] were re-evaluated using the WHO system. In accordance with the new classification system, another item was added as grade CEN. This is where the central optical zone of 3 mm in diameter is involved in cortical opacification in which vacuoles, watercleft and congenital opacities are not included. The lenses of the Monzen Eye Study were also analyzed applying the WHO system. Although the original WHO grading system is aimed at observers utilizing slitlamp microscopes, the grading and classification in this study utilized documented Scheimpflug and retroillumination images.

Data collection and analysis were similar to the previous studies [4–6]: number of subjects with advanced lens opacities, opacity types and grades; if each eye of a subject had a different type of lens opacity at the same grade, classification was done for the right eye only; when comparing prevalences of the three main types of opacities, cortical, nuclear and subcapsular, if each eye had the same type of opacity at different grades, classification was done for the higher grade only.

In the previous studies, subjects with aphakia or pseudophakia in one or both eyes were excluded; however, in this study, subjects with phakia in at least one eye were included; thus, subject numbers in this study differ from the previous ones (table 4).

Statistics. For data analysis, Student's t, χ^2 and Mantel-Haenszel tests were applied.

Table 4. The number of analyzable subjects

Age, years	Reykjavik			Singapore			Monzen		
	males	females	total	males	females	total	males	females	total
50–59	165	191	356	84	127	211	71	120	191
60–69	142	210	352	107	115	222	153	213	366
70–79	115	129	244	42	31	73	135	169	304
≥80	33	43	76	5	5	10	17	16	33
Total	455	573	1,028	238	278	516	376	518	894

Table 5. Light scattering intensity TP at points A, C, E and the distance between A and E (means ± SD) in the three groups

	A, cct				C, cct				E, cct				AE, mm			
	50s		60s		50s		60s		50s		60s		50s		60s	
Reykjavik	116.2±15.4	**	129.5±18.4	*	144.4±33.0	**	184.3±38.8	n.s.	81.2±11.5	**	101.2±13.8	n.s.	2.28±0.17	**	2.42±0.18	**
Singapore	122.2±13.2	**	135.5±21.1	**	155.5±31.2	**	187.4±36.8	**	90.6±9.2	**	99.5±10.9	**	2.45±0.19	**	2.51±0.22	**
Monzen	99.7±15.7		106.7±15.8		132.9±29.5		161.2±31.7		72.8±9.1		81.2±11.1		2.45±0.21	n.s.	2.55±0.23	n.s.

cct = Computer-compatible tapes. * $p < 0.05$, ** $p < 0.01$.

Table 6. LTP of the three groups (means ± SD)

		50s				60s			
Reykjavik	Males	413.8±55.3	n.s.	**	n.s.	558.2±74.4	*	**	n.s.
	Females	423.7±64.0				538.8±72.3			
Singapore	Males	578.5±76.7	n.s.			660.9±85.5	n.s.		
	Females	578.1±72.9				672.6±81.4			
Monzen	Males	422.4±74.9	**	**		502.3±70.6	***	**	
	Females	395.7±64.1				465.3±70.1			

* $p < 0.05$, ** $p < 0.01$, *** $p < 0.005$.

Results

Comparison of LTP in the Three Subject Groups

Light scattering intensity in layers A, C and E increased with aging in all groups. In the three layers, light scattering intensity was significantly higher in the Singaporeans followed by the Icelandic subjects. Lens thickness was significantly thinner in the Icelanders than in the other two groups in their 50s and 60s (table 5).

LTP in the three groups increased linearly with aging (fig. 2a–c). The rate of increase in LTP was 11.8/year, 10.1/year and 11.1/year in the Icelanders, Japanese and Singaporean subjects, respectively.

Table 6 shows comparisons of LTP among the three groups for ages of 50s and 60s and gender. LTP was significantly higher than in Singaporeans followed by the Icelandic subjects. LTP in Japanese was the lowest among the groups.

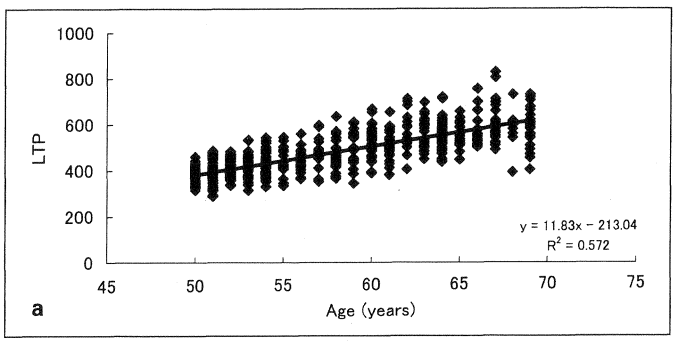

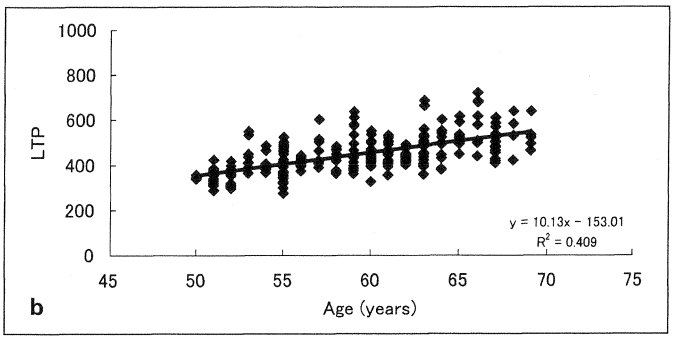

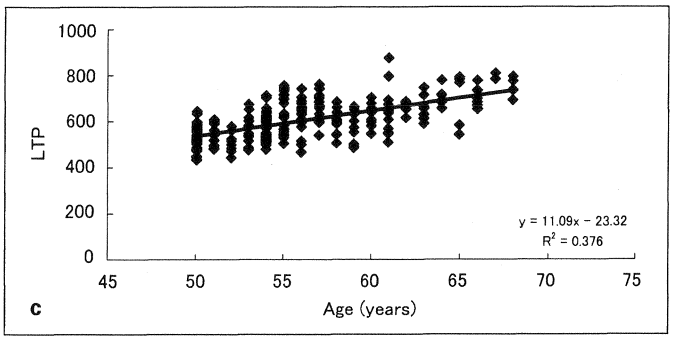

Fig. 2. Individual LTP in the subjects of Reykjavik (**a**), Monzen (**b**) and Singapore (**c**).

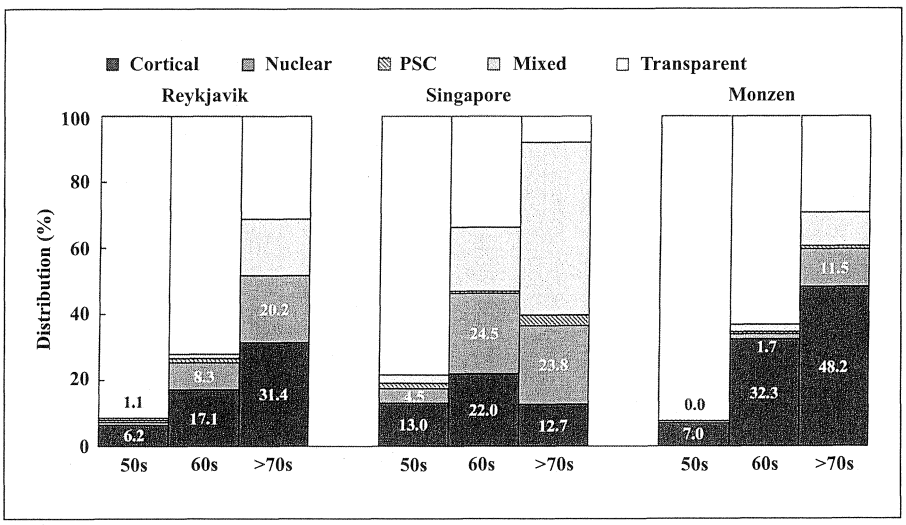

Fig. 3. Distribution of the three main pure types of lens opacification by age over 50 years. PSC = Posterior subcapsular cataract. Number in columns shows % of cortical and nuclear opacification.

Comparison of Lens Opacification Prevalence in the Three Subject Groups

Figure 3 shows the distribution of three main pure types and mixed types of opacification in the three subject groups by age.

The pure cortical type in Singaporeans was found in 13.0, 22.0 and 12.7% of subjects in their 50s, 60s and 70s, respectively. The Japanese displayed 7.0, 32.3 and 48.2%, and Icelanders 6.2, 17.1 and 31.4% similarly. The pure nuclear type was evident in 4.5, 24.5 and 23.8% of Singaporeans in their 50s, 60s and 70s. In the Japanese, prevalence was 1.7 and 11.5% in their 60s and 70s, and in Icelanders 1.1, 8.3 and 20.2% in their 50s, 60s and 70s, respectively. The prevalence of pure subcapsular opacification was quite rare in all groups. The prevalence of mixed type opacification in Singaporeans in their 60s and

Table 7. Prevalence (%) of three types of lens opacification of grades I–III and II–III

Subject groups		〈Cortical opacification〉									〈Nuclear opacification〉									〈Subcapsular opacification〉								
		Reykjavik			Singapore			Monzen			Reykjavik			Singapore			Monzen			Reykjavik			Singapore			Monzen		
Gender																												
Age (years)		M	F	M+F	M	F	M+F	M	F	M+F	M	F	M+F	M	F	M+F	M	F	M+F	M	F	M+F	M	F	M+F	M	F	M+F
	Gr.																											
50–59	I–III	7.9	5.8	6.7	11.0	20.0	16.4	8.5	7.6	7.9	1.8	1.6	1.7	11.3	6.6	8.4	0.0	0.0	0.0	0.0	1.6	0.8	6.0	1.6	3.4	1.4	0.0	0.5
	II–III	3.6	2.1	2.8	7.3	15.2	12.1	4.2	5.1	4.8	0.6	0.0	0.3	2.5	0.8	1.5	0.0	0.0	0.0	0.0	1.0	0.6	2.4	1.6	1.9	0.0	0.0	0.0
60–69	I–III	20.4	16.8	18.3	39.6	38.9	39.3	22.8	43.3	34.7	11.3	9.1	10.0	41.2	43.9	42.6	2.6	1.9	2.2	2.1	1.4	1.7	11.8	7.9	9.7	3.3	2.8	3.0
	II–III	11.3	12.5	12.0	34.7	28.3	31.3	16.1	32.7	25.8	4.2	2.9	3.4	15.5	10.3	12.7	2.0	1.0	1.4	1.4	0.5	0.9	8.8	4.4	6.5	1.3	0.9	1.1
70–	I–III	46.0	54.0	50.2	48.6	63.3	55.4	55.7	59.0	57.5	33.3	42.8	38.2	74.4	82.8	77.9	22.4	18.3	20.2	4.3	5.3	4.8	48.6	30.0	40.3	5.7	4.4	5.0
	II–III	30.9	36.0	33.6	45.7	40.0	43.1	42.1	45.8	44.1	16.3	13.8	15.0	51.3	51.7	51.5	9.8	9.5	9.6	2.9	3.3	3.1	21.6	26.7	23.9	2.9	3.1	3.0

* $p < 0.05$, ** $p < 0.01$.

Table 8. Prevalence (%) of grade CEN of cortical opacification

Age	Reykjavik			Singapore			Monzen		
	males	females	both	males	females	both	males	females	both
50–59 years	4.8	1.6	3.1	4.8	15.7	11.4	2.8	5.0	4.2
60–69 years	12.7	13.8	13.4	24.3	27.8	26.1	10.5	25.4	19.1
70–79 years	33.0	38.8	36.1	31.0	32.3	31.5	31.9	40.2	36.5
≥80 years	54.5	51.2	52.6	20.0	80.0	50.0	47.1	25.0	36.4

* $p < 0.05$, ** $p < 0.01$, *** $p < 0.005$.

70s was markedly higher than in the Japanese and Icelanders of the same age. In both Japanese and Icelandic subject groups, the pure type of cortical cataract increased with aging. In particular, Japanese aged over 70 years showed a quite high percentage of 48.2%.

Table 7 shows the distribution of the three main types of opacities by age, gender and grade. This analysis was different from the distribution of pure type. In cases where subjects had more than one type of opacity, each type was picked up. Overall, the prevalence of all three types increased with aging. In detail, cortical opacification in Singaporeans was significantly higher than in Japanese and Icelanders; furthermore, a significant difference in prevalence between Asians and Caucasians was observed for ages 60–69 where no significant difference was observed between the two Asian groups. The cortical type predominated in Japanese and Icelanders of all ages, whereas it was only dominant for Singaporeans in their 50s and grade II–III of those in their 60s. Regarding the central optical zone involvement shown in table 8, the prevalence of grade CEN was significantly higher in the Singaporeans than the other two nationalities in their 50s and 60s.

Interestingly (table 7), the prevalence of nuclear opacification in Singaporeans was markedly higher than that in the other two nationalities for any age. A prevalence of

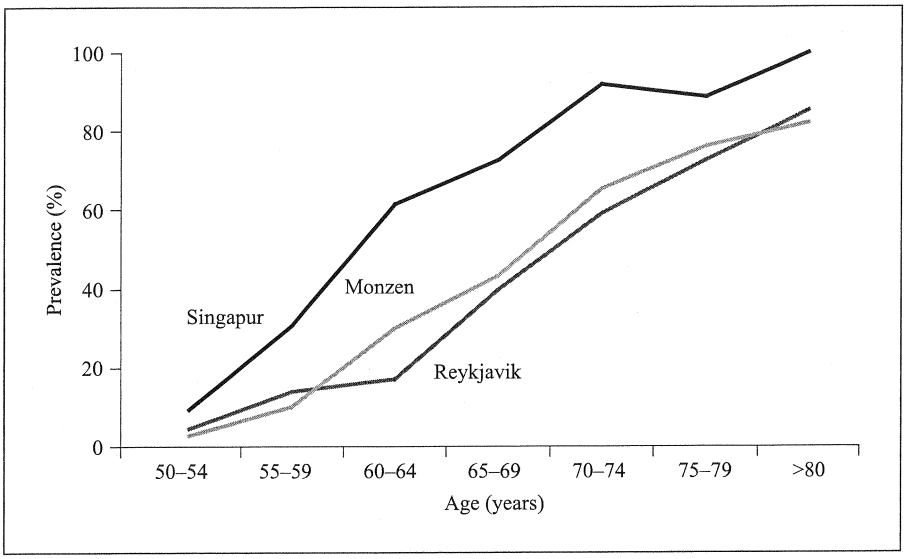

Fig. 4. Prevalence of lens opacification in the three subject groups including whole types with over grade I.

progressed nuclear opacification (grade II and over) was not detected in the Japanese and Icelandic groups aged 50–59, and no significant difference at this grade existed between Japanese and Icelanders aged 60–69; however, at this age these subjects showed a significant difference in prevalence of nuclear opacification of grades I–III.

Although the prevalence of subcapsular opacification was very low in all nationalities and age groups, that seen in Singaporeans was significantly higher ($p < 0.05$, $p < 0.01$) than those of the other two groups at every age.

Discussion

Among the majority of recent large-scale cataract epidemiologic studies, there are almost no discussions about lens transparency changes with age from the standpoint of lens research. Vrensen and Willekens [8] showed that transparent lenses themselves reveal important information regarding their future processes. Later, Fujisawa and Sasaki [9] reported that light scattering intensity in lens layers detected from Scheimpflug slit images increased exponentially with age and estimated that the decreasing ratio might accelerate from as early as the middle 40s and there might exist racial differences. Based on the above investigation, Sasaki et al. [1] proposed the concept of LTP in 1999. Since this index is a useful measure of lens clarity in relation to age, the authors aimed to reveal characteristics of LTP in the three different racial groups Japanese, Chinese-Singaporeans and Icelanders. There was a high correlation of LTP increase with age for all three groups. This result shows that LTP is an appropriate index to evaluate age-related changes in transparent lenses.

Since the prevalence of nuclear cataract was significantly higher in Singaporeans compared to the other races, the authors presume that the significantly higher LTP seen in the Singaporean subjects showed that the transparent lenses in Singaporeans are more aged than those of the Japanese and Icelanders and are at higher risk of lens opacification, especially nuclear cataract. Although there was no significant difference in LTP between the Japanese and Icelanders, it was higher in Icelanders than in Japanese in their 60s, which might indicate the higher prevalence of nuclear cataract in Icelanders than that in Japanese. Regarding gender differences, male Japanese in their 50s and 60s showed significantly higher values of LTP than the respective females. The prevalence of nuclear cataract was slightly higher in males than in females in their 60s, which might correlate with this difference. Furthermore, we found that, in the subjects who were followed up for more than 5 years, the incidence of early lens opacity was higher in those with high LTP for age and that it was very low in those with low LTP for age (unpublished data). Although further investigation is needed, we assume that LTP may be a useful tool for the early diagnosis of cataract.

In the mid 1990s, the WHO working group established a new worldwide unified cataract classification system that was officially released in 2002 [2]. Although this system lends itself to observations of actual slitlamp images, we had to convert data from judgments of photographed

images from our previous studies for the present study. Intraobserver and interobserver agreement of the classification of photographed images with the WHO system was 95.0% with a κ value of 0.925, and 77.5% with a κ value of 0.700 for cortical cataract, 91.9% with a κ value of 0.851 and 82.4% with a κ value of 0.763 for nuclear cataract and 92.6% with a κ value of 0.876 and 88.4% with a κ value of 0.824 for posterior subcapsular cataract, respectively. The above results suggest that without very high-quality lens images from Scheimpflug or retroillumination photographs, this conversion would have been impossible. This kind of conversion had only been recommended in special cases, but from now, researchers are recommended to use this world unified classification system together with their own classification system if the latter is required. In fact Dr. West, a contributor to the development of the new WHO system, was first to apply the WHO system in a survey of cataract epidemiology in an African population [10]. We hope that such comparative studies will become commonplace in the field of cataract epidemiology research in the near future. Another characteristic of the WHO grading system, the one for grading cortical opacification with central optical zone involvement (CEN), correlates very well with visual acuity. Grading of CEN may become a useful indicator in judging visual impairment not only in epidemiologic studies, but in daily clinical use.

Since discussion about the prevalence of lens opacification in the three subject groups has previously been covered [4–6], only the main characteristic points are briefly mentioned in this article. As shown in figure 4, the prevalence of lens opacification of grade over I in the three subject groups seems to correspond with LTP change with aging. The increase in prevalence in both Japanese and Icelanders aged over 55 years shows almost the same pattern. On the other hand, prevalence in the Singaporeans is markedly higher than that of the other two groups. Figure 4 suggests that the progression rate of lens opacification in Singaporeans might be faster than that of Japanese and Icelanders. The comparison of age-related change in the prevalence of pure cortical cataract shows a characteristic result (fig. 3). The prevalence in Japanese and Icelanders increased with aging; however, the Singaporeans did not display the same tendency. The prevalence of the pure type of cortical cataract in 12.7% of Singaporeans in their 70s would be quite meaningful. In the prevalence of 52.4% of mixed type in Singaporeans aged over 70 years, the rate of cortical opacification was included; however, the high value of 48.2% pure type cortical opacity prevalence in Japanese over 70 years might be specific to the Japanese race. Among the three main types of opacities, cortical cataract was the predominant type in Japanese and Icelanders in their 50s, 60s and over 70s.

Icelanders as Caucasians and Japanese as Asians showed the same tendency for prevalence of age-related opacification, but it should be noted that the Japanese and Singaporeans, both Asians, did not. Solar UV exposure rather than race could be considered as one of the risk factors for cortical cataract formation and/or progression. As shown in table 3, the irradiation dose of UVB was 5.5 kJ/m^2 in Reykjavik/Iceland, 29.2 kJ/m^2 in Singapore and 17.6 kJ/m^2 in Monzen/Japan. The irradiation dose in Singapore is 5.3 times higher and in Monzen/Japan 3.2 times higher than in Reykjavik/Iceland. Although we cannot simply state that this shows a relationship between dose of solar UV irradiation and prevalence of cortical opacification in the general population for a corresponding area, the significantly higher prevalence of cortical opacification in Singaporeans in their 50s and 60s was particularly interesting for us having been strongly involved in UV-related lens research. The prevalence of nuclear opacity in Singaporeans was significantly higher than in the other subjects for all age groups. The prevalence in Icelanders in their 60s and over 70s was higher than in Japanese ($p < 0.01$) but that in Singaporeans was remarkably higher. We conducted similar cataract epidemiologic surveys in several locations in Japan including the subtropical Amami islands [6, 11]. Including the above studies, we knew that before the prevalence of nuclear opacification exceeded 50% of subjects, it increased 2.1–5.4 times per decade [6]. This result may suggest that once nuclear opacification has started in a population, it increases rapidly with aging. In Singaporeans, 8.4% of participants developed nuclear opacity in their 50s, and prevalence reached 42.6% in their 60s. The high prevalence of nuclear opacification at a rather young age is an important indicator for a high prevalence after the age of 60. This tendency is reported for the general population of Sumatra, Indonesia [12]. Furthermore, climatically different places in Japan, i.e. Hokkaido in the north, Noto in the central area and Okinawa in the south, have been compared [11], and the prevalence of nuclear opacity in the population of Okinawa was found to be significantly higher than that of the two other places. Based on all of the above studies, we are able to state that the general population living in tropical and subtropical areas is at a high risk for developing nuclear lens opacity at a rather early age. West et al. [13] reported that Caucasians were significantly more likely to have nuclear opacification

than African Americans. However, another study in an African (Tanzanian) population performed by Congdon et al. [10], using the new WHO classification system, reported a prevalence of nuclear cataract (grade I and over) in Tanzanians in their 50s, 60s and over 70 years of 13.2, 28 and 59.2%, respectively. The corresponding prevalence in the Singaporeans in this study was 8.4, 42.6 and 77.9% (table 7). In contrast, their reported prevalence of cortical opacification in Tanzanians was different from ours (8.0, 17.0 and 23.5% for the 50s, 60s and over 70 years) [10]. Since both studies applied the same classification system, the data are comparable. We do not have enough information about the climatic conditions and life style in Tanzania; however, their prevalence of nuclear opacification showed a similarity to that of the Singaporeans.

Regarding the effect of high environmental temperatures on cataract, few studies have been done [14]. A high ambient temperature in daily life might be said to accelerate the aging process of inhabitants. The high prevalence of nuclear opacification or the high value of LTP in Singaporeans might possibly have been influenced by such conditions. Separately from the above speculation, Kojima et al. [15] observed that the light scattering intensity in the nuclear part of rat lenses was significantly higher in the rats kept at a higher ambient temperature (35.2 ± 2°C) than those kept at their usual temperature (24 ± 2°C) after 78 weeks. They stated that paying attention to the effects of temperature on the lens is worthwhile [15].

Although further epidemiologic and experimental investigations are scheduled, at present, the authors hold the view that the high prevalence of nuclear opacification in the Singaporeans was not specifically related to race but rather to environmental conditions.

Acknowledgements

This article was part of an Ophthalmic Research Lecture given by K.S. at the EVER 2003 meeting. On behalf of the authors, K. Sasaki would like to thank the committee members of EVER 2003 for that honorable occasion.

The international co-work studies were carried out by the Kanazawa Medical University Cataract Study Group, the Reykjavik Eye Study Group of the Department of Ophthalmology, Iceland University, and the Singapore-Japan Cooperative Cataract Study Group. The authors express their sincere gratitude to all parties for their contribution to these studies.

This research was supported by a Grant-in-Aid for Scientific Research (C) from the MEXT (15591880) and a Grant for Promoted Research from the Kanazawa Medical University (S2003-6).

References

1 Sasaki H, Hockwin O, Kasuga T, Nagai K, Sakamoto Y, Sasaki K: An index for human lens transparency related to age and lens layers: Comparison between normal volunteers and diabetic patients with still clear lens. Ophthalmic Res 1999;31:93–103.

2 Thylefors B, Chylack LT Jr, Konyama K, Sasaki K, Sperduto R, Taylor HR, West S: A simplified cataract grading system: The WHO Cataract Grading Group. Ophthalmic Epidemiol 2002;9:83–95.

3 Sasaki K, Shibata T, Obazawa H, Fujuwara T, Kogure F, Obara Y, Itoi M, Katou K, Akiyama K, Okuyama S: Classification for cataract: Application by Japanese Cooperative Cataract Epidemiology Study Group. Ophthalmic Res 1990;22(suppl):46–50.

4 Sasaki H, Jonasson F, Kojima M, Katoh N, Ono M, Takahashi N, Sasaki K: The Reykjavik Eye Study – Prevalence of lens opacification with reference to identical Japanese studies. Ophthalmologica 2000;214:412–420.

5 Sasaki H, Shui YB, Kojima M, Chew SJ, Ono M, Katoh N, Cheng HM, Takahashi N, Sasaki K: Characteristics of cataract in the Chinese Singaporeans. J Epidemiol 2001;11:16–23.

6 Sasaki H, Jonasson F, Shui YB, Kojima M, Ono M, Cheng HM, Takahashi N, Sasaki K: High prevalence of nuclear cataract in the population of tropical and subtropical areas; in Hockwin O, Kojima M, Takahashi N, Sliney DH (eds): Progress in Lens and Cataract Research. Dev Ophthalmol. Basel, Karger, 2002, vol 35, pp 60–69.

7 Sasaki K, Shibata T, Sakamoto Y, Emori Y: The multi-purpose camera: A new anterior eye segment analysis system. Ophthalmic Res 1990;22(suppl):3–8.

8 Vrensen G, Willekens B: Classification and prevalence of early senile lens opacities in human donor eyes; in Hockwin O, Sasaki K, Leske MC (eds): Risk Factors for Cataract Development. Dev Ophthalmol. Basel, Karger, 1989, vol 17, pp 181–187.

9 Fujisawa K, Sasaki K: Changes in light scattering intensity of the transparent lenses of subjects selected from population-based surveys depending on age: Analysis through Scheimpflug images. Ophtalmic Res 1995;27:89–101.

10 Congdon N, West SK, Bubrmann RR, Kouzis A, Munoz B, Mkocha H: Prevalence of the different type of age-related cataract in African population. Invest Ophthalmol Vis Sci 2001; 42:2478–2482.

11 Sasaki K, Ono M, Aoki K, Katou N, Morine Y, Nakaizumi H, Fujisawa K, Kojima M, Sakamoto Y, Hatano T: Cataract epidemiology survey in three different areas in Japan – Prevalence of cataract and types of lens opacification. J Jpn Ophthalmol Soc 1995;99: 204–211.

12 Sasaki K, Zainuddin J, Fujisawa K, Kojima M, Sakamoto Y: Cataract epidemiology study in West Sumatra; in Hockwin O, Sasaki K, Leske MC (eds): Risk Factors for Cataract Development. Dev Ophthalmol. Basel, Karger, 1980, vol 17, pp 26–32.

13 West SK, Munoz B, Schein OD, Duncan DD, Rubin GS: Racial differences in lens opacities: The Salisbury Eye Evaluation (SEE) Project. Am J Epidemiol 1998;148:1033–1039.

14 Miranda MN: Environmental temperature and senile cataract. Trans Am Ophthalmol Soc 1980;78:255–264.

15 Kojima M, Okuno T, Miyakashi M, Sasaki K: Effect of environmental temperature on cataract progression in an experimental cataract rat model; in Hockwin O, Kojima M, Sliney DH (eds): Progress in Lens and Cataract Research. Dev Ophthalmol. Basel, Karger, 2002, vol 35, pp 125–134.

1．研究課題名：敗血症血管におけるαカテコラミン受容体刺激時の平滑筋収縮および内皮機能変化の検討（研究番号 S2003-7）

2．キーワード：1）内皮細胞由来弛緩因子（EDRF; endothelium-derived relaxing factor）
2）内皮細胞由来過分極因子
（EDHF; endothelium- derived hyperpolarizing factor）
3）αアドレナリン受容体（alfa-adrenergic receptor）
4）βアドレナリン受容体（alfa-adrenergic receptor）
5）敗血症（sepsis）

3．研究者氏名：関　純彦・医学部・助教授・侵襲制御学(麻酔学)

4．研究目的

敗血症性ショックでは、カテコラミンα受容体刺激薬による血管収縮反応が減弱することが知られている。その機序として、平滑筋での誘導型一酸化窒素（NO）産生による血管拡張反応、活性酸素によるカテコラミンα受容体の不活化、平滑筋収縮機構自体の破綻などが考えられているが、敗血症の進行度や血管の部位によって機序が異なる可能性がある。

正常血管におけるカテコラミンα受容体刺激による収縮では、同時に血管内皮細胞の NO 産生も増加し、収縮を抑制する方向に働くことで血管の緊張性が調節されている。一方、敗血症時の血管内皮機能の変化はあまり知られておらず、カテコラミンα受容体性収縮に内皮がどのような影響を与えているのかは不明である。

そこで本研究では、ラット腹膜炎敗血症モデルから大動脈および微小腸間膜動脈を摘出し、カテコラミンα受容体刺激薬フェニレフリンによる収縮反応を観察し、内皮機能との関係を検討する。

また、実際の臨床現場では、敗血症性ショック時には血管拡張作用を持つカテコラミンβ受容体刺激薬や鎮静薬プロポフォールがよく用いられる。そこで、フェニレフリン前収縮状態の血管で、これらの薬剤の血管拡張作用がどのように変化するのかも合わせて検討する。

5．研究計画

(1)腹膜炎敗血症ラットの作成

12 時間絶食としたラットをセボフルラン麻酔下に開腹し、虫垂を取り出して結紮するとともに 2 カ所に穿孔を開け、閉腹する。対象群（シャム手術群）では、同様に開腹し虫垂を取り出すが、何も操作を加えないままに閉腹する。12 時間、または 24 時間経過したラットを実験に用いる。

(2)大動脈実験

胸部大動脈を摘出し、長さ約 5 mm のリング状標本を作成する。一部は内腔を綿棒で擦って内皮を除去する。オルガン・バスを 25 ml の栄養液で満たす。リング状切片の一端はオルガン・バスの底に固定し、他端は張力トランスデューサーに接続する。標本に至適静止張力（約 2g）をかけた後、60 mM KCl で収縮を確認する。通常の栄養液に置換し張力が前値に復した後、実験を開始する。

フェニレフリン（10^{-8} −10^{-4} M）を累積投与し、その張力変化を記録する。内皮温存標本において収縮反応減弱が観察された場合、NO 合成酵素阻害薬（L-NAME）、誘導型 NO 合成酵素阻害薬を前投与し、収縮反応減弱が改善するかどうかを検討する。また、フェニレフリンによる前収縮後、β_1受容体刺激薬であるドブタミン（10^{-9} - 10^{-5} M）またはβ_2受容体刺激薬であるサルブタモール（10^{-9} - 10^{-5} M）を累積的に投与し、拡張反応を観察する。

(3)微小腸間膜動脈実験

直径 200μm 以下の腸間膜動脈を摘出し、長さ約 10 mm の標本を作成する。一部標本では、内皮を擦過して除去する。採取した血管標本の両端に微小ガラス・ピペットを挿入し、微小血管チャンバー内で、灌流圧・流量制御ポンプにて内圧を一定に保つ。灌流圧は、灌流圧モニターで監視する。顕微鏡に装着した CCD カメラにて観察し、壁厚と内径の変化を測定・記録する。

血管内圧を 60mmHg で一定に制御し、フェニレフリンを累積的に投与する。次に内皮温存標本にて、NO 合成酵素阻害薬（L-NAME）およびプロスタサイクリン産生を阻害する薬剤（シクロオキシゲナーゼ阻害薬、インドメタシン）を同時に前投与した状態でフェニレフリンを累積的に投与する。また、この反応に麻酔薬プロポフォールがどのように影響するのかを検討する。

6．研究成果

(1)大動脈におけるフェニレフリン収縮の変化

対照群では、２回目、３回目のフェニレフリン累積投与においても１回目と同様の反応を示したが、24 時間後の敗血症モデルの内皮温存標本では、１回目の収縮反応に比較し、２回目、３回目の収縮が有意に抑制されるという現象が観察された。このフェニレフリン反復投与による収縮反応の減弱は、内皮除去標本では全く認めなかった。敗血症群におけるフェニレフリン反復投与時の収縮反応減弱は、L-NAME あるいはアミノグアニジンを前投与すると観察されなかった。

(2)大動脈におけるβ受容体刺激薬による拡張反応の変化

対照群では、内皮除去によりドブタミンによる拡張反応が大きく抑制されたが、サルブタモールによる拡張反応の抑制は軽度であった。12 時間後の敗血症群におけるドブタミンの拡張反応は、内皮の有無に係わらず、対照群と比較して差はなかった。内

皮温存標本におけるサルブタモールの血管拡張反応は、対照群と比較して敗血症群で有意に抑制された。しかし、内皮除去標本では、対照群と差がなかった。

(3)微小腸間膜動脈におけるフェニレフリン収縮の変化

微小腸間膜動脈も大動脈同様フェニレフリンによって濃度依存性に収縮したが、高濃度では収縮弛緩を繰り返す律動運動を呈した。この律動運動は内皮除去で消失するが L-NAME およびインドメタシンを同時に前投与しても完全には消失せず、カルシウム感受性カリウムチャネルの阻害薬（カリブドトキシン、アパミン）投与で消失する。このことから、律動には EDHF が関与している可能性が強い。

敗血症モデルにおける EDHF 依存性律動の観察は今回の研究の目的のひとつであったが、微小細動脈は敗血症による平滑筋細胞自体の障害が大きく標本化が困難であるため、まだ観察できていない。

(4) 微小腸間膜動脈におけるプロポフォールの影響

敗血症モデルにおける微小腸間膜動脈の標本化が困難であったため、対照群でのみフェニレフリン収縮に及ぼすプロポフォールの影響を観察した。その結果、臨床使用濃度（10^{-5} - 10^{-6} M）のプロポフォールはフェニレフリンによる収縮そのものには影響を与えないが、EDHF 依存性律動運動を明らかに増強するという新たな知見を得た。

7．研究の考察・反省

前項目（1）の結果から、腹膜炎 24 時間後の敗血症では、まず内皮に誘導型 NO 合成酵素が誘導され、これによる NO 産生がフェニレフリン収縮反応を減弱させると予想される。血管内皮には主に β_1 受容体が存在すると言われているが、（2）の結果から、内皮依存性拡張には内皮 β_2 受容体も弱いながら介在しており、腹膜炎 12 時間後ではまず内皮 β_2 受容体が障害を受けると推察される。また、（4）の結果から微小腸間膜動脈においてプロポフォールは EDHF 反応を増強させる可能性があることが示唆された。

（1）の結果に引き続き、現在内皮細胞への好中球集積や誘導型 NO 合成酵素の発現など、病理学的・生化学的な検討を加え、さらに収縮反応減弱の機序を解明する予定である。現在のところ敗血症モデルでの微小腸間膜動脈の標本化が達成できていない。したがって今後は敗血症モデルでの微小腸間膜動脈標本化に力を入れ、EDHF 依存性律動は敗血症で影響を受けるのか、またその時のプロポフォールの増強作用はどうなるのか、研究を進めていく必要があると考えている。

8．研究発表

現在、（3）（4）の結果について投稿準備中である。（1）（2）の結果についてはさらに病理学的・生化学的な検討を加え、１－２年以内に投稿する予定である。

1．研究課題名：IL-2 投与が肺胞上皮細胞の分子生物学的機能特性に及ぼす影響に関する研究
（研究番号 S2003-8）

2．キーワード：1）癌免疫療法（cancer immunotherapy）
2）肺水腫（pulmonary edema）
3）肺胞上皮水分クリアランス（alveolar fluid clearance, AFC）

3．研究者氏名：杉田　真・医学部・講師・呼吸機能治療学（呼吸器外科）

4．研究目的

【背景】遺伝子組み換え技術によって作成されたインターロイキン－２（IL－２）製剤を用いた免疫療法が、腎細胞癌、悪性黒色腫、血管肉腫等の悪性腫瘍と、その転移巣に対して、著明な抗腫瘍作用を有することが知られている。しかし、IL－２製剤投与では、25％程度の確率で重篤な肺水腫を発症させ、この副作用が大きな障壁となっている。これまでの基礎研究では、IL－２の全身投与は急性肺傷害を惹起し、これがこの肺水腫成立の原因である可能性が示唆されてきた。しかし、詳細なメカニズムに関してはいまだに不明である。一方、近年の研究により、肺胞上皮細胞の Na イオン輸送に依存する水分輸送能が、肺の水分バランス、さらには肺水腫からの回復に中心的な役割を担っていることが明確になってきている。また、肺胞上皮細胞の機能特性は各種サイトカインに影響を受け、肺胞上皮細胞には IL－２受容体が存在し、免疫担当細胞の制御を受ける可能性が示唆されている。

【研究目的】IL－２投与が肺胞上皮細胞の分子生物学的機能特性に及ぼす影響を詳細に検討し、より安全な免疫療法の確立を目指す事である。第一に、生理学的手法を用いて、IL－２投与が肺胞上皮細胞の水分輸送能に及ぼす影響を検討し、第二に、これら生理学的影響に関して、その詳細なメカニズムを分子生物学的に解明することである。そして、究極的には、より安全な癌免疫療法の確立を目指す事である。

5．研究計画

【実験項目１】ラットを用い、アドレナリン受容体刺激によって、肺胞上皮細胞の水分輸送能が上昇するか否かを検討する。肺水腫の治療において、気道内へのアドレナリン受容体刺激物質の投与が有望である可能性が示唆されているが、α受容体への刺激に関するデータはいまだに少ない。よって、*in vivo* のレベルにおいて、IL－２投与によって惹起される肺水腫に対する治療の可能性として、α受容体の投与が、肺胞上皮細胞の水分輸送能に与える影響に関して実験を行う。肺胞上皮細胞の水分輸送能の量的な判定には、肺胞水分クリアランスを用いる。肺胞水分クリアランスの測定は、肺循環の影響を除外するために、ラットと犠牲死させた直後に心肺を一塊として摘出し、体外（*ex vivo*）にて行う（以後の実験項目でも同様の方法を用いる）。

【実験項目２】ラットに各種濃度の IL－２を投与し、肺水腫の程度を検討する。IL－２投与が、肺胞上皮細胞の水分輸送能に与える影響に関しては、肺胞水分クリアランスにて判定する。

【実験項目３】IL－２投与による肺胞水分クリアランスの変化の詳細に関しメカニズムを生理学的に明らかにする目的に、Na^+ channel ならびに Na^+-K^+-ATPase の阻害薬を用いて、さらにはその他のチャンネルブロッカーや刺激薬を用いて検討する。

【実験項目４】IL-２投与が肺胞上皮細胞の機能に及ぼす影響を分子生物学的に検討する。肺胞上皮細胞の Na^+ channel ならびに Na^+-K^+-ATPase に規定されることが知られている。そこで、IL-２投与が、Na^+ channel ならびに Na^+-K^+-ATPase の発現に与える影響を検討する。タンパクの発現の変化と mRNA の発現の変化を検討する。

６．研究成果

【実験項目１】肺水腫の治療として有望と考えるα1アドレナリン受容体刺激であるフェニレフリンを気道内に投与し、肺胞水分クリアランスに及ぼす影響を検討した。

a)　フェニレフリンの濃度依存性の肺胞水分クリアランスが上昇する結果を得た。

b)　α1アドレナリン受容体刺激役の拮抗薬であるプラゾシンとα2アドレナリン受容体刺激役の拮抗薬であるヨヒンビンを同時に投与し肺胞水分クリアランスを測定した。その結果、プラゾシンを投与することによって、フェニレフリンによって得られる肺胞水分クリアランスの上昇を抑制することが可能であった

c)　ヨヒンビン投与は、肺胞水分クリアランスの上昇を抑制することができなかった。

以上の結果より、α1アドレナリン受容体刺激であるフェニレフリンが、肺胞上皮細胞の水分輸送能を有意に上昇させることが明らかになり、肺水腫に対する治療薬として有望であることが分かった。

【実験項目２】気道内に IL-２を直接投与して、肺胞上皮水分輸送能に関して、肺胞水分クリアランスを測定することで生理学的な影響を検討した。

a)　気道内に IL-２を 50IU/ml～10^4IU/ml の濃度で投与し、肺胞上皮細胞の水分輸送能の指標として、肺胞水分クリアランスを測定した。その結果、濃度依存性に肺胞水分クリアランスが上昇し、0.5×10^4IU/ml 以上の濃度では、有意に肺胞水分クリアランスが亢進することが明らかになった。

以上の結果より、IL-２投与は濃度依存性に肺胞水分クリアランスを亢進させ、肺胞上皮水分輸送能を亢進させることが明らかになった。

【実験項目３】気道内に各種刺激薬、阻害薬を直接投与して、肺胞上皮水分輸送能に関して、肺胞水分クリアランスを測定することで生理学的な影響を検討した。

a)　β受容体に対する刺激薬であるテルブタリン（10^{-5}M）投与でも同程度の肺胞水分クリアランスの亢進を認めることを確認した。

b)　テルブタリン（10^{-5}M）と IL－２（10^4IU/ml）を同時に投与しても、肺胞水分クリアランスは相乗的に亢進することはなかった。

c)　β受容体の阻害薬であるプロプラノロール（10^{-4}M）を同時に投与すると、テルブタリン投与群では肺胞水分クリアランスの亢進が有意に抑制されたが、IL-２群では肺胞水分クリアランスの亢進は抑制されなかった。

以上の結果より、IL-２投与による肺胞水分輸送能の亢進はβ受容体を介さないメカニズムであることが示唆された。

【実験項目４】現在、Na^+ channel の阻害薬であるアミロライドを用いて実験を進めており、この肺胞水分クリアランスの亢進がアミロライド感受性の Na^+ channel を介しているか否かを検討している。今後、これまでの生理学的な実験結果をふまえて、各種膜タンパクの変化に関してタンパクレベル（ウエスタン・ブロッティングを用いる）と mRNA レベル（Real Time PCR を用いる）にて検討する予定である。

7．研究の考察・反省

これまでの臨床報告、研究報告によると、IL-２を血管内に投与した場合、肺水腫が惹起されることが明らかになっていた。しかし、その詳細なメカニズムに関しては不明であった。今回の研究では、IL-２を気道内に直接投与し、さらに、*ex vivo*にて肺胞水分クリアランスを測定することにより、IL-２が血管内皮細胞に及ぼす影響を除外し、肺胞上皮細胞の水分輸送機能に直接及ぼす影響に関して詳細に検討することが可能であった。その結果、IL-２は肺胞上皮細胞の水分輸送能を亢進させることが明らかになった。さらに、この亢進のメカニズムは、β受容体を介さないことが示唆された。

本研究の結果は、これまでの知見と矛盾するようだが、すでに発表されている研究では、IL-２の血管内投与の影響を検討したものであり、血管内皮細胞の障害が大きく関与していると推測できる。すなわち、IL-２の全身投与は、血管内皮細胞障害を惹起し、血管透過性が亢進する事に起因する過性亢進型肺水腫が、その病態の本体である可能性が高いと考えることが可能である。そして、本研究の結果は、この内皮細胞障害に対して、肺胞上皮細胞は水分輸送能を亢進させて肺水腫の病態に対して保護的な作用を有している可能性が高いことを示唆する。今後、血管内皮細胞に及ぼす影響に関する研究を本研究と並行して行うことにより、より詳細な IL-２投与による肺水腫発生のメカニズムの詳細が明らかになることと思う。

反省点

a)　本研究は、国内および国外の学会で発表済み、もしくは予定している。ただし、論文の形式ではいまだに発表がない。現在、英文を作成中である。英文論文の完成が遅れており、大変に申し訳ないと思っている。

b)　予定していた実験の約 70%のみが達成されており、いまだに 30%程度が未達成である。今後、可及的にかつ慎重に残りの実験を遂行するように予定している。

1. 研究課題名：異なる感覚情報の大脳新皮質における統合機序及びその生後発達に関する研究（研究番号 S2003-9）

2. キーワード：1）大脳皮質味覚野（gustatory insular cortex）
2）大脳皮質口腔体性感覚野（oral somatosensory cortex）
3）膜電位振動（voltage oscillation）
4）カフェイン（caffeine）
5）ラット（rat）

3. 研究代表者名：吉村　弘・医学部・助教授・顎口腔機能病態学（口腔科学）

4. 研究目的

広義の味覚認知とは、純粋な基本味覚情報に、触覚、温度覚、浸透圧、刺激覚、さらには嗅覚や視覚などが加わった複合感覚として認識されるものと考えられる。この複合味覚認知や嗜好性は成長過程で一様ではなく、発達期前後で変化する。カフェインは嗜好性を有する苦味物質であるが、一方で強力な中枢神経作動薬としても知られており、脳における神経回路の機能を顕在化させるための有用な薬物である。我々の以前のカフェインを用いた研究により、情報伝達の場であるシナプスにおいて NMDA 受容体-Ca^{2+}誘発性 Ca^{2+}放出の機能連関が生後発達に伴って強化されることにより、大脳新皮質に振動性活動の発現することが明らかになった（Yoshimura, et. al, 2001、2002、2003）。そこで、本研究において、感覚認知と深くかかわっていると予想されている同期性膜電位振動現象を視点として、大脳皮質味覚野と口腔体性感覚野に焦点をあて、これら二つの大脳皮質間における機能的神経ネットワークの形成機序および生後発達にともなう機能獲得の様式について調べた。

5. 研究計画

＜平成 15 年度＞

内因性信号計測法を用いて、大脳皮質における味覚野を同定する。つぎに、電気生理学的計測と膜電位感受性色素を用いた光学的計測実験を相補的におこない、味覚、口腔体性感覚などの神経性入力がいかにして大脳皮質味覚野－口腔体性感覚野間の神経回路の発達・形成を促すのかについて、ラット脳スライスを用いて調べる。

＜平成 16 年度＞

味覚情報と視覚情報が融合する可能性のある脳梁膨大後野に注目し、この領域に存在する振動源の性質を調べる。さらに、異なる感覚情報が融合するために、膜電位振動現象がどのように関わっているのかを調べ、異なる感覚情報の統合機序や神経回路網発達の関係などを探る。

6. 研究成果

我々は、温度、触、圧などの体性感覚情報と味覚などの化学感覚情報の異なる感覚情報が、口腔という閉じた環境の中で融合することに注目した。内因性信号計測法という新手法をもちいて、2 種類の化学物質 NaCl と Sucrose に関して、化学感覚情報の空間的符号化が大脳島皮質に存在することを明らかにした（NeuroReport 2004, Yoshimura et al)。

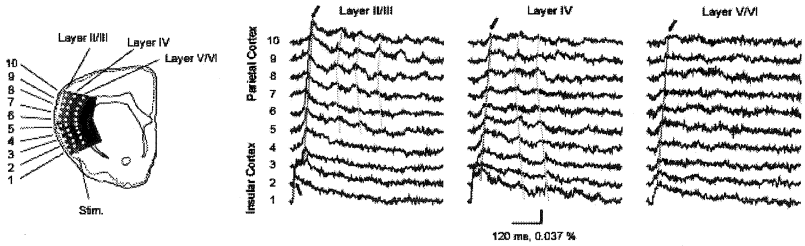

図 1　大脳皮質味覚野（島皮質）-口腔体性感覚野間の神経情報の往来（Brain Research 2004, Yoshimura et

脳における情報処理に重要な役割を演じているグルタミン酸受容体を、カフェインを用いて活性化させるという手法を用いて、味覚野-口腔体性感覚野間の情報伝播の動的な振る舞いを観察した。図 1 に示すように、味覚野からの信号が口腔体性感覚野へ伝播した後、口腔体性感覚野に振動性信号配信が出現した。味覚-口腔体性感覚野間の情報伝達は双方向性であり、また、振動現象は口腔体性感覚野で引き起こされることがわかった。ところが、幼弱期においては、味覚情報と口腔体性感覚情報を融合させるネットワークが形成されていなかった。この振動発生装置は生後発達に伴って獲得されることがわかった（図 2 参照)。

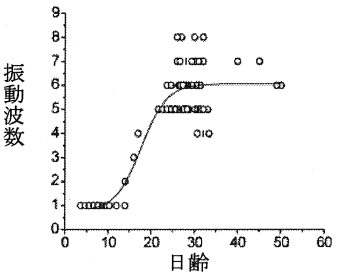

図 2　口腔体性感覚野における振動装置の生後発達

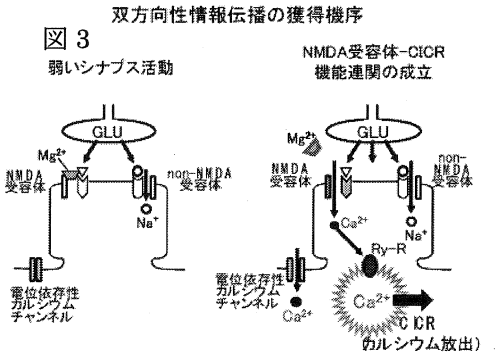

次に、脳における情報処理活動の中心的役割を演じている NMDA 受容体に注目し、細胞内カルシウム動態を調べたところ、幼弱期においては、NMDA 受容体と細胞内カルシウム放出の機能連関が未発達で、成長に従ってこの機能連関が強化され、味覚-口腔体性感覚野間の双方向性情報伝達が形成されてくる、ということが示唆された（図 3)。これらの結果より振動活動に依存する味覚-口腔体性感覚の情報連絡強化のメカニズムが示唆された（図 4)。

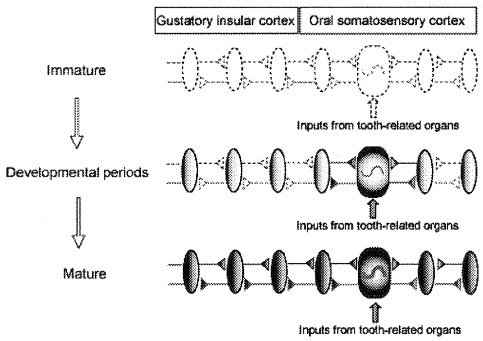

図4　振動活動依存性皮質情報伝播の強化機序
（上段）幼弱期；振動装置未発達。
（中段）発達期；振動装置が形成され、NMDA 受容体依存性信号の配信。
（下段）成熟期；味覚野-口腔体性感覚野間の神経連絡の強化。

味覚情報と視覚情報が融合する可能性のある脳梁膨大後野にも振動装置が存在していることがわかった（図 5)。脳梁膨大後野の振動装置が、中継装置として情報のやりとりを強化している可能性が示唆された。

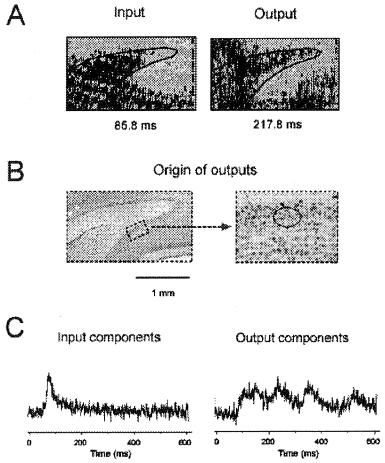

図5　脳梁膨大後野における入力信号および出力信号
(A) 内因性信号計測による入力および出力信号の画像化。出力は脳梁膨大後野の深層で発生している。(B) 振動発生源の細胞構築。(C) 入力および出力信号の膜電位波形。 振動性の出力が確認された。視覚情報をより遠方に伝播させるために、振動性活動が必要であった。
(Brain Research 2005 Yoshimura et al.)

7.　研究の考察・反省

「異なる情報を処理する大脳皮質間の連絡を強化するために、皮質振動中継装置が存在し、その振動装置は発達期に形成され、経験依存的にネットワークを形成する。」という概念は、今回の研究により始めて提唱された。従来の神経可塑性の概念をシナプスレベルから大脳皮質間ネットワークレベルに発展させることができた。奨励研究期間中に上記発見ができたことは有意義であった。今後さらに認知や嗜好性成立過程のメカニズムに迫るために、大脳新皮質-辺縁系の機能連関について調べていく必要がある。

8.　研究発表

Yoshimura H, Sugai T, Fukuda M, Segami N, Onoda N. Cortical spatial aspects of optical intrinsic signals in response to sucrose and NaCl stimuli. NeuroReport 2004; 15: 17-20. (MLDB)

Yoshimura H, Kato N, Sugai T, Honjo M, Sato J, Segami N, Onoda N. To-and-fro optical voltage signal propagation between the insular gustatory and parietal oral somatosensory areas in rat cortex slices. Brain Research 2004;1015: 114-121. (MLDB)

Yoshimura H, Sugai T, Segami N, Onoda N. Chemotopic arrangement for taste quality discrimination in the cortical taste area. Chemical Senses, 2005; Suppl1: i164-i165. (MLDB)

Yoshimura H, Sugai T, Segami N, Onoda N. Strengthening of non-NMDA receptor dependent horizontal pathways between primary and lateral secondary visual cortices after NMDA receptor-dependent oscillatory neural activities. Brain Research 2005; 1036: 60-69. (MLDB)

Yoshimura H, Sugai T, Honjo M, Segami N, Onoda N. NMDA receptor-dependent oscillatory signal outputs from the retrpsplenial cortex triggered by a non-NMDA receptor-dependent signal input from the visual cortex. Brain Research, 2005;1045: 12-21. (MLDB)

Cortical spatial aspects of optical intrinsic signals in response to sucrose and NaCl stimuli

Hiroshi Yoshimura,[1,2,CA] Tokio Sugai,[2] Mitsuhiro Fukuda,[3] Natsuki Segami[1] and Norihiko Onoda[2]

Departments of [1]Oral and Maxillofacial Surgery; [2]Physiology, Kanazawa Medical University, Uchinada-cho 920-0293; [3]Laboratory for Integrative Neural System, Brain Science Institute, RIKEN, Japan

[CA,1]Corresponding Author: hyoshimu@kanaza-med.ac.jp

Received 19 March 2003; accepted 24 April 2003

DOI: 10.1097/01.wnr.0000107520.38715.21

To examine whether cortical taste neurons use spatial codes for discriminating taste information, we investigated the spatial aspects of optical intrinsic signal (OIS) responses in the gustatory insular cortex (GC) elicited by the administration of two essential tastants, sucrose and NaCl, on the tongue. OIS responses to sucrose appeared in the rostral part of the GC, whereas those to NaCl appeared in the central part of the GC. Local anesthetization of the tongue abolished OIS responses, and the administration of distilled water elicited no OIS response. Thus, taste information elicited by sucrose and NaCl from the peripheral sensory organs is segregated in the GC, suggesting that the information from two essential tastants is assembled as spatial codes in the primary cortical taste area through the process of taste quality perception. *NeuroReport* 15:17–20 © 2004 Lippincott Williams & Wilkins.

Key words: Cortical taste area; Gustatory insular cortex; Guinea-pig; Spatial code

INTRODUCTION

Sucrose and NaCl are essential molecules for cell metabolism, and are essential appetitive tastants for feeding. Sensation and discrimination between the two tastants are indispensable when animals ingest foods for survival. In general, temporal and spatial codes of neural signals play a significant role in sensory information processing in the brain [1], and has been well established in visual information processing [2,3] and olfactory information processing [4,5]. As for taste information processing, controversy still exists as to whether cortical taste neurons use temporal codes or spatial codes for discriminating taste information in the cortical taste area. Recent electrophysiological studies revealed that many cortical taste neurons are multimodal [6–8], responding to several tastants or other sensory stimulation, and have an ability to discriminate source of information by the frequency code of firing [9,10]. These results suggest that temporal codes are involved in the discrimination of taste information. However, in order to discriminate taste information efficiently, cortical taste neurons may use spatial codes, as well as frequency codes. Previous electrophysiological studies predict that there is a chemotopic arrangement for taste quality discrimination in the cortical taste area [11], but this hypothesis has not been confirmed because of lacking for the evidence with high resolution of spatial dimension. Optical imaging based on intrinsic signals has a high spatial resolution [12], and is useful for studying the functional organization of the brain [13]. Using this imaging method, spatial aspects of neural activities in olfactory bulb [14], somatosensory cortex [15], auditory cortex [16] and visual cortex [17,18] have been reported. In the present study, we investigated the spatial aspects of optical intrinsic signal (OIS) responses in the gustatory insular cortex that were elicited by delivering a solution of appetitive tastants, sucrose and NaCl on the tongue.

MATERIALS AND METHODS

Guinea-pigs (350–450 g) were anesthetized with Na-barbiturate (35 mg/kg, i.p.). A specially designed head attachment was fixed to the skull with tiny stainless steel screws and dental cement, as described elsewhere [19]. The animal's head was fixed on the stereotaxic frame, and the insular cortex, including rhinal sulcus and medial central artery (MCA), was exposed with dura mater and a thinned skull. The heart rate, rectal temperature and pneumorate were monitored continuously. To prevent pain and discomfort, the need for additional anesthesia was monitored by EEG activity, and Na-barbiturate to maintain the animal in a drowsy state was administered as needed. Local anesthetics were applied periodically to the wound margin to avoid pain.

Optical intrinsic signals (OIS; absorption changes at 602 nm) were recorded from the insular cortex with a video camera (CS8310, Tokyo Electronic Industry, Tokyo, Japan). The imaged area was $3.7 \times 5.9\,mm^2$ and contained 137×216 pixels. The focusing depth was adjusted to 400–450 μm below the cortical surface. Gustatory stimulation was administered by delivering a solution of sucrose and NaCl, respectively, on the tongue in the oral cavity. For control experiments, distilled water (DW) was administered instead of tastant solution. The trials were repeated 8–10 times, and

each trial consisted of a pair of records with and without a stimulation session. During the inter-trial period, the oral cavity was washed with DW. Data were collected for 7 s with a frame length of 500 ms (14 frames/record). In the stimulating session, the stimulation was applied at frames 3–14, i.e. the stimulation was continued for 6 s.

Data analysis was performed using IDL (Research Systems Inc., Boulder, Co., USA) as follows. The OISs in the first and second frames were averaged, and the basal image that composed of the averaged signals was obtained. Then, the OISs in all frames (from 1 to 14) were divided by the averaged signals in the basal image, and we obtained ratio images from frames 1–14. These individual ratio images were collected from the records with and without stimulation session, respectively. The collected ratio images were filtered by using a Gausian spatial filter to eliminate non-specific darkening (increased light absorption) caused by the stimulus in the recording region and high frequency noise [20]. For statistical analysis, a t-test was applied to the intensities of each pixel in the filtered images between

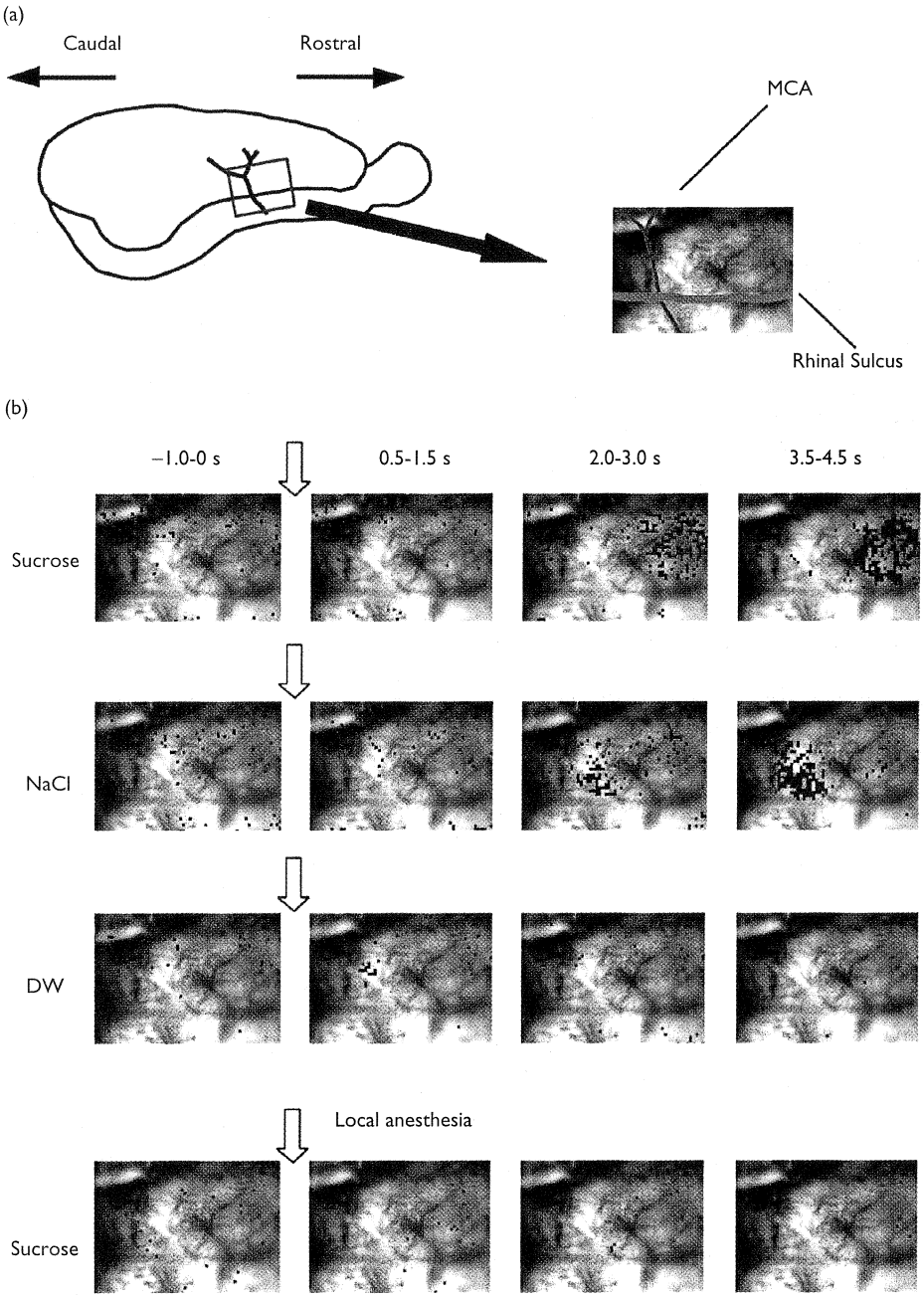

Fig. 1. Time course comparison of OIS response images. (**a**) Optical recording area in the brain and a real image of the recording area. Location of rhinal sulcus (blue line) and MCA (red line) are superimposed on the brain images. (**b**) Statistical responsive pixels ($p < 0.05$, red spots) are superimposed on real images of the recording area. Open arrows indicate the start of tastant or DW application on the tongue. The time windows at which OISs were recorded are indicated above the images. (top, second top) Time course comparison of OIS images in the case of sucrose application and NaCl application. (third top) Time course comparison of OIS images in the case of DW application. (bottom) Time course of OIS images in the case of sucrose application under anesthetization of the tongue by a local injection of lidocaine.

the with and without stimulation sessions. The statistical analysis was applied to the data collected at frames 1–2, 4–5, 7–8, and 10–11 in 8–10 trials, that is, the data collected 1.0–0 s before, 0.5–1.5 s after, 2.0–3.0 s after and 3.5–4.5 s after the start of solution delivery to the tongue in one course of experiments. We defined the statistically significant pixels ($p<0.05$) as active signals in response to stimuli.

RESULTS

A time course comparison of statistical OIS images showed that OIS responses to 0.5 M sucrose appeared 2.0–3.0 s after the start of tongue stimulation. The responsive area was localized in the anterolateral insular cortex, dorsal to rhinal sulcus, which is the rostral part of gustatory insular cortex (Fig. 1b, top). OIS responses to 0.5 M NaCl appeared 2.0–3.0 s after the start of tongue stimulation. The responsive area was localized in the centrolateral insular cortex, dorsal to rhinal sulcus and straddling MCA, which is the central part of the gustatory insular cortex (Fig. 1b, second top). Thus, the sucrose-responsive area is located relatively rostral of the gustatory insular cortex when compared with the NaCl-responsive area. The same relativities between sucrose- and NaCl-responsive areas were observed in all seven animals.

In order to examine whether OIS responses to sucrose and NaCl solution were responses to the tastants themselves, DW was administered on the tongue. A time course comparison of statistical OIS images clearly showed that no OIS response was generated within the gustatory insular cortex (Fig. 1b, third top). In order to examine whether OIS responses to the tastants were responses to neural inputs from peripheral organs on the tongue, the tongue was anesthetized by a local injection of lidocaine, and sucrose was administered on the tongue. A time course comparison of statistical OIS images clearly showed that no OIS response was generated within the gustatory insular cortex, despite the delivery of the tastants on the tongue (Fig. 1b, bottom). These results indicate that the OIS responses to tastants we observed in this study are responses to gustatory information from the tongue, and not responses to somatosensory information from the oral cavity.

The contribution of tastant concentration to gustatory information processing was investigated by comparing the OIS responses of high concentrations of NaCl with that of lower concentrations of NaCl. When 0.05 M NaCl was administered on the tongue, OIS responses began to appear after 2.0–3.0 s (Fig. 2b, top). When 0.2 M NaCl was administered, OIS response began after 0.5–1.5 s (Fig. 2b, second top). In addition, the density of statistical spots, in the case of 0.2 M NaCl applications, was higher than that of 0.05 M NaCl.

DISCUSSION

The OIS recording methods for investigation of sensory information processing allows a high resolution of spatial dimension [12,13]. We can, therefore, identify the relative location between areas in the same window of the brain surface, if each area is responsive to appropriate sensory stimulation and is localized. Figure 1 shows that the sucrose-responsive area is localized relatively rostral

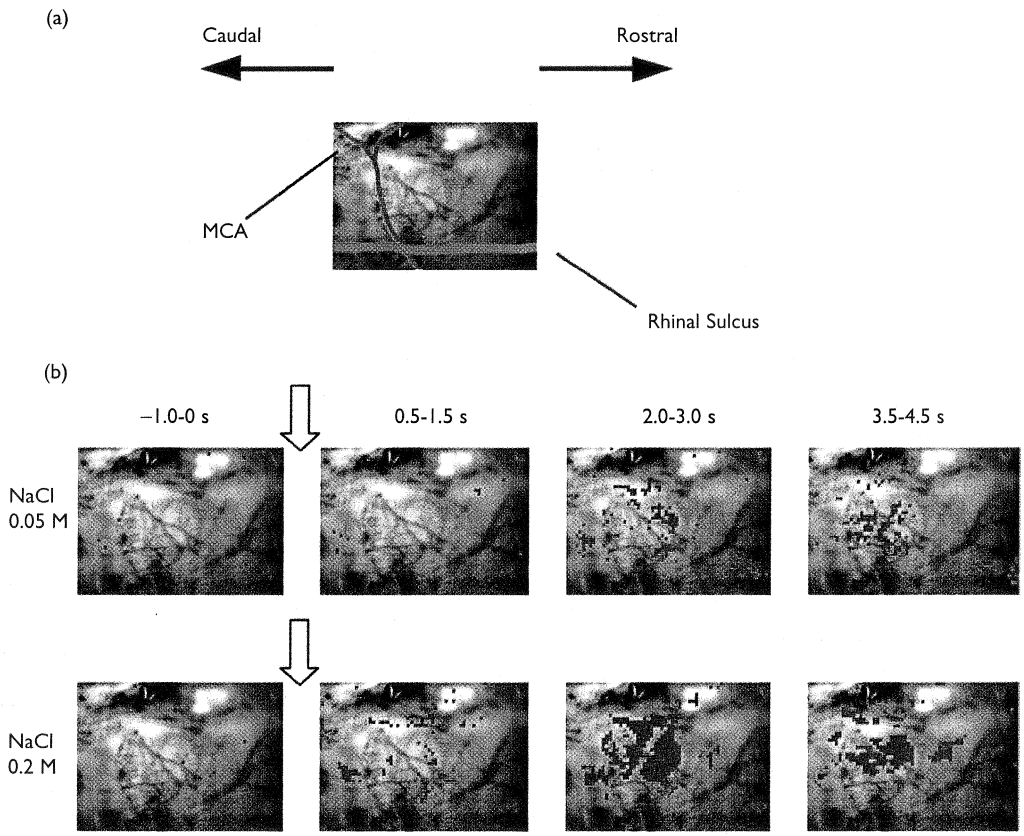

Fig. 2. Contribution of tastant concentration to cortical responses. (**a**) The real image of the recording area. (**b**) (top) Time course comparison of OIS images in the case of 0.05 M NaCl application. (second top) Time course comparison of OIS images in the case of 0.2 M NaCl application.

compared with the NaCl-responsive area in the gustatory insular cortex. This result strongly suggests that cortical taste neurons use spatial codes for discriminating taste information between sucrose and NaCl. Thus, chemotopy for the taste quality of two essential tastants may be organized in the primary cortical taste area. This cortical chemotopy may be assisted by a previous finding at the subcortical level that the chemotopic organization for taste quality is in the nucleus of solitary tract [21]. As for the temporal dimension, the concentration of tastants may be discriminated by the onset time of responses to taste stimulation (Fig. 2b), as reported in a previous electrophysiological study [22]. However, the contribution of frequency code could not be addressed by the present methods, due to their low temporal resolution. General taste sensation is recognized as an integration of chemosensory and somatosensory information, which should require both spatial and temporal coding [9,23]. Electrophysiological methods with high resolution of temporal codes may have difficulty in interpreting the spatial aspects of neural activities in the primary cortical taste area, since gustatory insular cortex neurons receive not only chemosensory afferents, but also somatosensory afferents by way of thalamo-cortical pathways or horizontal cortico-cortical pathways with frequency code information [23,24]. In the present study, owing to a low temporal resolution of OIS imaging methods, desynchronized elements or short activity elements might be canceled, resulting in the detection of spatial aspects of chemosensory elements in the OIS images.

The results of the present study suggest that taste information of sucrose and NaCl from the peripheral sensory organs is segregated at the level of the gustatory insular cortex. Further, the taste information of the two essential tastants may be assembled as spatial codes in the primary cortical taste area through the process of taste quality perception. We examined only two basic tastants. In general, the recognition of the source of sensory information may require neural oscillation and synchronization between functional neuron clusters [3,25]. In order to understand the precise mechanisms of discriminating complicated taste information, further investigations should examine how different sensory information is integrated with frequencies and temporal dynamics, based on spatial coding.

CONCLUSION

OIS imaging revealed that gustatory responses to the administration of sucrose and NaCl on the tongue assembled separately in the gustatory insular cortex, suggesting that cortical taste neurons use spatial codes for the discrimination of taste information between the two essential tastants at the level of primary cortical taste area.

REFERENCES

1. Florey E. Frequency and amplitude codes of neuronal signals. In: Deecke L, Eccles JC and Mountcastel VB (eds). *From Neuron to Action. An Appraisal of Fundamental and Clinical Research.* New York: Springer-Verlag; 1990, pp. 413–419.
2. Gilbert CD, Das A, Ito M, Kapadia M and Westheimer G. Spatial integration and cortical dynamics. *Proc Natl Acad Sci USA* **93**, 615–622 (1996).
3. Singer W and Gray CM. Visual feature integration and the temporal correlation hypothesis. *Annu Rev Neurosci* **18**, 555–586 (1995).
4. MacLeod K, Bäcker A and Laurent G. Who reads temporal information contained across synchronized and oscillatory spike trains? *Nature* **395**, 693–698 (1998).
5. Stopfer M, Bhagavan S, Smith BH and Laurent G. Impaired odour discrimination on desynchronization of odour-encoding neural assemblies. *Nature* **390**, 70–74 (1997).
6. Hanamori T, Kunitake T, Kato K and Kannan H. Responses of neurons in the insular cortex to gustatory, visceral, and nociceptive stimuli in rats. *J Neurophysiol* **79**, 2535–2545 (1999).
7. Ogawa H, Hasegawa K and Murayama N. Difference in taste quality coding between two cortical taste areas, granular and dysgranular insular areas, in rats. *Exp Brain Res* **91**, 415–424 (1992).
8. Yamamoto T, Matsuo R, Kiyomitsu Y and Kitamura R. Taste responses of cortical neurons in freely ingesting rats. *J Neurophysiol* **61**, 1244–1258 (1989).
9. Katz DB, Simon SA and Nicolelis MA. Dynamic and multimodal responses of gustatory cortical neurons in awake rats. *J Neurosci* **21**, 4478–4489 (2001).
10. Katz DB, Simon SA and Nicolelis MA. Taste-specific neuronal ensembles in the gustatory cortex of awake rats. *J Neurosci* **22**, 1850–1857 (2002).
11. Yamamoto T, Yuyama N, Kato T and Kawamura Y. Gustatory responses of cortical neurons in rats. II. Information processing of taste quality. *J Neurophysiol* **53**, 1356–1369 (1984).
12. Frostig RD, Lieke EE and Ts'o DY and Grinvald A. Cortical functional architecture and local coupling between neuronal activity and the microcirculation revealed by *in vivo* high-resolution optical imaging of intrinsic signals. *Proc Natl Acad Sci USA* **87**, 6082–6086 (1990).
13. Bonhoeffer T and Grinvald A. Optical imaging based on intrinsic signals: the methodology. In: Toga A and Mazziotta JC (eds). *Brain Mapping: The Methods.* San Diego: Academic Press; 1996, pp. 55–97.
14. Rubin BD and Katz LC. Optical imaging of odorant representations in the mammalian olfactory bulb. *Neuron* **23**, 499–511 (1999).
15. Blood AJ, Pouratian N and Toga AW. Temporally staggered forelimb stimulation modulates barrel cortex optical intrinsic signal responses to whisker stimulation. *J Neurophysiol* **88**, 422–437 (2002).
16. Tsytsarev V and Tanaka S. Intrinsic optical signals from rat primary auditory cortex in response to sound stimuli presented to contralateral, ipsilateral and bilateral ears. *NeuroReport* **13**, 1661–1666 (2002).
17. Bonhoeffer T and Grinvald A. Iso-orientation domains in cat visual cortex are arranged in pinwheel-like patterns. *Nature* **353**, 429–431 (1991).
18. Das A and Gilbert CD. Long-range horizontal connections and their role in cortical reorganization revealed by optical recording of cat primary visual cortex. *Nature* **375**, 780–784 (1995).
19. Onoda N, Imamura K, Obata E and Iino M. Response selectivity of neocortical neurons to specific odors in the rabbit. *J Neurophysiol* **52**, 638–652 (1984).
20. Tsunoda K, Yamane Y, Nishizaki M and Tanifuji M. Complex objects are represented in macaque inferotemporal cortex by the combination of feature columns. *Nature Neurosci* **4**, 832–838 (2001).
21. Harrer MI and Travers SP. Topographic organization of Fos-like immunoreactivity in the rostral nucleus of the solitary tract evoked by gustatory stimulation with sucrose and quinine. *Brain Res* **711**, 125–137 (1996).
22. Yamamoto T, Yuyama N, Kato T and Kawamura Y. Gustatory responses of cortical neurons in rats. I. Response characteristics. *J Neurophysiol* **51**, 616–635 (1984).
23. Katz DB, Nicolelis MA and Simon SA. Gustatory processing is dynamic and distributed. *Curr Opin Neurobiol* **12**, 448–454 (2002).
24. Yoshimura H, Kato N, Sugai T, Segami N and Onoda N. Age-dependent appearance an insulo-parietal cortical signal propagation that elicits a synchronized population oscillation in the parietal cortex of rats. *Dev Brain Res* **143**, 245–251 (2003).
25. Salinas E and Sejnowski TJ. Correlated neuronal activity and the flow of neural information. *Nature Rev Neurosci* **2**, 539–550 (2001).

Acknowledgements: We thank Dr N. Kato for his valuable advice on our manuscript, and Mr H. Adachi and Mr S. Muramoto for technical assistance. This work was supported in part by grants from the Ministry of Health, Labour and Welfare of Japan (a Health Science Research Grant to H. Y. and S. N.) and Kanazawa Medical University (a Grant for Collaborative Research, No. S2003-9, to H. Y. and N. O.).

Available online at www.sciencedirect.com

SCIENCE DIRECT®

Brain Research 1015 (2004) 114–121

BRAIN RESEARCH

www.elsevier.com/locate/brainres

Research report

To-and-fro optical voltage signal propagation between the insular gustatory and parietal oral somatosensory areas in rat cortex slices

Hiroshi Yoshimura[a,b], Nobuo Kato[c,*], Tokio Sugai[b], Makoto Honjo[a], Jun Sato[a], Natsuki Segami[a], Norihiko Onoda[b]

[a] *Department of Oral and Maxillofacial Surgery, Kanazawa Medical University, Uchinada 920-0293, Japan*
[b] *Department of Physiology, Kanazawa Medical University, Uchinada 920-0293, Japan*
[c] *Department of Integrative Brain Science, Kyoto University Graduate School of Medicine, Kyoto 606-8501, Japan*

Accepted 9 April 2004
Available online 4 June 2004

Abstract

Taste perception depends not only on special taste information processed in the insular cortex, but also on oral somesthetic processing in the parietal cortex. Many insular cortex neurons show multimodal responsiveness. Such multimodality may be enabled by signal exchange between these two cortices. By using the protocol that we have developed, a synchronized population oscillation of synaptic potentials was induced in the parietal cortex by stimulation to the insular cortex in rat neocortex slices. The spatiotemporal pattern of propagation of this oscillation was studied by recording voltage-sensitive optical signals and field potentials. The first wavelet of the oscillation was propagated from the insular stimulation site to the parietal cortex. However, the second and later wavelets propagated back from the parietal cortex to the insular cortex. The oscillation was detected in the insular cortex as well, but was actually generated in the parietal cortex. Thus, the initial peak of optical signal, sent from the insular to parietal cortex, served to generate oscillatory responses in the parietal cortex, which propagated back to the insular cortex wave-by-wave. We propose that this to-and-fro propagation may be an artificially exaggerated demonstration of an intrinsic mechanism relevant to signal exchange between the parietal and insular cortices.

Theme: Excitable membranes and synaptic transmission
Topic: Postsynaptic mechanisms

Keywords: Insular cortex; Parietal cortex; Caffeine; Optical recording; Horizontal propagation; Population oscillation

1. Introduction

The insular cortex, located dorsal to the rhinal sulcus, is regarded as the primary taste area [5,9,11,13,20,22,23, 30,32]. General somesthetic sensation of the oral cavity, on the other hand, is held to be projected onto the ventral part of the parietal cortex adjacent to the insular cortex [5–7,9,23]. In the insular cortex, many neurons respond to both gustatory and oral somatosensory stimulation, hence exhibiting multimodal responsiveness [2,9,12,24]. Responses of some insular multimodal neurons to tastant stimulation are reported to have a complex temporal structure lasting for a few second, during which time neurons respond first to somatosensory aspects of tastants, then to gustatory aspects and finally to both [6,7]. To maintain such a temporally structured multimodal responsiveness, a sustained communication between the insular and parietal cortex would be beneficial, even though subcortical structures may also participate in this processing.

Recently we have reported that insular cortex stimulation can elicit synchronized population oscillation of synaptic potentials in the parietal cortex, but not in the insular cortex [27], by using the procedure that we have developed in rat visual cortex slices [25,26,28]. In complementary experiments, stimulation to the parietal cortex itself elicited the same oscillation in the parietal cortex but not in the insular cortex, suggesting that the parietal cortex is more prone to

* Corresponding author. Tel.: +81-75-753-4678; fax: +81-75-753-4486.
E-mail address: f50207@sakura.kudpc.kyoto-u.ac.jp (N. Kato).

0006-8993/$ - see front matter © 2004 Elsevier B.V. All rights reserved.
doi:10.1016/j.brainres.2004.04.056

induce oscillation than the insular cortex [29]. Once tissue was ready for oscillation, an episode of stimulation was evoked in the parietal cortex by a single stimulation and lasted about 1 s. This oscillation might be suitable to support a sustained temporal structure of neuron responsiveness. However, insofar as remaining within the parietal cortex, the oscillation would never be relevant to the multimodality. In the present report, by using the optical recording method with a voltage-sensitive dye, we attempted to record optical signals in the window covering both the insular and parietal cortices to elucidate the spatiotemporal pattern of the oscillation on a wider scale.

2. Materials and methods

2.1. Animals and slice preparations

All the experiments were performed in accordance with the guideline for ethical use of animals approved by the Japanese Physiological Society. Wistar rats (28–40 days of age) were decapitated under ether anesthesia, and the brains were quickly removed and soaked into cold medium (2–4 °C) consisting of (in mM) NaCl 124, KCl 3.3, KH_2PO_4 1.25, $MgSO_4$ 1.3, $CaCl_2$ 2, $NaHCO_3$ 26, and D-glucose 10, saturated with 95% O_2–5% CO_2. Coronal slices (350 μm thick) including the insular and parietal cortices anterior to the middle cerebral artery (MCA) were made. After cutting, slices were incubated in a chamber, different from the recording chamber, at room temperature (18–23 °C) for at least 1 h before starting the recording session.

2.2. Field potential recording

The slices were placed in a submerged-type chamber set on the stage of an upright microscope (Olympus IMT-2) and perfused with medium (30 °C) at 5 ml/min. Field potential recordings were made from the parietal cortex and the dorsal insular cortex facing the rhinal sulcus, as previously described [27]. Micropipettes for field potential recordings were filled with 3 M NaCl and inserted into layer II/III of the insular or the parietal cortex (6–10 MΩ). A bipolar tungsten electrode, consisting of parallel tungsten wires, was inserted into layer IV of the insular cortex (the border region between the agranular and dysgranular insular cortices) for stimulation (duration, 80 μs; intensity, 250–350 μA). Synaptic responses were evoked by single pulse stimulation at 0.03–0.3 Hz, recorded with a bridge-equipped amplifier (Axoclamp-2B, Axon Instruments, Foster City, USA), digitized by an AD converter (at the rate of 2.5–5 kHz; Digidata 1200, Axon Instruments), and stored in a PC for off-line analysis.

2.3. Optical recording

We used high-speed optical recording methods with voltage-sensitive dyes, so as to observe spatiotemporal dynamics of neural activities. The details of optical recording system used in this study have been described elsewhere [18,19,28]. Before optical recording started, the slices were incubated with the voltage-sensitive dye NK2761 (0.125 mg/ml, purchased from Nihon Kanko, Okayama, Japan) for 20 min, and then transferred to the recording chamber. The camera unit of the optical imaging system (Fujix HR Deltaron 1700; Fuji Photo Film, Tokyo, Japan) contains a photodiode array of 128 × 128 elements. With an × 10 objective, the whole array corresponded to a 2.24 × 2.24 mm^2 area of tissue. The light for absorption measurements, generated by a tungsten-halogen lamp (150 W), passed through a heat absorption filter and a narrow band interference filter, before being focused on the preparation. Illumination was controlled by electromagnetic shutter to avoid dye bleaching or photodynamic damages. Sixteen responses elicited by cortical stimulation were averaged to form a run. Neural activities were recorded as intensity changes of transmitted light hitting each photodiode. Images are captured every 0.6 ms. Recordings shown are averages over 16 traces. Relative increase of optical signal was expressed as a time-sequence of the whole image, or was plotted against time for each regions of interest (ROIs).

2.4. Drugs used

According to the purposes of experiments, the following chemicals (purchased from Wako, Osaka, Japan) were added to medium: caffeine, 3.0 mM; D-2-amino-5-phosphonovaleric acid (AP5), 15 μM; thapsigargin, 15 μM.

3. Results

Both the areal border between the insular and parietal cortices and the cortical laminar delineation were determined by observing cytoarchitectonic features in some slices and more macroscopic landmarks in the other slices, as discussed in our previous reports [27]. The criteria for delineation were based on description in the atlases by Swanson [20] and by Zilles [32]. Also, in the light of Remple et al. [14] and Shi and Cassell [16], it is clear that the slices used in the present study contained both the taste part of the insular cortex and the lingual part of the primary somatosensory area.

In slices containing both areas, intracortical electrical stimulation was delivered to layer IV of the insular cortex. In normal medium, both the field potentials and optical signals evoked by this stimulation were small and restricted (Fig. 1A; in 5/5 slices). Optical imaging showed that this small response was localized in the vicinity of the stimulated area, without spreading toward the parietal cortex (Fig. 1B). We then changed the medium into a caffeine-containing one, and attempted to evoke oscillation of synaptic potentials by using the same methods that we have developed for the induction of synchronous oscillation in the visual cortex

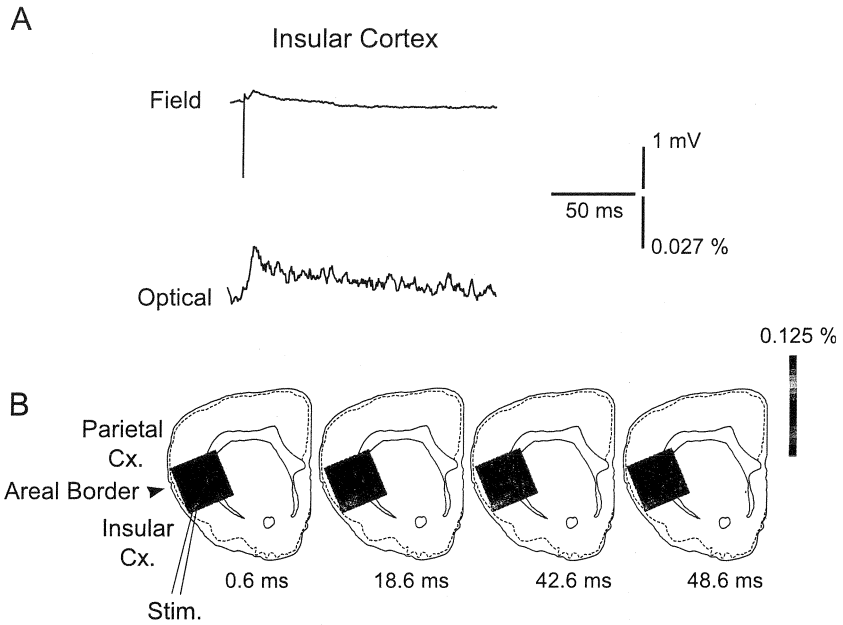

Fig. 1. A small solitary response elicited by stimulation to the insular cortex in normal medium. (A) The response was detected in layer II/III of the insular cortex by both field potential recording and optical recording. (B) Optical images superimposed on illustration of the recorded slice. The optical signal is restricted to the insular cortex. The post-stimulus time is indicated at the bottom of each image. The site of stimulation was illustrated (Stim.).

[25,26,28]. Once the oscillation was induced, insular cortex stimulation evoked voltage signals that spread to the parietal cortex (Fig. 2A; in 5/5 slices), in contrast to the locally restricted response in normal medium (Fig. 1B). All the experiments described below were done in caffeine-containing medium.

We looked into details of the spatiotemporal pattern of this voltage signal by plotting the time course of signal intensity recorded from each of 30 regions of interest (ROIs). These ROIs were aligned tangentially at each level of three different cortical depths (Fig. 2B). The voltage signals showed oscillation in layers II/III and IV of the parietal cortex and in layer IV of the insular cortex (Fig. 2C). The frequency of this oscillation was 9.6 ± 0.3 Hz ($N=5$). In our previous study [27], although the same procedure resulted in induction of the oscillation in the parietal cortex in slices obtained from rats of similar ages, we failed to detect the oscillation in layer IV of the insular cortex by field potential recording. Our previous field potential recordings, obtained strictly from narrow spots depending on the locations of recording electrodes, are likely to have missed the oscillation in the insular cortex. We presume that the present experiments finally detected this oscillation with optical recording, which offers a spatially continuous monitoring of the whole surface of a part of the insular cortex. Only the initial peak of the oscillatory episode (Fig. 2C, arrows) is illustrated in the sequence of images shown in Fig. 2A, while the second and following waves appear in images captured later.

Peak-by-peak comparison among signals obtained from the tangentially located ROIs in layer II/III (Fig. 2C, red line) indicates that the peak of the first wave came the later at more distant ROIs from the insular stimulation site, confirming the insulo-parietal propagation of the voltage signal revealed by imaging (Fig. 2A). Imaging also suggested that this initial propagation was mediated by three pathways along layer II/III, layer IV and layer V/VI, since elongation of apparently three parallel red bands, indicating relatively highest voltage signals, progressed from 42.6 to 54.6 ms post-stimulus (Fig. 2A; the third to fifth images from the left). How these three propagation paths are correlated is not investigated yet, though the propagation along layer II/III looks most prominent in the pseudo-color images. However, when the real intensity data, instead of the pseudo-color appearance in images, was used for calculation, the throughput velocity of propagation of the first wave was 72.8 ± 10.0 mm/s in layer II/III and 69.8 ± 11.2 mm/s in layer IV ($N=5$), which are not significantly different from each other. The peak amplitude of the first wave in layer II/III was $0.08 \pm 0.005\%$ at the border between the insular and parietal cortices, and significantly larger than in layer IV ($0.04 \pm 0.003\%$; $P<0.01$). Based on the peak amplitude, we presume that the major route of the present insulo-parietal propagation is through layer II/III. A possibility therefore arises that the signal propagation in layer IV may result from short-distance vertical propagation from layer II/III, rather than a real propagation through layer IV. However, the velocity data suggest, on the contrary, that the signal in layer IV may not necessarily follow that in layer II/III. It has yet to be further elucidated by which route the to-and-fro propagation spread.

The second and later peaks of the oscillation, by contrast, emerged first at ROI 8 (Fig. 2C). Peak-by-peak comparison indicated that these later waves propagated bi-directionally

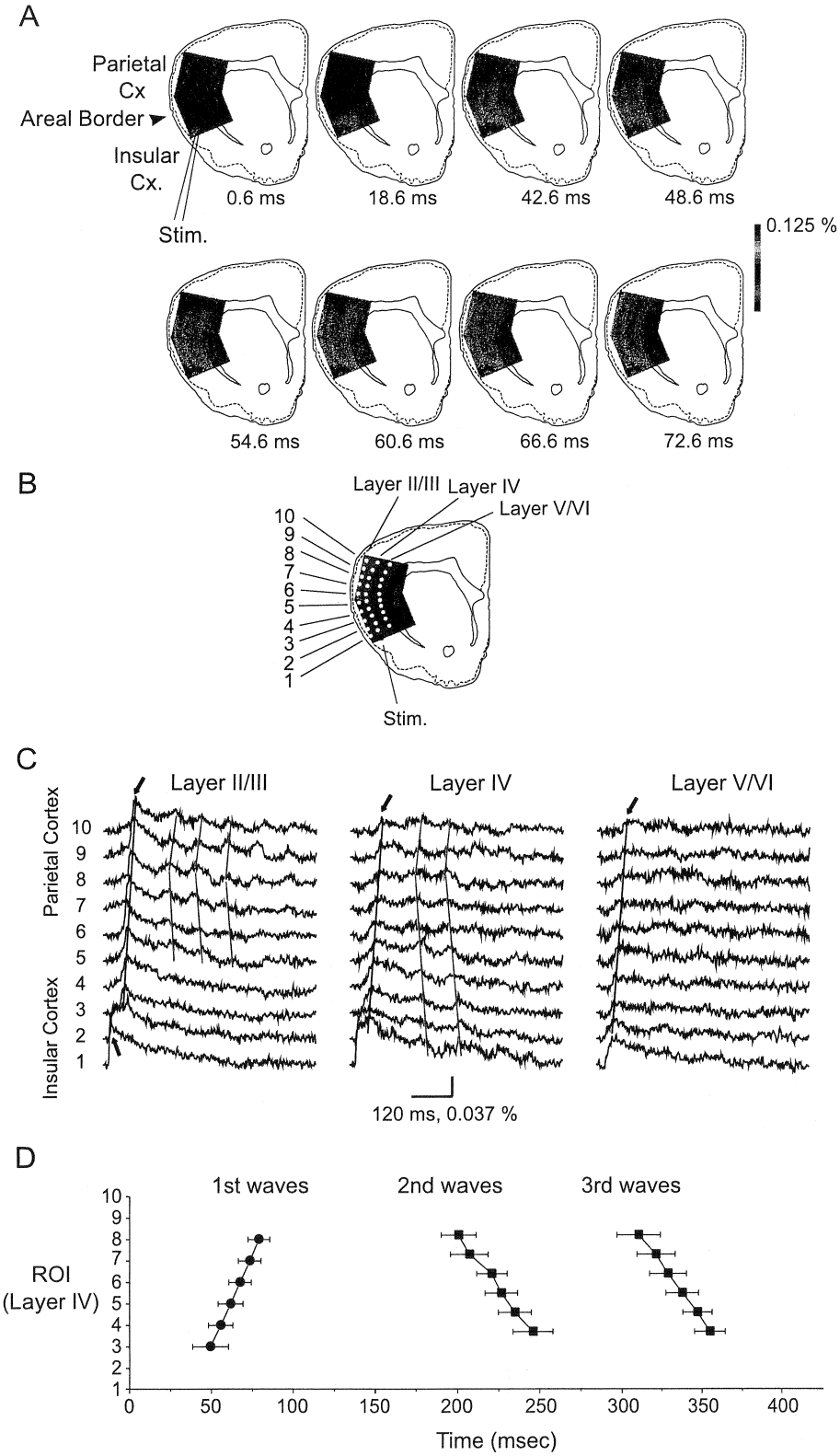

Fig. 2. Occurrence and propagation of oscillation evoked in the parietal cortex by insular stimulation. (A) The insulo-parietal propagation of the very initial part of the response detected by optical imaging. (B) Locations of ROIs. Optical signals were collected from these ROIs and illustrated in C. Three tangential series of ROIs are placed in layers II/III, IV and V/VI, respectively. The insulo-parietal border is located between ROI 4 and ROI 5. (C) The time courses of optical signals for 30 regions of interest (ROIs, Fig. 2B). The peaks of the first waves were fitted with the red lines, and the two series of later peaks with the blue lines. Note that blue lines are not straight but have a reflection point at ROI 8, indicating that the second and later peaks emerge first at ROI 8 and then propagate bi-directionally. (D) Averaged time-to-peak of first, second and third waves at ROI 3 to ROI 8. The ROI-by-ROI changes in the time-to-peak clearly indicate that the first wave propagated from the insular to parietal cortex, whereas the second and third waves propagated in the opposite direction.

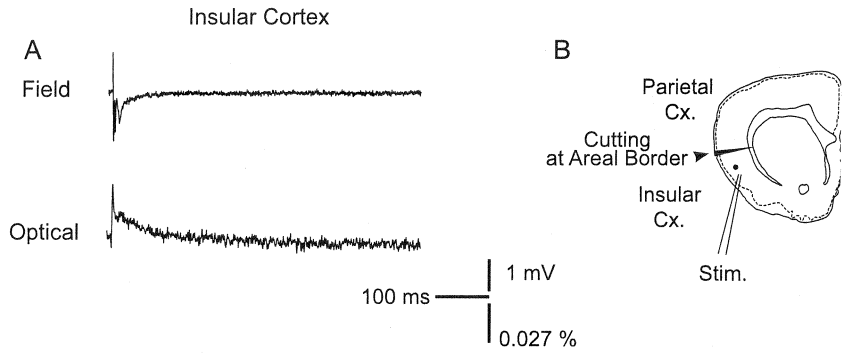

Fig. 3. Aborted induction of oscillation in the isolated insular cortex. (A) Arrangement of stimulation and recording electrodes and the location of cutting. (B) Although the same protocol to induce oscillation was imposed, no oscillation in field potentials was generated in the insular or parietal cortex by stimulating the insular cortex isolated from the parietal cortex.

from ROI 8 toward ROI 7 as well as toward ROI 9 (Fig. 2C, blue lines). Such bi-directional sequences of the peaks strongly suggest that the generator of the oscillation is located near ROI 8. Downward propagation of these waves, from ROI 8 through ROI 7, reached the insular cortex in layer IV only, whereas the oscillation disappeared within the parietal cortex in layer II/III. In layer V/VI, the oscillation was not obviously detectable even in the parietal cortex. It is thus shown that the initial wave propagated from the insular to parietal cortex along layer II/III and layer IV, while the oscillation is generated in the parietal cortex and traveled back to the insular cortex along layer IV (Fig. 2C, blue lines).

We then averaged the time-to-peak of the first three waves recorded at ROI 3–8 over different slices, and compared the ROI-by-ROI progression of time-to-peak of the waves (Fig. 2D), which convincingly confirmed the forward propagation of the first wave from the insular to parietal cortex, and the backward propagation of the second and third waves. For the second wave, the time-to-peak was 200.3 ± 10.6 ms ($N=5$) at ROI 8, which is significantly smaller than that at ROI 4 (234.7 ± 10.0 ms, $P<0.05$), confirming the backward propagation. For the third wave also, the time-to-peak was 310.0 ± 13.7 ms ($N=5$) at ROI 8, which is significantly smaller than that at ROI 4 (347.0 ± 9.1 ms, $P<0.05$), pointing again to a backward propagation. The inter-peak interval between the peak of the second and third waves was 117.7 ± 7.3 ms ($N=5$) at ROI 8 and 111.1 ± 9.3 ms ($N=5$) at ROI 5, indicating no significant phase shift during the backward propagation.

To confirm the inability of the insular cortex to generate oscillation, cutting was made between the insular and parietal cortices, and induction of oscillation was attempted by insular stimulation. No oscillation was observed in this isolated insular cortex (Fig. 3; in 4/4 slices), indicating that the insular cortex was unable to generate oscillation by itself. This result confirms that the oscillation recorded in layer IV of the insular cortex resulted from the parieto-insular propagation of the oscillation generated in the parietal cortex.

Robustness of the oscillation in the parietal cortex was confirmed by field potential recordings. Simultaneous recordings of optical signals and field potentials from layer II/III of the parietal cortex showed correspondence in both the frequency and phase between the oscillation recorded by these two different methods (Fig. 4). The frequency was 9.9 ± 0.5 Hz ($N=4$) for both field and optical recordings. There were no significant differences in the time-to-peak of the second wave (192.0 ± 19.4 ms for field recording vs. 191.0 ± 18.9 ms for optical recording, $N=4$) or the third

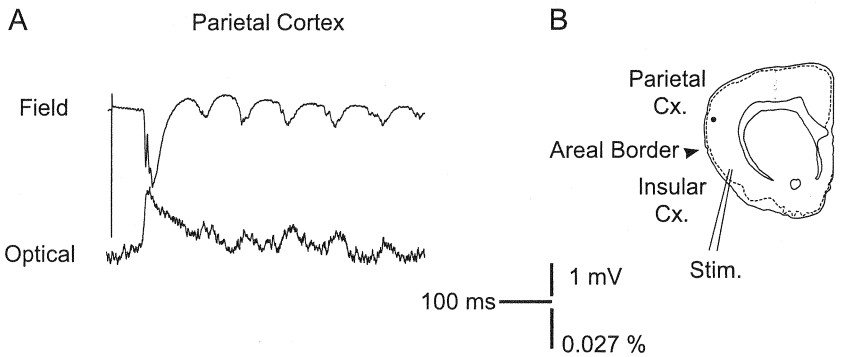

Fig. 4. (A) Synchronized population oscillation recorded simultaneously by field potential and optical recording from the parietal cortex. The oscillation appears more robust in field potential recording, presumably because of the better signal-to-noise ratio. (B) Stimulation and recording sites are illustrated. In the lower part of the illustration, the circle indicates the anterior commeasure.

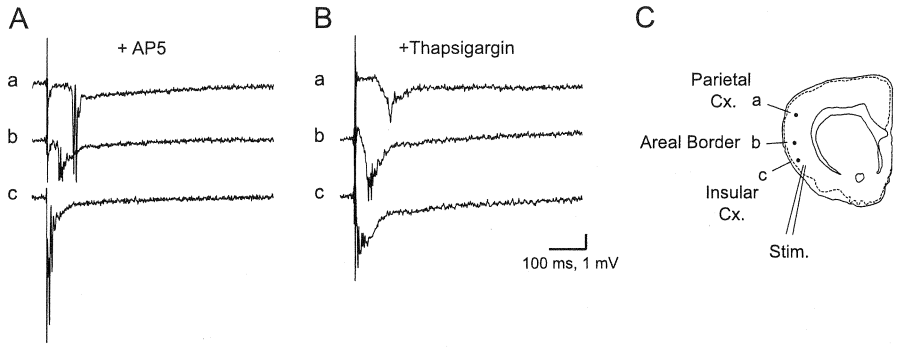

Fig. 5. Pharmacological dissection of the mechanisms whereby to elicit the oscillation and propagation. Once the oscillation was induced, the NMDA receptor blocker AP5 (A) or the calcium store depletor thapsigargine (B) was bath-applied. Both drugs left the insulo-parietal propagation of the first wave intact, but abolished the once-induced oscillation. Like the oscillation, backward propagation from the parietal cortex was once induced and abolished by either drug. The alphabets on the left of recordings correspond with the recording sites illustrated in C. Scale bars applicable to both A and B; 1 mV, 100 ms. (C) The stimulation and recording sites are illustrated. Alphabets indicate the recording sites.

wave (294.5 ± 22.1 vs. 293.5 ± 21.6 ms, $N=4$). The inter-peak interval between the second and third waves was 102.5 ± 7.6 ms ($N=4$) for field potential recording and 102.5 ± 6.7 ms for optical recording, which did not differ significantly. The signal-to-noise ratio was always better in field potential recordings. This oscillation in field potentials is likely to reflect synchronous oscillation of synaptic potentials, as we have shown precisely by dual intracellular recording in the visual cortex [25].

Our previous studies [25,26] showed that induction of this oscillation depend on NMDA receptors and intracellular calcium release. In the present experiments also, application of either the NMDAR blocker AP5 (15 μM; in 7/8 slices) or the intracellular calcium store depletor thapsigargin prevented induction of both the oscillation and insulo-parietal propagation of field potentials (15 μM; 4/5 slices). However, once tissue was prepared to generate the oscillation, both of these drugs abolished the oscillation in the parietal and insular cortex, but left the insulo-parietal propagation intact (in 5/5 slices for AP5 application, Fig. 5A; in 3/3 for thapsigargin application, Fig. 5B). On the other hand, either drug abolished the parieto-insular backward propagation along with the oscillation of the parietal cortex. This result is consistent with our conclusion that the oscillation recorded in the insular cortex (Fig. 2C) is actually not generated in the insular cortex but due to backward propagation of the oscillation generated in the parietal cortex.

4. Discussion

The present findings were obtained by using our oscillation model, in which a synchronized population oscillation is stably induced in caffeine-containing medium in rat neocortex slices [25–29]. The same type of oscillation, as in the present study, was generated previously in the secondary visual cortex [28] and the parietal cortex [27,29], whereas induction failed in the primary visual or insular cortex even under caffeine application. This difference of inducibility is presumably due to area-specific differences in neuron circuitry, since caffeine application is unlikely to affect an area specifically, but not another, in the same slice.

In the present experiments, although the same site was stimulated and the same oscillation generated as previously [27], we have recorded from the insular and parietal cortices at the same time by the optical method. It became thereby possible to reveal that the oscillation generated in the parietal cortex by insular stimulation backpropagates to the insular cortex. Thus, between these two cortices, a to-and-fro communication of voltage signal has been documented. These findings may originate from the combination of two artificial conditions that we used here, caffeine application and electrical stimulation. These two are likely to enhance output signals from the stimulation site, which could have induced a purely artifactual propagation of signals. However, another interpretation is also possible that the neuron circuitry in the parietal and insular cortices may be basically so organized as to enable this type of to-and-fro signal propagation, and such circuitry may be usually dormant but activated in the present experimental conditions. Such an innate organization of neuron circuits, if ever existed, would be consistent with the heterogeneity across cortical areas in the ability of generating synchronized population oscillation that we discussed above.

The crucial question at this point is whether the experimentally enhanced excitation is only too artificial, and never occurs in the real brain. Of course, a macroscopically observable excitation, synchronized over a wide cortical area, would be unrealistic in the physiological condition. However, at the level of neuron clusters or modules, a critical mass of neurons might fire synchronously to recruit a limited part of the neuron circuitry for a to-and-fro propagation. For instance, it is well known on the basis of extracellular unit studies that neurons within a single column in the visual cortex have the same or similar firing properties, and therefore could fire simultaneously on physiological stimulation such as moving bars. On the mass recording level also, such columnar activation has been

imaged in vivo by the optical method [4,10,21]. Also, it has been repeatedly documented that synchronized oscillation in the visual cortex in response to visual, as opposed to electrical, stimulation is detectable in the form of field potentials as well as single units [3]. Furthermore, corticocortical projections among the visual cortices are known to be linked in such a way that functionally relevant locations, which for example share the same orientation preference, are connected reciprocally and serve to refine receptive field properties [1,8,15,17,31]. Given these locally condensed corticocortical connections between neuron modules or columns, it might be quite reasonable to imagine that a highly excitable state comparable to that induced globally in the present study is reproduced to a much lesser extent by physiological stimulations. Then a similar to-and-fro propagation might really occur between functionally relevant neuron modules in vivo, and serve as a means of communication between two different sensory cortices.

Finally, a to-and-fro propagation between the insular gustatory and parietal oral somatosensory cortices was induced by an apparently peculiar procedure in the present study. If this propagation was not a pure artifact, it might serve as a means of communication between two different sensory cortices.

Acknowledgements

We thank Mr. H. Adachi and Mr. S. Muramoto for technical assistance. This work was supported in part by grants from Kanazawa Medical University (a Science Research Grant to H.Y., No. S2003-9) and the Ministry of Education, Science, Sports and Culture (Grants-in-Aid for Scientific Research to N.K.).

References

[1] J. Bullier, Integrated model of visual processing, Brain Res. Rev. 36 (2001) 96–107.

[2] D.F. Cechetto, C.B. Saper, Evidence for a viscerotopic sensory representation in the cortex and thalamus in the rat, J. Comp. Neurol. 262 (1987) 27–45.

[3] C.M. Gray, W. Singer, Stimulus-specific neuronal oscillations in orientation columns of cat visual cortex, Proc. Natl. Acad. Sci. U. S. A. 86 (1989) 1698–1702.

[4] A. Grinvald, E.F. Lieke, R.D. Frostig, R. Hildesheim, Cortical point-spread function and long-range lateral interactions revealed by real-time optical imaging of macaque monkey primary visual cortex, J. Neurosci. 14 (1994) 2545–2568.

[5] T. Hanamori, T. Kunitake, K. Kato, H. Kannan, Responses of neurons in the insular cortex to gustatory, visceral, and nociceptive stimuli in rats, J. Neurophysiol. 79 (1999) 2535–2545.

[6] D.B. Katz, S.A. Simon, M.A.L. Nicolelis, Dynamic and multimodal responses of gustatory cortical neurons in awake rats, J. Neurosci. 21 (2001) 4478–4489.

[7] D.B. Katz, M.A.L. Nicolelis, A.A. Simon, Gustatory processing is dynamic and distributed, Curr. Opin. Neurobiol. 12 (2002) 448–454.

[8] Z.F. Kisvarday, U.T. Eysel, Cellular organization of reciprocal patchy networks in layer III of cat visual cortex (area 17), Neuroscience 46 (1992) 275–286.

[9] E. Kosar, H.J. Grill, R. Norgren, Gustatory cortex in the rat. I: physiological properties and cytoarchitecture, Brain Res. 379 (1986) 329–341.

[10] K. Obermayer, G.C. Blasdel, Geometry of orientation and ocular dominance columns in monkey striate cortex, J. Neurosci. 13 (1993) 4114–4129.

[11] H. Ogawa, X.D. Wang, Neurons in the cortical taste area receive nociceptive inputs from the whole body as well as the oral cavity in the rat, Neurosci. Lett. 322 (2002) 87–90.

[12] H. Ogawa, K. Hasegawa, N. Murayama, Difference in taste quality coding between two cortical taste areas, granular and dysgranular insular areas, in rats, Exp. Brain Res. 91 (1992) 415–424.

[13] G. Paxinos, C. Watson, The Rat Brain in Stereotaxic Coordinates, 4th ed., Academic Press, San Diego, 1997.

[14] M.S. Remple, E.C. Henry, K.C. Catania, Organization of somatosensory cortex in the laboratory rat (*Rattus norvegicus*): evidence for two lateral areas joined at the representation of the teeth, J. Comp. Neurol. 467 (2003) 105–118.

[15] P.A. Salin, P. Girard, H. Kennedy, J. Bullier, Visuotopic organization of corticocortical connections in the visual of the cat, J. Comp. Neurol. 22 (1992) 415–434.

[16] C.J. Shi, M.D. Cassell, Cortical, thalamic, and amygdaloid connections of the anterior and posterior insular cortex, J. Comp. Neurol. 399 (1998) 440–468.

[17] W. Singer, Development and plasticity of cortical processing architectures, Science 270 (1995) 758–764.

[18] T. Sugai, M. Sugitani, N. Onoda, Subdivision of the guniea-pig accessory olfactory bulb revealed by the combined method with immunohistochemistry, electrophysiological and optical recordings, Neuroscience 79 (1997) 871–885.

[19] T. Sugai, M. Sugitani, N. Onoda, Novel subdivisions of the rat accessory olfactory bulb revealed by the combined method with lectin histochemistry, electrophysiological and optical recordings, Neuroscience 95 (2000) 23–32.

[20] L.W. Swanson, Brain Maps: Structure of the Rat Brain, 2nd ed., Elsevier, Amsterdam, 1992.

[21] N. Vnek, B.M. Ramsden, C.P. Hung, P.S. Goldman-Rakic, A.W. Roe, Optical imaging of functional domains in the cortex of the awake and behaving monkey, Proc. Natl. Acad. Sci. U. S. A. 96 (1999) 4057–4060.

[22] X. Wang, H. Ogawa, Columnar organization of mechanoreceptive neurons in the cortical taste area in the rat, Exp. Brain Res. 147 (2002) 114–123.

[23] T. Yamamoto, N. Yuyama, Y. Kawamura, Cortical neurons responding to tactile, thermal and taste stimulation of the rat's tongue, Brain Res. 221 (1981) 202–206.

[24] T. Yamamoto, N. Yuyama, T. Kato, Y. Kawamura, Gustatory responses of cortical neurons in rats. I: response characteristics, J. Neurophysiol. 51 (1984) 616–635.

[25] H. Yoshimura, T. Sugai, N. Onoda, N. Segami, N. Kato, Synchronized population oscillation of excitatory synaptic potentials dependent on calcium-induced calcium release in rat neocortex layer II/III neurons, Brain Res. 915 (2001) 94–100.

[26] H. Yoshimura, T. Sugai, N. Onoda, N. Segami, N. Kato, Age-dependent occurrence of synchronized population oscillation suggestive of a developing functional coupling between NMDA and ryanodine receptors in the neocortex, Dev. Brain Res. 136 (2002) 63–68.

[27] H. Yoshimura, N. Kato, T. Sugai, N. Segami, N. Onoda, Age-dependent appearance of an insulo-parietal cortical signal propagation that elicits a synchronized population oscillation in the parietal cortex in rats, Dev. Brain Res. 143 (2003) 245–251.

[28] H. Yoshimura, N. Kato, T. Sugai, N. Segami, N. Onoda, Age-dependent emergence of oscillatory signal flow between the primary and

secondary visual cortices in rat brain slices, Brain Res. 990 (2003) 172–181.

[29] H. Yoshimura, N. Kato, M. Honjo, T. Sugai, N. Segami, N. Onoda, Age-dependent emergence of a parieto-insuler corticocortical signal flow in developing rats, Dev. Brain Res. 149 (2004) 45–51.

[30] H. Yoshimura, T. Sugai, M. Fukuda, N. Segami, N. Onoda, Cortical spatial aspects of optical intrinsic signals in response to sucrose and NaCl stimuli, NeuroReport 15 (2004) 17–20.

[31] T. Yousef, T. Bonhoeffer, D.S. Kim, U.T. Eysel, E. Toth, Z.F. Kisvarday, Orientation topography of layer 4 lateral networks revealed by optical imaging in cat visual cortex (area 18), Eur. J. Neurosci. 11 (1999) 4291–4308.

[32] K. Zilles, The Cortex of the Rat, Springer-Verlag, Berlin, 1985.

Chem. Senses 30 (suppl 1): i164–i165, 2005

doi:10.1093/chemse/bjh165

Chemotopic Arrangement for Taste Quality Discrimination in the Cortical Taste Area

Hiroshi Yoshimura[1], Tokio Sugai[2], Natsuki Segami[1] and Norihiko Onoda[2]

[1]Department of Oral and Maxillofacial Surgery, Kanazawa Medical University, Uchinada, Ishilkawa, 920-0293, Japan and [2]Department of Physiology, Kanazawa Medical University, Uchinada, Ishilkawa, 920-0293, Japan

Correspondence to be sent to: Hiroshi Yoshimura, e-mail: hyoshimu@kanazawa-med.ac.jp

Key words: chemotopy, insular cortex, optical intrinsic signal, spatial code, taste

Introduction

Signals from various sensory organs are delivered to the brain where sensory information is generated from the signals. The information is represented on the brain in the form of temporal and spatial codes, which enable us to create inner an representation of the outer world (Florey, 1990). In the neocortex, the information consisting of the spatial codes is principally arranged in the primary sensory area as a receptive field, by way of anatomical column formation. The information consisting of temporal codes, such as frequency and phase dynamics, also plays an important role for synchronization of neural activities or strengthening signal amplitudes. Interaction or integration of the information by way of intra-cortical or cortico-cortical connections enables the temporal and spatial codes to link (Singer and Gray, 1995; Gilbert *et al.*, 1996; Salinas and Sejnowski, 2001).

As for taste information processing, controversy still exists as to whether cortical taste neurons use temporal codes or spatial codes for discriminating taste information in the cortical taste area. However, it may be presumed that cortical taste neurons use spatial codes as well as frequency codes in order to discriminate taste information efficiently. Previous electrophysiological studies predict that there is a chemotopic arrangement for taste quality discrimination in the cortical taste area, but this hypothesis has not been confirmed because of lacking for the evidence with high resolution of spatial dimension. Optical imaging based on intrinsic signals has a high spatial resolution (Frostig *et al.*, 1990) and is useful for studying the functional organization of the brain (Bonhoeffer and Grinvald, 1996). Here, we investigated the spatial aspects of optical intrinsic signal (OIS) responses in the gustatory insular cortex that were elicited by delivering a solution of tastants on the tongue.

Materials and methods

Guinea-pigs were anesthetized with Na-barbiturate. The insular cortex, including rhinal sulcus and middle cerebral artery (MCA), was exposed with dura mater and a thinned skull. Optical intrinsic signals (OISs) were recorded from the insular cortex with a video camera. An area dimension and number of pixels are 8.7×6.5 mm^2 and 320×240, respectively. The focusing depth was adjusted to ~400 μm below the cortical surface. Solutions of tastants were delivered on the tongue in the oral cavity. We used NaCl, sucrose, quinine and HCl for taste stimulation.

Gustatory stimulation was administered by delivering a solution of NaCl, sucrose, quinine and HCl, respectively, on the tongue. The trials were repeated eight to ten times and each trial consisted of a pair of records with and without a stimulation session. During the inter-trial period, the oral cavity was washed with distilled water (DW). OIS data were collected for 7 s with a frame length of 500 ms. There are 14 frames per record. In the stimulating session, the stimulation was applied at frames 3–14, i.e. the stimulation was continued for 6 s. The statistical analysis was applied to the data collected in frames between with and without a stimulation session. We defined the statistically significant pixels ($P < 0.05$) as active signals in response to stimuli. The details of the OIS recording system and the statistical analysis have been described in our recent report (Yoshimura *et al.*, 2004c).

Results

According to the methods above-mentioned, OIS recording and statistical analysis were executed. In the case of sucrose application, a time course comparison of OIS images showed that OIS responses to sucrose appeared at 2.0–3.0 s after the start of tongue stimulation. The responsive area was localized in the rostral part of gustatory insular cortex. In the case of NaCl application, a time course comparison of OIS images showed that OIS responses to NaCl appeared at 2.0–3.0 s after the start of tongue stimulation. The responsive area was localized near the MCA in the gustatory insular cortex. Thus, the sucrose-responsive area is located relatively rostral of the gustatory insular cortex when compared with the NaCl-responsive area.

In order to examine whether OIS responses to sucrose and NaCl solution were responses to the tastants themselves, DW was administered on the tongue. A time course comparison of OIS images clearly showed that no OIS response was generated within the gustatory insular cortex. In order to examine whether OIS responses to the tastants were responses to neural inputs from peripheral organs on the tongue, the tongue was anesthetized by a local injection of lidocaine and sucrose was administered on the tongue. A time course comparison of OIS images clearly showed that no OIS response was generated within the gustatory insular cortex, despite the delivery of the tastants on the tongue. These results indicate that the OIS responses to tastants we observed in this study are responses to gustatory information from the tongue, and not responses to somatosensory information from the oral cavity.

The contribution of tastant concentration to gustatory information processing was investigated by comparing the OIS responses of high concentrations of NaCl with that of lower concentrations of NaCl. When low concentration of NaCl was administered on the tongue, OIS responses began to appear after 2.0–3.0 s. On the other hand, when high concentration of NaCl was administered, OIS response began after 0.5–1.5 s. In addition, in case of high-NaCl applications, the area of statistical spots was wider in rostro-caudal dimension than that of low-NaCl application. As for the temporal dimension, the concentration of tastants may be discriminated by the onset time of responses to taste stimulation.

In the same way, sucrose-, NaCl-, HCl- and quinine-responsive areas were compared. When low-concentration of tastants were administered, the areas of OIS in response to each tastant were spatially separated. Sucrose-, HCl-, NaCl- and quinine-responsive areas were arranged in rostro-caudal direction. When high-concentration of tastants were administered, OIS responses appeared in the rostral part, near the MCA and caudal part to the MCA of the gustatory insular cortex.

The OIS recording methods for investigation of sensory information processing allows a high resolution of spatial dimension. There-

fore, we can identify the relative location between areas in the same window of the brain surface, if each area is responsive to appropriate sensory stimulation and is localized. Based on the data corrected from seven animals, we made chemosensory maps in the insular cortex. To identify relative location of tastant-responsive area clearly, center-of-each-OIS response was plotted on line drawing of insular cortex. It shows that sucrose and HCl-responsive areas locate rostral part of the insular cortex, NaCl-responsive area locates near the MCA, and quinine-responsive area locates caudal part to the MCA of the insular cortex. These results are partially consistent with the cortical taste map investigated by electrophysiological methods (Yamamoto, 1987). Thus, chemotopy for the taste quality of tastants may be organized in the primary cortical taste area. When high-concentration of tastants were administered, sucrose- and HCl-responsive areas appeared near the MCA and caudal part to MCA of the insular cortex respectively in addition to rostral parts, and NaCl-responsive area appeared in the caudal part to MCA in addition to near the MCA, whereas, quinine-responsive area appeared in the rostral part in addition to the caudal part to MCA. Thus, as for high concentration of tastants, chemotopy for the taste quality may be represented in the primary cortical taste area as combinations of high and low threshold tastant-responsive areas.

Discussion

The present results were based on relative location of OIS responses, but not absolute location. Optical imaging based on intrinsic signals enables us to compare relative location over several tastant-responsive areas in the same recording window. For the reason, the OIS recording method is useful for studying spatial aspects of sensory information processing. By using this method, here we demonstrated that chemotopy for the taste quality may be organized in the primary cortical taste area. In addition, as for information processing of tastant concentration, chemotopy for the taste quality may be represented as combinations of high and low threshold tastant-responsive areas. Thus, not only information of taste quality but also information of concentration may be assembled as spatial codes in the primary cortical taste area through the process of taste quality perception.

General taste sensation is recognized as an integration of chemosensory and somatosensory information, which should require both spatial and temporal coding. Gustatory insular cortex neurons receive not only chemosensory afferents, but also somatosensory afferents by way of thalamo-cortical pathways or horizontal cortico-cortical pathways with temporal code information (Katz *et al.*, 2002; Wang and Ogawa, 2002; Yoshimura *et al.*, 2003, 2004a,b). In general, the recognition of the source of sensory information may require neural oscillation and synchronization between functional neuron clusters. It may be presumed that, based on spatial coding in the primary cortical taste area, the brain integrates different sensory information with frequencies and temporal dynamics so as to discriminate complicated taste information. Further study should precisely investigate the contribution of temporal coding to integration of chemical and somatosensory information from the oral cavity.

Acknowledgments

This work was supported by grants from Kanazawa Medical University (Grant for Promoted Research to H.Y., No. S2003-9).

References

Bonhoeffer, T. and **Grinvald, A.** (1996) *Optical imaging based on intrinsic signals: the methodology.* In Toga, A. and Mazziotta, J.C. (eds), Brain Mapping: The Methods. Academic Press, San Diego, CA, pp. 55–97.

Florey, E. (1990) *Frequency and amplitude codes of neuronal signals.* In Deecke, L., Eccles, J.C. and Mountcastel, V.B. (eds), From Neuron to Action. An Appraisal of Fundamental and Clinical Research. Springer, New York, pp. 413–419.

Frostig, R.D., Lieke, E.E., Ts'o, D.Y. and Grinvald, A. (1990) *Cortical functional architecture and local coupling between neuronal activity and the microcirculation revealed by* in vivo *high-resolution optical imaging of intrinsic signals.* Proc. Natl Acad. Sci. USA, 87, 6082–6086.

Gilbert, C.D., Das, A., Ito, M., Kapadia, M. and Westheimer, G. (1996) *Spatial integration and cortical dynamics.* Proc. Natl Acad. Sci. USA, 93, 615–622.

Katz, D.B., Nicolelis, M.A. and Simon, S.A. (2002) *Gustatory processing is dynamic and distributed.* Curr. Opin. Neurobiol., 12, 448–454.

Salinas, E. and **Sejnowski, T.J.** (2001) *Correlated neuronal activity and the flow of neural information.* Nat. Rev. Neurosci., 2, 539–550.

Singer, W. and **Gray, C.M.** (1995) *Visual feature integration and the temporal correlation hypothesis.* Annu. Rev. Neurosci., 18, 555–586.

Wang, X. and **Ogawa, H.** (2002) *Columnar organization of mechanoreceptive neurons in the cortical taste area in the rat.* Exp. Brain Res., 147, 114–123.

Yamamoto, T. (1987) *Cortical organization in gustatory perception.* Ann. NY Acad. Sci., 510, 49–54.

Yoshimura, H., Kato, N., Sugai, T., Segami, N. and Onoda, N. (2003) *Age-dependent appearance an insulo-parietal cortical signal propagation that elicits a synchronized population oscillation in the parietal cortex of rats.* Dev. Brain Res., 143, 245–241.

Yoshimura, H., Kato, N., Honjo, M., Sugai, T., Segami, N. and Onoda, N. (2004a) *Age-dependent emergence of a parieto-insular corticocortical signal flow in developing rats.* Dev. Brain Res., 149, 45–51.

Yoshimura, H., Kato, N., Sugai, T., Honjo, M., Sato, J., Segami, N. and Onoda, N. (2004b) *To-and-fro optical voltage signal propagation between the insular gustatory and parietal oral somatosensory areas in rat cortex slices.* Brain Res., 1015, 114–121.

Yoshimura, H., Sugai, T., Fukuda, M., Segami, N. and Onoda, N. (2004c) *Cortical spatial aspects of optical intrinsic signals in response to sucrose and NaCl stimuli.* Neuroreport, 15, 17–20.

Available online at www.sciencedirect.com

SCIENCE DIRECT

Brain Research 1036 (2005) 60–69

BRAIN RESEARCH

www.elsevier.com/locate/brainres

Research report

Strengthening of non-NMDA receptor-dependent horizontal pathways between primary and lateral secondary visual cortices after NMDA receptor-dependent oscillatory neural activities

Hiroshi Yoshimura[a,b,*], Tokio Sugai[b], Natsuki Segami[a], Norihiko Onoda[b]

[a]*Department of Oral and Maxillofacial Surgery, Kanazawa Medical University, Uchinada-cho 920-0293, Japan*
[b]*Department of Physiology, Kanazawa Medical University, Uchinada-cho 920-0293, Japan*

Accepted 4 December 2004

Abstract

Emergence of oscillatory signal flows between the primary visual cortex (Oc1) and medial secondary visual cortex (Oc2M) was previously dynamically demonstrated in rat brain slices by us. Applying caffeine, a neural modulator, to the slices and using optical recording methods revealed this facilitation along horizontal intrinsic pathways in which initial forward propagation from Oc1 to Oc2M was dependent on both *N*-methyl-D-aspartate receptors (NMDARs) and non-NMDARs. Conversely, oscillatory backward propagation from Oc2M to Oc1 was entirely dependent on NMDARs. The present study examined: (1) whether the signal behavior between Oc1 and lateral secondary visual cortex (Oc2L) is based on the same mechanism with that between Oc1 and Oc2M; and (2) how non-NMDAR and NMDAR activities underlie opening of horizontal corticocortical pathways between Oc1 and Oc2. Under NMDAR blockade, signals elicited in the Oc1 either could not or only weakly penetrated the Oc2L, even in caffeine-containing medium. In contrast, once forward propagation from Oc1 to Oc2L and oscillatory backward propagation from Oc2L to Oc1 was established in caffeine-containing medium, signals elicited in Oc1 could strongly penetrate the Oc2 even during blockade of NMDA activities, when forward penetrating components were dependent on non-NMDARs. These findings suggest that: (1) signal behavior and its mechanism between Oc1and Oc2L are the same with those between Oc1 and Oc2M; and (2) NMDAR activation results in non-NMDAR activity, resulting in opening and strengthening of intrinsic signal pathways between Oc1 and Oc2. NMDAR-dependent forward and backward propagation might be involved in cortical reorganization of the visual cortex.

Theme: Excitable membranes and synaptic transmission
Topic: Postsynaptic mechanisms

Keywords: Primary visual cortex; Secondary visual cortex; Horizontal propagation; Oscillation; NMDA receptor; Non-NMDA receptor; Caffeine

1. Introduction

Functional linkage between the primary visual cortex (Oc1) and secondary visual cortex (Oc2) is critical to cognition of the visual world [1,4,11,12,24]. Specialization of receptive fields requires the development of functional intrinsic connections between two areas [3,14–16,28,29, 39]. As animals mature, horizontal anatomical connectivity between the Oc1 and Oc2 is strengthened [10,15,19, 30,33]. We recently reported enhancement of signal interactions along horizontal directions between Oc1 and the medial part of the secondary visual cortex (Oc2M) during development [38]. Dynamics of these developmental changes were successfully shown by applying the neural modulator, caffeine, to visual cortex slices of rats, and by using optical recording methods with voltage-sensitive dyes. Signal

* Corresponding author. Department of Oral and Maxillofacial Surgery, Kanazawa Medical University, Uchinada-cho 920-0293, Japan. Fax: +81 76 286 2010.
E-mail address: hyoshimu@kanazawa-med.ac.jp (H. Yoshimura).

0006-8993/$ - see front matter © 2004 Elsevier B.V. All rights reserved.
doi:10.1016/j.brainres.2004.12.028

propagation elicited by Oc1 stimulation was restricted within Oc1 before caffeine application, while evoked signals spread from Oc1 to Oc2M by way of layer II/III principally after low-frequency stimulation to Oc1 on application of caffeine, and oscillatory signals emerged in Oc2M and spread back to Oc1. *N*-methyl-D-aspartate receptor (NMDAR) activation was required for oscillatory activities in Oc2M, but was not necessarily required for initial forward propagation from Oc1 to Oc2M. Focusing on initial forward propagation, initial horizontal components comprised fast non-NMDAR and slow NMDAR components.

Oc2 is located not only at the medial part of the Oc1, but also at the lateral parts, named Oc2L. Cytoarchitectural differences between Oc1 and Oc2M are also preserved between Oc1 and Oc2L [27,32,40]. If the manner of neural activity is dependent on cytoarchitectural features, signal penetration from Oc1 to Oc2L could generate neural oscillation in Oc2L, and oscillatory signals might spread back to Oc1, which may represent a similar pattern of propagation and oscillation to that between Oc1 and Oc2M. The present study examined whether the signal behavior between Oc1 and Oc2L is based on the same mechanism with that between Oc1 and Oc2M.

In general, activation of non-NMDARs and NMDARs is mutually controlled and is relevant to synapse plasticity in the central nervous system (CNS) [21,22]. In particular, the activities of NMDA receptors are indispensable for the induction of functional synapses mediated by non-NMDA receptors in the CNS [17,18,25]. In addition, a previous study predicted that intrinsic horizontal connections are concerned with remapping in the visual cortex [8]. Together, these findings suggest the possibility that NMDAR activities modify non-NMDAR activities, opening the horizontal intrinsic pathways to traffic. The aim of this study was to elucidate cause-and-effect during the process of establishing functional corticocortical interactions between Oc1 and Oc2.

2. Materials and methods

All experiments were performed in accordance with the guidelines for the ethical use of animals approved by the Japanese Physiological Society. Wistar rats (27- to 35-days-old) were decapitated under ether anesthesia, and the brains were quickly removed and soaked in cold medium (2–4 °C) comprising NaCl 124 mM, KCl 3.3 mM, NaH_2PO_4 1.25 mM, $MgSO_4$ 1.3 mM, $CaCl_2$ 2 mM, $NaHCO_3$ 26 mM, and D-glucose 10 mM, saturated with 95% O_2–5% CO_2. Visual cortex slices (350 μm thick) including the Oc1 and Oc2 were prepared using a slicer. Once cut, slices were left at room temperature for at least 1 h before starting the recording session.

To observe spatiotemporal dynamics of spreading neural activities, high-speed optical recording methods were used with voltage-sensitive dyes. Details of the optical recording system used in this study have been described elsewhere [13,23,26,31,34,37,38]. Slices were placed in a submerged-type chamber set on the stage of an IMT-2 upright microscope (Olympus, Tokyo, Japan) and perfused with medium (30 °C) at 5 mL/min. For optical recordings, slices were incubated with voltage-sensitive dye NK2761 (0.125 mg/mL; Nihon Kanko, Okayama, Japan) for 20 min, then transferred to the recording chamber. A bipolar tungsten electrode for stimulation was inserted into the border region between gray and white matter (WM) in Oc1 (WM stimulation). Duration and intensity of stimuli were 80 μs and 200–350 μA, respectively. Synaptic responses were elicited by WM stimulation at 0.03–0.3 Hz. Field potentials were recorded for monitoring electrical activities using a glass micropipette filled with 3 M NaCl, and

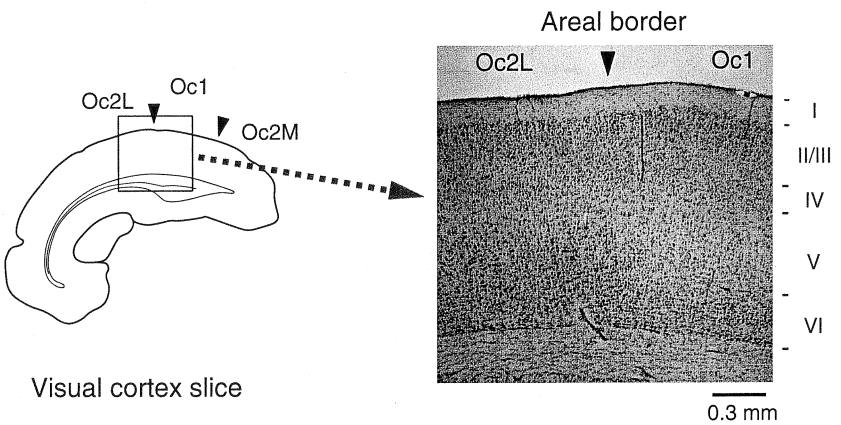

Fig. 1. Photomicrographs of a Nissl-stained visual cortex slice showing cytoarchitectonic features, in which the border of Oc1 and Oc2L is delineated. Photomicrographs were taken from the rectangular region indicated in the line drawing of the slice. Laminar borders of cortical layers and the Oc1/Oc2L border are indicated.

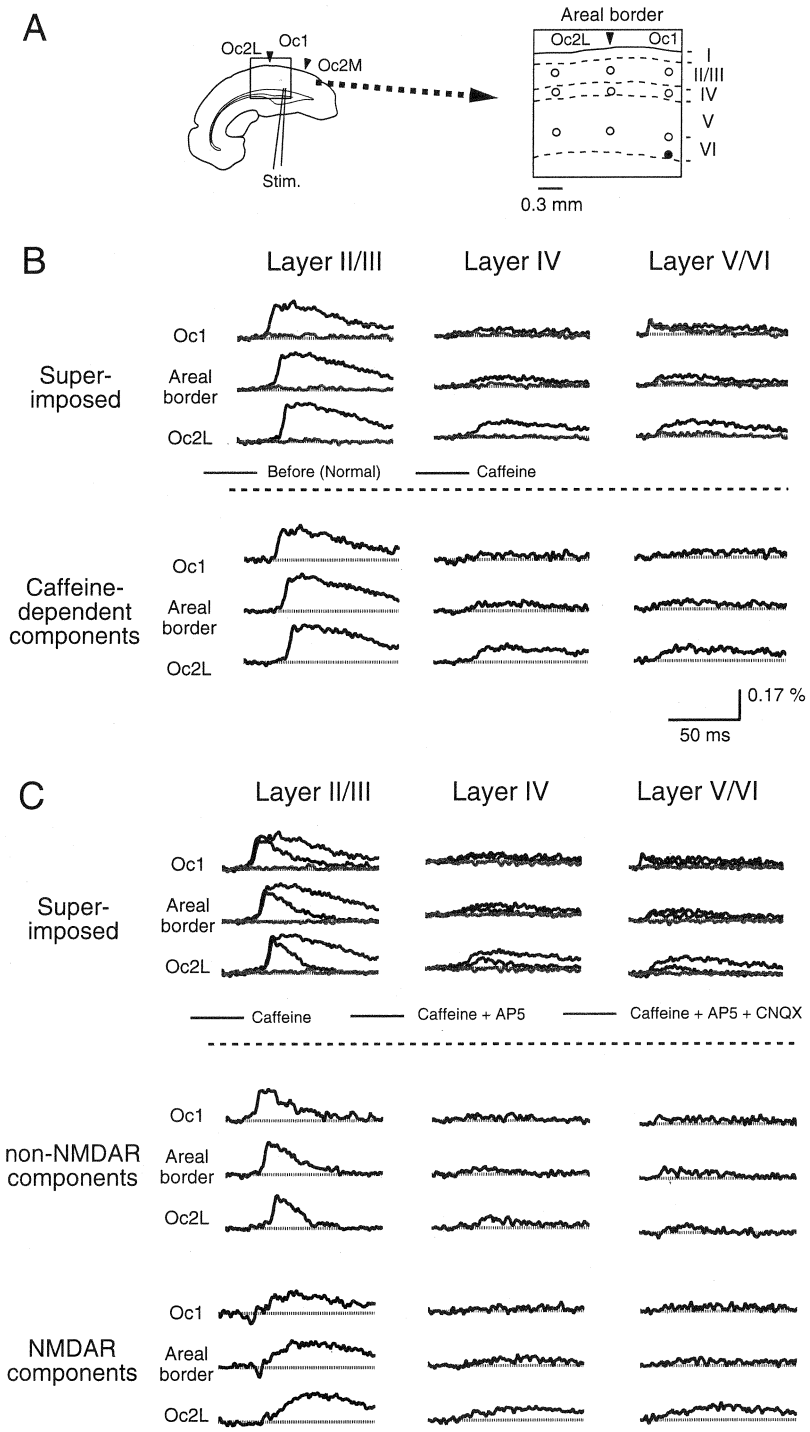

Fig. 2. Properties of initial propagating components from Oc1 to Oc2L. Time courses of optical responses obtained from ROIs arranged horizontally and vertically, as indicated in the line drawing in panel (A), where open and filled circles indicate ROIs and stimulation sites, respectively. (B) Time course responses after caffeine application are superimposed on those before caffeine application. Colored lines indicate before (dark green) and after (blue) caffeine application (upper). Recordings labeled 'Caffeine-dependent components' were obtained by subtracting recordings after caffeine application from those before application (lower). (C) Time course responses with 'caffeine + AP5' and 'caffeine + AP5 + CNQX' were superimposed on those with 'caffeine' (upper). Recordings labeled 'non-NMDAR-dependent components' were obtained by subtraction of recordings with 'caffeine + AP5 + CNQX' from recordings with 'caffeine + AP5' (middle). Recordings labeled 'NMDAR-dependent components' were obtained by subtraction of recordings with 'caffeine + AP5' from recordings with 'caffeine' (lower).

stored on a personal computer for off-line analysis. The camera unit of the Fujix HR Deltaron 1700 optical imaging system (Fuji Photo Film, Tokyo, Japan) contains a photodiode array of 128 × 128 elements. Using a ×10 objective lens, the whole array corresponded to a 2.24 × 2.24 mm area of tissue. A tungsten–halogen lamp (150 W) was used as the light source for absorption measurements. Light passed through a heat absorption filter and a narrow band interference filter, and was focused on the preparation. Illumination was controlled using an electromagnetic shutter to avoid dye bleaching or photodynamic damage. A total of 16 responses elicited by WM stimulation were averaged to form a run. Neural activities were recorded as intensity changes of transmitted light hitting each photodiode, with a temporal resolution of 0.6 ms per frame.

According to the purposes of the experiments, the following chemicals (Wako, Osaka, Japan) were added to the perfusion medium: caffeine, 3.5 mM; D-2-amino-5-phosphonovaleric acid (AP5), 10 μM; 6-cyano-7-nitroquinoxaline-2, 3-dione (CNQX), 20 μM. In this study, all recordings were performed in the medium with 0.5 mM $[Mg^{2+}]_o$.

3. Results

The present study applied the same protocol used previously to visual cortex slices including Oc1 and Oc2L [35,36,38]. Histological examination of Oc1 and Oc2M has been described previously [38]. Delineation of the areal border was based on descriptions by Swanson and Zilles [32,40]. Cytoarchitecture of recording areas was examined in the same way in the present study. Oc1 and Oc2L were identified by cytoarchitectural features. One clear difference between the two areas is that cell density in layer V is relatively high in Oc2L and relatively low in Oc1 (Fig. 1).

We previously reported that low frequency stimulation to the Oc1 WM in caffeine-containing medium induced initial signal propagation from Oc1 to Oc2M and oscillatory backward propagation from Oc2M to Oc1 [38]. Likewise, the present study found low frequency stimulation to Oc1 WM in caffeine-containing medium induced initial signal propagation from Oc1 to Oc2L and oscillatory backward propagation from Oc2L to Oc1 (18 slices in total). Attention was initially focused on the properties of initial signal flow from Oc1 to Oc2L. Fig. 2B (upper) shows initial optical responses before and after application of caffeine at the 9 ROIs illustrated in Fig. 2A. This indicates that signals propagate from Oc1 to Oc2L horizontally, and from layer V/VI to layer II/III vertically. Horizontal propagation was notably dominant in layer II/III and vertical propagation was dominant in Oc2L. Fig. 2C indicates that the initial propagating components comprise early non-NMDAR and late NMDAR components, with NMDAR components in Oc2L dominant compared to those in Oc1.

Fig. 3 showed spatiotemporal properties of both initial signal propagation from Oc1 to Oc2L and oscillatory backward propagation from Oc2L to Oc1. Before caffeine application, optical responses elicited by WM stimulation in Oc1 spread vertically, and reached layer II/III (Fig. 3A-1). However, responses were restricted to Oc1. After caffeine application, optical responses elicited by WM stimulation penetrated Oc2L along layer V/VI and layer II/III (Fig. 3A-2 upper). When initial responses were attenuated, secondary signals emerged in layer II/III in O2L and spread back to Oc1, principally along layer II/III. In the same way as secondary signals, succeeding oscillatory signals emerged at the same area in Oc2L and spread back to Oc1 several times (Fig. 3A-2 lower). According to our previous reports [38], generation and backward propagation of oscillatory signals from Oc2M to Oc1 was NMDAR-dependent. To address whether the same relativity is observed between Oc1 and Oc2L, NMDARs were blocked with application of AP5 after induction of oscillatory activities in caffeine-containing medium. Similar to the results in Oc1 and Oc2M [38], generation and backward propagation of oscillatory signals from Oc2L to Oc1 disappeared, whereas initial forward propagation remained (Fig. 3A-3). These findings were observed in 6 of 6 slices.

"To-and-fro" signal propagation was marked in layer II/III between Oc1 and Oc2L. Time courses of optical responses in layer II/III obtained from the same data displayed in Fig. 3A were thus plotted to investigate precise direction of signal propagation. Before caffeine application, horizontal propagation was restricted above the stimulation site in Oc1 (Fig. 3B-1). After caffeine application, amplitudes of optical responses were enlarged, and initial signals propagated bi-directionally from ROI 7 to ROI 10 and ROI 1 (Fig. 3B-2). This shows that initial responses penetrated from Oc1 to Oc2L along layer II/III. After initial signals were attenuated, oscillatory signals emerged from ROIs 2–3 and spread back toward ROI 10. Additional application of AP5 blocked both emergence of oscillatory responses and backward propagation, but initial bi-directional propagation remained, showing that oscillation and backward propagation are completely NMDAR-dependent, whereas the initial propagating components are non-NMDAR-dependent (Fig. 3B-3). Decay of the first waves was marked under application of AP5 compared with first waves in medium with caffeine alone, indicating that slow components of the first waves are NMDAR-dependent.

Caffeine application induced signal propagation and oscillation between Oc1 and Oc2L. Real caffeine-enhanced components can thus be obtained by subtracting time course responses in normal medium from those in caffeine-containing medium (Fig. 3C-1). This shows that both signal penetrations from Oc1 to Oc2L and backward propagation of oscillatory responses represent caffeine-enhanced com-

ponents. Time courses of NMDAR-dependent components in propagation and oscillation were obtained by subtracting time courses in medium with additional AP5 from time courses in medium with caffeine alone (Fig. 3C-2). This revealed that small first waves propagate bi-directionally from ROI 7, whereas marked oscillatory waves propagate back from ROIs 7–8 to ROI 10. These propagating components were NMDAR-dependent. Interestingly, NMDARs were active during the emergence of caffeine-enhanced components.

To investigate the contribution of NMDAR activities to the induction of propagation and oscillation during caffeine application, the next experiments were performed in the condition that AP5, an NMDAR blocker, was co-applied to the medium from the beginning of caffeine application. In normal medium, similar to Fig. 3A-1, optical responses elicited by WM stimulation in Oc1 spread vertically and reached layer II/III (Fig. 4A-1), and responses were restricted. In medium with co-application of caffeine and AP5, horizontal propagation from Oc1 to Oc2L along layer II/III and layer I/VI was enhanced, but signal amplitude was small (Fig. 4A-2). To investigate the precise direction of signal propagation, time courses of optical responses in layer II/III obtained from the same data were plotted. In normal medium, horizontal propagation was restricted in Oc1 (Fig. 4B-1). After application of caffeine with AP5, amplitudes of optical responses were slightly enlarged, and initial signals propagated bi-directionally from ROI 7 (Fig. 4B-2). However, the initial response was almost non-existant in Oc2L, and neither oscillatory responses nor backward propagation were present. These findings were observed in 5 of 5 slices.

The question arouses as to whether NMDAR activation alone can induce signal propagation and oscillation under caffeine application. In general, sufficient activation of NMDARs for induction of synaptic changes requires activation of non-NMDARs in glutamatergic synapses [2,25]. The next experiments were thus performed with co-application of non-NMDAR blocker, CNQX, to the medium from the beginning of caffeine application. In normal medium, similar to Figs. 3A and 4A, optical responses elicited by WM stimulation in Oc1 spread vertically, and reached layer II/III (Fig. 5A-1). After application of caffeine with CNQX, only small vertical propagation was appeared (Fig. 5A-2), but responses disappeared quickly. Caffeine application was thus unable to enhance horizontal propagation under non-NMDAR blockade, nor could oscillatory responses or backward propagation be induced. These findings were observed in 3 of 3 slices.

Since we were focusing attention on facilitation of horizontal propagation induced by caffeine application, responses after caffeine washout should be compared with those before caffeine application. Fig. 6B shows that once oscillation was induced with caffeine application, signals penetrated to Oc2L from Oc1 along horizontal pathways even after caffeine washout. However, when induction of oscillation was blocked with co-application of caffeine and D-AP5, signals could barely penetrate to the areal border, and did not reach Oc2L, after washout of both caffeine and D-AP5 (Fig. 6C). Indeed, caffeine, a membrane-permeable chemical, is difficult to washout completely, but comparison of Fig. 6B with C revealed that the caffeine-dependent facilitation of horizontal pathways from Oc1 to Oc2L requires NMDAR-dependent oscillatory signal propagation. These findings were observed in 5 of 5 and 4 of 4 slices, respectively.

4. Discussion

We have previously described signal propagation and oscillation in the area between Oc1 and Oc2M under caffeine application [38]. According to that report, signals penetrating from Oc1 to Oc2M generate oscillatory activity in Oc2M, and signals spread back to Oc1 repeatedly for several times. Generation of neural oscillation in Oc2M was entirely dependent on NMDAR. In the same way, the

Fig. 3. Properties of signal propagation and oscillation between Oc1 and Oc2L. (A) Spatiotemporal dynamics of propagation and oscillation recorded from a visual cortex slice. Illustrations indicating the locations of stimulation site (Stim.) and Oc1/Oc2M and Oc1/Oc2L borders (arrowheads) (right side). (A1–3) Selected pseudo-color images of optical signals. Recordings were made in normal medium (before), in medium containing caffeine alone (caffeine), and in medium containing caffeine + AP5. Time after stimulation is indicated at the bottom and applies to all recordings on the same columns from top to bottom. (A1–2) At 6.6 ms after stimulation, a small area became slightly depolarized in layer II/III immediately above the simulation site in both normal and caffeine-containing media. (A2) In contrast with control medium, the area expanded bilaterally and, on the left, spread into Oc2L in caffeine-containing medium (Forward propagation). At 106.8 ms, the second wave started to travel from Oc2L, and at 150.0 ms, the traveling wave had already penetrated Oc1 (2nd wave). In similar ways, the 3rd to 5th waves propagated periodically from Oc2L to Oc1 (Backward propagation; 3rd to 5th waves). (A3) Additional application of AP5 abolished the 2nd to 5th waves, but the initial wave remained. Note that AP5 was applied after propagation and oscillation between Oc1 and Oc2L were established. (B) Time courses of optical responses obtained from ROIs arranged horizontally in layer II/III (ROIs 1–10), as indicated in the line drawing on the right. The filled circle indicates stimulation site. (B1–3) Time courses of optical responses in normal medium (before), medium containing caffeine alone (caffeine), and medium containing caffeine + AP5. These time causes were obtained from the same data as presented in Fig. 1. (C) Recordings labeled 'NMDAR-dependent components' were obtained by subtraction of recordings labeled 'caffeine + AP5' from recordings labeled 'caffeine'. For each experimental group, traces obtained from ROIs 1–10 are arranged in numerical order from bottom to top. ROI 7 is located just above the stimulation site. Trace-by-trace comparison of wave peaks in recordings labeled 'caffeine' indicates that the first wave propagates from ROI 7 to both ROIs 1 and 10, whereas later waves always propagate from ROIs 2–3 to ROI 10.

present study demonstrated that signals penetrating from Oc1 to Oc2L generate oscillatory activity in Oc2L, and signals spread back to Oc1 repeatedly. Generation of neural oscillation in Oc2L was also dependent on NMDAR. Oc2M and Oc2L are similar in that cell density is relatively high in layer V and relatively low in Oc1.

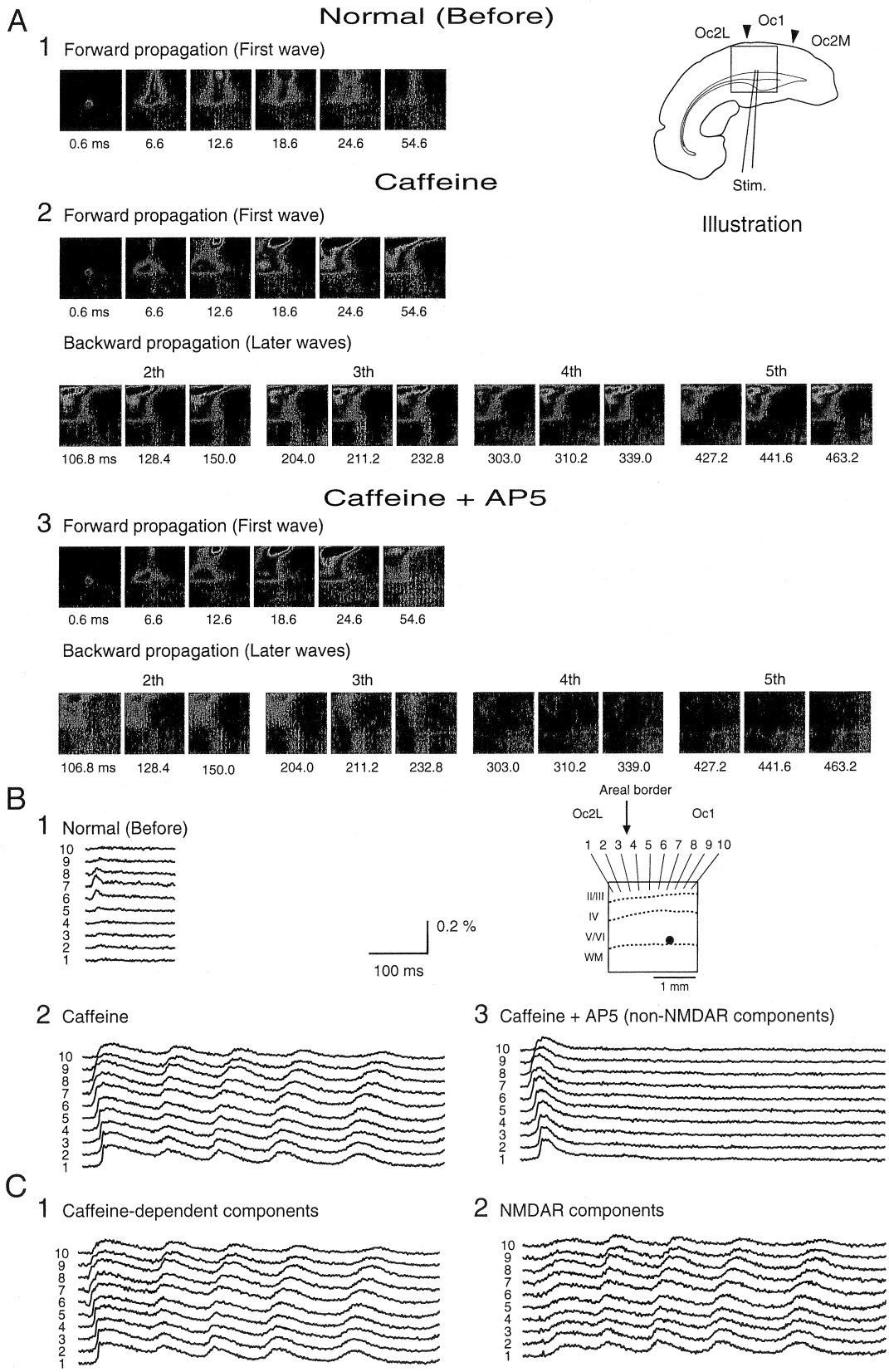

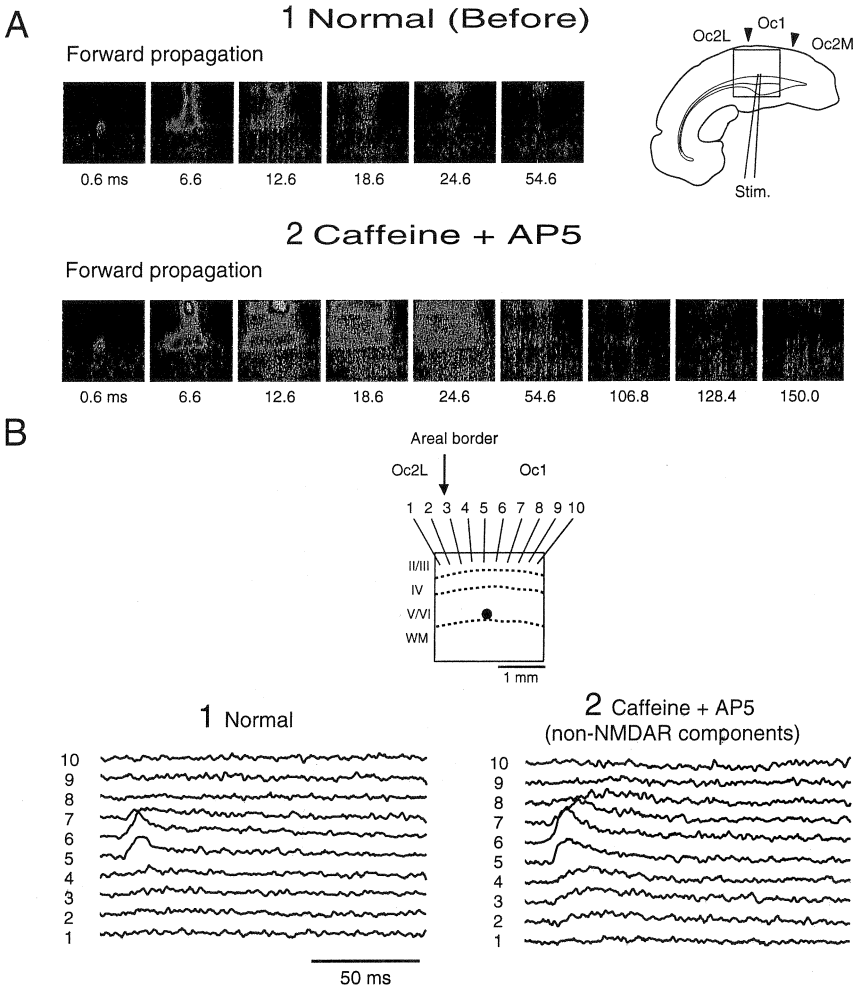

Fig. 4. Effects of NMDAR blockade on induction of propagation and oscillation between Oc1 and Oc2L. (A) Spatiotemporal dynamics of signal propagation recorded from a visual cortex slice. Illustrations indicating locations of the stimulation site (Stim.) and Oc1/Oc2M and Oc1/Oc2L borders (arrowheads) (right side). (B) Time courses of optical responses obtained from ROIs arranged horizontally in layer II/III (ROIs 1–10), as indicated in the line drawing on the right. Filled circle indicates the stimulation site. (B1–2) Time courses of optical responses in normal medium, and medium containing caffeine + AP5. Time courses were obtained from the same data as presented in panel A. For each experimental group, traces obtained from ROIs 1–10 are arranged in numerical order from bottom to top. ROI 5 is located just above the stimulation site.

From the perspective of cytoarchitectural features, Oc2M and Oc2L are bilaterally symmetrical around Oc1. Interestingly, the manner of signal interactions between Oc2M and Oc1 and between Oc2L and Oc1 displayed bilateral symmetry. Optical responses were relatively high through all layers in both Oc2M and Oc2L, whereas responses were dominant in the upper layer of Oc1. This might reflect differences in cell density between Oc1 and Oc2. Considering the three-dimensional relationship between Oc1 and Oc2, Oc2 is located around Oc1 [24,27,32,40]. Our previous and present results demonstrate that neurons in Oc2 located around Oc1 are liable to oscillate and deliver signals to Oc1, where both the induction and propagation of oscillatory activities are NMDAR-dependent. Since NMDAR activation is largely required for inducing synaptic plasticity in the CNS [6,7,9,20,22,25], Oc2 might be involved in modulating neural function in Oc1. This may support the hypothesis that synaptic plasticity underlies cortical map reorganization [5].

The induction mechanism underlying horizontal signaling pathways between Oc1 and Oc2L represents the most interesting finding in the present study. Once initial horizontal propagation and oscillation are established between Oc1 and Oc2L under caffeine application in conditions where NMDARs are active, initial forward propagation no longer requires NMDAR activities. Non-NMDAR activities are enough to convey signals from Oc1 to Oc2L (Figs. 2, 3). In contrast, when NMDAR activities are blocked before the establishment of propagation and oscillation, signals from Oc1 can no longer penetrate to Oc2L, even under caffeine application (Fig. 4). Moreover, signal penetration from Oc1 to Oc2L remained even after washout of caffeine in cases where caffeine-dependent oscillation was induced, whereas in cases with oscillation blocked by co-application of caffeine and AP5, signal

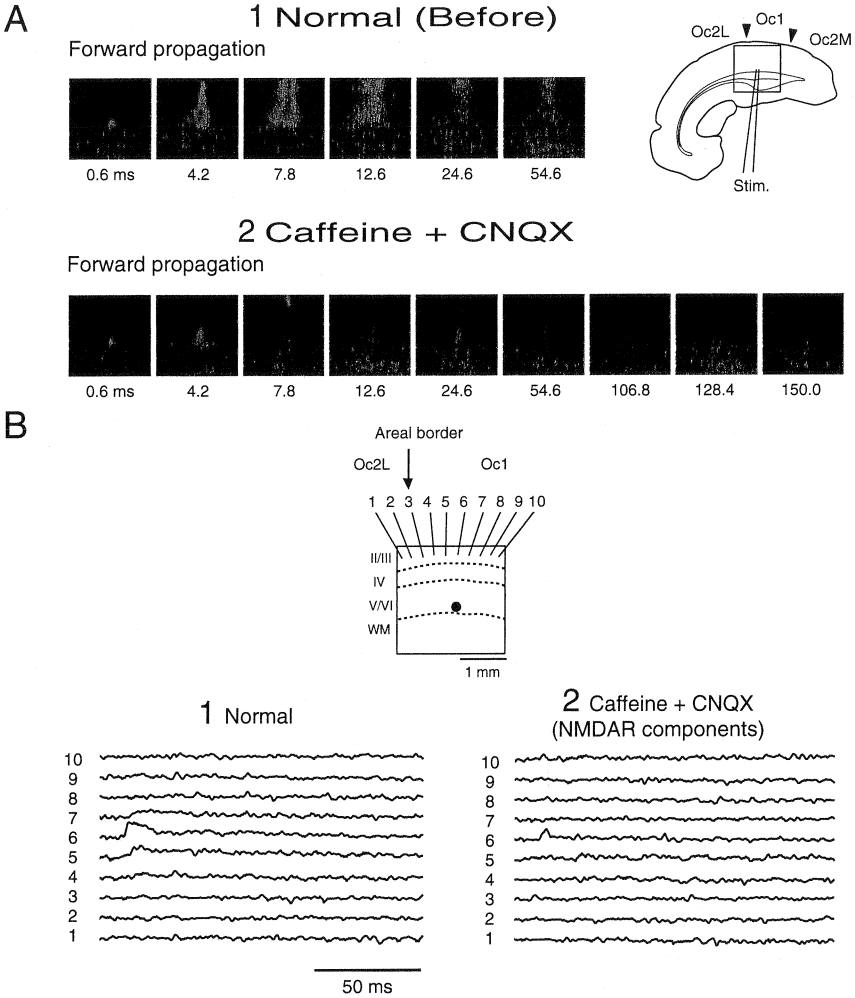

Fig. 5. Effects of non-NMDAR-blockade on induction of propagation and oscillation between Oc1 and Oc2L. (A) Spatiotemporal dynamics of signal propagation recorded from a visual cortex slice. Illustrations indicating locations of stimulation site (Stim.) and Oc1/Oc2M and Oc1/Oc2L borders (arrowheads) (right side). (B) Time courses of optical responses obtained from ROIs arranged horizontally in layer II/III (ROIs 1–10), as indicated in the line drawing on the right. Filled circle indicates the stimulation site. (B1–2) Time courses of optical responses in normal medium, and medium containing caffeine + CNQX. Time courses were obtained from the same data as presented in panel A. For each experimental group, traces obtained from ROIs 1–10 are arranged in numerical order from bottom to top. ROI 6 is located just above the stimulation site.

penetration was blocked after washout of both caffeine and AP5. Comparing responses in normal medium after caffeine conditioning under conditions of NMDAR activity with responses under NMDAR blockade, signals after conditioning with NMDAR activation could travel more widely than those without NMDAR activation (Fig. 6). These findings suggest that NMDAR activities are crucial to the induction of signal penetration from Oc1 to Oc2. In other words, horizontal signal pathways between Oc1 and Oc2 are opened to traffic by NMDAR activation. Causality may be described as follows: NMDAR activity causes the effect of opening non-NMDAR-dependent intrinsic pathways between Oc1 and Oc2L.

For initial signals traveling in a horizontal direction (Fig. 3A-2), deep layer signals start just after delivery of stimulation to Oc1 WM, whereas upper layer signals start after arrival of vertical signals to layer II/III above the stimulation site. In contrast, for backward signals traveling horizontally, upper layer signals start after the appearance of later waves from layer II/III in Oc2L, whereas deep layer signals start behind upper layer signals. From the perspective of Oc2L, initial signals were inputs from Oc1, whereas backward signals were outputs to Oc1. Again considering causality, output signal traveling caused the effect of facilitating input signal traveling. Precise traveling pathways must differ between input and output signals, but the spatial regions for dominant depolarization of membrane potentials are the same (Fig. 3A-2). Amplitudes of responses recorded by optical recording using voltage-sensitive dyes are considered to reflect excitable synaptic potentials [34]. The dominant region for synaptic activities is thus layer II/III, when input and output signals travel between Oc1 and Oc2. We propose that input signals from Oc1 manage to switch on neural

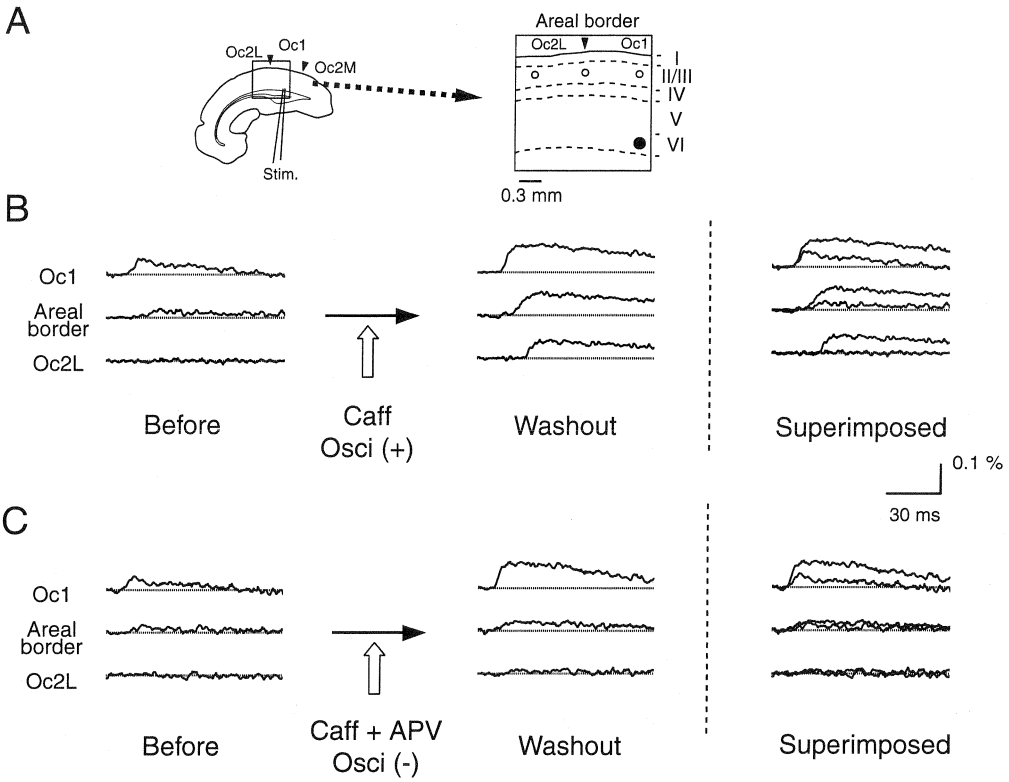

Fig. 6. Comparing signal propagations in normal medium after caffeine conditioning under NMDAR activity with propagations under NMDAR blockade. Time courses of optical responses obtained from ROIs arranged horizontally, as indicated in the line drawing in panel A. Open and filled circles indicate ROIs and stimulation site, respectively. (B) After optical responses were stable, oscillation was induced with caffeine application. Caffeine was then removed from the medium. Time courses of optical responses before caffeine application and 60 min after caffeine washout were illustrated. (C) After optical responses stabilized, induction of oscillation was blocked with co-application of caffeine and D-AP5. Both caffeine and D-AP5 were then removed from the medium. Time courses of optical responses before co-application of caffeine and D-AP5 and 60 min after washout are shown.

oscillators in Oc2, and output signals from Oc2 then repetitively stimulate NMDARs located at layer II/III, which in turn induce modification or recruitment of non-NMDARs located near each active NMDAR, resulting in opening and strengthening of intrinsic signal pathways between Oc1 and Oc2.

Acknowledgments

We wish to thank Dr. N. Kato for his valuable advice on our manuscript, and Mssrs. H. Adachi and S. Muramoto for technical assistance. This work was supported by grants from Kanazawa Medical University (Grant for Promoted Research No. S2003-9 to H.Y.).

References

[1] T.D. Albright, G.R. Stoner, Contextual influences on visual processing, Annu. Rev. Neurosci. 25 (2002) 339–379.
[2] T.P.V. Bliss, G.L. Collingridge, A synaptic model of memory: long term potentiation in the hippocampus, Nature 361 (1993) 31–39.
[3] V. Bringuier, F. Chavane, L. Glaeser, Y. Frégnac, Horizontal propagation of visual activity in the synaptic integration field of area 17 neurons, Science 283 (1999) 695–699.
[4] J. Bullier, Integrated model of visual processing, Brain Res. Rev. 36 (2001) 96–107.
[5] D.V. Buonomano, M.M. Merzenich, Cortical plasticity: from synapses to maps, Annu. Rev. Neurosci. 21 (1998) 149–186.
[6] R.C. Carroll, R.S. Zukin, NMDA-receptor trafficking and targeting: implications for synaptic transmission and plasticity, Trends Neurosci. 25 (2002) 571–577.
[7] G.L. Collingridge, T.V.P. Bliss, NMDA receptors: their role in long-term potentiation, Trends Neurosci. 10 (1987) 288–293.
[8] A. Das, C.D. Gilbert, Long-range horizontal connections and their role in cortical reorganization revealed by optical recording of cat primary visual cortex, Nature 375 (1995) 780–784.
[9] N.W. Daw, P.S.G. Stein, K. Fox, The role of NMDA receptors in information processing, Ann. Rev. Neurosci. 16 (1993) 207–222.
[10] M.B. Delva, L.C. Katz, Rearrangement of synaptic connections in visual cortex revealed by laser photostimulation, Science 265 (1994) 255–258.
[11] C.D. Gilbert, T.N. Weisel, Columnar specificity of intrinsic horizontal and cortico-cortical connections in cat visual cortex, J. Neurosci. 9 (1989) 2432–2442.
[12] C.D. Gilbert, A. Das, M. Ito, M. Kapadia, G. Westheimer, Spatial integration and cortical dynamics, Proc. Natl. Acad. Sci. U. S. A. 93 (1996) 615–622.
[13] A. Grinvald, Real time optical mapping of neural activity; from single growth cones to the intact mammalian brain, Annu. Rev. Neurosci. 8 (1985) 263–305.
[14] J.M. Hupé, A.C. James, B.R. Payne, S.G. Lomber, P. Girard, J. Bullier, Cortical feedback improves discrimination between figure and background by V1, V2 and V3 neurons, Nature 394 (1998) 784–787.

[15] L.C. Katz, E.M. Callaway, Development of local circuits in mammalian visual cortex, Annu. Rev. Neurosci. 15 (1992) 31–56.
[16] Z.F. Kisvarday, U.T. Eysel, Cellular organization of reciprocal patchy networks in layer III of cat visual cortex (area 17), Neuroscience 46 (1992) 275–286.
[17] D. Liao, R.H. Scannevin, R. Huganir, Activation of silent synapses by rapid activity-dependent synaptic recruitment of AMPA receptors, J. Neurosci. 21 (2001) 6008–6017.
[18] W. Lu, H. Man, W. Ju, W.S. Trimble, J.F. MacDonald, Y.T. Wang, Activation of synaptic NMDA receptors induces membrane insertion of new AMPA receptors and LTP in cultured hippocampal neurons, Neuron 29 (2001) 243–254.
[19] H.L. Luhmann, L. Mattinez Millan, W. Singer, Development of horizontal intrinsic connections in cat striate cortex, Exp. Brain Res. 63 (1986) 443–448.
[20] R.C. Malenka, Postsynaptic factors control the duration of synaptic enhancement in area CA1 of the hippocampus, Neuron 6 (1991) 53–60.
[21] R.C. Malenka, R.A. Nicoll, Long-term potentiation—a decade of progress? Science 285 (1999) 1870–1874.
[22] S.J. Martin, P.D. Grimwood, G.M. Morris, Synaptic plasticity and memory: an evaluation of the hypothesis, Annu. Rev. Neurosci. 23 (2000) 649–711.
[23] Y. Momose-Sato, K. Sato, H. Mochida, I. Yazawa, S. Sasaki, K. Kamino, Spreading depolarization waves triggered by vagal stimulation in the embryonic chick brain: optical evidence for intracellular communication in the developing central nervous system, Neuroscience 102 (2001) 245–262.
[24] V.M. Monetero, Retinotopy of cortical connections between the striate cortex and extrastriate visual areas in the rat, Exp. Brain Res. 94 (1993) 1–15.
[25] R.A. Nicoll, R.C. Malenka, Expression mechanisms underlying NMDA receptor-dependent long-term potentiation, Ann. N.Y. Acad. Sci. 868 (1999) 515–525.
[26] A.L. Obaid, B.M. Salzberg, Micromolar 4-aminopyridine enhances invasion of a vertebrate neurosecretory terminal arborization: optical recording of action potential propagation using an ultrafast photodiode-MOSFET camera and a photodiode array, J. Gen. Physiol. 107 (1996) 353–368.
[27] G. Paxinos, C. Watson, The Rat Brain in Stereotaxic Coordinates, 4th ed., Academic Press, San Diego, 1997.
[28] P.A. Salin, P. Girard, H. Kennedy, J. Bullier, Visuotopic organization of corticocortical connections in the visual of the cat, J. Comp. Neurol. 22 (1992) 415–434.
[29] P.A. Salin, P. Girard, J. Bullier, Visuotopic organization of corticocortical connections in the visual system, Prog. Brain Res. 95 (1993) 169–178.
[30] W. Singer, Development and plasticity of cortical processing architectures, Science 270 (1995) 758–764.
[31] T. Sugai, M. Sugitani, N. Onoda, Novel subdivision of the rat accessory olfactory bulb revealed by the combined method with lectin histochemistry, electrophysiological and optical recordings, Neuroscience 95 (2000) 23–32.
[32] L.W. Swanson, Brain Maps: Structure of the Rat Brain, 2nd ed., Elsevier, Amsterdam, 1992.
[33] M. Sur, C.A. Leamey, Development and plasticity of cortical areas and networks, Nature Rev. 2 (2001) 251–262.
[34] M. Tanifuji, T. Sugiyama, K. Murase, Horizontal propagation excitation in rat visual cortex slices revealed by optical imaging, Science 266 (1994) 1057–1059.
[35] H. Yoshimura, T. Sugai, N. Onoda, N. Segami, N. Kato, Synchronized population oscillation of excitatory synaptic potentials dependent on calcium-induced calcium release in rat neocortex layer II/III neurons, Brain Res. 915 (2001) 94–100.
[36] H. Yoshimura, T. Sugai, N. Onoda, N. Segami, N. Kato, Age-dependent occurrence of synchronized population oscillation suggestive of a developing functional coupling between NMDA and ryanodine receptors in the neocortex, Dev. Brain Res. 13 (2002) 663–668.
[37] H. Yoshimura, N. Kato, T. Sugai, N. Segami, N. Onoda, Age-dependent emergence of oscillatory signal flow between the primary and secondary visual cortices in rat brain slices, Brain Res. 990 (2003) 172–181.
[38] H. Yoshimura, N. Kato, T. Sugai, M. Honjo, J. Sato, N. Segami, N. Onoda, To-and-fro optical voltage signal propagation between the insular gustatory and parietal oral somatosensory areas in rat cortex slices, Brain Res. 1015 (2004) 114–121.
[39] T. Yousef, T. Bonhoeffer, D.S. Kim, U.T. Eysel, E. Toth, Z.F. Kisvarday, Orientation topography of layer 4 lateral networks revealed by optical imaging in cat visual cortex (area 18), Eur. J. Neurosci. 11 (1999) 4291–4308.
[40] K. Zilles, A. Wree, Cortex: areal and laminar structure, in: G. Paxinos (Ed.), The Rat Nervous System, 2nd ed., Academic Press, San Diego, 1995, pp. 649–685.

Available online at www.sciencedirect.com

SCIENCE DIRECT

Brain Research 1045 (2005) 12–21

BRAIN RESEARCH

www.elsevier.com/locate/brainres

Research report

NMDA receptor-dependent oscillatory signal outputs from the retrosplenial cortex triggered by a non-NMDA receptor-dependent signal input from the visual cortex

Hiroshi Yoshimura[a,b,*], Tokio Sugai[b], Makoto Honjo[a], Natsuki Segami[a], Norihiko Onoda[b]

[a]*Department of Oral and Maxillofacial Surgery, Kanazawa Medical University, Uchinada-cho 920-0293, Japan*
[b]*Department of Physiology, Kanazawa Medical University, Uchinada-cho 920-0293, Japan*

Accepted 23 February 2005
Available online 28 April 2005

Abstract

The retrosplenial cortex is located at a critical juncture between the visual cortex and hippocampal formation. Functions of the retrosplenial cortex at the local circuit level, however, remain unclear. Herein, we show how signals traveling from the visual cortex behave in local circuits of the retrosplenial cortex, using optical recording methods and application of caffeine to rat brain slices. Electrical signals evoked in the primary visual cortex penetrated into the deep layer of the retrosplenial granular a cortex (RSGa) and propagated further toward postsubiculum and upper layer. Non-*N*-methyl-D-aspartate (NMDA) receptor-dependent initial traveling signal from the visual cortex triggered NMDA receptor-dependent neural oscillation in the RSGa. Oscillatory signals originated from the local area in the deep layer of the RSGa, and the signal spread back and forth toward the visual cortex and postsubiculum, in addition to spreading toward the upper layer. From the perspective of the RSGa, extrinsic signal inputs from the visual cortex switched on neural oscillators in the RSGa that deliver NMDA receptor-dependent intrinsic signal outputs. Opening and strengthening of non-NMDA receptor-dependent input pathways from the visual cortex required NMDA receptor-dependent oscillatory neural activities. These input and output relationships indicate that the retrosplenial cortex may represent an important relay station between the visual cortex and hippocampal formation.

Theme: Excitable membranes and synaptic transmission
Topic: Postsynaptic mechanisms

Keywords: Visual cortex; Retrosplenial cortex; Caffeine; Optical recording; Horizontal propagation; Oscillation

1. Introduction

The neocortex and hippocampal formation play important roles in cognitive functions of the brain [16,17]. The retrosplenial cortex is located between these two areas and is thought to be concerned with processing of spatial information and episodic memory [1–3,6,7,19,22]. Neuroanatomically, the retrosplenial cortex receives innervations from the visual cortex and projects fibers to the hippocampal formation, and these connections are reciprocal [12,26–29,31]. The retrosplenial cortex might therefore act as an interface between these two areas. Despite the important location, functions of the retrosplenial cortex at the local circuit level have not been clarified.

We recently succeeded in demonstrating the dynamics of signal propagation and oscillation between the primary and secondary visual cortices (Oc1 and Oc2, respectively) of rats [35,37]. To demonstrate spatiotemporal dynamics, optical recording methods were used with voltage-sensitive dyes applied to slices of visual cortex, and caffeine was used to enhance overall synaptic activities. The results of those studies led us to propose that *N*-methyl-D-aspartate (NMDA) receptor-dependent oscillatory activ-

* Corresponding author. Department of Oral and Maxillofacial Surgery, Kanazawa Medical University, Uchinada-cho 920-0293, Japan. Fax: +81 76 286 2010.
E-mail address: hyoshimu@kanazawa-med.ac.jp (H. Yoshimura).

0006-8993/$ - see front matter © 2005 Elsevier B.V. All rights reserved.
doi:10.1016/j.brainres.2005.02.084

ities originating in Oc2 strengthen non-NMDA receptor-dependent horizontal pathways between Oc1 and Oc2. These findings suggest that a device delivering NMDA receptor-dependent oscillatory signals may also be equipped outside the visual cortex to open longer-range corticocortical pathways from the visual cortex. The present study focused attention on the retrosplenial cortex, and our experimental protocol and recording methods [35,37] were applied in an attempt to demonstrate that the retrosplenial cortex includes a generator of neural oscillation that delivers NMDA receptor-dependent signals to the surrounding areas.

2. Methods

All experiments were performed in accordance with the guidelines for the ethical use of animals approved by the Japanese Physiological Society. Wistar rats (27 to 32 days old) were decapitated under ether anesthesia, and the brains were quickly removed and soaked in cold medium (2–4 °C) comprising NaCl 124 mM, KCl 3.3 mM, NaH_2PO_4 1.25 mM, $MgSO_4$ 1.3 mM, $CaCl_2$ 2 mM, $NaHCO_3$ 26 mM, and D-glucose 10 mM, saturated with 95% O_2–5% CO_2. Brain slices (350 μm thick) including visual cortex, retrosplenial cortex, postsubiculum, and subiculum were prepared using a slicer. Once cut, slices were left at room temperature for at least 1 h before starting the recording session.

High-speed optical recording methods were used with voltage-sensitive dyes to observe spatiotemporal dynamics of spreading neural activities. Details of the optical recording system used in this study have been described elsewhere by us and other groups [5,13,21,24,35,37]. For optical recordings, slices were incubated with voltage-sensitive dye NK2761 (0.125 mg/ml; Nihon Kanko, Okayama, Japan) for 20 min then transferred to the recording system. Slices were placed in a submerged-type chamber set on the stage of an IMT-2 upright microscope (Olympus, Tokyo, Japan) and perfused with medium (30 °C; 5 ml/min). A bipolar tungsten electrode for stimulation was inserted into the border region between gray and white matter (WM) in Oc1 (WM stimulation). Duration and intensity of stimuli were 80 μs and 250–350 μA, respectively. Synaptic responses were elicited by WM stimulation at 0.03–0.3 Hz. Field potentials were recorded for monitoring electrical activities using a glass micropipette filled with 3 M NaCl and stored on a personal computer for off-line analysis. The camera unit of the Fujix HR Deltaron 1700 optical imaging system (Fuji Photo Film, Tokyo, Japan) contains a photodiode array of 128 × 128 elements. Using a ×10 objective lens, the whole array corresponded to a 2.24 × 2.24 mm area of tissue. A 150-W tungsten–halogen lamp was used as the light source for absorption measurements. Light passed through a heat absorption filter and a narrow band interference filter and was focused on the preparation. Illumination was controlled using an electromagnetic shutter to avoid dye bleaching or photodynamic damage. A total of 16 responses elicited by WM stimulation were averaged to form a run. Neural activities were recorded as intensity changes of transmitted light hitting each photodiode, with a temporal resolution of 0.6 ms/frame.

The following chemicals (Wako, Osaka, Japan) were added to the perfusion medium according to the purposes of the experiments: caffeine, 3.5 mM; D-2-amino-5-phosphonovaleric acid (AP5), 10 μM; and 6-cyano-7-nitroquinoxaline-2, 3-dione (CNQX), 20 μM. In this study, all recordings were performed in medium with 0.5 mM $[Mg^{2+}]_o$.

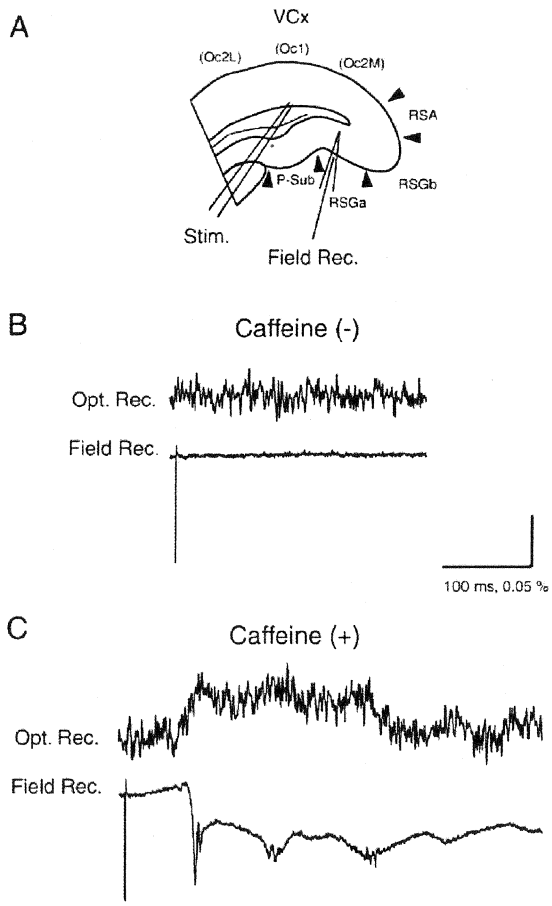

Fig. 1. Simultaneous recording of optical signal and field potentials from the same site in the ventral part of the retrosplenial cortex, RSGa. (A) Illustration of a slice used for optical recordings, indicating locations of the stimulation site, field potential recording site, and areal borders between several cortices (arrowheads). VCx, visual cortex; Oc2L, lateral secondary visual cortex; Oc1, primary visual cortex; Oc2M, medial secondary visual cortex; RSA, retrosplenial agranular cortex; RSGa, retrosplenial granular a cortex; RSGb, retrosplenial granular b cortex; P-Sub, postsubiculum. (B) No response was detected by either optical recording or field potential recording in medium without caffeine. (C) After application of low-frequency WM stimulation, stable synchronized population oscillation was detected by both optical recording and field potential recording in medium with caffeine.

3. Results

In the previous studies [32,33,35,37], we found a protocol whereby synchronized membrane potential oscillations of α-range frequency can be induced in rat visual cortex slices. Stable membrane potential oscillation will finally appear after continuing low-frequency stimulation to WM in medium containing caffeine with 0.5 mM $[Mg^{2+}]_o$. In those studies, optical recording methods were used with voltage-sensitive dyes to observe the spatiotemporal dynamics of oscillation. These studies revealed that: (1) oscillation comprised both initial forward propagation from Oc1 that is non-NMDA receptor-dependent, and subsequent backward propagation from Oc2 that is NMDA receptor-dependent; and (2) backward propagation from Oc2 causes strengthening of forward propagation from Oc1.

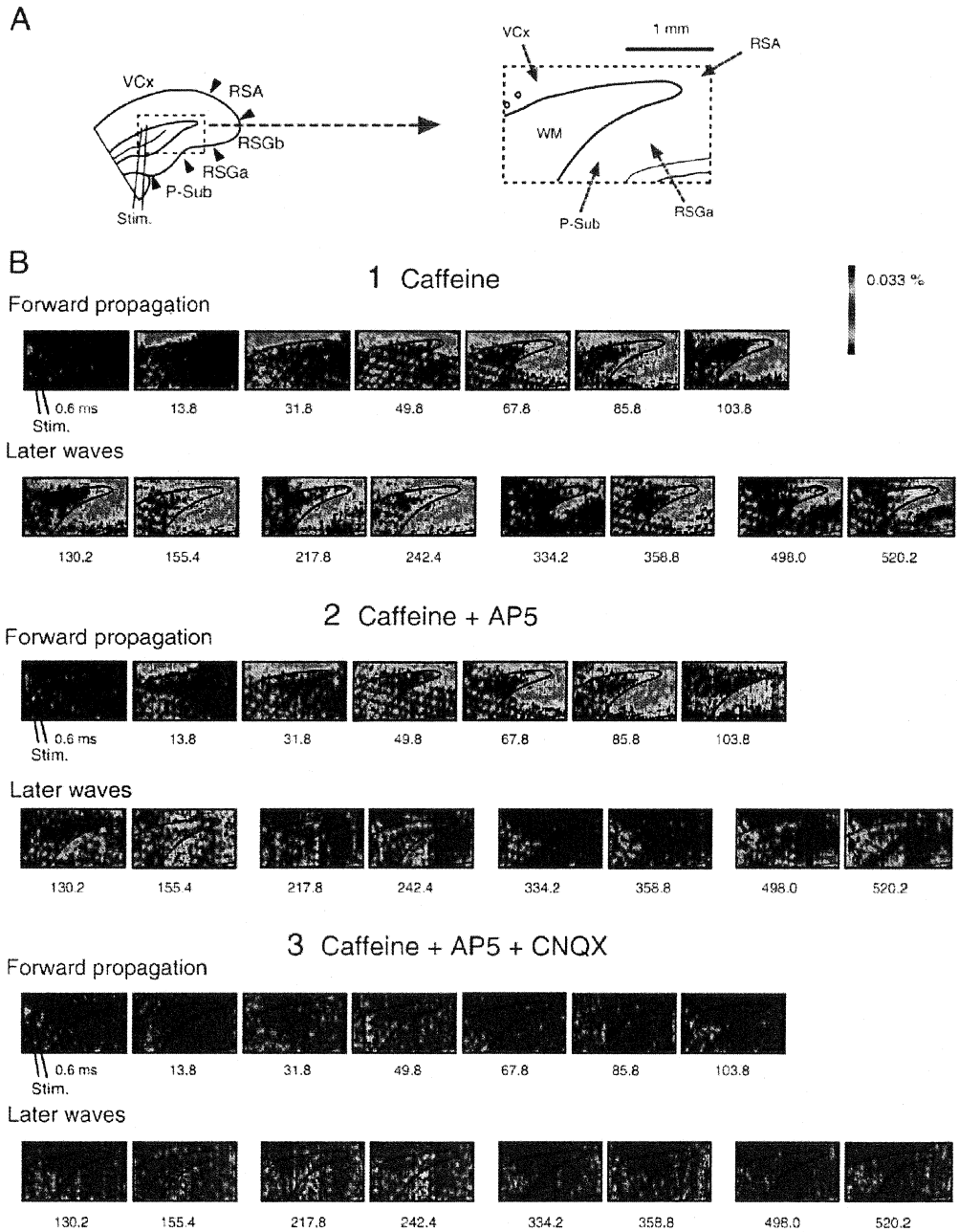

Fig. 2. Spatiotemporal dynamics of voltage signal propagation in the RSGa. (A) Illustration of a slice (right) and a window of interest that includes RSGa (left). (B) Selected pseudo-color images of optical signals. Recordings were made in medium containing "Caffeine" alone, "Caffeine + AP5", or "Caffeine + CNQX + AP5". Time after stimulation is indicated at the bottom. (1 Caffeine) After delivery of stimulation, the initial signal begins to propagate and penetrates into P-Sub, while later signals come from the deep layer of the RSGa. (2 Caffeine + AP5) Additional application of AP5 abolishes later waves, but forward propagation remains. (3 Caffeine + AP5 + CNQX) Additional application of CNQX abolishes later waves, and all waves disappear.

The retrosplenial cortex is divided into the retrosplenial agranular cortex (RSA), retrosplenial granular b cortex (RSGb), and retrosplenial granular a cortex (RSGa) (Fig. 1A) [23,26,29,38]. The RSGa is the ventral part of the retrosplenial cortex and, compared with the RSGb, is more closely related to the hippocampal formation than to the neocortex, suggesting that the RSGa is situated in a critical position for processing "limbic information" [26–28]. For these reasons, the present study focused on the RSGa.

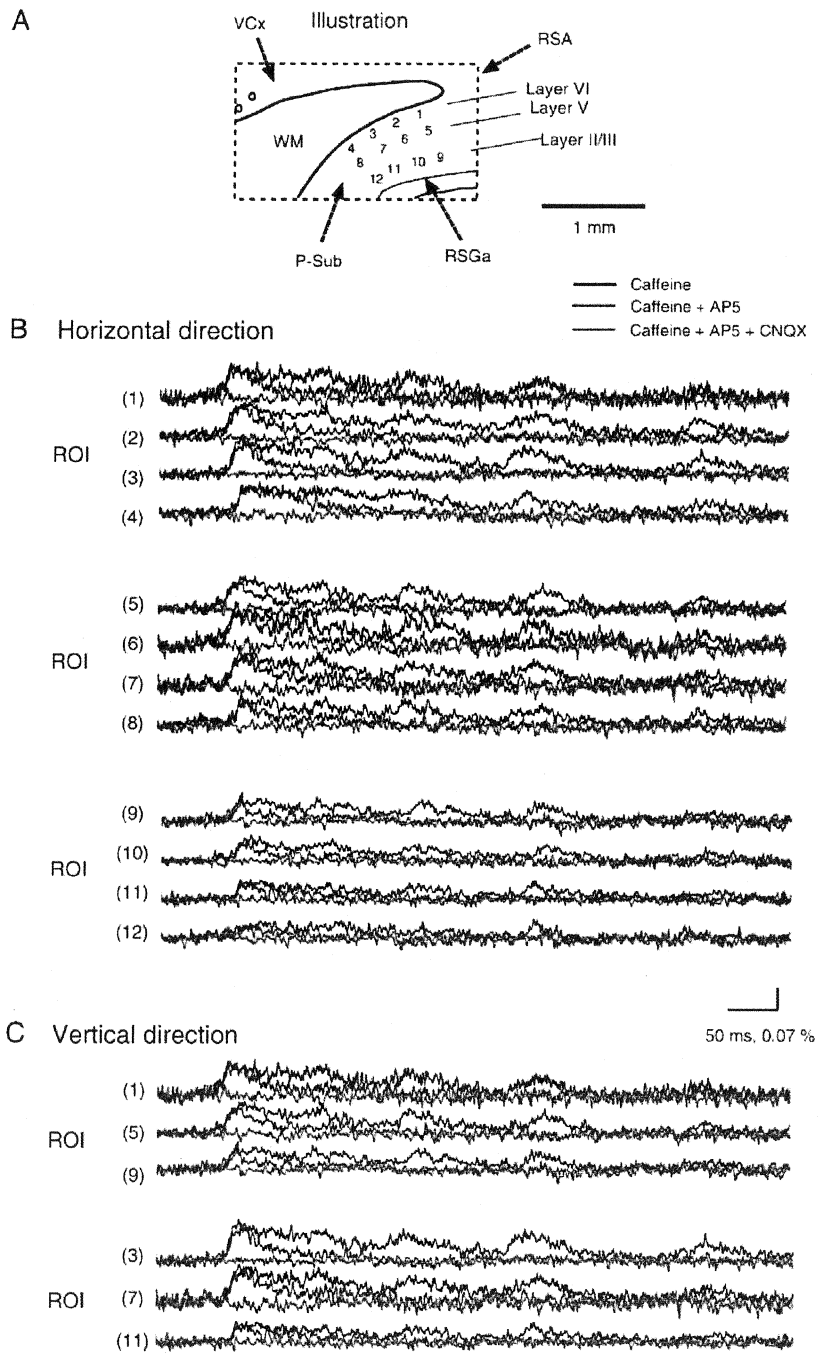

Fig. 3. Time courses of optical responses in RSGa, obtained from optical recordings illustrated in Fig. 2B. (A) Regions of interests (ROI 1–12) are shown in an illustration of the RSGa. (B) Time courses of optical responses obtained from ROIs arranged horizontally in layers VI (ROIs 1–4), V (ROIs 5–8), and II/III (ROIs 9–12) (1 Horizontal direction) or vertically (ROIs 1, 5, 9) and (ROIs 3, 7, 11) (Vertical direction), respectively in the same slice, which was used for recordings described in Fig. 2B. Time courses of optical responses recorded in the 3 media, "Caffeine" "Caffeine + AP5", and "Caffeine + CNQX + AP5" were superimposed at every ROI.

Electrical stimulation was delivered to WM of the primary visual cortex (Fig. 1A). Field potential recordings and optical recordings with voltage sensitive dyes were made simultaneously from the RSGa. In normal medium, WM stimulation elicited no response in the RSGa (Fig. 1B). After application of caffeine into the medium with low-

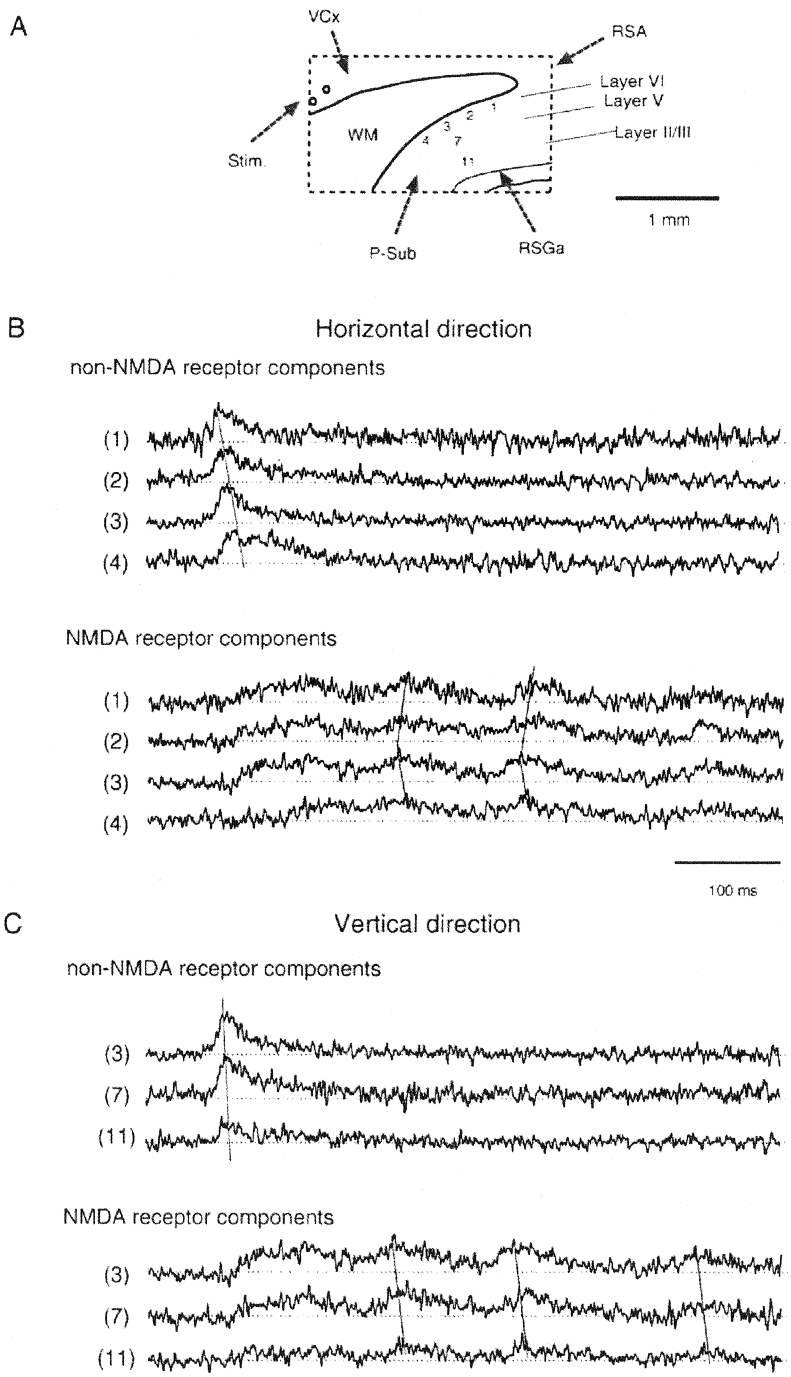

Fig. 4. Properties of propagating components horizontally and vertically in the RSGa. (A) Regions of interests (ROI 1–4, ROI 3, 7, 11) shown in an illustration of the RSGa. (B) Recordings labeled "non-NMDA receptor components" were obtained by subtracting recordings with "Caffeine + AP5 + CNQX" from recordings with "Caffeine + AP5" in Fig. 3B. Recordings labeled "NMDA receptor components" were obtained by subtracting recordings with "Caffeine + AP5" from recordings with "Caffeine" in Fig. 3B. Peaks of the first waves and 2–3 series of later waves were fitted with the blue and red lines, respectively. Note that fitting lines on later waves in the horizontal direction display reflection points, indicating that later peaks emerge within the RSGa. Scale bars apply to all recordings shown in panel B.

frequency WM stimulation, marked voltage oscillation was generated in the RSGa. Oscillation was observed from both the field potential recording and optical recording, and timing of voltage reflection was the same between the two time course responses (Fig. 1C). Simultaneous recording revealed that optical responses reflected the electrical activities of neurons. These RSGa oscillations were observed in 21 of 25 slices.

The recording windows were set on the deep layer of the visual cortex and RSGa to observe spatiotemporal optical responses between stimulation site and RSGa (Fig. 2A). Evoked signal propagated horizontally in the deep layer of the visual cortex and penetrated into the RSGa (Fig. 2B-1). After arrival of the signal to layer VI in the RSGa, the signal propagated further toward the postsubiculum and layer II/III (Fig. 2B-1, forward propagation). After attenuation of the first wave, a secondary wave emerged in the deep layer of the RSGa and propagated back and forth horizontally and vertically. These oscillatory dynamics were repeated several times (Fig. 2B-1, later waves). In our previous reports, initial forward components of first wave from primary to secondary visual cortex were largely dependent on non-NMDA receptors, with subsequent oscillatory components dependent on NMDA receptors. Here again, blockade of NMDA receptors abolished oscillation in the RSGa, whereas initial forward propagation from the visual cortex to the RSGa remained intact (Fig. 2B-2, caffeine + AP5). Additional application of CNQX completely blocked signal propagation (Fig. 2B-3, caffeine + AP5 + CNQX). Initial forward components of the first wave from the visual to the retrosplenial cortex are thus dependent on non-NMDA receptors, and subsequent oscillatory components originating from the RSGa depend on NMDA receptors. These findings were confirmed in all 5 slices.

To observe the precise temporal course of optical responses in the RSGa, 12 regions of interest (ROIs) were selected (Fig. 3A). To understand vertical signal propagation, time courses of optical signals obtained from ROIs in layers VI, V, and II/III were arranged vertically (Fig. 3C; ROIs 1, 5, 9, ROIs 3, 7, 11). Time courses under application of caffeine, additional application of AP5, and further additional application of CNQX were superimposed. Peak-by-peak comparisons of signals obtained from time course responses located vertically in the RSGa indicate that the initial wave propagates from layer VI to layer II/III, and later oscillatory waves also propagate from layer VI to layer

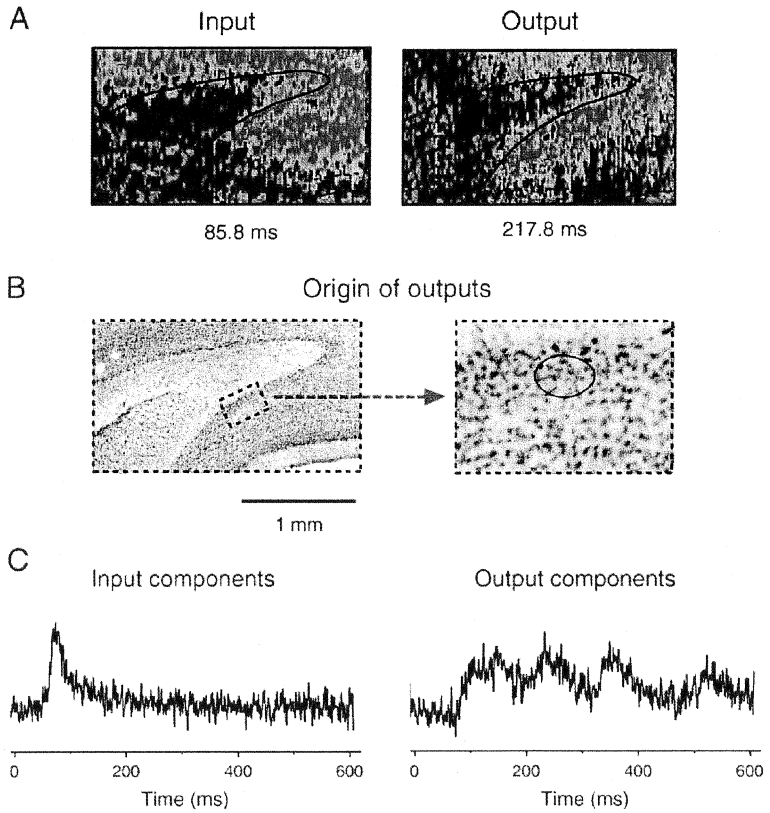

Fig. 5. Features of cytoarchitecture and electromotive force at the area of output origin. (A) Optical images at 80.6 ms and 217.8 ms after WM stimulation show input and output signals, respectively. (B) Photomicrograph of a Nissl-stained brain slice showing cytoarchitectural features of recording window, taken after optical recordings illustrated in Figs. 2–4 and panel A of this figure (right) and cytoarchitectural features of the output origin (ellipse in right box). (C) Features of electromotive force at the area of output origin, taken from ROI 3 in Fig. 4. Note that "Input components" switch on the voltage oscillators that generate "Output components".

II/III. Additional application of AP5 depressed later waves in addition to the late phase of the initial wave, and further additional application of CNQX flattened responses. These results show that the initial wave comprises fast non-NMDA receptor components and slow NMDA receptor components, whereas later oscillatory waves comprise NMDA receptor components only.

To facilitate understanding of horizontal signal propagation, time courses of optical signals obtained from layer VI of the RSGa were arranged horizontally (Fig. 3B; ROIs 1–4; ROIs 5–8; ROIs 9–12). This shows that the initial wave propagates horizontally from the dorsal retrosplenial cortex to the postsubiculum, whereas direction of propagation for later waves is not the same as the initial wave. Peak-by-peak comparison of signals indicates that later waves first emerge at ROI 3 and propagate bi-directionally. Signal flows between the visual cortex and RSGa are reciprocal. The same tendency was observed in layers V and II/III. Time courses of optical signals on additional application of AP5 and further additional application of CNQX were superimposed with time courses for application of caffeine alone. These results also show that the initial wave comprises fast non-NMDA receptor components and slow NMDA receptor components, whereas later oscillatory waves comprise NMDA receptor components only.

The origin of later oscillatory waves thus seems to lie in layer V/VI in the RSGa (ROI 3), and signals propagate repetitively both vertically and horizontally from the origin. To observe precise time courses of optical responses for non-NMDA receptor and NMDA receptor components around the origin of oscillation in the RSGa, 6 ROIs including ROI 3 were selected (Fig. 4A). Time courses of NMDA receptor-dependent components were obtained by subtracting time courses in medium with additional AP5 from time courses in medium with caffeine alone (Figs. 4B lower, C lower). Time courses of non-NMDA receptor-dependent components were obtained by subtracting time courses in medium with additional CNQX from time courses in medium with caffeine + AP5 (Figs. 4B upper, C upper). Horizontally, initial non-NMDA receptor components propagated from the dorsal retrosplenial cortex to the postsubiculum, whereas later NMDA receptor components propagated bi-directionally from ROI 3 (Fig. 4B). Vertically, initial non-NMDA receptor components

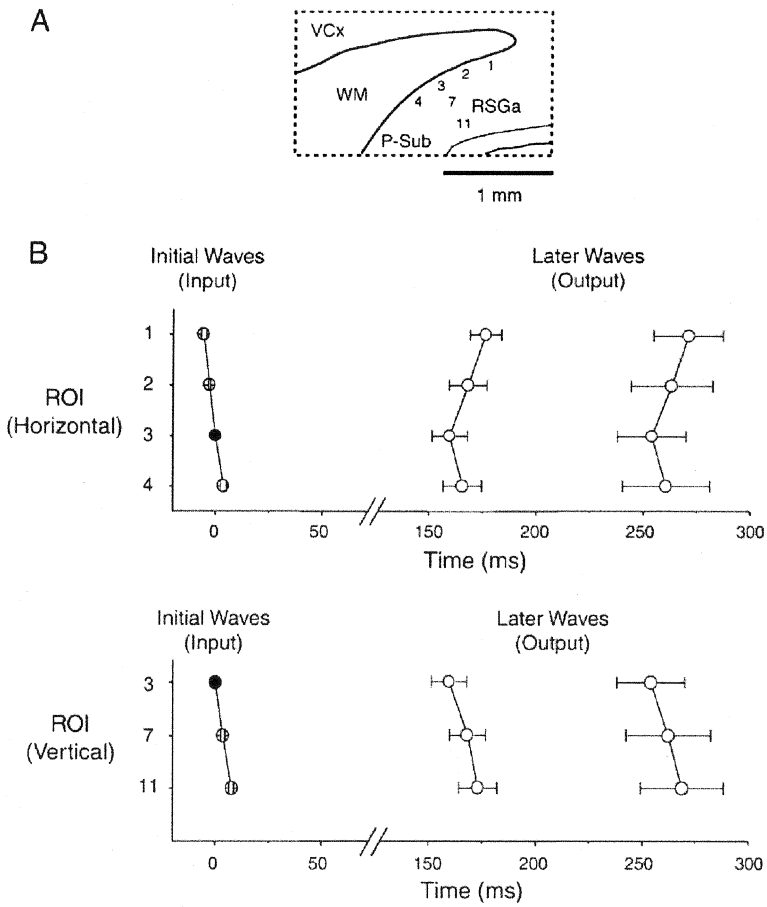

Fig. 6. Averaged time-to-peak of first and later waves in layer VI of the RSGa. Time-to-peak of the initial wave at ROI 3 was considered zero, and time-to-peak of initial and later waves at ROIs 1, 2, 4, 7, and 11 were normalized and averaged. Mean time (open circle) and standard deviation (cap) were plotted. ROI-by-ROI changes in time-to-peak indicate that first waves propagate from ROIs 1–4, whereas later waves propagate bi-directionally from ROI 3.

propagated from layer VI to layer II/III, and later NMDA receptor components propagated in the same direction from ROI 3 (Fig. 4C).

From the perspective of the RSGa, signal inputs from the visual cortex switched on the neural oscillators in the RSGa that deliver NMDA receptor-dependent oscillatory signal outputs. An optical recording frame at 85.8 ms after WM stimulation (Fig. 5A left) shows input signal propagation, and an optical recording frame at 217.8 ms (Fig. 5A right) shows generation of output signals. Cytoarchitectural features were observed from the same slice used for optical recording (Fig. 5B), showing that the origin of oscillatory outputs is located layer VI in the RSGa and revealing no marked differences in cytoarchitectural features compared with the surrounding area. Electromotive force of input and output at the origin of oscillatory outputs is illustrated in Fig. 5C. Non-NMDA receptor-dependent extrinsic input switches on NMDA receptor-dependent intrinsic generator of oscillation. Neurons of the output origin have the ability to intrinsically generate electromotive force as shown in Fig. 5C right.

To obtain and estimate accurate time differences between peak times of input and output signals, time-to-peak of the initial wave at ROI 3 was considered zero, and peak times of initial and later waves at various ROIs (Fig. 6A) were averaged respectively over 5 slices. Mean times are shown in Fig. 6B. Horizontally, time-to-peak of later waves at ROI 3 (159.7 ± 8.2 ms) was significantly smaller than that at ROI 1 (176.3 ± 7.2 ms; $n = 5$). Vertically, time-to-peak of later waves at ROI 3 (159.7 ± 8.2 ms) was significantly smaller than that at ROI 11 (173.2 ± 8.9 ms; $n = 5$). These results show that the first wave propagated horizontally from ROI 1 to ROI 4, whereas later waves emerged first at ROI 3 and propagated bi-directionally toward both ROI 1 and ROI 4. Vertically, initial waves propagated from ROI 3 to ROI 11, and later waves propagated in the same direction from ROI 3. These findings suggest that initial waves propagate from the visual cortex to the postsubiculum by way of the retrosplenial cortex, whereas later waves emerge first within the RSGa and propagate horizontally back-and-forth in addition to vertically.

The contribution of NMDA receptor activities to the induction of signal propagation from the visual cortex to the RSGa during caffeine application was investigated in the next experiment. Application of AP5 to the medium from the beginning abolished both signal propagation from the visual cortex and oscillation in the RSGa. Additional application of CNQX kept the response flat. Non-NMDA receptor-dependent components were obtained in the same way as mentioned above (Fig. 7B lower). To clearly demonstrate the contribution of NMDA receptor-dependent oscillation to the generation of non-NMDA receptor-dependent signal inputs to the RSGa from the visual cortex, two experimental protocols were used, and the respective time courses were shown (Fig. 7B). The results showed that establishment of long-range signals traveling from the visual

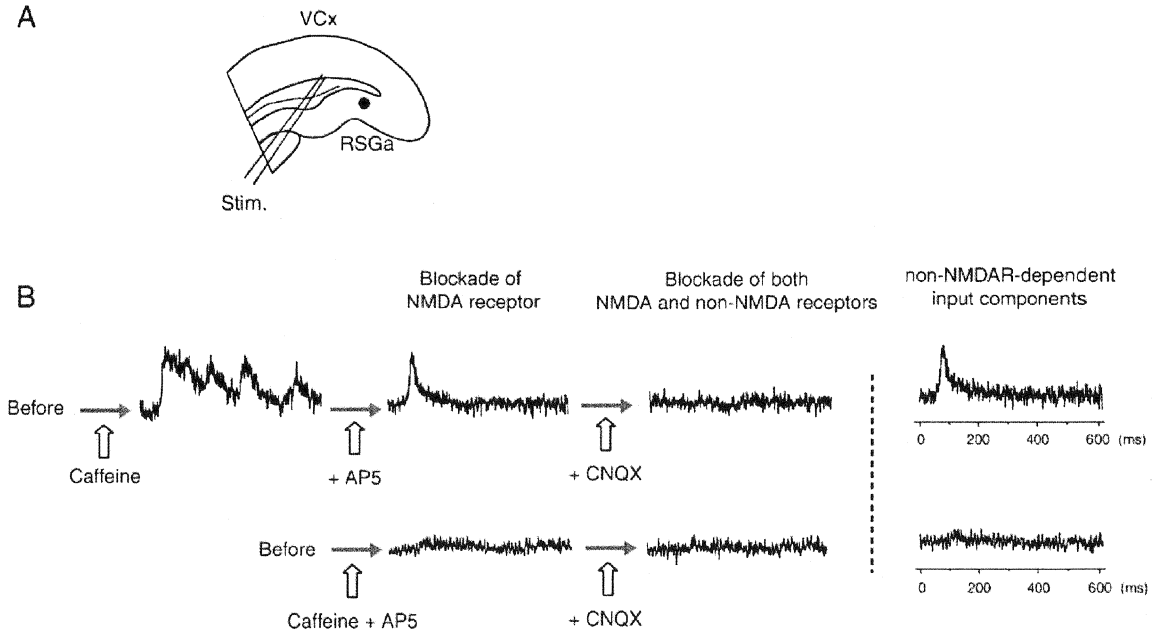

Fig. 7. Comparing non-NMDA receptor-dependent input components at the RSGa after caffeine conditioning under NMDA receptor activity with those under NMDA receptor blockade. (A) ROI (●) and stimulation site are illustrated. (B) Two experimental protocols are schematically illustrated, and the respective time course responses are shown. Labeled "non-NMDA receptor-dependent input components" were obtained by subtracting recordings with "Caffeine + AP5 + CNQX" from recordings with "Caffeine + AP5". Note that once NMDA receptor-dependent oscillation is induced, non-NMDA receptor-dependent components remain even after NMDA receptor blockade (upper), but when oscillation is blocked from the beginning under NMDA receptor blockade, non-NMDA receptor-dependent components are not observed (lower).

cortex toward the RSGa and postsubiculum require NMDA receptor-dependent activities.

4. Discussion

In general, electrical signals cannot travel a long distance in slice preparations in normal artificial cerebrospinal fluid (ASCF). This may be because many input and output fibers are severed, and the population of neurons in the slice preparation does not represent a complete neural formation, with the result that it is difficult to induce spatiotemporal integration or amplification of signals. Glutamatergic networks play important roles in information processing in the cortical region [4,9,10,15,18,20,25,30]. If heterogeneity of functions exists between different cortical regions, functional differences may be exaggeratedly when elicited by accelerating glutamatergic network activities, even if the cortical regions are transferred into slices. Several experimental protocols were developed by us and another group, in which caffeine effectively enhances activities of both NMDA and non-NMDA receptors in local circuits of neocortical slices [32–37] and hippocampal slices [8]. Using our protocols, the action of caffeine was found to be heterogeneous rather than homogenous in cortical regions of slices. The visual cortical region equips local combustible areas where NMDA receptor-dependent oscillatory outputs are generated, when the area receives intracortical or corticocortical inputs [35,37]. The local combustible area thus acts as a booster and signal relay station. Our protocols may be helpful for detecting "hot spots" from cortical slice preparations.

We have already reported the existence of generators of NMDA receptor-dependent neural oscillation at local areas in lateral part of the secondary visual cortex (Oc2L) and medial part of the secondary visual cortex (Oc2M) [35,37]. The present study focused attention on the RSGa. Neuroanatomical examination revealed that the RSGa receives not only visual cortical innervations, but also thalamic, hippocampal, and other neocortical innervations and projects information to the hippocampal formation and other cortical areas [12,26–29,31]. The RSGa is thus connected with numerous neural fibers. In general, the higher order cortex may equip diffuse projections and spatial reciprocity of feedforward and feedback connections [18]. The present study found the generators of NMDA receptor-dependent neural oscillation in this RSGa area. Behaviors of signals in the RSGa were as follows. The initial non-NMDA receptor-dependent signal traveling from the visual cortex triggers NMDA receptor-dependent neural oscillators in the deep layer of the RSGa, from which oscillatory signals originate and signals spread back and forth toward the visual cortex and postsubiculum and also spread toward the upper layer of the RSGa. From the perspective of the RSGa, extrinsic signal inputs switch on neural oscillators in the RSGa, which repetitively deliver NMDA receptor-dependent intrinsic signal outputs. These input and output relationships indicate that the retrosplenial cortex acts as a signal distributor and may represent an important rely station between the visual cortex and hippocampal formation.

No cytoarchitectural differences, such as cell density or somatic morphology, are apparent between the oscillatory origin and the surrounding area (Fig. 5). The precise mechanisms underlying the generation of NMDA receptor-dependent neural oscillation is unclear. However, showing that the relay station is located outside the visual cortex is very important. Our previous study found that NMDA receptor-dependent forward and backward signal propagation from Oc2 strengthens the non-NMDA receptor-dependent intrinsic signal pathway between Oc1 and Oc2 [37]. In the same way, delivery of NMDA receptor-dependent oscillatory signals from the RSGa was required to open signal pathways from the visual cortex toward the postsubiculum in the present study. The NMDA receptor-dependent voltage oscillator may induce use-dependent strengthening of wiring between the two cortices, since NMDA receptors are deeply concerned with use-dependent synapse plasticity [11,14], such as plastic changes in reciprocal assembly-forming cortical connections [9,20]. One function of the oscillators in the Oc2 and RSGa that might be expected is strengthening of functional connections between the visual cortex and hippocampal formation, allowing visual information from the external world to travel further toward the "limbic system".

Acknowledgments

We wish to thank Dr. N. Kato for providing valuable advice on the manuscript and Mssrs. H. Adachi and S. Muramoto for technical assistance. This work was supported by grants from Kanazawa Medical University (Grant for Promoted Research No. S2003-9 to H.Y.).

References

[1] M. Bar, E. Aminoff, Cortical analysis of visual context, Neuron 38 (2003) 347–358.

[2] L.L. Chen, L.H. Lin, E.J. Green, C.A. Barnes, B.L. McNaughton, Head-direction cells in the rat posterior cortex: I. Anatomical distribution and behavioral modulation, Exp. Brain Res. 101 (1994) 8–23.

[3] J. Cho, P.E. Sharp, Head direction, place, and movement correlates for cells in the rat retrosplenial cortex, Behav. Neurosci. 115 (2001) 3–25.

[4] A. Compte, N. Brunel, P.S. Goldman-Rakic, X.J. Wang, Synaptic mechanisms and network dynamics underlying spatial working memory in a cortical network model, Cereb. Cortex 10 (2000) 910–923.

[5] W. Fu, T. Sugai, H. Yoshimura, N. Onoda, Convergence of olfactory and gustatory connections onto the endopiriform nucleus in the rat, Neurosci. 126 (2004) 1033–1041.

[6] M. Gabriel, S. Sparenborg, Posterior cingulate cortical legions eliminate learning-related unit activity in the anterior cingulate cortex, Brain Res. 409 (1987) 151–157.

[7] K.T. Harker, I.Q. Whishaw, Impaired spatial performance in rats with letrosplenial regions: importance of the spatial problem and the rat strain in identifying lesion effects in a swimming pool, J. Neurosci. 22 (2002) 1155–1164.
[8] S.-J. He, C. Xiao, Z.-Y. Wu, D.-Y. Ruan, Caffeine-dependent stimulus-triggered oscillations in the CA3 region of hippocampal slices from rats chronically exposed to lead, Exp. Neurol. 190 (2004) 525–534.
[9] L.C. Katz, C.J. Shatz, Synaptic activity and the construction of cortical circuits, Science 274 (1996) 1133–1138.
[10] A.A. Koulakov, S. Raghavachari, A. Kepecs, J.E. Lisman, Model for a robust neural integrator, Nat. Neurosci. 5 (2002) 775–782.
[11] R.C. Malenka, R.A. Nicoll, Long-term potentiation—A decade of progress? Science 285 (1999) 1870–1874.
[12] M.W. Miller, B.A. Vogt, Direct connections of rat visual cortex with sensory, motor, and association cortices, J. Comp. Neurol. 226 (1984) 184–202.
[13] Y. Momose-Sato, K. Sato, K. Kamino, Optical approaches to embryonic development of neural functions in the brainstem, Prog. Neurobiol. 63 (2001) 151–197.
[14] R.A. Nicoll, R.C. Malenka, Expression mechanisms underlying NMDA receptor-dependent long-term potentiation, Ann. N.Y. Acad. Sci. 868 (1999) 515–525.
[15] R.J. Reimer, R.T. Fremeau Jr., E.E. Bellocchio, R.H Edwards, The essence of excitation, Curr. Opin. Cell Biol. 13 (2001) 417–421.
[16] E.T. Rolls, Hippocampo-cortical and cortico-cortical backprojections, Hippocampus 10 (2000) 380–388.
[17] L.A. Rothblat, L.F. Kromer, Object recognition memory in the rat: the role of the hippocampus, Behav. Brain Res. 42 (1991) 25–31.
[18] P.-A. Salin, J. Bullier, Corticocortical connections in the visual system: structure and function, Physiol. Rev. 75 (1995) 107–154.
[19] R. Sayed, W. Mubrak, A. Ohtsuka, T. Taguchi, T. Murakami, Histochemical study of perineuronal nets in the retrosplenial cortex of adult rats, Ann. Anat. 184 (2002) 333–339.
[20] W. Singer, Development and plasticity of cortical processing architectures, Science 270 (1995) 758–764.
[21] T. Sugai, M. Sugitani, N. Onoda, Novel subdivisions of the rat accessory olfactory bulb revealed by the combined method with lectin histochemistry, electrophysiological and optical recordings, Neuroscience 95 (2000) 23–32.
[22] R.J. Sutherland, I.Q. Whishaw, B. Kolb, Contributions of cingulate cortex to two forms of spatial learning and memory, J. Neurosci. 8 (1988) 1863–1872.
[23] L.W. Swanson, Brain maps: structure of the rat brain, 2nd ed., Elsevier, Amsterdam, 1992.
[24] M. Tanifuji, T. Sugiyama, K. Murase, Horizontal propagation excitation in rat visual cortex slices revealed by optical imaging, Science 266 (1994) 1057–1059.
[25] J. Tegner, A. Compte, X.J. Wang, The dynamical stability of reverberatory neural circuits, Biol. Cybern. 87 (2002) 471–481.
[26] T. van Groen, M. Wyss, Connections of the retrosplenial granular a cortex in rats, J. Comp. Neurol. 300 (1990) 593–606.
[27] T. van Groen, M. Wyss, The postsubicular cortex in the rat: characterization of the forth region of the subicular cortex and its connections, Brain Res. 529 (1990) 165–177.
[28] T. van Groen, M. Wyss, Connections of the retrosplenial granular b cortex in rats, J. Comp. Neurol. 463 (2003) 249–263.
[29] B.A. Vogt, M.W. Miller, Cortical connections between rat cingulated cortex and visual, motor, and postsubicular cortices, J. Comp. Neurol. 216 (1983) 192–210.
[30] X.J. Wang, Synaptic basis of cortical persistent activity: the importance of NMDA receptors to working memory, J. Neurosci. 19 (1999) 9587–9603.
[31] J.M. Wyss, T. van Groen, Connections between the retrosplenial cortex and the hippocampal formation in the rat: a review, Hippocampus 2 (1992) 1–11.
[32] H. Yoshimura, T. Sugai, N. Onoda, N. Segami, N. Kato, Synchronized population oscillation of excitatory synaptic potentials dependent on calcium-induced calcium release in rat neocortex layer II/III neurons, Brain Res. 915 (2001) 94–100.
[33] H. Yoshimura, T. Sugai, N. Onoda, N. Segami, N. Kato, Age-dependent occurrence of synchronized population oscillation suggestive of a developing functional coupling between NMDA and ryanodine receptors in the neocortex, Dev. Brain Res. 136 (2002) 63–68.
[34] H. Yoshimura, N. Kato, T. Sugai, N. Segami, N. Onoda, Age-dependent appearance of an insulo-parietal cortical signal propagation that elicits a synchronized population oscillation in the parietal cortex in rats, Dev. Brain Res. 143 (2003) 245–251.
[35] H. Yoshimura, N. Kato, T. Sugai, N. Segami, N. Onoda, Age-dependent emergence of oscillatory signal flow between the primary and secondary visual cortices in rat brain slices, Brain Res. 990 (2003) 172–181.
[36] H. Yoshimura, N. Kato, M. Honjo, T. Sugai, N. Segami, N. Onoda, Age-dependent emergence of a parieto-insular corticocortical signal flow in developing rats, Dev. Brain Res. 149 (2004) 45–51.
[37] H. Yoshimura, T. Sugai, N. Segami, N. Onoda, Strengthening of non-NMDA receptor-dependent horizontal pathways between primary and lateral secondary visual cortices after NMDA receptor-dependent oscillatory neural activities, Brain Res. (in press).
[38] K. Zilles, A. Wree, Cortex, in: G. Paxinos (Ed.), The Rat Nervous System, 2nd ed., Academic Press Inc., San Diego, 1995, pp. 649–685.

1．研究課題名：ヒト口唇小唾液腺由来の幹細胞の同定（研究番号 S2003-10）

2．キーワード：1）唾液腺（salivary gland）
2）再生医療（regenerative medicine）
3）組織幹細胞（tissue stem cell）

3．研究者氏名：河南崇典・医学部・助手・血液免疫制御学(血液免疫内科学)

4．研 究 目 的

シェーグレン症候群（以下SS）は唾液腺、涙腺等の外分泌腺を系統的に冒す自己免疫疾患である。SSは唾液腺や涙腺などへの著しいリンパ球浸潤により腺組織を傷害し、唾液、涙液の分泌低下、乾燥症状を呈する。この唾液分泌減少による口腔乾燥症状は、う歯の増加や口渇、口内炎の反復による嚥下困難や摂食障害、不眠の原因となり、患者の生活の質の点で重大な問題となっている。腺組織の障害が無く分泌が低下した患者に対しては分泌を促進することも可能であるが、一度萎縮した唾液腺機能の回復は現在のところほとんど期待できず、唾液腺組織の再生、機能回復を目的とした根治的治療法が強く望まれている。近年、組織の再生において成体組織幹細胞に高い注目が寄せられている。動物の体を構成する多種多様な組織細胞の多くは恒常性の維持のために常に更新され続ける。このような個体の維持のため新たな細胞を供給する源となる細胞が組織幹細胞である。再生医療の材料として組織幹細胞は、自分自身の組織から単離できるので生命倫理問題が少なく、また移植による免疫拒絶を心配する必要がないといった利点がある。そこで本研究では、ヒト唾液腺組織より組織幹細胞を分離・同定し、増幅する技術を確立し、唾液腺の再生医療を創始することを目的とした。

5．研 究 計 画

当研究室では既に SS の診断に必須な口唇小唾液腺組織より、ヒト唾液腺培養上皮細胞を特異的に分離培養する技術を確立している。そこでまず、この細胞を用いて組織幹細胞の同定を行うこととした。組織幹細胞はこれまでにいくつかの組織から発見されているが、それらの性質は組織により異なり、幹細胞の特異的マーカーとなり得るものが非常に少ない。ヒト唾液腺における組織幹細胞の効率的な分離には、培養唾液腺上皮細胞中の特異的な組織幹細胞マーカーが必要となる。既に我々は、唾液腺上皮細胞の培養に伴う各種遺伝子発現、表面抗原変化について検討した際に、継代初期の幼若な細胞にのみ EGF-R（epidermal growth factor receptor)が発現し、また培養細胞が経時的に、いくつかの機能分子の発現を変化させる事象を見いだしている。これは培養唾液腺上皮細胞が継代初期には主に導管細胞からなり、培養経時的に腺房細胞へ分化していることを示唆するものであった。そこで幼若で未分化な唾液腺組織幹細

胞を分離するため、FACS (fluorescence activated cell sorting)を用い、EGF-R をマーカーとした、個体中に極少数しか存在しない唾液腺幹細胞の純化を試みた。その結果、ヒト唾液腺培養上皮細胞には EGF-R 弱陽性、強陽性の分画が存在し、強陽性群には、他の幹細胞において発現が認められる prostate stem cell antigen (PSCA)、clusterin 遺伝子の特異的な発現が確認された。ヒト唾液腺培養細胞は EGF-R 強陽性分画に幹細胞を含む可能性が示唆されたが、より純度の高い分離を行うにはいくつかのマーカーを組み合わせる必要がある。そこで、近年、抗体を使用しない新しい幹細胞純化法として使用され始めた DNA 結合色素 Hoechst33342 を排出する能力を指標として分離する side population (SP)法を組み合わせ、ヒト唾液腺組織幹細胞の更なる純化を試みている。予備的実験において、SP 法によりヒト唾液腺培養上皮細胞の解析を行ったところ、0.5〜0.9%の SP 細胞集団を得ることに成功している。今後、この SP 細胞群と EGF-R 強陽性群との各種プロファイルを比較し、唾液腺の幹細胞を選択的に認識するマーカーの検索を行い、ヒト唾液腺培養上皮細胞からの幹細胞の分離同定を行う。

6．研究成果

ヒト口唇小唾液腺組織から上皮細胞を特異的に分離培養する系を確立し、このヒト唾液腺培養細胞のcharacterizationから、次の結果を明らかにした。

1）培養細胞は接着性で、上皮系のマーカーであるEMA、Cytokeratin8/18が陽性であり、上皮細胞であることを明らかにした。

2）表面抗原の解析から、唾液腺上皮細胞はIFN刺激によりHLA-DR, CD40, Fasを発現し、また、SS患者由来の唾液腺上皮細胞とnon-SS由来の唾液腺上皮細胞ではIL-1β, IL-6, TNFαなどいくつかの分子で発現する量が異なることを明らかにした。

3）遺伝子発現の解析において、培養細胞は継代初期にEGF-Rを発現するが、経時的にその発現を徐々に低下させ、継代後期にEGF-Rは陰性化し、α-amylase1の発現を増大させる機能分子の経時的な発現の変化を見いだした。これは培養唾液腺上皮細胞が初期には主に導管細胞からなり、徐々に腺房細胞に分化していることを示している。発現する機能分子が、分化により変化することから、培養細胞中の組織幹細胞の存在が示唆された。

4）唾液腺培養上皮細胞をIFNγの存在また非存在下にて培養し、IP-10, Mig, I-TAC分子のmRNA発現と、培養上清中のこれら分子をELISA法にて定量を行った。IFN刺激によりIP-10, Mig, I-TACのＴ細胞遊走性ケモカインが誘導され、その蛋白産生量はnon-SS唾液腺上皮細胞に比べ、SS唾液腺上皮細胞では増大していることを明らかにした。

5）SS唾液腺上皮細胞において、IFN刺激により大量のIL-6産生を示す例を認め、高IL-6産生例ではTGFβ産生量が低下している現象を見いだした。TGFβは基本的に免疫調節性サイトカインであることから、SS唾液腺上皮細胞のTGFβ産生能低下が、IFN刺激によるIP-10, MigやIL-6の過剰産生をもたらしている可能性を示した。

6）EGF, IL-1β, IL-4, IL-6, IL-10などの種々のサイトカインに対する増殖反応が、non-SS細胞に比較して、SS唾液腺上皮細胞では増大している傾向があることを見いだした。

7）継代初期の幼若な細胞に発現するEGF-Rをマーカーとし、FACSにより、個体中に極少数しか存在しない唾液腺幹細胞の純化を試みた。その結果、ヒト唾液腺培養上皮細胞にはEGF-R弱陽性、強陽性の分画が存在し、強陽性群に、他の幹細胞において発現が認められるPSCA、clusterin遺伝子が特異的に発現する事象を見いだした。

8）より純度の高い分離を行うため、抗体を使用しない新しい幹細胞純化法として使用され始めたDNA結合色素Hoechst33342を排出する能力を指標として分離するSP法を施行した。その結果、ヒト唾液腺培養上皮細胞には0.5〜0.9 %のSP細胞集団が存在することを明らかにした。

9）高い割合で幹細胞が存在すると考えられるSP分画の細胞に、PSCAが特異的に発現していることを明らかにした。

7．研究の考察・反省

唾液腺再生の試みについては、動物を用いた組織学的、生化学的検討は行われているものの、ヒト培養細胞からの唾液腺細胞の再生の取り組みについては世界でも初めての試みである。そのため唾液腺組織幹細胞に関する特異的なマーカーや、分化の指標となる分子についての知見は未だほとんど得られておらず、ヒト唾液腺組織および培養上皮細胞の特異的マーカー検索が必須であった。今回、我々は、ヒト唾液腺培養上皮細胞が培養に伴い、いくつかの機能分子の発現を変化させる事象に注目した。そこから継代初期の幼若な細胞に発現するEGF-Rを見いだし、この分子を指標としたFACSによる唾液腺幹細胞分離を行った。その結果、このEGF-R強陽性の分画に、他の幹細胞において発現が認められるPSCA, clusterin遺伝子の特異的な発現を見いだした。また、もう一つの幹細胞純化のアプローチとしてDNA結合色素Hoechst33342を排出する能力を指標として分離するSP法を施行し、ヒト唾液腺培養上皮細胞のSP細胞集団とmain population(MP)細胞集団の遺伝子発現解析を行った。その結果、高い割合で幹細胞が存在すると考えられるSP分画の細胞にもPSCAが特異的に発現することを明らかにした。これらの結果から、ヒト唾液腺培養上皮細胞中には組織幹細胞が存在し、EGF-R強陽性分画に幹細胞を含む可能性を示した。またPSCAを更なるマーカーとして使用することで、より純度の高い幹細胞分離法を行うことが出来ると考えている。今後、EGF-RとPSCAを用いて細胞の分取を行い、これらの細胞が放出するサイトカインなどの因子を同定し、この細胞集団の分化制御や自己複製能について検討を行いたい。

1．　研究課題名：Chorea-acanthocytosis の発症機序に関する研究（研究番号 S2003-11）

2．　キーワード：1）chorea-acanthocytosis

2）常染色体優性遺伝（autosomal　dominant　heredity）

3）遺伝性舞踏病（hereditary　chorea）

3．　研究者氏名：　斉木臣二・医学部・助手・脳脊髄神経治療学（神経内科学）

（現　ケンブリッジ大学、英国）

4．　研究目的

大脳基底核変性による錐体外路症状と末梢有棘赤血球を呈する諸疾患は neuroacanthocytosis 症候群[chorea-acanthocytosis（以下 ChAc），McLeod 症候群、abetalipoproteinemia、Huntington's disease-like 2 with acanthocytosis（以下 HDL2 associated with acanthocytosis）]とされ、わが国では最も ChAc が多い。ChAc の病態機序解明は、neuroacanthocytosis 症候群だけでなく、phenotype の類似する Huntington 病（以下 HD）などの多くの大脳基底核変性疾患の機序解明に寄与すると考えられる。また ChAc 常染色体劣性遺伝家系において同定された CHAC（その後 VPS13A と改称された）の機能を、我々が世界で初めて見出した常染色体優性遺伝家系（以下 AD-ChAc）における変異の解析により明らかにする。さらに VPS13A 遺伝子産生タンパク chorein の機能を免疫学的手法にて解析し、他の遺伝性舞踏病との鑑別に用いることができるかを検討する。

5．　研究計画

網掛けの計画は時間的問題から完遂不能であった。

1）AD-ChAc2 家系における遺伝子変異同定、他の neuroacanthocytosis 症候群責任遺伝子との関連の検討

2）ChAc における不随意運動に対する 5-HT_{1A} agonist である tandospirone citrate（以下 TC）内服効果の評価

3）患者と他疾患の骨格筋組織における独自に合成した抗原ペプチドに対する 3 種類の抗体を用いた CHAC protein（chorein）発現の免疫学的検討（患者骨格筋、他疾患患者、正常コントロールとの比較及びミトコンドリア呼吸鎖異常の検討）

4）上記抗体を用いたウイスターラットの各脳組織における検討

5）我々が同定した変異遺伝子のクローニング

6）クローニングした遺伝子を導入したトランスジェニックマウスの作製

6．　研究成果

1) AD-ChAc 2家系においてまったく新しいVPS13A変異を同定し、AR-ChAcでの責任遺伝子CHACの変異がAD-ChAcの原因にもなりうることを証明した。これらは先天性ミオトニア（Becker型、Thomsen型）と同様に、常染色体劣性遺伝でも常染色体優性遺伝でも同一の疾患が発症しうることを示し、chorein機能不全が、dominant negative effectを獲得する可能性を示唆する。

2) 我々の同定したAD-ChAc 2家系は、Walker[a)]らが報告したAD-ChAcとはgenotype、phenotypeとも異なることを報告した。

3) 抗chorein抗体によるヒト骨格筋組織の染色が、ATP染色、NADH-TR染色と同様のパターンを呈することを見出し、ChAc患者骨格筋では筋膜のchorein発現が不十分であり、他の遺伝性舞踏病との鑑別が可能であることを証明した。ミトコンドリア機能異常に関しては証明できなかった。

a) Walker RH, et al. Neurology 2003;61:1002-4

7．　研究の考察・反省

1) 抗chorein抗体による骨格筋染色では、ChAcにのみ異常を認め、他の遺伝性舞踏病では異常を認めなかったことから、ChAcとHuntington病などの他の遺伝性舞踏病とのcommon pathwayを明らかにすることはできなかった。

2) 抗chorein抗体による免疫染色では、筋膜が不連続で時にdepositを認めた。これはVPS13AのhomologyMaintainに重要である）と一致すると考えられた。

3) 患者数が少なかったため、TCの治療効果に関しては英文でpublishされるレベルの論文を出すことができなかった。

4) 現在、研究成果3)の論文はNeurology誌に投稿中である。

5) トランスジェニックマウスの作製は、時間的問題から断念した。

8．　研究発表

Saiki S, Sakai K, Kitagawa Y, Saiki M, Kataoka S, Hirose G. Mutation in the CHAC gene in a family of autosomal dominant chorea-acanthocytosis. Neurology2003; 61: 1614-1616 (MLDB)

Mutation in the *CHAC* gene in a family of autosomal dominant chorea–acanthocytosis

S. Saiki, MD; K. Sakai, MD, PhD; Y. Kitagawa, AS; M. Saiki, MD; S. Kataoka, MD, PhD; and G. Hirose, MD, PhD

Abstract—Although mutations in the CHAC gene have been identified in autosomal recessive chorea–acanthocytosis (AR-ChAc), the molecular basis of autosomal dominant ChAc (AD-ChAc) remains to be determined. The authors investigated abnormalities in the *CHAC* gene in an AD-ChAc family with mRNA and sequencing analyses of mRNA and genomic DNA. A novel single heterozygous mutation in the last nucleotide of exon 57 of the *CHAC* gene, which could cause skipping of the exon, was detected in affected siblings.

NEUROLOGY 2003;61:1614–1616

Although most cases of chorea–acanthocytosis (ChAc) are transmitted as an autosomal recessive trait (AR-ChAc), some cases have been inherited as an autosomal dominant trait (AD-ChAc).[1] The gene (*CHAC*) responsible for AR-ChAc and its encoded protein, chorein, have been identified.[2,3] Several mutations in the exons and introns of the *CHAC* gene led to missense or nonsense mutations in chorein protein. A recent extensive study conducted of AR-ChAc found various abnormalities in the *CHAC* gene,[4] confirming that it is responsible for AR-ChAc. We have found abnormalities in the *CHAC* gene in a Japanese family with AD-ChAc.

Patients and methods. *Patients.* Clinical features of the pedigree are shown in the table. Neurologic examinations and studies of red blood cells in a wet preparation were performed in five affected individuals (II-1, II-9, III-1, III-2, and III-3) and the proband's mother (II-4). Blood smears were prepared from venous blood by placing a small drop of blood on the surface near the end of a clean glass slide. The spreader slide was kept at a 45° angle against the horizontal slide and was then drawn rapidly and

From the Department of Neurology, Kanazawa Medical University, Ishikawa, Japan.

Supported in part by Scientific Research Grant-in-Aid from the Ministry of Education of Japan, a grant for Neuroimmunological Disease Research from the Ministry of Health and Welfare of Japan, a grant for Project Research from High-Technology Center of Kanazawa Medical University (H2003-8), and a grant for Promoted Research from Kanazawa Medical University (S2003-11).

Received June 4, 2003. Accepted in final form August 5, 2003.

Address correspondence and reprint requests to Dr. K. Sakai, Department of Neurology, Kanazawa Medical University, 1-1 Daigaku, Uchinada-machi, Kahoku-gun, Ishikawa, 920-0293, Japan; e-mail: ksakai@kanazawa-med.ac.jp

Table *Clinical features of the family*

Patient	Age of death, y	Onset, y	Involuntary movement	DTRs	MMSE	CK [U/ml]	Acanthocyte	NCV	Muscle biopsy
I-1	62	30–35	chorea, ballism	NE	NE	NE	NE	NE	NE
II-1	62	38	chorea, tics	hypoactive	NE	710	15%	NE	NE
II-3	50	25–30	choreoathetosis	NE	NE	NE	*	NE	NE
II-4	64	—	none	normoactive	29	167	none	NE	NE
II-9	65	25–30	chorea, tics	hypoactive	NE	NE	20%	NE	NE
III-1	42	20–25	choreoathetosis, ballism	hypoactive	NE	NE	15%	NE	NE
III-2	37	35	chorea, tics, oral dyskinesia	hypoactive	28	851	15%	delayed	variable fiber diameter
III-3	34	25	chorea, tics, OCB	hypoactive	25	1179	20%	delayed	variable fiber diameter

* Although acanthocytes were detected, the percentage was unknown.

DTR = deep tendon reflex; MMSE = Mini mental state examination; CK = serum creatine kinase [normal value: 47–212 U/ml]; NCV = nerve conduction velocity; NE = not examined; OCB = obsessive compulsive behavior.

smoothly over the entire length of the slide. Blood biochemistry tests were performed in three affected individuals (II-1, III-2, and III-3) and the proband's mother, whereas nerve conduction velocity studies, biceps brachii muscle biopsy, and brain MRI were undertaken in two affected siblings (III-2 and III-3).

Reverse transcription PCR and sequencing analysis. Five micrograms of total RNA was prepared from lymphocytes from the affected individuals and their unaffected mother and used for the reverse transcription (RT) reaction with Moloney murine leukemia virus reverse transcriptase. The cDNA were amplified by PCR using primers specific to human chorein mRNA. Independently amplified products were purified, and >10 independent subclones were sequenced.

Genome analysis. Genomic DNA was extracted from the blood samples from affected individuals and their unaffected mother. Exon 57 and exon–intron boundaries of the *CHAC* gene were amplified and used for direct sequencing.

Results. We identified a pedigree of ChAc (figure 1A). The proband (III-2) and her sibling (III-3) were affected with ChAc and their father (II-3) and grandfather (I-1) presumptively affected. But their mother (II-4), who has no consanguinity, had been in good health and had neither neurologic symptoms nor acanthocytosis. Furthermore, as another three members were found to have the disease, we concluded that the inheritance trait of this pedigree is autosomal dominant. Five affected individuals showed peripheral acanthocytosis (see figure 1B). Abetalipoproteinemia was not detected in the proband or her brother, and their brain MRI study revealed bilateral caudate atrophy (see figure 1C). Three members, the proband, her brother, and their unaffected mother, consented to provide research samples for genetic analyses, and the other family members declined.

First, we investigated mutations, deletions, or insertions in the chorein mRNA of the two affected siblings and their unaffected mother. We carried out RT-PCR with mRNA from lymphocytes using 10 pairs of overlapping primers encompassing the entire coding region of the chorein mRNA (figure 2A). Subcloning the PCR products and sequencing revealed that 82 bp, corresponding to exon 57, were deleted in the chorein mRNA from the two affected siblings (see figure 2A) but not in the mRNA from

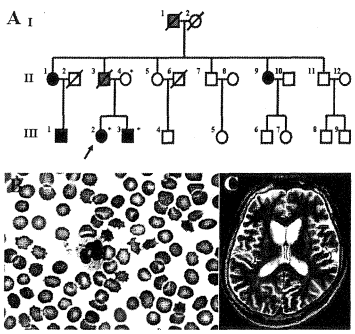

Figure 1. (A) The pedigree of the Japanese family with chorea–acanthocytosis analyzed here. Black symbols = affected individuals; gray symbols = presumptively affected individuals; open symbols = unaffected members. Patients with an asterisk underwent genetic analysis. (B) Wet blood smear showing many acanthocytes with spiky projections in peripheral blood (Patient III-2). (C) Brain MRI study showing atrophy of bilateral caudate nuclei and mild cortical atrophy (Patient III-2).

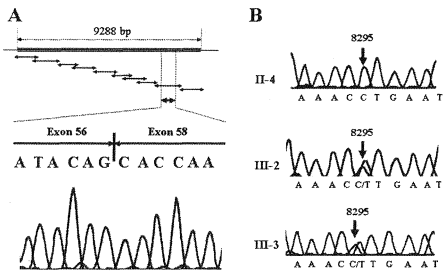

Figure 2. (A) Overlapping primers used for reverse transcription (RT) PCR analysis of the chorein mRNA. Primers encompass the entire coding region. RT-PCR result with the chorein mRNA from the affected siblings. Deletion of an 82-bp nucleotide, corresponding to exon 57, was detected in the affected siblings. This deletion could cause a frameshift mutation, leading to premature termination of translation of the chorein mRNA. (B) Sequence chromatograms around nucleotide 8,295 in the CHAC *gene. Mutation in the last nucleotide in exon 57 (8,295G→A) of the* CHAC *gene from two affected siblings (III-2 and III-3) is heterozygous, whereas their unaffected mother (II-4) is a homozygote wild type.*

their unaffected mother. This deletion could cause a frameshift, leading to a premature termination of translation of the chorein mRNA. In materials from the affected siblings, some subclones had a deletion and others had wild type, indicating that the deletion was heterozygous. No other abnormalities were detected in the coding region of the chorein mRNA from the affected siblings.

To determine the genome abnormality responsible for this deletion in the chorein mRNA, we investigated abnormalities in exon 57 and introns 56 and 57 of the *CHAC* gene from the two affected siblings and their unaffected mother. Genome analysis revealed a heterozygous G→A transversion at the last nucleotide of exon 57 of the *CHAC* genes from the affected siblings, but the *CHAC* gene from their unaffected mother showed homozygote wild type (see figure 2B). This mutation in exon 57 of the *CHAC* gene has not previously been reported in AR-ChAc families.

Discussion. The clinical features of this family were typical of ChAc. Although neither mutations of the *XK* gene nor Kell antigen expression was looked for in the family, we have ruled out McLeod syndrome based on male–male transmission over two generations and three women presenting with typical ChAc symptoms. Four women carriers with a heterozygous *XK* gene mutation in a single family have been identified, whereas only one has shown clinical abnormalities.[5]

It is well established that abnormalities in the *CHAC* gene are responsible for AR-ChAc, whereas the molecular mechanism of AD-ChAc remains to be determined. Although several cases of AD-ChAc families have been reported, the evidence for autosomal dominant inheritance is somewhat unclear and suggests reduced penetrance and variable clinical presentations. There is an AD-ChAc family without *CHAC* mutation,[6] and the possibility that AD-ChAc is due to expanded trinucleotide repeats has been suspected. However, the affected members of the kindred did not show typical AR-ChAc symptoms such as seizure, peripheral neuropathy, and myopathy, whereas the clinical phenotypes of AR-ChAc and AD-ChAc are the same.

Different mutations in one gene can result in either dominant or recessive phenotype. Autosomal recessive congenital myotonia (Becker) and autosomal dominant congenital myotonia (Thomsen) show similar clinical phenotype, and both have genetic defects in the same *ClC-1* gene.[7] A mutation Gly275 (1-bp ins) in retinal pigment epithelium G protein-coupled receptor has been reported to cause dominant retinitis pigmentosa, whereas the Ser66Arg mutation in the same gene appears to be recessive.[8] In this study, we have investigated abnormalities in chorein mRNA and the *CHAC* gene from AD-ChAc. We found a single heterozygous mutation (G→A) in the last nucleotide of exon 57 of the *CHAC* gene of the affected members. It has been demonstrated that the substitution of an A for G in the last nucleotide of the exon causes an exon skipping in a collagen gene associated with Ehlers–Danlos syndrome type VII and an ornithine transcarbamylase gene.[9] Thus, this single heterozygous mutation in the last nucleotide of an exon in the *CHAC* gene can be predicted to induce skipping of exon 57 and cause a frameshift, leading to premature termination of translation of chorein mRNA. Both affected siblings were heterozygotes, and the unaffected mother was homozygote wild type. These findings suggest that the *CHAC* gene may be responsible for AD-ChAc as well as AR-ChAc.

It remains unclear why a clinical disease with one mutation appears to be recessive, whereas the disease with another mutation appears dominant. In congenital myotonia, whether a mutation behaves in a dominant or recessive manner might depend on the severity of its effect on kinetics and current density.[10] Although the precise neurobiologic function of the chorein protein is not known, this feature possibly implicates a common etiology for a variety of neurodegenerative disorders, including the disorder in this AD-ChAc family. Loss-of-function mechanism of the chorein protein encoded by the *CHAC* gene is likely to contribute to the pathogenesis of ChAc unless there is dominant negative effect. Further investigation with genetically manipulated models harboring the identified mutations of the *CHAC* gene could provide more information about the relevance of the mutation to the pathogenesis of AD-ChAc.

References

1. Hardie RJ, Pullon HW, Harding AE, et al. Neuroacanthocytosis. Brain 1991;114:13–49.
2. Rampoldi L, Dobson–Stone C, Rubio JP, et al. A conserved sorting-associated protein is mutant in chorea–acanthocytosis. Nat Genet 2001; 28:118–119.
3. Ueno S, Maruki Y, Nakamura M, et al. The gene encoding a newly discovered protein, chorein, is mutated in chorea–acanthocytosis. Nat Genet 2001;28:120–121.
4. Dobson–Stone C, Danek A, Rampoldi L, et al. Mutational spectrum of the CHAC gene in patients with chorea–acanthocytosis. Eur J Hum Genet 2002;10:773–781.
5. Ho MF, Chalmers RM, Davis MB, Harding AE, Monaco AP. A novel point mutation in the McLeod syndrome gene in neuroacanthocytosis. Ann Neurol 1996;39:672–675.
6. Walker RH, Morgello S, Davidoff–Feldman B, et al. Autosomal dominant chorea–acanthocytosis with polyglutamine-containing neuronal inclusions. Neurology 2002;58:1031–1037.
7. Koch MC, Steinmeyer K, Lorenz C, et al. The skeletal muscle chloride channel in dominant and recessive human myotonia. Science 1992;257: 797–800.
8. Morimura H, Saindelle–Ribeaudeau F, Berson EL, Dryja TP. Mutations in RGR, encoding a light-sensitive rhodopsin homologue, in patients with retinitis pigmentosa. Nat Genet 1999;23:393–394.
9. Talerico M, Berget SM. Effects of 5' splice site mutations on splicing of the preceding intron. Mol Cell Biol 1990;10:6299–6305.
10. Kubisch C, Schmidt–Rose T, Fontaine B, Bretag AH, Jentsch TJ. ClC-1 chloride channel mutations in myotonia congenital: variable penetrance of mutations shifting the voltage dependence. Hum Mol Genet 1998;7: 1753–1760.

1．研究課題名：ミトコンドリア障害に関与する活性酸素生成酵素の研究（研究番号 S2003-12）

2．キーワード：1）ミトコンドリア（mitochondria）
2）パラコート（paraquat）
3）活性酸素（reactive oxygen）
4）フリーラジカル（free radical）
5）細胞障害（cytotoxicity）

3．研究者氏名：島田ひろき・医学部・講師・分子細胞形態科学（解剖学）

4．研究目的

世界各地で使用されている除草剤パラコートは，Parkinson 病のリスクファクターとして近年注目されている。従来，パラコートの細胞毒性機構は小胞体薬物代謝系酵素によるものとされてきたが，我々はこの機構がミトコンドリア外膜に局在する新規酵素 NADH-quinone oxidoreductase$_m$ (NQO_m) によって引き起こされるというミトコンドリア障害説を電顕細胞化学的，生化学的に証明してきた。即ち，パラコートは NQO_m によって NADH を電子供与体として還元されてパラコートラジカルとなり，引き続き生成する各種活性酸素種がミトコンドリアを障害して細胞死へ至らしめるという説である。

我々のこれまでの研究から，NQO_m は分子量約 500kDa の膜タンパク質複合体であることがわかっている。本研究の目的はこの構成タンパク質成分を解析して NQO_m の本態を明らかにすることである。

5．研究計画

1) ラット肝より単離したミトコンドリアで，パラコート由来の活性酸素生成を測定し，各種薬剤，抗体を用いて酵素成分を解析する。

2) 単離ミトコンドリアより調製した外膜から，界面活性剤処理およびクロマトグラフィーを行って酵素活性陽性成分を抽出・分画する。

3) 酵素画分の活性に対する各種薬剤，抗体の影響を解析する。また，免疫沈降を行って酵素成分を解析する。

4) Zymography により酵素を特定し，Western blot により酵素成分を解析する。

6．研究成果

ラット肝臓より単離したミトコンドリアをガラス上に吸着させ，10 mM パラコート，2 mM NADH を基質として反応させた。生成した superoxide の不均化反応によって生ずる過酸化水素を，dichlorofluorescin-diacetate 蛍光法によって検出すると，パラコートまたは NADH 単独では，ブランクと比べて蛍光強度に差は見られなかったが，両者を同時に添加すると蛍光を発する数，強度とも増加した。

この反応はアニオンチャンネルブロッカーである4,4'-diisothiocyanatostilbene-2,29-disulfic acid (DIDS), voltage-dependent anion channel (VDAC)の結合物質である N,N'-dicyclohexylcarbodiimide (DCCD), および抗VDAC抗体によって抑制された。

次にミトコンドリア外膜より1% Triton X-100/1%デオキシコール酸および0.06% SDS/0.1% NP-40の２段階処理で活性成分を抽出し，陰イオン交換クロマトグラフィーにより酵素画分を調製した。パラコートによるsuperoxide生成をnitroblue tetrazorium(NBT)還元法により測定したところ，単離ミトコンドリアでの実験と同様に,NADHとパラコートの同時添加により活性が現れ,DIDS, DCCDおよび抗VDAC抗体によって抑制された。また，抗VDAC抗体による免疫沈降を行い，画分中のVDACを減少させたところ，活性は抑制された。

さらに酵素画分をnative-ポリアクリルアミド電気泳動(PAGE)し，NBT法によるzymographyを行ったところ，分子量500 kDaに活性が現れた。このバンドをSDS-PAGEにかけたところ，複数の蛋白バンドが検出された。抗VDAC抗体でWestern blotしたところ，抗体に反応する蛋白質が含まれていた。

7．研究の考察・反省

本研究より,NQO_mが１)NADHを電子供与体としてパラコートを還元してラジカルを生成すること，２）分子量500 kDaの外膜に結合した蛋白複合体であること，３）複合体の成分に外膜イオンチャネルのVDACが含まれていることが明らかとなった。VDACはミトコンドリアの外膜に存在し，アデニンヌクレオチドトランスロケーター(ANT)，シクロフィリンＤなどと複合体を形成して，膜電位の維持やアポトーシスに関連しているといわれている。また，最近になって，細胞膜型VDACに酸化還元酵素活性をもつという報告がなされている。NQO_m活性がVDAC単独によるものなのか，ANTやシクロフィリンＤなど他の成分を必要とするのかは今後の課題であり，現在，ANTやシクロフィリンＤを修飾する薬剤のNQO_m活性におよぼす影響を解析中である。さらに，細胞内でVDACがNQO_m成分としてどのように働いているかを調べるため，VDAC遺伝子導入をおこなって，細胞内でのNQO_m活性や細胞障害の変化を解析中である。

2003　平成15年度金沢医科大学奨励研究成果報告書

平成17年12月発行

編　集　　研究推進評価特別委員会

発行所　　金沢医科大学出版局

石川県河北郡内灘町大学 1丁目1番地